Non-equilibrium phase transition to the polariton OPO regime

Kirsty Dunnett

University College London

A dissertation submitted for the degree of

Doctor of Philosophy

June 2016

Declaration

I, Kirsty Dunnett, confirm that the work presented in this thesis is my own. Where information has been derived from other sources, I confirm that this has been indicated in the thesis. The work contains nothing which is the outcome of work done in collaboration except where specifically indicated in the text. In particular, the work in chapter 4 was done in collaboration with G. Dagvadorj who provided me with all data from numerical integration of the cGPEs, and Dr. A. Zamora whose observations provided direction for the investigation.

Parts of this dissertation have been published, or submitted for publication, as follows.

Chapter 3 is summarised for the case of constant polariton decay in K. Dunnett and M. H. Szymańska, *"Keldysh Field theory for nonequilibrium condensation in a parametrically pumped polariton system"*, Physical Review B. 93. 195306 [1]. The plots in sections **3.5.1** and **3.6** are all from this paper.

Kirsty Dunnett
June 2016

Abstract

Exciton-polaritons are the quasi-particles that form when cavity photons couple strongly to quantum well excitons in semiconductor microcavities. When a pump laser is applied near the point of inflection of the lower polariton dispersion, a phase transition to the polariton optical parametric oscillator regime where two additional, 'signal' and 'idler', modes with macroscopic occupation appear can occur. The steady state of the non-equilibrium polariton system is maintained by continuous pumping and the Keldysh functional integral approach is used to study the phase transition. Despite its highly non-equilibrium nature, an effective chemical potential is identified and the phase transition occurs when the effective chemical potential crosses the normal modes. The Keldysh formalism also gives access to the occupations of the modes and experimentally observable properties such as the incoherent luminescence and absorption spectra are calculated.

One of the key properties of the signal mode is that it occurs near the minimum of the lower polariton dispersion with zero momentum. To calculate the mean field occupation of the three mode optical parametric oscillator regime analytically, the signal momentum has to be chosen explicitly. A simple method to determine the signal momentum by using linear response analysis for any system parameters is proposed and the predictions compared with numerical integration of the complex Gross-Pitaevskii equations describing the system. At weak pump strengths, the signal momentum is found best by the linear response analysis of the three mode description, while at higher pumping, a linear response analysis of the single pump mode gives best agreement with the numerical simulations.

Acknowledgements

Although many people have helped and supported me over the last few years, several deserve particular mention. First my parents, who, after my move to UCL in September 2013, patiently put up with all my complaints about London, delayed trains and a myriad of other topics.

Without the guidance of and numerous long discussions with my supervisor Dr. M. H. Szymańska, this project would neither have started nor reached its current state. Dr. J. M. Fellows provided invaluable assistance with the development of the Fortran code used. The project that forms the second half of this thesis was done in collaboration with G. D. Dagvarodj and Dr. A. Zamora; their hard work has made the project as complete as it is. Others who have provided useful discussions include colleagues Dr. T. K. Mavrogordatos and R. T. Juggins at UCL, Dr. F. M. Marchetti and A. C. Berceanu of the Universidad Autónoma de Madrid and the group of Dr. D. Sanvitto at CNR Nanotec, Lecce.

My sincere thanks also go to Dr. P. A. Bartlett whose trust and encouragement has enabled me to develop my teaching since I joined UCL. The time spent demonstrating for the first year undergraduate laboratory courses provided a welcome break from the computer screen.

Contents

List of Figures

List of Tables

1 Introduction

The non-equilibrium phase transition of a system of coherently pumped exciton-polaritons in a semiconductor microcavity is studied in this thesis. This chapter provides a brief background to the equilibrium Bose-Einstein condensation (BEC) and Berezhinskii-Kosterlitz-Thouless (BKT) phase transitions (section 1.1) which have featured in descriptions of the phase transition of interest. The polariton system is introduced in some detail in section 1.2, and section 1.2.3 reviews existing studies on the polariton optical parametric oscillator (OPO) regime which is studied. Here, the Keldysh Green's function approach is used to study the non-equilibrium phase transition to the OPO regime. The details of the Keldysh approach for the system studied are left to chapter 3, but in section 1.3 some systems that have been studied using the Keldysh approach are mentioned briefly. The structure of the thesis is outlined in section 1.4.

1.1 BEC and BKT

The Bose-Einstein distribution function that describes a gas of ideal bosons in equilibrium is [2,3]:

$$\overline{n}_k = \frac{1}{e^{(\epsilon_k - \mu)/T} - 1} \tag{1.1}$$

where $\overline{n}_k$ is the average occupation of state k with has energy ϵ_k and μ is the chemical potential which must be less than the lowest energy eigenvalue (ϵ_0) [3]. As $\mu \to \epsilon_0$, the occupation of the lowest energy state (with energy ϵ_0) becomes macroscopic; this is the characteristic mechanism of BEC [3, 4].

Before the experimental realisation of BEC, the macroscopic quantum phenomena of superfluidity and superconductivity were taken as evidence of the existence of a Bose-Einstein condensate [3, 5]. Experimental observation of equilibrium BEC was initially in dilute atomic gases [6–9] that are close to weakly interacting bosonic gases [6]. Even though light elements were studied, transition temperatures were low; between a couple of hundred nano-Kelvin [6] and a few micro-Kelvin [8, 9].

In an uniform Bose gas in two dimensions, BEC cannot occur at finite temperatures since thermal fluctuations of the phase destroy the condensate [3]. When interactions are included, a phase transition to a condensate can occur at a finite temperature T_c, however vortices can

be excited thermally above a particular temperature T_{BKT} [3]. The BKT transition defines the point at which the addition of vortices no longer reduces the free energy of the system. Above T_c, all vortices are free, while at temperatures below T_{BKT}, vortices of opposite circulation are bound in pairs [3]. The BKT transition is particularly important for defining the transition to superfluidity since vortices lead to friction between the superfluid and normal densities in a superfluid and therefore destroy the superfluid [3].

1.2 Polaritons

Polaritons are the quasi-particles that form as a result of strong-coupling between a radiation field and a polarisation field [10]. Although exciton-polaritons (where the polarisation field is the excitons) were observed in bulk materials [11–13], the creation of polaritons in bulk semiconductors was difficult to control [14]. The first experimental observation of polaritons in a semiconductor microcavity demonstrated the level of control available in these systems [14]. This section introduces these semiconductor microcavity exciton-polaritons (hereafter referred to simply as polaritons) and some of the main phenomena that have been observed. A detailed theoretical description is left for subsequent chapters.

1.2.1 Polaritons in semiconductor microcavities

A semiconductor microcavity consists of alternating layers of semiconductors, with different refractive indices, on either side of a central cavity containing one or more quantum wells [14,15], as shown schematically in Fig. 1.1. The layers of semiconductor material act as a distributed Bragg reflector (DBR) or Fabry-Pérot cavity and therefore trap incoming photons [14]. Although most microcavities used in polariton experiments have about 20 layers forming the front mirror and 30 forming the back mirror [15], increasing the number of mirrors can lead to polaritons with a lifetime longer than the thermalisation time [16, 17].

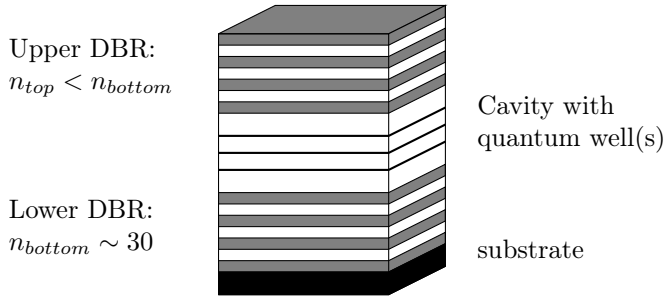

Figure 1.1: A semiconductor microcavity consists of alternating layers of semiconductor to form two distributed Bragg reflectors that trap photons. Excitons are formed in the central region which contains one or more quantum wells.

The photons are confined in the vertical direction of the microcavity, but not in the plane of

the quantum wells [15]. These cavity photons have a very small effective mass [15,18,19], and can create excitons in the quantum wells. If the interconversion rate is large enough, quantum well excitons and cavity photons can form quasi-particles, polaritons, that inherit properties from both excitons and photons [15, 18, 19].

The polariton dispersions are unusual in that the lower polariton branch is approximately quadratic at low momenta while at higher momenta the dispersion is almost flat and approaches the exciton energy, while the upper polariton branch is approximately quadratic at all momenta [15]. Due to the one to one correspondance between the in plane momentum of the polaritons and escaping photons, the polariton dispersions are determined by reflection or transmission experiments under weak pumping [15]; their exact forms are introduced in chapter 2. One of the key properties that the polaritons inherit from the photons is their finite lifetime, typically 10-100 ps, which facilitates their detection via emitted photons [15].

1.2.2 Pumping regimes

There are several ways in which polaritons can be created [18,19] and some of the most common are outlined below. The pumping regimes discussed focus on the semiconductor microcavity system described above, and a quick comment is made about the search for polaritons at room temperature.

In non-resonant excitation, a large exciton bath is created at large energies and momenta. The excitons then relax via multiple non-radiative scattering events to form polaritons which end up in a 'bottleneck' near the inflection point of the lower polariton curve [15,18,19]. Above a threshold pump power, spontaneous macroscopic occupation of the low energy modes near $\mathbf{k} = \mathbf{0}$ is observed [15, 19–21].

When polaritons are created by pumping resonantly with the lower polariton dispersion, near the point of inflection [22–31], two interesting behaviours can occur. First, if the pump is applied at energies above the polariton dispersion, the pump mode occupation may become bistable with two possible polariton occupations for a given pump strength [25, 28–30]. Second, at sufficiently strong pumping, two additional modes with macroscopic occupation may appear spontaneously, and the polariton system enter the OPO regime [26, 27, 32].

The polariton OPO regime is characterised by energy and momentum conservation of pairs of pump mode polaritons (P) that are scattered into the new 'signal' (S) and 'idler' (I) states [26–31]. This parametric scattering regime is referred to as the polariton optical parametric oscillation (OPO) regime in analogy to nonlinear optics phenomenon of the same name [33] where a photon in a χ^2 nonlinear medium is converted into a signal and idler photon whose energies satisfy the energy conservation $\omega_p = \omega_s + \omega_i$ and whose momenta satisfy momentum conservation $\mathbf{k}_p = \mathbf{k}_s + \mathbf{k}_i$ [34].

In nonlinear optics, an optical parametric oscillator is the device that results from adding mirrors that are highly reflective at the signal and/or idler frequencies around a χ^2 nonlinear optical material in which optical parametric amplification can occur. The frequency tuneable

mirrors of an optical parametric oscillator make it useful for creating light at specific frequencies. Optical parametric amplification, second harmonic generation and sum frequency generation, can all occur in χ^2 nonlinear media and produce an output wave with a different frequency to the input(s). The optical parametric amplifier uses two input beams, a strong pump beam and a weak idler at a lower frequency. The nonlinear mixing of these two waves can lead to the appearance of a signal wave with energy $\omega_p - \omega_i = \omega_s$; once the signal is established, the same process also amplifies the idler wave [35]. The work in this thesis considers the transition to and properties of the polariton OPO regime which is discussed phenomenologically in the next section; a detailed theoretical description occurs in chapters 3 and 4.

The spontaneous macroscopic occupations of a low energy state that were observed in both the excitation schemes discussed above were seen as the signature of BEC of polaritons, even though the system is two dimensional and held in a steady state far from equilibrium [20,26,27,32]. BEC of exciton-polaritons was first observed in the OPO regime of coherently pumped polaritons [26, 27] and later in non-resonantly excited polaritons [20].

Before discussing resonantly pumped polaritons in more detail, it is worth mentioning some of the other methods that can be used to create polaritons. Resonant pumping at small momenta create polaritons with finite velocity without the appearance of the additional modes; this can be used to probe superfluid behaviour, particularly by scattering against a defect [36]. It is possible to design and create extremely precise microcavity structures [37] in which polaritons can be created [38–41]. Further, real-space potentials can be created by applying external strain to a sample [42–45] or via an optical potential from an additional laser [17, 46].

Although polaritons are typically thought of in semiconductor microcavity systems, there is currently much research into creating polaritons in systems where the quantum wells are replaced by organic dyes, sometimes with modifications to the cavity structure [47–53] which have the advantage that polaritons can be created at room temperature [49, 52, 54]. Both the strong coupling [47,51,53] and ultra-strong coupling regimes [49–52] can be accessed, sometimes within a single sample [51].

The BEC phenomena discussed so far occur in the lower polariton branch of the spectrum, and the upper polariton branch has been neglected. This is common since the quest for non-equilibrium Bose-Einstein condensation focussed on the peculiar properties of the lower polariton branch; the very low polariton mass at low momenta being advantageous for BEC [15]. In a centro-symmetric system parity considerations forbid transitions between a doublet of dressed states [55]. This means that transitions between the two polariton branches by radiative decay are forbidden. By doping the quantum wells to produce an asymmetric system, radiative transitions between the polariton branches can occur at terahertz frequencies [56]. Further, in a polariton system where the excitons can occupy the first and second subbands of the quantum well, the Rabi frequency can be a large fraction of the intersubband transition frequency and the anti-resonant terms of the light-matter coupling become significant, and the upper polariton branches can no longer be neglected in theoretical analyses [57].

1.2.3 Polariton OPO: theory and experiments

Stimulated scattering of polaritons was first observed in pulsed experiments with a weak probe applied resonantly to the minimum of the lower polariton dispersion and a pulsed pump beam tuned to the point of inflection of the lower polariton dispersion [22]. The signal and idler properties were set by the probe beam, and the polariton occupation at the probe showed large gains when the pump beam was applied [22, 23].

Extending this pulsed parametric amplifier [22,23] to continuous wave experiments lead to the polariton OPO regime [26,27]. In early experiments, the pump was applied close to the inflection point of the lower polariton dispersion, at the 'magic angle', to maximise the efficiency of the stimulated scattering [26,27,33] due to the energy and momentum conserving final states all lying on the lower polariton dispersion as seen shown in the left hand panel of Fig. 1.2 [22,31]. Tuning the applied pump away from the triple resonance condition does not prevent the transition into the OPO regime [33,58]; the signal remains near $\mathbf{k} = \mathbf{0}$ while the idler varies in order to conserve energy and momentum [25, 33]. In experiments, the pump energy is usually adjusted once the OPO regime is reached to maximise the efficiency of the stimulated scattering [26, 29, 33, 59].

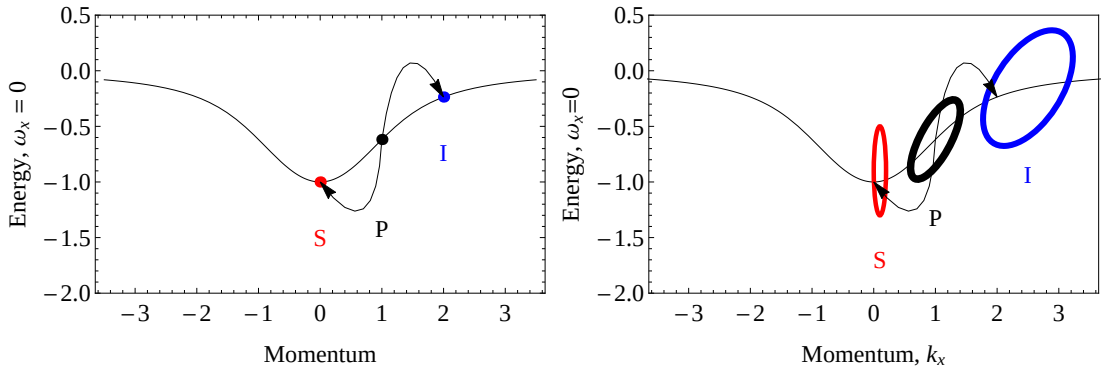

Figure 1.2: Left: example of OPO regime scattering: a pair of pump mode polaritons scatter while conserving energy and momentum into one signal and one idler polariton. In this example, the triple resonance condition is exactly satisfied and $2\omega_{lp}(\mathbf{k}_p) = \omega_{lp}(\mathbf{0}) + \omega_{lp}(2\mathbf{k}_p)$. Right: the OPO regime can occur for a pump chosen within a fairly large range of energies and momenta. The signal mode is always near $k = 0$ while the idler varies greatly with the pump properties to ensure that energy and momentum are conserved.

The energy and momentum conservation of the OPO states gives [26, 58, 59]:

$$2\omega_p = \omega_s + \omega_i, \tag{1.2}$$

$$2\mathbf{k}_p = \mathbf{k}_s + \mathbf{k}_i. \tag{1.3}$$

This assumes that there are only three states in the OPO regime [29,30,32,41,58]. In experiments and numerical simulations, additional peaks are observed in the polariton distribution that are sometimes far from the unperturbed lower polariton dispersion [31,60,61]. These satellite states

are equally spaced in energy and momentum and are the result of further parametric scattering between modes [19, 31, 60–62]. The first satellite states, S_2, I_2, are summarised in table 1.1 [31, 60, 61]. To include such satellite states into the theoretical description of the polariton OPO would require a mean field description for more than three states and is not done here.

State	energy	momentum	scattering channels
S_2	$\omega_s - \omega_p$	$\mathbf{k}_s - \mathbf{k}_p$	$S + S \to P + S_2$ $S + P \to I + S_2$ $P + P \to S_2 + I_2$
I_2	$\omega_i + \omega_p$	$\mathbf{k}_i + \mathbf{k}_p$	$I + I \to P + I_2$ $I + P \to S + I_2$ $P + P \to S_2 + I_2$

Table 1.1: Energy and momentum of the first satellite states and scattering channels (from the OPO regime signal S, pump P and idler I states) that can lead to their occupation.

The OPO regime requires a minimum pump strength that depends on the exact properties of the polariton sample studied and the applied pump [33]. There are two distinct phases of a resonantly pumped polariton system: below the OPO threshold there is only the pump mode that is macroscopically occupied while above the threshold, the OPO regime where the signal and idler modes are also macroscopically occupied, occurs [26, 27]. The signal and idler states have a large degree of spatial coherence [32, 63, 64] and long coherence times [65, 66]. These factors together lead to the description of the signal and idler states as Bose-Einstein condensates, even though the system is two dimensional and far from equilibrium [26, 27].

Since the polariton system is two dimensional, a BKT type rather than BEC type transition should be expected [67], this was seen in numerical simulations of the OPO regime where a narrow BKT region was observed at pump strengths slightly above the signal switch on [68]. In equilibrium, the long range order below the BKT transition temperature decays with a power law, and the maximum value of the exponent is $1/4$; above the transition the decay is exponential [3]. The BKT-type transition in coherently pumped polaritons considered the decay of long range order around the signal mode of the OPO regime. Immediately after the switch on of the signal mode, the long range order decayed exponentially while at slightly higher pump strengths there was a narrow band where the long range order had a power law decay, signifying a BKT type transition. In this far from equilibrium system, the exponent of the power law decay could be much larger than the equilibrium value, reaching 1.2 near the BKT threshold [68].

1.3 Keldysh approach for non-equilibrium phase transitions

The Keldysh functional integral approach can be used to study non-equilibrium systems and their phase transitions [69–71]. The technique enables the calculation of all two-time correlation

functions [69–71] and direct comparison with equilibrium phase transitions [69].

This approach has been used to study the phase transitions of several driven-dissipative systems including the superradiant and glassy phase transitions of the Dicke model [72,73], BEC of photons in dye-filled cavities [74], atoms in multimode cavities [75], a 1-D driven dissipative system near quantum criticality [76] and exciton-polaritons in semiconductor microcavities under incoherent excitation in which a BEC type phase transition and an upper threshold to a laser like behaviour were observed [5,21,77–80].

Further detail on the Keldysh method can be found in section 3.2 where the Keldysh functional integral is derived for a system of coherently pumped polaritons.

1.4 Scope of thesis

Two main projects form the bulk of this thesis. Before commencing with any analysis, chapter 2 introduces the generic description of the polariton system in terms of coupled excitons and photons, which is then rotated into the lower polariton basis. The Hopfield coefficients are derived in detail since they appear in several forms in the literature. In chapter 3, the Keldysh functional integral approach is applied to coherently pumped polaritons. The results reproduce existing work on the phase transition to the OPO regime and extends the analysis since the Keldysh formalism also gives the occupation of the system. The polariton system is studied for equal exciton and photon decays and for exciton decays much less than the photon decay. The work in chapter 4, which discusses the problem of choosing the signal momentum in the OPO regime, was done in collaboration with G. D. Dagvadorj at Warwick University and the results of the time integration of the complex Gross-Pitaevskii equations are from data that he provided. The signal momenta from the results of the time integration are compared with those that could be found through a simple linear response analysis with the aim of improving the choice of the signal momentum made in mean field analyses of the OPO regime. Finally, chapter 5 contains the conclusions and discusses possible future work based on work contained in this thesis.

2 | Descriptions of the system

The basic process of creating microcavity polaritons under any excitation regime is broadly the same [15, 18, 81]. An external laser introduces cavity photons, some of which are converted into quantum well excitons at a rate $\Omega_R/2$, which can convert back into cavity photons, again at a rate $\Omega_R/2$ [81]. In any real system, the cavity photons and quantum well excitons have finite lifetimes; the excitons so may decay into phonons while the photons are lost due to the imperfect reflectance of the microcavity mirrors [15].

In this chapter, the Hamiltonians describing the coherently pumped polariton system, including the losses, are written down. The exact description in the exciton-photon basis is introduced in section 2.1 and the rotation to the polariton basis performed in section 2.2. The lossless system is then used in section 2.3 to obtain the polariton dispersions and to derive the Hopfield coefficients.

2.1 Exciton-photon Hamiltonian

The most general description of exciton polaritons is as a system of interacting excitons ($\hat{b}, \hat{b}^\dagger$) coupled to cavity photons ($\hat{a}, \hat{a}^\dagger$) with a strength $\Omega_R/2$ [10, 15, 28, 31, 64]. The coherent pump introduces photons directly into the system, and both excitons and photons are coupled to decay baths [15, 31].

The Hamiltonian for the coherently pumped exciton-photon system coupled to incoherent decay baths contains several terms:

$$\hat{H}_{x-c} = \hat{H}_{syst} + \hat{H}_{int} + \hat{H}_{pump} + \hat{H}_{decay}(+\hat{H}_{sat}). \tag{2.1}$$

The last term of the Hamiltonian ($\hat{H}_{sat}$) accounts for the effects of the exciton saturation and this is the only place where it appears. Since excitons are composite bosons formed by the Coulomb coupling of an electron and a hole, their statistics are not defined [31]. However, if the exciton (and hence polariton) density is low or moderate, excitons (and also polaritons) can be treated as bosons [31]. Including the exciton saturation term would add an anharmonic term to the exciton-photon coupling [31]. This is often neglected for simplicity [15, 28] and is not used in this analysis; all results are valid only if the exciton density is moderate. In the lower

polariton basis, the exciton saturation would appear as an addition to the polariton-polariton interaction [23, 82, 83].

The first term of the Hamiltonian describes quantum well excitons and cavity photons with dispersions $\omega_x(\mathbf{k})$ and $\omega_c(\mathbf{k})$ and an interconversion rate $\Omega_R/2$:

$$\begin{aligned}\hat{H}_{syst} &= \sum_{\mathbf{k}} \left(\omega_c(\mathbf{k}) \hat{a}^\dagger_{\mathbf{k}} \hat{a}_{\mathbf{k}} + \omega_x(\mathbf{k}) \hat{b}^\dagger_{\mathbf{k}} \hat{b}_{\mathbf{k}} + \frac{\Omega_R}{2} (\hat{a}^\dagger_{\mathbf{k}} \hat{b}_{\mathbf{k}} + \hat{b}^\dagger_{\mathbf{k}} \hat{a}_{\mathbf{k}}) \right) \\ &= \sum_{\mathbf{k}} \begin{pmatrix} \hat{a}^\dagger_{\mathbf{k}} & \hat{b}^\dagger_{\mathbf{k}} \end{pmatrix} \begin{pmatrix} \omega_c(\mathbf{k}) & \frac{\Omega_R}{2} \\ \frac{\Omega_R}{2} & \omega_x(\mathbf{k}) \end{pmatrix} \begin{pmatrix} \hat{a}_{\mathbf{k}} \\ \hat{b}_{\mathbf{k}} \end{pmatrix}. \end{aligned} \tag{2.2}$$

$\Omega_R/2$ defines the coupling between the excitons and photons, or the rate at which photons become excitons and vice versa. This is due to the dipole interaction between excitons and the coupling only occurs between excitons and photons with the same momenta [15].

When the rate of exciton-photon interconversion exceeds the decay and decoherence rates, the excitons and photons are strongly coupled and polaritons, characterised by anti-crossing dispersions, appear [15, 18, 57, 84]. In the strong coupling regime considered here, Ω_R is small compared to the intersubband transition frequency [57], or the exciton and photon energies [19]. If Ω_R is a significant fraction of the intersubband transition frequency [57] or if Ω_R is comparable with the exciton and photon energies [19], then the system is in the ultra-strong coupling regime. Weak coupling occurs when the decay and decoherence of the excitons and photons dominate [19, 84].

The next term describes the exciton-exciton contact interaction with interaction constant g_{x}:

$$\hat{H}_{int} = \frac{1}{2} g_{\mathrm{x}} \sum_{\mathbf{k},\mathbf{k}',\mathbf{q}} \hat{b}^\dagger_{\mathbf{k}} \hat{b}^\dagger_{\mathbf{k}'} \hat{b}_{\mathbf{k}-\mathbf{q}} \hat{b}_{\mathbf{k}'+\mathbf{q}}. \tag{2.3}$$

The coherent pump has strength $F_{p,c}$ and introduces photons at a single energy ω_p and momentum $\mathbf{k}_p$:

$$\begin{aligned}\hat{H}_{pump} &= \sum_{\mathbf{k}} (\hat{a}^\dagger_{\mathbf{k}} F_{p,c} \delta_{\mathbf{k},\mathbf{k}_p} + F^\dagger_{p,c} \delta_{\mathbf{k},\mathbf{k}_p} \hat{a}_{\mathbf{k}}) \\ &= \hat{a}^\dagger_{\mathbf{k}_p} F_{p,c} + F^\dagger_{p,c} \hat{a}_{\mathbf{k}_p}. \end{aligned} \tag{2.4}$$

The finite lifetimes are included by coupling the photons (excitons) to incoherent decay baths $\hat{A}_{\mathbf{p}}(\hat{B}_{\mathbf{p}})$ with dispersions $\omega^{\Gamma^c}_{\mathbf{p}}(\omega^{\Gamma^x}_{\mathbf{p}})$:

$$\begin{aligned}\hat{H}_{decay} &= \sum_{\mathbf{p},\mathbf{k}} \left(\Gamma^c_{\mathbf{p},\mathbf{k}} (\hat{a}^\dagger_{\mathbf{k}} \hat{A}_{\mathbf{p},\mathbf{k}} + \hat{A}^\dagger_{\mathbf{p},\mathbf{k}} \hat{a}_{\mathbf{k}}) + \Gamma^x_{\mathbf{p},\mathbf{k}} (\hat{b}^\dagger_{\mathbf{k}} \hat{B}_{\mathbf{p},\mathbf{k}} + \hat{B}^\dagger_{\mathbf{p},\mathbf{k}} \hat{b}_{\mathbf{k}}) \right) \\ &\quad + \sum_{\mathbf{p}} \left(\omega^{\Gamma^c}_{\mathbf{p}} \hat{A}^\dagger_{\mathbf{p},\mathbf{k}} \hat{A}_{\mathbf{p},\mathbf{k}} + \omega^{\Gamma^x}_{\mathbf{p}} \hat{B}^\dagger_{\mathbf{p},\mathbf{k}} \hat{B}_{\mathbf{p},\mathbf{k}} \right). \end{aligned} \tag{2.5}$$

The coupling strengths are $\Gamma^c_{\mathbf{k},\mathbf{p}}(\Gamma^x_{\mathbf{k},\mathbf{p}})$, and each system mode is connected to a full set of

independent decay baths [21].

2.2 Change of basis: lower polariton Hamiltonian

To transform from one orthonormal basis to another, the new basis ψ' is defined as the rotation of the old basis ψ by an unitary operator $\hat{S}$ such that $\psi' = \hat{S}\psi$ [85]. If the matrix elements of a physical quantity f (in the new basis) are given by:

$$\int \psi_m'^{*} \hat{f} \psi_n' \mathrm{dq} = \int \hat{S}^{\dagger} \psi_m^{*} \hat{f} \hat{S} \psi_n \mathrm{dq} = \int \psi_m^{*} \hat{S}^{-1} \hat{f} \hat{S} \psi_n \mathrm{dq},$$

then in the old basis the matrix $\hat{f}'$ corresponding to the same physical quantity is

$$\begin{aligned} \hat{f}' &= \hat{S}^{-1} \hat{f} \hat{S} \\ \int \psi_m'^{*} \hat{f} \psi_n' \mathrm{dq} &= \int \psi_m^{*} \hat{f}' \psi_n \mathrm{dq}, \\ \hat{f} &= \hat{S} \hat{f}' \hat{S}^{-1}. \end{aligned}$$

In the polariton system $\hat{S}$ is the matrix operation that diagonalises $\hat{H}_{syst}$. Since S is unitary $S^{-1} = S^{\dagger}$; $\psi = (\hat{a}_{\mathbf{k}}, \hat{b}_{\mathbf{k}})^T$ and the operators of the upper $\hat{u}_{\mathbf{k}}$, and lower $\hat{p}_{\mathbf{k}}$ polaritons form the new basis: $\psi' = (\hat{u}_{\mathbf{k}}, \hat{p}_{\mathbf{k}})^T$. To transform from the exciton-photon Hamiltonian to a Hamiltonian of the polaritons, the following rotation is used [10, 15, 19, 31, 64]:

$$\begin{pmatrix} \hat{a}_{\mathbf{k}} \\ \hat{b}_{\mathbf{k}} \end{pmatrix} = \begin{pmatrix} X(\mathbf{k}) & C(\mathbf{k}) \\ -C(\mathbf{k}) & X(\mathbf{k}) \end{pmatrix} \begin{pmatrix} \hat{u}_{\mathbf{k}} \\ \hat{p}_{\mathbf{k}} \end{pmatrix} = \hat{S}^{-1} \begin{pmatrix} \hat{u}_{\mathbf{k}} \\ \hat{p}_{\mathbf{k}}. \end{pmatrix} \tag{2.6}$$

The elements of $S^{\dagger}$ are the Hopfield coefficients [10], and are derived in detail in section 2.3. The polariton operators are:

$$\begin{pmatrix} \hat{u}_{\mathbf{k}} \\ \hat{p}_{\mathbf{k}} \end{pmatrix} = \begin{pmatrix} X(\mathbf{k}) & -C(\mathbf{k}) \\ C(\mathbf{k}) & X(\mathbf{k}) \end{pmatrix} \begin{pmatrix} \hat{a}_{\mathbf{k}} \\ \hat{b}_{\mathbf{k}} \end{pmatrix}. \tag{2.7}$$

To write the entire Hamiltonian in the polariton basis, Eqs. (2.6) and

$$\begin{aligned} \begin{pmatrix} \hat{a}_{\mathbf{k}}^{\dagger} & \hat{b}_{\mathbf{k}}^{\dagger} \end{pmatrix} &= \left(\begin{pmatrix} X(\mathbf{k}) & C(\mathbf{k}) \\ -C(\mathbf{k}) & X(\mathbf{k}) \end{pmatrix} \begin{pmatrix} \hat{u}_{\mathbf{k}} \\ \hat{p}_{\mathbf{k}} \end{pmatrix} \right)^{\dagger} = \left(\hat{S}^{-1} \begin{pmatrix} \hat{u}_{\mathbf{k}} \\ \hat{p}_{\mathbf{k}} \end{pmatrix} \right)^{\dagger} \\ &= \begin{pmatrix} \hat{u}_{\mathbf{k}}^{\dagger} & \hat{p}_{\mathbf{k}}^{\dagger} \end{pmatrix} \begin{pmatrix} X(\mathbf{k}) & -C(\mathbf{k}) \\ C(\mathbf{k}) & X(\mathbf{k}) \end{pmatrix} = \begin{pmatrix} \hat{u}_{\mathbf{k}}^{\dagger} & \hat{p}_{\mathbf{k}}^{\dagger} \end{pmatrix} \hat{S} \end{aligned} \tag{2.8}$$

are used, which means that the following substitutions are made in Eqs. (2.2)-(2.5):

$$\begin{aligned} \hat{a}_{\mathbf{k}} &= X(\mathbf{k}) \hat{u}_{\mathbf{k}} + C(\mathbf{k}) \hat{p}_{\mathbf{k}}, \\ \hat{b}_{\mathbf{k}} &= -C(\mathbf{k}) \hat{u}_{\mathbf{k}} + X(\mathbf{k}) \hat{p}_{\mathbf{k}}, \end{aligned}$$

$$\hat{a}^\dagger_{\mathbf{k}} = X(\mathbf{k})\hat{u}^\dagger_{\mathbf{k}} + C(\mathbf{k})\hat{p}^\dagger_{\mathbf{k}},$$
$$\hat{b}^\dagger_{\mathbf{k}} = -C(\mathbf{k})\hat{u}^\dagger_{\mathbf{k}} + X(\mathbf{k})\hat{p}^\dagger_{\mathbf{k}}.$$

Performing the rotation on the entire exciton-photon Hamiltonian (except the exciton saturation) gives a system of upper and lower polaritons with dispersions $\omega_{up}(\mathbf{k})$ and $\omega_{lp}(\mathbf{k})$:

$$\hat{H}_{syst-pol} = \sum_{\mathbf{k}} \left(\omega_{lp}(\mathbf{k})\hat{p}^\dagger_{\mathbf{k}}\hat{p}_{\mathbf{k}} + \omega_{up}(\mathbf{k})\hat{u}^\dagger_{\mathbf{k}}\hat{u}_{\mathbf{k}} \right). \tag{2.9}$$

The external laser adds photons to the system and can excite both upper and lower polaritons:

$$\hat{H}_{pump-pol} = F_{p,c}\left(X(\mathbf{k}_p)\hat{u}^\dagger_{\mathbf{k}_p} + C(\mathbf{k}_p)\hat{p}^\dagger_{\mathbf{k}_p} \right) + F^\dagger_{p,c}\left(X(\mathbf{k}_p)\hat{u}_{\mathbf{k}_p} + C(\mathbf{k}_p)\hat{p}_{\mathbf{k}_p} \right). \tag{2.10}$$

The existing exciton and photon decay baths are unaffected by the change of basis, but are now coupled to the polaritons:

$$\begin{aligned}
\hat{H}_{decay-pol} \;=\; & \sum_{\mathbf{p},\mathbf{k}} \Bigg(\Gamma^c_{\mathbf{p},\mathbf{k}} \left[\left(X(\mathbf{k})\hat{u}^\dagger_{\mathbf{k}} + C(\mathbf{k})\hat{p}^\dagger_{\mathbf{k}} \right) \hat{A}_{\mathbf{p}} + \hat{A}^\dagger_{\mathbf{p}} \left(X(\mathbf{k})\hat{u}_{\mathbf{k}} + C(\mathbf{k})\hat{p}_{\mathbf{k}} \right) \right] \\
& + \Gamma^x_{\mathbf{p},\mathbf{k}} \left[\left(-C(\mathbf{k})\hat{u}^\dagger_{\mathbf{k}} + X(\mathbf{k})\hat{p}^\dagger_{\mathbf{k}} \right) \hat{B}_{\mathbf{p}} + \hat{B}^\dagger_{\mathbf{p}} \left(-C(\mathbf{k})\hat{u}_{\mathbf{k}} + X(\mathbf{k})\hat{p}_{\mathbf{k}} \right) \right] \Bigg) \\
& + \sum_{\mathbf{p}} \left(\omega^{\Gamma^c}_{\mathbf{p}} \hat{A}^\dagger_{\mathbf{p},\mathbf{k}} \hat{A}_{\mathbf{p},\mathbf{k}} + \omega^{\Gamma^x}_{\mathbf{p}} \hat{B}^\dagger_{\mathbf{p},\mathbf{k}} \hat{B}_{\mathbf{p},\mathbf{k}} \right).
\end{aligned} \tag{2.11}$$

The polariton interactions are complicated since terms of the type: $\hat{u}^\dagger\hat{p}^\dagger\hat{u}\hat{p}, \hat{u}^\dagger\hat{u}^\dagger\hat{u}\hat{p}, \hat{u}^\dagger\hat{u}^\dagger\hat{p}\hat{p}$ (and Hermitian conjugates), that describe interactions between polaritons on the different branches are present. For simplicity, $\mathbf{k}' + \mathbf{q} = \mathbf{k}_1$ and $\mathbf{k} - \mathbf{q} = \mathbf{k}_2$ are used in the following expression of the complete polariton-polariton interaction:

$$\begin{aligned}
\hat{H}_{int-pol} = \frac{1}{2} g_{\mathrm{x}} \sum_{\mathbf{k},\mathbf{k}',\mathbf{q}} \Big(& C(\mathbf{k})C(\mathbf{k}')C(\mathbf{k}_2)C(\mathbf{k}_1)\hat{u}^\dagger_{\mathbf{k}}\hat{u}^\dagger_{\mathbf{k}'}\hat{u}_{\mathbf{k}_2}\hat{u}_{\mathbf{k}_1} \\
& - C(\mathbf{k})C(\mathbf{k}')C(\mathbf{k}_2)X(\mathbf{k}_1)\hat{u}^\dagger_{\mathbf{k}}\hat{u}^\dagger_{\mathbf{k}'}\hat{u}_{\mathbf{k}_2}\hat{p}_{\mathbf{k}_1} - C(\mathbf{k})C(\mathbf{k}')X(\mathbf{k}_2)C(\mathbf{k}_1)\hat{u}^\dagger_{\mathbf{k}}\hat{u}^\dagger_{\mathbf{k}'}\hat{p}_{\mathbf{k}_2}\hat{u}_{\mathbf{k}_1} \\
& + C(\mathbf{k})X(\mathbf{k}')X(\mathbf{k}_2)X(\mathbf{k}_1)\hat{u}^\dagger_{\mathbf{k}}\hat{u}^\dagger_{\mathbf{k}'}\hat{p}_{\mathbf{k}_2}\hat{p}_{\mathbf{k}_1} - C(\mathbf{k})X(\mathbf{k}')C(\mathbf{k}_2)C(\mathbf{k}_1)\hat{u}^\dagger_{\mathbf{k}}\hat{p}^\dagger_{\mathbf{k}'}\hat{u}_{\mathbf{k}_2}\hat{u}_{\mathbf{k}_1} \\
& + C(\mathbf{k})X(\mathbf{k}')C(\mathbf{k}_2)X(\mathbf{k}_1)\hat{u}^\dagger_{\mathbf{k}}\hat{p}^\dagger_{\mathbf{k}'}\hat{u}_{\mathbf{k}_2}\hat{p}_{\mathbf{k}_1} + C(\mathbf{k})X(\mathbf{k}')X(\mathbf{k}_2)C(\mathbf{k}_1)\hat{u}^\dagger_{\mathbf{k}}\hat{p}^\dagger_{\mathbf{k}'}\hat{p}_{\mathbf{k}_2}\hat{u}_{\mathbf{k}_1} \\
& - C(\mathbf{k})X(\mathbf{k}')X(\mathbf{k}_2)X(\mathbf{k}_1)\hat{u}^\dagger_{\mathbf{k}}\hat{p}^\dagger_{\mathbf{k}'}\hat{p}_{\mathbf{k}_2}\hat{p}_{\mathbf{k}_1} - X(\mathbf{k})C(\mathbf{k}')C(\mathbf{k}_2)C(\mathbf{k}_1)\hat{p}^\dagger_{\mathbf{k}}\hat{u}^\dagger_{\mathbf{k}'}\hat{u}_{\mathbf{k}_2}\hat{u}_{\mathbf{k}_1} \\
& + X(\mathbf{k})C(\mathbf{k}')C(\mathbf{k}_2)X(\mathbf{k}_1)\hat{p}^\dagger_{\mathbf{k}}\hat{u}^\dagger_{\mathbf{k}'}\hat{u}_{\mathbf{k}_2}\hat{p}_{\mathbf{k}_1} + X(\mathbf{k})C(\mathbf{k}')X(\mathbf{k}_2)C(\mathbf{k}_1)\hat{p}^\dagger_{\mathbf{k}}\hat{u}^\dagger_{\mathbf{k}'}\hat{p}_{\mathbf{k}_2}\hat{u}_{\mathbf{k}_1} \\
& - X(\mathbf{k})C(\mathbf{k}')X(\mathbf{k}_2)X(\mathbf{k}_1)\hat{p}^\dagger_{\mathbf{k}}\hat{u}^\dagger_{\mathbf{k}'}\hat{p}_{\mathbf{k}_2}\hat{p}_{\mathbf{k}_1} + X(\mathbf{k})X(\mathbf{k}')C(\mathbf{k}_2)C(\mathbf{k}_1)\hat{p}^\dagger_{\mathbf{k}}\hat{p}^\dagger_{\mathbf{k}'}\hat{u}_{\mathbf{k}_2}\hat{u}_{\mathbf{k}_1} \\
& - X(\mathbf{k})X(\mathbf{k}')C(\mathbf{k}_2)X(\mathbf{k}_1)\hat{p}^\dagger_{\mathbf{k}}\hat{p}^\dagger_{\mathbf{k}'}\hat{u}_{\mathbf{k}_2}\hat{p}_{\mathbf{k}_1} - X(\mathbf{k})X(\mathbf{k}')C(\mathbf{k}_2)X(\mathbf{k}_1)\hat{p}^\dagger_{\mathbf{k}}\hat{p}^\dagger_{\mathbf{k}'}\hat{u}_{\mathbf{k}_2}\hat{p}_{\mathbf{k}_1} \\
& + X(\mathbf{k})X(\mathbf{k}')X(\mathbf{k}_2)X(\mathbf{k}_1)\hat{p}^\dagger_{\mathbf{k}}\hat{p}^\dagger_{\mathbf{k}'}\hat{p}_{\mathbf{k}_2}\hat{p}_{\mathbf{k}_1} \Big).
\end{aligned} \tag{2.12}$$

If the upper polariton branch is energetically far from the lower polariton branch, it can be neglected [28, 41]. This is allowed if Ω_R is much greater than the detuning of the applied pump away from the lower polariton dispersion ($\Omega_R \gg \Delta^p \equiv [\omega_p - \omega_{lp}(\mathbf{k}_p)]$) and also if the nonlinear shift of the lower polariton mode due to finite occupation at the pump mode is small [41]. The second condition reinforces the existing condition that the descriptions of the polariton system used are only valid for low (exciton or polariton) density. Only the last term of Eq. (2.12) remains and the Hamiltonian that describes the lower polaritons only is [28, 31]:

$$\begin{aligned}\hat{H}_{lp} &= \sum_{\mathbf{k}} \omega_{lp}(\mathbf{k})\hat{p}^\dagger_{\mathbf{k}}\hat{p}_{\mathbf{k}} + \frac{1}{2}\sum_{\mathbf{k},\mathbf{k}',\mathbf{q}} V_{\mathbf{k},\mathbf{k}',\mathbf{q}}\hat{p}^\dagger_{\mathbf{k}}\hat{p}^\dagger_{\mathbf{k}'}\hat{p}_{\mathbf{k}-\mathbf{q}}\hat{p}_{\mathbf{k}'+\mathbf{q}} \\ &+ \sum_{\mathbf{p},\mathbf{k}} \left(\Gamma^c_{\mathbf{p},\mathbf{k}} \left(C(\mathbf{k})\hat{p}^\dagger_{\mathbf{k}}\hat{A}_{\mathbf{p}} + \hat{A}^\dagger_{\mathbf{p}} C(\mathbf{k})\hat{p}_{\mathbf{k}} \right) + \Gamma^x_{\mathbf{p},\mathbf{k}} \left(X(\mathbf{k})\hat{p}^\dagger_{\mathbf{k}}\hat{B}_{\mathbf{p}} + \hat{B}^\dagger_{\mathbf{p}} X(\mathbf{k})\hat{p}_{\mathbf{k}} \right) \right) \\ &+ \sum_{\mathbf{p}} \left(\omega^{\Gamma^c}_{\mathbf{p}} \hat{A}^\dagger_{\mathbf{p}}\hat{A}_{\mathbf{p}} + \omega^{\Gamma^x}_{\mathbf{p}} \hat{B}^\dagger_{\mathbf{p}}\hat{B}_{\mathbf{p}} \right) + (F_{lp}\hat{p}^\dagger_{\mathbf{k}_p} + F^\dagger_{lp}\hat{p}_{\mathbf{k}_p}) \end{aligned} \tag{2.13}$$

where $F_{lp} = C(\mathbf{k}_p)F_{p,c}$ has been introduced as the polariton pump operator, and $V_{\mathbf{k},\mathbf{k}',\mathbf{q}} = g_{\mathrm{x}} X(\mathbf{k})X(\mathbf{k}')X(\mathbf{k}-\mathbf{q})X(\mathbf{k}'+\mathbf{q})$ is the momentum dependent strength of the lower polariton interactions.

2.3 Derivation of the Hopfield coefficients

In different places in the literature, different expressions are given for the Hopfield coefficients [15, 31, 86, 87]. In this section, the Hopfield coefficients are derived and the different forms shown to be equivalent.

In the absence of pump and decay, the exciton-photon system is described by the simple Hamiltonian of Eq. (2.2) [15]. The eigenvalues of the matrix

$$S(\mathbf{k}) = \begin{pmatrix} \omega_c(\mathbf{k}) & \frac{\Omega_R}{2} \\ \frac{\Omega_R}{2} & \omega_x(\mathbf{k}) \end{pmatrix} \tag{2.14}$$

therefore give the dispersions of the upper and lower polaritons [15]:

$$\omega_{up,lp}(\mathbf{k}) = \frac{\omega_c(\mathbf{k}) + \omega_x(\mathbf{k})}{2} \pm \frac{1}{2}\sqrt{\left(\omega_c(\mathbf{k}) - \omega_x(\mathbf{k})\right)^2 + \Omega_R^2}. \tag{2.15}$$

The exciton dispersion is usually assumed flat, $\omega_x(\mathbf{k}) = \omega_x$, since the exciton mass is much larger than the cavity photons' which have a quadratic dispersion: $\omega_c(\mathbf{k}) = \omega_x + \Delta^0 + |\mathbf{k}|^2/2m_c$, where $\Delta^0 = \omega_c(\mathbf{0}) - \omega_x$ is the exciton-photon detuning. The dispersions for $\Delta^0 = 0$ are shown in Fig. 2.1.

In Eq. (2.7), both the polariton operators were written using the Hopfield coefficients of the lower polaritons only, here the Hopfield coefficients for both the upper and lower polaritons are

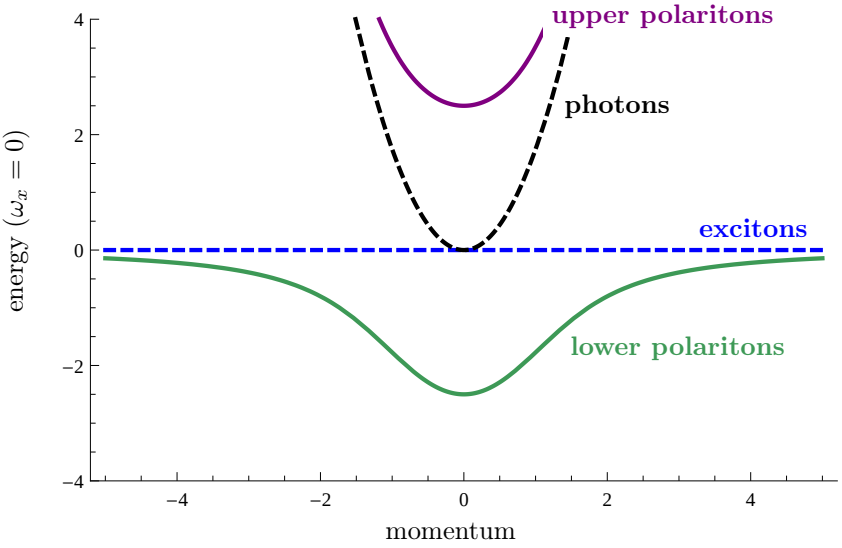

Figure 2.1: Dispersions of the quantum well excitons, cavity photons and the upper and lower polaritons for $\Delta^0 = 0$ and a flat exciton dispersion.

derived and the minus sign explained. To do so, the polariton operators are written as linear superpositions of excitons and photons with the weightings [15, 87]:

$$\begin{aligned} \hat{u}_{\mathbf{k}} &= C_{up}(\mathbf{k})\hat{a}_{\mathbf{k}} + X_{up}(\mathbf{k})\hat{b}_{\mathbf{k}} \\ \hat{p}_{\mathbf{k}} &= C_{lp}(\mathbf{k})\hat{a}_{\mathbf{k}} + X_{lp}(\mathbf{k})\hat{b}_{\mathbf{k}}. \end{aligned} \tag{2.16}$$

The eigenvectors are the solutions of [10, 64, 87]:

$$S(\mathbf{k}) \begin{pmatrix} C_{up,lp}(\mathbf{k}) \\ X_{up,lp}(\mathbf{k}) \end{pmatrix} = \omega_{up,lp}(\mathbf{k}) \begin{pmatrix} C_{up,lp}(\mathbf{k}) \\ X_{up,lp}(\mathbf{k}) \end{pmatrix} \tag{2.17}$$

with the constraint [15, 87]

$$|X_{lp,up}(\mathbf{k})|^2 + |C_{lp,up}(\mathbf{k})|^2 = 1. \tag{2.18}$$

Since $S(\mathbf{k})$ is a unitary matrix so $S^\dagger S = SS^\dagger = 1$, and Eq. (2.18) ensures the correct normalisation after rotation [85]; the exciton $|X(\mathbf{k})|^2$ and photon $|C(\mathbf{k})|^2$ fractions of the polaritons must add up to unity.

The lower polaritons are considered first and $C_{lp}(\mathbf{k})$ and $X_{lp}(\mathbf{k})$ are calculated. Expanding Eq. (2.17) gives:

$$\omega_{lp}(\mathbf{k})C_{lp}(\mathbf{k}) = \epsilon_c(\mathbf{k})C_{lp}(\mathbf{k}) + \frac{\Omega_R}{2}X_{lp}(\mathbf{k}), \tag{2.19}$$

$$\omega_{lp}(\mathbf{k})X_{lp}(\mathbf{k}) = \frac{\Omega_R}{2}C_{lp}(\mathbf{k}) + \epsilon_x(\mathbf{k})X_{lp}(\mathbf{k}). \tag{2.20}$$

Eq. (2.19) is rearranged for $C_{lp}(\mathbf{k})$ which is substituted into Eq. (2.18):

$$\begin{aligned}
C_{lp}(\mathbf{k}) &= \frac{\Omega_R}{2(\omega_{lp}(\mathbf{k})-\epsilon_c(\mathbf{k})}X_{lp}(\mathbf{k}),\\
1 &= |X_{lp}(\mathbf{k})|^2\left(1+\frac{\Omega_R^2}{4(\omega_{lp}(\mathbf{k})-\omega_c(\mathbf{k}))^2}\right),\\
|X_{lp}(\mathbf{k})|^2 &= \frac{1}{1+\frac{\Omega_R^2}{4(\omega_{lp}(\mathbf{k})-\omega_c(\mathbf{k}))^2}},\\
X_{lp}(\mathbf{k}) &= \frac{2(\omega_{lp}(\mathbf{k})-\omega_c(\mathbf{k}))}{\sqrt{4(\omega_{lp}(\mathbf{k})-\omega_c(\mathbf{k}))^2+\Omega_R^2}}, \qquad (2.21)\\
C_{lp}(\mathbf{k}) &= \frac{\Omega_R}{\sqrt{4(\omega_{lp}(\mathbf{k})-\omega_c(\mathbf{k}))^2+\Omega_R^2}}. \qquad (2.22)
\end{aligned}$$

The same procedure for the upper polaritons yields:

$$\begin{aligned}
\omega_{up}(\mathbf{k})C_{up}(\mathbf{k}) &= \omega_c(\mathbf{k})C_{up}(\mathbf{k})+\frac{\Omega_R}{2}X_{up}(\mathbf{k}), \qquad (2.23)\\
\omega_{up}(\mathbf{k})X_{up}(\mathbf{k}) &= \frac{\Omega_R}{2}C_{up}(\mathbf{k})+\omega_x(\mathbf{k})X_{up}(\mathbf{k}). \qquad (2.24)
\end{aligned}$$

Rearranging Eq. (2.24) for $C_{up}(\mathbf{k})$ and again substituting into Eq. (2.18) leads to:

$$\begin{aligned}
C_{up}(\mathbf{k}) &= \frac{2(\omega_{up}(\mathbf{k})-\omega_x(\mathbf{k}))}{\Omega_R}X_{up}(\mathbf{k}),\\
1 &= |X_{up}(\mathbf{k})|^2\left(1+\frac{4(\omega_{up}(\mathbf{k})-\omega_x(\mathbf{k}))^2}{\Omega_R^2}\right),\\
|X_{up}(\mathbf{k})|^2 &= \frac{\Omega_R^2}{4(\omega_{up}(\mathbf{k})-\omega_x(\mathbf{k}))^2+\Omega_R^2},\\
X_{up}(\mathbf{k}) &= \frac{\Omega_R}{\sqrt{4(\omega_{up}(\mathbf{k})-\omega_x(\mathbf{k}))^2+\Omega_R^2}}, \qquad (2.25)\\
C_{up}(\mathbf{k}) &= \frac{2(\omega_{up}(\mathbf{k})-\omega_x(\mathbf{k}))}{\sqrt{4(\omega_{up}(\mathbf{k})-\omega_x(\mathbf{k}))^2+\Omega_R^2}}. \qquad (2.26)
\end{aligned}$$

From the definitions of the upper and lower polariton dispersions given in Eq. (2.15), $\omega_{up}(\mathbf{k})-\omega_x(\mathbf{k})=-(\omega_{lp}(\mathbf{k})-\omega_c(\mathbf{k}))$ so

$$\begin{aligned}
X_{up}(\mathbf{k}) &= \frac{\Omega_R}{\sqrt{\Omega_R^2+4(\omega_{lp}(\mathbf{k})-\omega_c(\mathbf{k}))^2}}, \qquad (2.27)\\
C_{up}(\mathbf{k}) &= \frac{-2(\omega_{lp}(\mathbf{k})-\omega_c(\mathbf{k}))}{\sqrt{\Omega_R^2+4(\omega_{lp}(\mathbf{k})-\omega_c(\mathbf{k}))^2}}. \qquad (2.28)
\end{aligned}$$

Then $X_{up}(\mathbf{k})=C_{lp}(\mathbf{k})$ and $C_{up}(\mathbf{k})=-X_{lp}(\mathbf{k})$ [87]. If the lower polariton Hopfield coefficients are calculated by first rearranging Eq. (2.19) for $C_{lp}(\mathbf{k})$, the lower polariton Hopfield coeffients

are:

$$C_{lp}(\mathbf{k}) = \frac{2(\omega_{lp}(\mathbf{k}) - \omega_x(\mathbf{k}))}{\sqrt{4(\omega_{lp}(\mathbf{k}) - \omega_x(\mathbf{k}))^2 + \Omega_R^2}}, \tag{2.29}$$

$$X_{lp}(\mathbf{k}) = \frac{\Omega_R}{\sqrt{4(\omega_{lp}(\mathbf{k}) - \omega_x(\mathbf{k}))^2 + \Omega_R^2}}. \tag{2.30}$$

Meanwhile, calculating the upper polariton Hopfield coefficients by rearranging Eq. (2.23) for $X_{up}(\mathbf{k})$ gives:

$$C_{up}(\mathbf{k}) = \frac{\Omega_R}{\sqrt{4(\omega_{up}(\mathbf{k}) - \omega_c(\mathbf{k}))^2 + \Omega_R^2}}, \tag{2.31}$$

$$X_{up}(\mathbf{k}) = \frac{2(\omega_{up}(\mathbf{k}) - \omega_c(\mathbf{k})}{\sqrt{4(\omega_{up}(\mathbf{k}) - \omega_c(\mathbf{k}))^2 + \Omega_R^2}}. \tag{2.32}$$

Using that $\omega_{up}(\mathbf{k}) - \omega_c(\mathbf{k}) = -(\omega_{lp}(\mathbf{k}) - \omega_x(\mathbf{k}))$ gives

$$C_{up}(\mathbf{k}) = \frac{\Omega_R}{\sqrt{4(\omega_{lp}(\mathbf{k}) - \omega_x(\mathbf{k}))^2 + \Omega_R^2}} = X_{lp}(\mathbf{k}), \tag{2.33}$$

$$X_{up}(\mathbf{k}) = \frac{-2(\omega_{lp}(\mathbf{k}) - \omega_x(\mathbf{k})}{\sqrt{4(\omega_{lp}(\mathbf{k}) - \omega_x(\mathbf{k}))^2 + \Omega_R^2}} = -C_{lp}(\mathbf{k}). \tag{2.34}$$

which is the convention used in the previous section and the remainder of this thesis where $X(\mathbf{k}) = X_{lp}(\mathbf{k})$ and $C(\mathbf{k}) = C_{lp}(\mathbf{k})$ are the lower polariton Hopfield coefficients. The polariton operators are then defined using the lower polariton Hopfield coefficients only and Eqs. (2.16) become [15]:

$$\begin{pmatrix} \hat{u}_{\mathbf{k}} \\ \hat{p}_{\mathbf{k}} \end{pmatrix} = \begin{pmatrix} X(\mathbf{k}) & -C(\mathbf{k}) \\ C(\mathbf{k}) & X(\mathbf{k}) \end{pmatrix} \begin{pmatrix} \hat{a}_{\mathbf{k}} \\ \hat{b}_{\mathbf{k}} \end{pmatrix}. \tag{2.35}$$

Inverting the rotation gives [19]:

$$\begin{pmatrix} \hat{a}_{\mathbf{k}} \\ \hat{b}_{\mathbf{k}} \end{pmatrix} = \begin{pmatrix} X(\mathbf{k}) & C(\mathbf{k}) \\ -C(\mathbf{k}) & X(\mathbf{k}) \end{pmatrix} \begin{pmatrix} \hat{u}_{\mathbf{k}} \\ \hat{p}_{\mathbf{k}} \end{pmatrix}. \tag{2.36}$$

To compare these definitions of the Hopfield coefficients with other expressions, the energy difference between the exciton and photon dispersions at any momentum is introduced: $\delta_{\mathbf{k}} = \epsilon_c(\mathbf{k}) - \epsilon_x(\mathbf{k})$. Then $\omega_{lp}(\mathbf{k}) - \epsilon_c(\mathbf{k}) = -\left(\delta_{\mathbf{k}} + \sqrt{\delta_{\mathbf{k}}^2 + \Omega_R^2}\right)/2$ is substituted into Eqs. (2.21) and (2.22) giving:

$$X_{lp}(\mathbf{k}) = -\frac{\delta_{\mathbf{k}} + \sqrt{\delta_{\mathbf{k}}^2 + \Omega_R^2}}{\sqrt{\left(\delta_{\mathbf{k}} + \sqrt{\delta_{\mathbf{k}}^2 + \Omega_R^2}\right)^2 + \Omega_R^2}} = \left(\frac{\delta_{\mathbf{k}} + \sqrt{\delta_{\mathbf{k}}^2 + \Omega_R^2}}{2\sqrt{\delta_{\mathbf{k}}^2 + \Omega_R^2}}\right)^{\frac{1}{2}}, \tag{2.37}$$

and

$$C_{lp}(\mathbf{k}) = \frac{\Omega_R}{\left(\delta_\mathbf{k} + \sqrt{\delta_\mathbf{k}^2 + \Omega_R^2}\right)^2 + \Omega_R^2} = \left(\frac{\Omega_R^2}{2\left(\delta_\mathbf{k} + \sqrt{\delta_\mathbf{k}^2 + \Omega_R^2}\right)\sqrt{\delta_\mathbf{k}^2 + \Omega_R^2}}\right)^{\frac{1}{2}}. \tag{2.38}$$

Eqs. (2.37) and (2.38) are identical to the expressions for $X_\mathbf{k}$, and $C_\mathbf{k}$ in Ref. [86]. Calculating $|X_{lp}(\mathbf{k})|^2$ from Eq. (2.37) gives:

$$|X_{lp}(\mathbf{k})|^2 = \frac{1}{2}\left(1 + \frac{\delta_\mathbf{k}}{\sqrt{\delta_\mathbf{k}^2 + \Omega_R^2}}\right), \tag{2.39}$$

$$|C_{lp}(\mathbf{k})|^2 = \frac{1}{2}\left(1 - \frac{\delta_\mathbf{k}}{\sqrt{\delta_\mathbf{k}^2 + \Omega_R^2}}\right), \tag{2.40}$$

as in Ref. [15], where the second line uses the normalisation condition $|X_{lp}(\mathbf{k})|^2 + |C_{lp}(\mathbf{k})|^2 = 1$. It is not possible to reproduce the expressions for X_U, C_U in Ref. [87]. For $\delta_{\mathbf{k}=\mathbf{0}} = 0$, $X_{lp}^2(0) = C_{lp}^2(0) = 1/2$, which holds for all the derived expressions. In Ref. [87], the Hopfield coefficients for the upper polaritons are given in terms of the exciton E_x and upper polariton dispersions E_{up} as:

$$C_{up} = \frac{2\hbar\Omega}{\sqrt{4\hbar^2\Omega^2 + (E_{up} - E_x)^2}},$$

$$X_{up} = \frac{E_{up} - E_x}{\sqrt{4\hbar^2\Omega^2 + (E_{up} - E_x)^2}}.$$

These are very similar to Eqs. (2.28) and (2.27), but the weight of the exciton-photon interconversion term used up to now has been $\Omega_R/2$, while here it is $\hbar\Omega$. Considering the case at $\mathbf{k} = 0$, where $E_{up} - E_x = \hbar\Omega$:

$$X_{up}^2(0) = C_{lp}(0) = \frac{1}{5}; \qquad C_{up}^2(0) = X_{lp}(0) = \frac{4}{5}$$

which is not correctly normalised for $E_c(0) = E_x(0)$. This may be due to an inconsistency in the definition of the exciton-photon coupling energy, which, in different places differs by a factor of 2 [15, 19, 87].

3 | Keldysh Green's functions for coherently pumped polaritons

This chapter contains all work on the Keldysh functional integral approach applied to the system of coherently pumped polaritons, both above and below the OPO threshold. First, a brief sketch of the Keldysh method is given in section 3.1. Section 3.2 contains a detailed derivation of the Keldysh functional integral for an arbitrary number of modes coupled to two incoherent decay baths, while the pumping directly occupies one mode. The Keldysh actions and the inverse Green's functions found by taking fluctuations to second order for the pump only and OPO regimes are presented in sections 3.3 and 3.4 respectively, with numerical results in sections 3.5 and 3.6.

3.1 Sketch of Keldysh method

The basis of the Green's function approach is that the partition function Z of a system described by an Hamiltonian $\hat{H}$ with operators written in the Heisenberg representation can be written in the form [69–71]:

$$Z = N \int D(\overline{\phi}, \phi) e^{iS} = \int D(\overline{\phi}, \phi) \exp\left\{ i \int_C [\overline{\phi}(t) G^{-1} \phi(t)] dt \right\}, \tag{3.1}$$

where N provides the correct normalisation, S is the action: $S = S[\overline{\phi}, \phi]$ and G^{-1} is the inverse Green's function. The particular method used here uses a (Keldysh) closed time contour, shown schematically in Fig. 3.1, whereby the interactions are switched on and then switched off so that there is no reference to the system's state at $t = +\infty$ [70]. The system can be considered to evolve from the distant past ($t = -\infty$) to the distant future ($t = +\infty$) on the forwards branch of the time contour and then return from $t = +\infty$ to $t = -\infty$ along the backwards branch, closing the time contour.

To construct the functional integral, the time evolution is initially considered to consist of $2N$ discrete steps, N of which are on the forwards branch of the time contour (t_{n+1} after t_n) and N of which are on the backwards branch of the time contour (t_{n+1} *before* t_n), as included

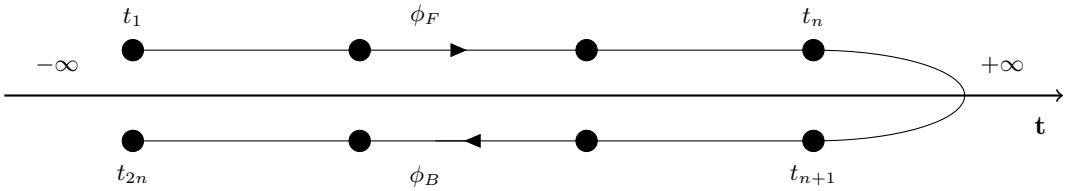

Figure 3.1: (Keldysh) Closed time contour: start from a 'known' state ϕ_0 at $t = -\infty$, switch interactions on adiabatically to $t = \infty$, 'unwind' back to ϕ_0. The fields on the forwards branch are ϕ_F and those on the backwards branch ϕ_B. The points on the contour illustrate how $2n$ points are used to construct the functional integral [70].

in Fig. 3.1. The partition function is calculated in the coherent state basis and the properties of any coherent state ϕ are given in table 3.1 [69–71].

$$\begin{aligned}
\hat{a}_i|\phi\rangle &= \psi_i|\phi\rangle \\
\langle\phi|\hat{a}_i^\dagger &= \langle\phi|\overline{\phi}_i \\
\langle\phi'|\phi\rangle &= e^{\overline{\phi}'\phi} \\
I &= \int D(\overline{\phi},\phi)e^{-\overline{\phi}\phi}|\phi\rangle\langle\phi| \\
D(\overline{\phi},\phi) &= \prod_i \frac{d(\Re\phi_i)d(\Im\phi_i)}{\pi}
\end{aligned}$$

Table 3.1: Properties of the coherent state for a general coherent state basis ϕ, operator $\hat{a}$. I is a resolution of identity and can be inserted at any point.

In order to calculate the partition function, it is necessary to use the property that the closed time contour returns the system to its original state through the time evolution

$$Tr(\hat{\rho}) = Tr(U_t\hat{\rho}). \tag{3.2}$$

The partition function is defined as $Z = Tr(\hat{\rho}) = Tr(e^{-\beta(\hat{H}-\mu\hat{a}^\dagger\hat{a})})$, where $\hat{\rho}$ is the initial density matrix of the system and can be chosen to be the equilibrium density matrix. This leads to the second expression where β is the inverse temperature and μ the chemical potential at equilibrium [70, 71].

The trace is defined as the sum

$$Tr(U_t\hat{\rho}) = \sum_n \langle n|U_t\hat{\rho}|n\rangle,$$

where $\hat{\rho}$ is the density matrix, $|n\rangle$ is a basis state and U_t is a time evolution operator [69]. To calculate the trace, resolutions of identity of the coherent state basis are inserted. Since summation and integration commute, groups of $\langle|\rangle$ can be moved around and:

$$Tr(U_t\hat{\rho}) = \sum_n \langle n|U_t\hat{\rho}|n\rangle \tag{3.3}$$

$$
\begin{aligned}
&= \sum_n \langle n| \int d(\overline{\phi},\phi) e^{-\overline{\phi}\phi} |\phi\rangle\langle\phi|U_t\hat{\rho}|n\rangle \\
&= \int d(\overline{\phi},\phi) e^{-\overline{\phi}\phi} \sum_n \langle n|\phi\rangle\langle\phi|U_t\hat{\rho}|n\rangle \\
&= \int d(\overline{\phi},\phi) e^{-\overline{\phi}\phi} \langle\phi|U_t\hat{\rho}\Big(\sum_n |n\rangle\langle n|\Big)|\phi\rangle.
\end{aligned}
$$

$\sum_n |n\rangle\langle n| = I$ is just another resolution of identity and can therefore be removed to give:

$$
Tr(U_t\hat{\rho}) \quad = \quad \int d(\overline{\phi},\phi) e^{-\overline{\phi}\phi} \langle\phi|U_t\hat{\rho}|\phi\rangle.
$$

For the construction of the Keldysh contour, $|\phi\rangle$ in the above is the $2N^{th}$ element (first and last) of the closed time contour: $|\phi\rangle \equiv |\phi_{2N}\rangle$. The time evolution is therefore split into $2N$ segments with $U_{\pm\delta t} = e^{\mp iH\delta t}$ with $U_{+\delta t}$ on the forwards branch and $U_{-\delta t}$ on the backwards branch. Steps N and $N+1$ are identical so $U_{\delta t}(N, N+1) = 1$. The forwards branch runs from step 1 at $t = -\infty$ to step N at $t = +\infty$ and the backwards branch from step $N+1$ at $t = +\infty$ to step $2N$ at $t = -\infty$ as defined in Fig. 3.1.

The action is initially written in terms of the fields on the forwards and backwards branches of the closed time contour with Green's functions defined as $G(t,t') \equiv -i\langle\phi(t)\phi(t')\rangle$ where the two times are somewhere on the Keldysh contour. The key aspect of the Keldysh approach is to define a pair of new fields:

$$
\phi_{cl}(t) \quad = \quad \frac{1}{\sqrt{2}}\left(\phi_F(t) + \phi_B(t)\right), \tag{3.4}
$$

$$
\phi_q(t) \quad = \quad \frac{1}{\sqrt{2}}\left(\phi_F(t) - \phi_B(t)\right), \tag{3.5}
$$

where the F, B subscripts refer to the forwards and backwards branches of the time contour and the subscripts 'cl' and 'q' denote the classical and quantum components of the fields [70]. In the Keldysh basis, the inverse Green's function in Eq. (3.1) is defined as a matrix formed of retarded, advanced and Keldysh components:

$$
G^{-1} = \begin{pmatrix} G^K & G^R \\ G^A & 0 \end{pmatrix}^{-1} = \begin{pmatrix} 0 & [G^{-1}]^A \\ [G^{-1}]^R & [G^{-1}]^K \end{pmatrix}. \tag{3.6}
$$

The inverse Green's functions have the following key properties and relations [70]:

$$
[G^{-1}]^{R,A} = [G^{R,A}]^{-1}, \tag{3.7}
$$

$$
[G^{-1}]^A = \left([G^{-1}]^R\right)^\dagger, \tag{3.8}
$$

$$
G^A = \left(G^R\right)^\dagger, \tag{3.9}
$$

$$
[G^{-1}]^K = -[G^R]^{-1}G^K[G^A]^{-1} = [G^R]^{-1}F_s - F_s[G^A]^{-1}, \tag{3.10}
$$

$$G^K = -G^R[G^{-1}]^K G^A = G^R F_s - F_s G^A, \tag{3.11}$$

where F_s is the distribution function that parameterises the Keldysh Green's function. The retarded and advanced Green's functions can be found through simple inversion of their inverses and are Hermitian conjugates of each other [69–71].

In the basis of classical and quantum fields, the action has the form:

$$S[\phi_{cl}, \phi_q] = \iint_{-\infty}^{\infty} dt dt' (\overline{\phi}_{cl}, \overline{\phi}_q)_t \begin{pmatrix} 0 & [G^{-1}]^A \\ [G^{-1}]^R & [G^{-1}]^K \end{pmatrix}_{t,t'} \begin{pmatrix} \phi_{cl} \\ \phi_q \end{pmatrix}_{t'}, \tag{3.12}$$

and the inverse Green's functions are found by inspecting the action.

3.2 Detailed derivation of Keldysh action

In this section, a non-equilibrium field theory for a system of coherently pumped polaritons is constructed starting from the Hamiltonian of Eq. (2.13).

3.2.1 Heisenberg operators and gauge transformation

The functional integral can only be constructed when the operators in the Hamiltonian are in the Heisenberg representation [70, 71]. This means that a gauge transformation to move the system described by Eq. (2.13) to the reference frame of the pump mode while making the Hamiltonian time-independent has to be performed. New operators $\tilde{p} = \hat{p} e^{i\omega_p t} e^{-i\mathbf{k}_p \cdot \mathbf{x}}$ and $\tilde{p}^\dagger = \hat{p}^\dagger e^{-i\omega_p t} e^{i\mathbf{k}_p \cdot \mathbf{x}}$ are defined. Without any loss of generality, $F_{lp} \in \Re$ can be chosen so the pump term becomes:

$$\hat{H}_{pump} \rightarrow F_{lp}(\tilde{p}_{\mathbf{0}} + \tilde{p}^\dagger_{\mathbf{0}}).$$

To write the Hamiltonian with the new operators ($\tilde{p}$), it is noted that the existing operators can be defined in terms of the new operators as $\hat{p} = \tilde{p} e^{-i\omega_p t} e^{i\mathbf{k}_p \cdot \mathbf{x}}$. The exponents cancel in all terms of the Hamiltonian that are quadratic or quartic in the the original operators.

The terms that relate to the decay baths now contain both the new operators and the old operators. By defining the bath operators as $\hat{A} = \tilde{A} e^{-i\omega_p t} e^{i\mathbf{k}_p \cdot \mathbf{x}}$, $\hat{B} = \tilde{B} e^{-i\omega_p t} e^{i\mathbf{k}_p \cdot \mathbf{x}}$, and including the ω_p shift into the bath energies (from here onwards, $\omega^{\Gamma^i}_{\mathbf{p}}$ includes an implicit contribution $-\omega_p$), the entire system is written relative to the pump energy ω_p, and momentum $\mathbf{k}_p$. The time

independent Hamiltonian $\hat{H}'$ is:

$$\begin{aligned}\hat{H}'_{lp} &= \sum_{\mathbf{k}}(\omega_{lp}(\mathbf{k}+\mathbf{k}_p)-\omega_p)\tilde{p}^\dagger_{\mathbf{k}}\tilde{p}_{\mathbf{k}} + F_{lp}(\tilde{p}^\dagger_{\mathbf{0}}+\tilde{p}_{\mathbf{0}}) + \frac{1}{2}\sum_{\mathbf{k},\mathbf{k}',\mathbf{q}} V_{\mathbf{k},\mathbf{k}',\mathbf{q}}\tilde{p}^\dagger_{\mathbf{k}}\tilde{p}^\dagger_{\mathbf{k}'}\tilde{p}_{\mathbf{k}-\mathbf{q}}\tilde{p}_{\mathbf{k}'+\mathbf{q}} \\ &+\sum_{\mathbf{p}}\left(\omega^{\Gamma^c}_{\mathbf{p}}\tilde{A}^\dagger_{\mathbf{p}}\tilde{A}_{\mathbf{p}}+\omega^{\Gamma^x}_{\mathbf{p}}\tilde{B}^\dagger_{\mathbf{p}}\tilde{B}_{\mathbf{p}}\right)+\sum_{\mathbf{p},\mathbf{k}}\Bigg(\Gamma^c_{\mathbf{p},\mathbf{k}}\left(C(\mathbf{k}+\mathbf{k}_p)\tilde{p}^\dagger_{\mathbf{k}}\tilde{A}_{\mathbf{p}}+\tilde{A}^\dagger_{\mathbf{p}}C(\mathbf{k}+\mathbf{k}_p)\tilde{p}_{\mathbf{k}}\right) \\ &+\Gamma^x_{\mathbf{p},\mathbf{k}}\left(X(\mathbf{k}+\mathbf{k}_p)\tilde{p}^\dagger_{\mathbf{k}}\tilde{B}_{\mathbf{p}}+\tilde{B}^\dagger_{\mathbf{p}}X(\mathbf{k}+\mathbf{k}_p)\tilde{p}_{\mathbf{k}}\right)\Bigg). \qquad (3.13)\end{aligned}$$

All momenta are shifted such that $\mathbf{k}=0$ is at the pump; $\mathbf{k}_p$ is included explicitly in the polariton dispersion and the Hopfield coefficients since these are the standard definitions of these functions, without the gauge transformation, are used. The shift of the momentum in the polariton dispersion is due to the kinetic energy shift found through Fourier transforming the term of the original Hamiltonian into real space, performing the change of operators and then Fourier transforming back into the momentum space description used throughout.

3.2.2 Coherent state bases

The Hamiltonian (Eq. (3.13)) contains summations over momenta as well as operators for the polaritons and the exciton and photon decay baths. The properties of the coherent state bases remain as in table 3.1, but the notation for the three fields needs to be set and the implications of the three different operators and the different momenta considered.

Each type of boson in the Hamiltonian couples to its own coherent state basis and resolutions of identity can be written for each basis. There is a summation over momentum states in the Hamiltonian each of which has its own coherent state basis. Here, the coherent states are written without any momentum arguments, but instead include an implicit product over momenta:

$$\tilde{p}_{\mathbf{k}}|\psi\rangle = \psi_{\mathbf{k}}|\psi\rangle \qquad (3.14)$$

where ψ is the coherent state basis of the polaritons, defined as [69]:

$$|\psi\rangle \equiv |(\prod_{\mathbf{k}=\mathbf{k}_1}^{\mathbf{k}_n}\psi_{\mathbf{k}})\rangle = |\psi_{\mathbf{k}_1}\psi_{\mathbf{k}_2}\ldots\psi_{\mathbf{k}_n}\rangle. \qquad (3.15)$$

with a resolution of identity that now includes a summation over momenta:

$$I = \int D(\overline{\psi},\psi)e^{-\sum_{\mathbf{k}}\overline{\psi}_{\mathbf{k}}\psi_{\mathbf{k}}}|\psi\rangle\langle\psi|. \qquad (3.16)$$

The measure of integration, $D(\overline{\psi},\psi)$, now contains a product over momenta. The coherent state

bases of the exciton and photon decay baths can be defined in a similar way:

$$\tilde{A}_{\mathbf{p}}|\chi_c\rangle = \chi_{c,\mathbf{p}}|\chi_c\rangle, \tag{3.17}$$

$$\tilde{B}_{\mathbf{p}}|\chi_x\rangle = \chi_{x,\mathbf{p}}|\chi_x\rangle. \tag{3.18}$$

The fact that the decay baths are separate from the polariton system and each other means that acting on the coherent state basis of one species with an operator of another species yields zero, that is:

$$\tilde{A}_{\mathbf{p}}|\chi_x\rangle = \tilde{A}_{\mathbf{p}}|\psi\rangle = 0; \qquad \tilde{B}_{\mathbf{p}}|\chi_c\rangle = \tilde{B}_{\mathbf{p}}|\psi\rangle = 0; \qquad \tilde{p}_{\mathbf{k}}|\chi_c\rangle = \tilde{p}_{\mathbf{k}}|\chi_x\rangle = 0. \tag{3.19}$$

3.2.3 Constructing the functional integral

The functional integral is constructed by considering the $N = 3$ case explicitly and generalising to any N before taking the continuum limit.

As well as the $|\psi\chi_c\chi_x\rangle$ shorthand used above, the measure of integration is shortened further: $d(\overline{\psi}, \psi, \overline{\chi}_c, \chi_c, \overline{\chi}_x, \chi_x) \rightarrow d(\psi, \chi_c, \chi_x)$ which includes both the fields and their conjugates, the product over the polariton momenta $\mathbf{k}$ and the product over the bath momenta $\mathbf{p}$. Starting from the definition of the trace, Eq. (3.3), and following the procedure outlined in section 3.1 where summation and integration are commuted and resolutions of identity are included as appropriate, the $2N = 6$ step time contour becomes:

$$\begin{aligned}
Tr(U_t\hat{\rho}) = &\int d(\psi_6, \chi_{a,6}, \chi_{b,6}) e^{-\sum_{\mathbf{k}}|\psi_{\mathbf{k},6}|^2 - \sum_{\mathbf{p}}(|\chi_{\mathbf{p},c,6}|^2 + |\chi_{\mathbf{p},x,6}|^2)} \times \\
&\langle(\psi\chi_c\chi_x)_6|U_{-\delta t}\int d(\psi_5, \chi_{c,5}, \chi_{x,5}) e^{-\sum_{\mathbf{k}}|\psi_{\mathbf{k},5}|^2 - \sum_{\mathbf{p}}(|\chi_{\mathbf{p},c,5}|^2 + |\chi_{\mathbf{p},x,5}|^2)}|(\psi\chi_c\chi_x)_5\rangle \times \\
&\langle(\psi\chi_c\chi_x)_5|U_{-\delta t}\int d(\psi_4, \chi_{c,4}, \chi_{x,4}) e^{-\sum_{\mathbf{k}}|\psi_{\mathbf{k},4}|^2 - \sum_{\mathbf{p}}(|\chi_{\mathbf{p},c,4}|^2 + |\chi_{\mathbf{p},x,4}|^2)}|(\psi\chi_c\chi_x)_4\rangle \times \\
&\langle(\psi\chi_c\chi_x)_4|\int d(\psi_3, \chi_{c,3}, \chi_{x,3}) e^{-\sum_{\mathbf{k}}|\psi_{\mathbf{k},3}|^2 - \sum_{\mathbf{p}}(|\chi_{\mathbf{p},c,3}|^2 + |\chi_{\mathbf{p},x,3}|^2)}|(\psi\chi_c\chi_x)_3\rangle \times \\
&\langle(\psi\chi_c\chi_x)_3|U_{\delta t}\int d(\psi_2, \chi_{c,2}, \chi_{x,2}) e^{-\sum_{\mathbf{k}}|\psi_{\mathbf{k},2}|^2 - \sum_{\mathbf{p}}(|\chi_{\mathbf{p},c,2}|^2 + |\chi_{\mathbf{p},x,2}|^2)}|(\psi\chi_c\chi_x)_2\rangle \times \\
&\langle(\psi\chi_c\chi_x)_2|U_{\delta t}\int d(\psi_1, \chi_{c,1}, \chi_{x,1}) e^{-\sum_{\mathbf{k}}|\psi_{\mathbf{k},1}|^2 - \sum_{\mathbf{p}}(|\chi_{\mathbf{p},c,1}|^2 + |\chi_{\mathbf{p},x,1}|^2)}|(\psi\chi_c\chi_x)_1\rangle \times \\
&\langle(\psi\chi_c\chi_x)_1|\hat{\rho}|(\psi\chi_c\chi_x)_6\rangle \\
&= \int(\prod_{j=1}^{6} d(\psi_j, \chi_{c,j}, \chi_{x,j}) e^{-\sum_{\mathbf{k}}|\psi_{\mathbf{k},j}|^2 - \sum_{\mathbf{p}}(|\chi_{\mathbf{p},c,j}|^2 + |\chi_{\mathbf{p},x,j}|^2)})\langle(\psi\chi_c\chi_x)_6|U_{-\delta t}|(\psi\chi_c\chi_x)_5\rangle \times \\
&\quad\langle(\psi\chi_c\chi_x)_5|U_{-\delta t}|(\psi\chi_c\chi_x)_4\rangle\langle(\psi\chi_c\chi_x)_4|(\psi\chi_c\chi_x)_3\rangle\langle(\psi\chi_c\chi_x)_3|U_{\delta t}|(\psi\chi_c\chi_x)_2\rangle \times \\
&\quad\langle(\psi\chi_c\chi_x)_2|U_{\delta t}|(\psi\chi_c\chi_x)_1\rangle\langle(\psi\chi_c\chi_x)_1|\hat{\rho}|(\psi\chi_c\chi_x)_6\rangle.
\end{aligned} \tag{3.20}$$

The elements that need explicit calculation are of the form: $\langle(\psi\chi_c\chi_x)_{j+1}|U_{\pm\delta t}|(\psi\chi_c\chi_x)_j\rangle$ and

the last term: $\langle(\psi\chi_c\chi_x)_1|\hat{\rho}|(\psi\chi_c\chi_x)_6\rangle$.

The simpler of the two terms $\eta = \langle(\psi\chi_c\chi_x)_1|\hat{\rho}|(\psi\chi_c\chi_x)_6\rangle$ is considered first. The equilibrium density matrix

$$\hat{\rho} = \exp\Big(-\beta(\omega_{lp}(\mathbf{k}) - \mu_{\mathbf{k},\psi})\tilde{p}^\dagger\tilde{p} - \beta(\omega^{\Gamma^c}(\mathbf{p}) - \mu_{\chi_c,\mathbf{p}})\tilde{A}^\dagger_{\mathbf{p}}\tilde{A}_{\mathbf{p}} - \beta(\omega^{\Gamma^x}(\mathbf{p}) - \mu_{\chi_x,\mathbf{p}})\tilde{B}^\dagger_{\mathbf{p}}\tilde{B}_{\mathbf{p}}\Big) \quad (3.21)$$

is used since the interactions, between the polaritons and between the polaritons and the baths, are supposed to be adiabatically switched on and off and therefore only affect the matrix elements of the evolution operator [70, 71] (the summation over the system and bath momenta has been dropped for simplicity while the summation over the two baths has been written as a $\sum_i$). This element is therefore calculated by using that the coherent state basis has the following property [70, 71]:

$$\langle\phi|e^{\kappa a^\dagger a}|\phi'\rangle = \exp\{\overline{\phi}\phi' e^\kappa\}.$$

Since the three operators act on different coherent state bases, there is one copy for each of the three parts of the system:

$$\langle(\psi\chi_c\chi_x)_1|\hat{\rho}|(\psi\chi_c\chi_x)_{2N}\rangle = \exp\left\{\overline{\psi}_1\psi_{2N}e^{-\beta(\omega_{lp}(\mathbf{k})-\mu_{\mathbf{k},\psi})} + \sum_{i\in\{x,c\}}\overline{\chi}_{i,1}\chi_{i,2N}e^{-\beta(\omega^{\Gamma^i}(\mathbf{p})-\mu_{\chi_i,\mathbf{p}})}\right\}, \quad (3.22)$$

and the two baths have been written compactly.

In the terms containing the time evolution, the operator is $U_{\pm\delta t}$ and all terms have the form $\langle(\psi\chi_x\chi_b)_{j+1}|U_{\pm\delta t}|(\psi\chi_x\chi_b)_j\rangle = \nu_j$. The time evolution operator is defined as

$$\begin{aligned}
U_{\pm\delta t} &= e^{\mp i\hat{H}'\delta t} \\
&= \exp\Bigg\{\mp i\Big(\sum_{\mathbf{k}}(\omega_{lp}(\mathbf{k}+\mathbf{k}_p) - \omega_p)\tilde{p}^\dagger_{\mathbf{k}}\tilde{p}_{\mathbf{k}} + \frac{1}{2}\sum_{\mathbf{k},\mathbf{k}',\mathbf{q}}V_{\mathbf{k},\mathbf{k}',\mathbf{q}}\tilde{p}^\dagger_{\mathbf{k}}\tilde{p}^\dagger_{\mathbf{k}'}\tilde{p}_{\mathbf{k}-\mathbf{q}}\tilde{p}_{\mathbf{k}'+\mathbf{q}} \\
&\quad + \sum_{\mathbf{p},\mathbf{k}}\Big[\Gamma^c_{\mathbf{p},\mathbf{k}}\Big(C(\mathbf{k}+\mathbf{k}_p)\tilde{p}^\dagger_{\mathbf{k}}\tilde{A}_{\mathbf{p}} + \tilde{A}^\dagger_{\mathbf{p}}C(\mathbf{k}+\mathbf{k}_p)\tilde{p}_{\mathbf{k}}\Big) \\
&\qquad + \Gamma^x_{\mathbf{p},\mathbf{k}}\Big(X(\mathbf{k}+\mathbf{k}_p)\tilde{p}^\dagger_{\mathbf{k}}\tilde{B}_{\mathbf{p}} + \tilde{B}^\dagger_{\mathbf{p}}X(\mathbf{k}+\mathbf{k}_p)\tilde{p}_{\mathbf{k}}\Big)\Big] \\
&\quad + \sum_{\mathbf{p}}\Big[\omega^{\Gamma^c}_{\mathbf{p}}\tilde{A}^\dagger_{\mathbf{p}}\tilde{A}_{\mathbf{p}} + \omega^{\Gamma^x}_{\mathbf{p}}\tilde{B}^\dagger_{\mathbf{p}}\tilde{B}_{\mathbf{p}}\Big] + F_{lp}(\tilde{p}^\dagger_{\mathbf{0}} + \tilde{p}_{\mathbf{0}})\Big)\delta t\Bigg\}.
\end{aligned} \quad (3.23)$$

Since δt is small, a Taylor expansion of the exponential is made, the action of the operators calculated and the exponential reformed by using the overlap properties of the coherent state basis [70, 71]. The generic result, between any two consecutive points on the time contour t_j and

t_{j+1}, is:

$$\begin{aligned}\nu_j &= \exp\Bigg\{ \sum_{\mathbf{k}} \overline{\psi}_{\mathbf{k},j+1}\psi_{\mathbf{k},j} + \sum_{\substack{\mathbf{p}\\ i\in\{c,x\}}} \overline{\chi}_{\mathbf{p},i,j+1}\chi_{\mathbf{p},i,j+1} \mp i\delta t\Big(\sum_{\mathbf{k}} (\omega_{lp}(\mathbf{k}+\mathbf{k}_p)-\omega_p)\overline{\psi}_{j+1}\psi_j \\ &\quad + F_{lp}(\overline{\psi}_{\mathbf{0},j+1}+\psi_{\mathbf{0},j}) + \frac{1}{2}\sum_{\mathbf{k},\mathbf{k}',\mathbf{q}} V_{\mathbf{k},\mathbf{k}',\mathbf{q}}\overline{\psi}_{\mathbf{k},j+1}\overline{\psi}_{\mathbf{k}',j+1}\psi_{\mathbf{k}-\mathbf{q},j}\psi_{\mathbf{k}'+\mathbf{q},j} \\ &\quad + \sum_{\substack{\mathbf{p}\\ i\in\{c,x\}}} \Big[\omega_{\mathbf{p}}^{\Gamma^i}\overline{\chi}_{\mathbf{p},i,j+1}\chi_{\mathbf{p},i,j} + \sum_{\mathbf{k}} h_{\mathbf{k}}^i\Gamma_{\mathbf{p},\mathbf{k}}^i(\overline{\psi}_{\mathbf{k},j+1}\chi_{\mathbf{p},i,j} + \overline{\chi}_{\mathbf{p},i,j+1}\psi_{\mathbf{k},j})\Big]\Big)\Bigg\}. \end{aligned} \tag{3.24}$$

The decay bath terms have been written compactly by summing over the baths $i \in \{c, x\}$ as well as the momenta by introducing $h_{\mathbf{k}}^i$ for the Hopfield coefficients ($h_{\mathbf{k}}^c = C(\mathbf{k}+\mathbf{k}_p), h_{\mathbf{k}}^x = X(\mathbf{k}+\mathbf{k}_p)$).

With $N = 3$, the terms of the exponent can be written as elements of a matrix and a sum over the elements performed. The presence of the constant pump term F_{lp} requires that it either acquires a time label or that the pump term is separated out as a vector, as below. The general matrix form of the exponent is $\eta + \sum_{j=1}^{2N}\nu_j$:

$$\begin{pmatrix} -|\phi_1|^2 & 0 & 0 & 0 & 0 & (\overline{\phi}_1,\phi_6) \\ (\overline{\phi}_2,\phi_1) & -|\phi_2|^2 & 0 & 0 & 0 & 0 \\ 0 & (\overline{\phi}_3,\phi_2) & -|\phi_3|^2 & 0 & 0 & 0 \\ 0 & 0 & (\overline{\phi}_4,\phi_3) & -|\phi_4|^2 & 0 & 0 \\ 0 & 0 & 0 & (\overline{\phi}_5,\phi_4) & -|\phi_5|^2 & 0 \\ 0 & 0 & 0 & 0 & (\overline{\phi}_6,\phi_5) & -|\phi_6|^2 \end{pmatrix} + F_{lp}\begin{pmatrix} \delta t\psi_{\mathbf{0},1} \\ \delta t\overline{\psi}_{\mathbf{0},2} + \delta t\psi_{\mathbf{0},2} \\ \delta t\overline{\psi}_{\mathbf{0},3} \\ \delta t\psi_{\mathbf{0},4} \\ \delta t\overline{\psi}_{\mathbf{0},5} + \delta t\psi_{\mathbf{0},5} \\ \delta t\overline{\psi}_{\mathbf{0},6} \end{pmatrix}.$$

All fields, except those related to the external pump, contain an implicit summation over momenta and the form ϕ_j include all fields (system plus decay baths). The terms are not written out explicitly, but show the relevant time arguments on the fields and their conjugates.

The next step is to write the exponent in a convenient form as an integral in which top right hand element $(\overline{\phi}_1,\phi_6) = (\overline{\psi}_1,\psi_6,\overline{\chi}_{c,1},\chi_{c,6},\overline{\chi}_{x,1},\chi_{x,6})$ appears to be lost, but this is only an artefact of the continuum notation [70, 71]. The momentum and bath field summations are restored and the matrix can be written compactly as a summation over the $2N$ time steps:

$$\begin{aligned} &-\sum_{j=2}^{2N}\delta t_j\Bigg(\sum_{\mathbf{k}}\overline{\psi}_{\mathbf{k},j}\frac{\psi_{\mathbf{k},j}-\psi_{\mathbf{k},j-1}}{\delta t_j} + \sum_{\substack{\mathbf{p}\\ i\in\{c,x\}}}\overline{\chi}_{\mathbf{p},i,j}\frac{\chi_{\mathbf{p},i,j}-\chi_{\mathbf{p},i,j-1}}{\delta t_j} \\ &+ i\Big\{\sum_{\mathbf{k}}(\omega_{lp}(\mathbf{k}+\mathbf{k}_p)-\omega_p)\overline{\psi}_{\mathbf{k},j}\psi_{\mathbf{k},j-1} + \frac{1}{2}\sum_{\mathbf{k},\mathbf{k}',\mathbf{q}} V_{\mathbf{k},\mathbf{k}',\mathbf{q}}\overline{\psi}_{\mathbf{k},j+1}\overline{\psi}_{\mathbf{k}',j+1}\psi_{\mathbf{k}-\mathbf{q},j}\psi_{\mathbf{k}'+\mathbf{q},j} \\ &+ F_{lp}(\psi_{\mathbf{0},j-1}+\overline{\psi}_{\mathbf{0},j}) + \sum_{\substack{\mathbf{p}\\ i\in\{c,x\}}}\Big[\omega_{\mathbf{p}}^{\Gamma^i}\overline{\chi}_{\mathbf{p},i,j}\chi_{\mathbf{p},i,j-1} + \sum_{\mathbf{k}} h_{\mathbf{k}}^i\Gamma_{\mathbf{p},\mathbf{k}}^i\left(\overline{\chi}_{\mathbf{p},i,j}\psi_{\mathbf{k},j-1} + \overline{\psi}_{\mathbf{k},j}\chi_{\mathbf{p},i,j-1}\right)\Big]\Big\}\Bigg). \end{aligned}$$

In the limit of $N \to \infty$, $\psi_{\mathbf{k},j} \to \psi_{\mathbf{k}}(t), \chi_{\mathbf{p},j} \to \chi_{\mathbf{p}}(t)$ and $\sum_j$ becomes an integral over the entire closed time contour $\int_C dt$ with $(\psi_{\mathbf{k},j} - \psi_{\mathbf{k},j-1})/\delta t \to \partial_t \psi_{\mathbf{k}}(t)$ and likewise for the bath fields.

$$
\begin{aligned}
-\int_C dt \Bigg\{ & \sum_{\mathbf{k}} \overline{\psi}_{\mathbf{k}} \partial_t \psi_{\mathbf{k}} + \sum_{\substack{\mathbf{p} \\ i \in \{c,x\}}} \overline{\chi}_{\mathbf{p},i} \partial_t \chi_{\mathbf{p},i} + i \Big(\sum_{\mathbf{k}} (\omega_{lp}(\mathbf{k}+\mathbf{k}_p) - \omega_p) \overline{\psi}_{\mathbf{k}} \psi_{\mathbf{k}} + F_{lp}(\overline{\psi}_{\mathbf{0}} + \psi_{\mathbf{0}}) \\
& + \frac{1}{2} \sum_{\mathbf{k},\mathbf{k}',\mathbf{q}} V_{\mathbf{k},\mathbf{k}',\mathbf{q}} \overline{\psi}_{\mathbf{k}} \overline{\psi}_{\mathbf{k}'} \psi_{\mathbf{k}-\mathbf{q}} \psi_{\mathbf{k}'+\mathbf{q}} + \sum_{\substack{\mathbf{p} \\ i \in \{c,x\}}} \left[\omega_{\mathbf{p}}^{\Gamma^i} \overline{\chi}_{\mathbf{p},i} \chi_{\mathbf{p},i} + \sum_{\mathbf{k}} h_{\mathbf{k}}^i \Gamma_{\mathbf{p},\mathbf{k}}^i (\overline{\chi}_{\mathbf{p},i} \psi_{\mathbf{k}} + \overline{\psi}_{\mathbf{k}} \chi_{\mathbf{p},i}) \right] \Big) \Bigg\}.
\end{aligned}
\tag{3.25}
$$

To proceed further, the desired form of the trace:

$$
Tr(U_t \hat{\rho}) = N \int D(\psi, \chi_c, \chi_x) e^{iS},
$$

is considered, where the measure of integration $D(\psi, \chi_c, \chi_x)$ includes products over all fields (and conjugate fields) and momenta [69]:

$$
D(\psi, \chi_c, \chi_x) = \lim_{j \to \infty} \prod_{j=1}^{2N} \left(\prod_{\mathbf{k}} \frac{d(\Re(\psi_{\mathbf{k},j})) d(\Im(\psi_{\mathbf{k},j}))}{\pi} \prod_{\substack{\mathbf{p} \\ i \in \{c,x\}}} \frac{d(\Re(\chi_{\mathbf{p},i,j})) d(\Im(\chi_{\mathbf{p},i,j}))}{\pi} \right).
$$

The action S is simply $-i$ times the exponent calculated above:

$$
\begin{aligned}
S[\psi, \chi_c, \chi_x] = \int_C dt \Bigg\{ & i \Big(\sum_{\mathbf{k}} \overline{\psi}_{\mathbf{k}}(t) \partial_t \psi_{\mathbf{k}}(t) + \sum_{\substack{\mathbf{p} \\ i \in \{c,x\}}} \overline{\chi}_{\mathbf{p},i}(t) \partial_t \chi_{\mathbf{p},i}(t) \Big) - F_{lp} \left(\psi_{\mathbf{0}}(t) + \overline{\psi}_{\mathbf{0}}(t) \right) \\
& - \Big(\sum_{\mathbf{k}} (\omega_{lp}(\mathbf{k}+\mathbf{k}_p) - \omega_p) \overline{\psi}_{\mathbf{k}}(t) \psi_{\mathbf{k}}(t) + \frac{1}{2} \sum_{\mathbf{k},\mathbf{k}',\mathbf{q}} V_{\mathbf{k},\mathbf{k}',\mathbf{q}} \overline{\psi}_{\mathbf{k}}(t) \overline{\psi}_{\mathbf{k}'}(t) \psi_{\mathbf{k}-\mathbf{q}}(t) \psi_{\mathbf{k}'+\mathbf{q}}(t) \\
& + \sum_{\substack{\mathbf{p} \\ i \in \{c,x\}}} \left[\omega_{\mathbf{p}}^{\Gamma^i} \overline{\chi}_{\mathbf{p},i}(t) \chi_{\mathbf{p},i}(t) + \sum_{\mathbf{k}} h_{\mathbf{k}}^i \Gamma_{\mathbf{p},\mathbf{k}}^i \left(\overline{\chi}_{\mathbf{p},i}(t) \psi_{\mathbf{k}}(t) + \overline{\psi}_{\mathbf{k}}(t) \chi_{\mathbf{p},i}(t) \right) \right] \Big) \Bigg\},
\end{aligned}
\tag{3.26}
$$

in which the integral runs over the entire closed time contour.

3.2.4 Quantum and classical fields

In order to calculate quantities of interest, the action is written in terms of quantum and classical components of the fields as outlined in section 3.1. The time integration in Eq. (3.26) is over the entire closed time contour, while the quantum and classical parts of the fields are defined in terms of the fields on the forwards and backwards branches of the contour according to Eqs. (3.4) and (3.5). The first step is to split the closed time contour into its forwards and backwards

branches so the action is of the form:

$$S[\psi,\chi_c,\chi_x]=\int_{-\infty}^{\infty}dtS_F[\psi_F,\chi_{c,F},\chi_{x,F}]-\int_{-\infty}^{\infty}dtS_B[\psi_B,\chi_{c,B},\chi_{x,B}]. \tag{3.27}$$

The minus sign comes from $\int_\alpha^\beta=-\int_\beta^\alpha$, and $F(B)$ indicates that the fields are on the forwards (backwards) branch of the time contour.

The fields on the forwards and backwards branches are now written in terms of the quantum and classical components according to Eqs. (3.4) and (3.5). The action in the Keldysh basis is:

$$\begin{aligned}iS[\Psi,\chi_{c,x}] &= i\int dt\Bigg\{\sum_{\mathbf{k}}\Psi^\dagger_{\mathbf{k}}(i\partial_t-\omega_{lp}(\mathbf{k}+\mathbf{k}_p)+\omega_p)\sigma_1^K\Psi_{\mathbf{k}}+\sum_{\substack{\mathbf{p}\\ i\in\{c,x\}}}\chi^\dagger_{\mathbf{p},i}(i\partial_t-\omega_{\mathbf{p}}^{\Gamma^i})\sigma_1^K\chi_{\mathbf{p},i}\\ &-\sum_{\mathbf{k}}\sum_{\substack{\mathbf{p}\\ i\in\{c,x\}}}h^i_{\mathbf{k}}\Gamma^i_{\mathbf{p},\mathbf{k}}(\chi^\dagger_{\mathbf{p},i}\sigma_1^K\Psi_{\mathbf{k}}+\Psi^\dagger_{\mathbf{k}}\sigma_1^K\chi_{\mathbf{p},i})-\sqrt{2}F_{lp}(\overline{\psi}_{\mathbf{0},q}+\psi_{\mathbf{0},q})\\ &-\frac{1}{4}\sum_{\mathbf{k},\mathbf{k}',\mathbf{q}}V_{\mathbf{k},\mathbf{k}',\mathbf{q}}\left[\Psi^\dagger_{\mathbf{k}}\sigma_1^K\Psi_{\mathbf{k}-\mathbf{q}}\Psi^\dagger_{\mathbf{k}'}\Psi_{\mathbf{k}'+\mathbf{q}}+\Psi^\dagger_{\mathbf{k}}\Psi_{\mathbf{k}-\mathbf{q}}\Psi^\dagger_{\mathbf{k}'}\sigma_1^K\Psi_{\mathbf{k}'+\mathbf{q}}\right]\Bigg\}\end{aligned} \tag{3.28}$$

which has double the number of terms as the original action due to the presence of the classical and quantum components [70], and σ_1^K is the Pauli matrix

$$\sigma_1^K=\begin{pmatrix}0&1\\1&0\end{pmatrix},$$

that acts on the vectors $\Psi_{\mathbf{k}},\chi_{\mathbf{p},i}$ that have the form

$$\Phi\equiv\begin{pmatrix}\phi_{cl}\\ \phi_q\end{pmatrix};\qquad \Phi^\dagger\equiv\begin{pmatrix}\overline{\phi}_{cl}, & \overline{\phi}_q\end{pmatrix}.$$

The field arguments of the action include the conjugate fields by implication.

All terms in the action, except the pump term, contain both classical and quantum fields. The pump term contains only quantum fields, but the pump is classical by construction. Terms relating to the incoherent decay are very similar to the photon decay of the incoherently pumped polariton system [21] since all decay baths are bosonic. The action is quadratic in the bath fields ($\chi_{c,x}$) which can be integrated out using Gaussian integrals (or a Hubbard-Stratonovich transformation) [21, 69].

3.2.5 Integrating out the decay baths

The process of integrating out the decay baths is analogous to a Hubbard-Stratonovich transformation, and follows the procedure used to integrate out the photon decay bath in the case of incoherently pumped polaritons [21]. Only one bath is treated explicitly since the second has the

same properties and the derivation is identical up to the different Hopfield coefficient and decay constant.

Let T be the integral that is of interest for disposing of the bath fields, it is a part of the partition function where the terms in the 'action' are those containing the decay bath

$$T = \int \prod_{\substack{\mathbf{p} \\ i\in\{c,x\}}} D(\chi^{\dagger}_{\mathbf{p},i}, \chi_{\mathbf{p},i}) \exp\left(i \int dt \sum_{\substack{\mathbf{p} \\ i\in\{c,x\}}} \Big[\chi^{\dagger}_{\mathbf{p},i}(i\partial_t - \omega^{\Gamma^i}_{\mathbf{p}})\sigma_1^K \chi_{\mathbf{p},i} - \sum_{\mathbf{k}} h^i_{\mathbf{k}} \Gamma^i_{\mathbf{p},\mathbf{k}} (\chi^{\dagger}_{\mathbf{p},i}\sigma_1^K \psi_{\mathbf{k}} + \overline{\psi}_{\mathbf{k}}\sigma_1^K \chi_{\mathbf{p},i}) \Big] \right). \tag{3.29}$$

A Gaussian integral for a functional integral of complex variables is required. This is the generalisation of the Gaussian integrals of real and complex vectors and a functional integral of real variables [69]:

$$\int D(\overline{v}(x), v(x)) \exp\left(- \int dx dx' \overline{v}(x) A(x,x') v(x') + \int dx (\overline{w}(x) v(x) + \overline{v}(x) w'(x)) \right) \propto (detA)^{-1} \exp\left(\int dx dx' \overline{w}(x) A^{-1}(x,x') w'(x') \right). \tag{3.30}$$

$v(x), \overline{v}(x)$ are complex functions (the bath fields that want to be removed), $w(x), \overline{w}(x)$ are complex functions (the system fields that want to be kept), and the inverse of the operator kernal $A(x,x')$ can be interpreted as the Green's function [69].

Returning to the problem at hand and the part of the action that concerns the bath fields, the exponent that comes from performing the integral T is of interest. Comparing Eq. (3.29) with Eq. (3.30) leads to the relations summarised in table 3.2. The summations over the polariton and decay bath fields are extracted from the integrands at the start of the process, and remain unchanged.

$D(\overline{v}(x), v(x))$	$D(\chi^{\dagger}_{\mathbf{p}}(t), \chi_{\mathbf{p}}(t))$
dx	dt
dx'	dt'
$\overline{v}(x)$	$\chi^{\dagger}_{\mathbf{p},i} \rightarrow \chi^{\dagger}_{\mathbf{p},i}(t)$
$A(x,x')$	$-(i\partial_t - \omega^{\Gamma^i}_{\mathbf{p}})\sigma_1^K \rightarrow -(i\partial_t - \omega^{\Gamma^i}_{\mathbf{p}})\sigma_1^K \delta(t-t')$
$v(x')$	$\chi_{\mathbf{p},i} \rightarrow \chi_{\mathbf{p},i}(t')$
$\overline{w}(x)$	$-h^i_{\mathbf{k}}\Gamma^i_{\mathbf{p},\mathbf{k}}\Psi^{\dagger}_{\mathbf{k}}\sigma_1^K \rightarrow -h^i_{\mathbf{k}}\Gamma^i_{\mathbf{p},\mathbf{k}}\Psi^{\dagger}_{\mathbf{k}}(t)\sigma_1^K$
$v(x)$	$\chi_{\mathbf{p},i} \rightarrow \chi_{\mathbf{p},i}(t)$
$w'(x)$	$-h^i_{\mathbf{k}}\Gamma^i_{\mathbf{p},\mathbf{k}}\sigma_1^K\Psi_{\mathbf{k}} \rightarrow -h^i_{\mathbf{k}}\Gamma^i_{\mathbf{p},\mathbf{k}}\sigma_1^K\Psi_{\mathbf{k}}(t)$

Table 3.2: Elements of the generic equation for the Gaussian integral of a functional integral of complex fields with specific terms in the notation of the incoherent exciton and photon decay baths (given by superscripts and subscripts i).

The part of the action that contained the decay baths is now written in terms of the system

fields, the couplings and the bath dispersions:

$$iS_{baths,\Psi} = -i\int dtdt' \sum_{\substack{\mathbf{p},\mathbf{k}\\ i\in\{c,x\}}} (h^i_{\mathbf{k}}\Gamma^i_{\mathbf{p},\mathbf{k}})^2 \Psi^\dagger_{\mathbf{k}}(t)\sigma_1^K((i\partial_t - \omega^{\Gamma^i}_{\mathbf{p}})\sigma_1^K)^{-1}\sigma_1^K\Psi_{\mathbf{k}}(t'). \tag{3.31}$$

If it is assumed that the baths are large and therefore unaffected by the behaviour of the polariton system, $((i\partial_t - \omega^{\Gamma^i}_{\mathbf{p}})\sigma_1^K)^{-1} = D_{\mathbf{p},i}(t-t')$, the Green's function for a free boson [21, 70, 71], which has the matrix form [21].

$$((i\partial_t - \omega^{\Gamma^i}_{\mathbf{p}})\sigma_1^K)^{-1} = \begin{pmatrix} D^K_{\mathbf{p},i}(t-t') & D^R_{\mathbf{p},i}(t-t') \\ D^A_{\mathbf{p},i}(t-t') & 0 \end{pmatrix}.$$

The Fourier transform and it inverse are defined as

$$\begin{aligned} f(t) &= \frac{1}{2\pi}\int_{-\infty}^{\infty} f(\omega)e^{i\omega t}d\omega, \\ f(\omega) &= \int_{-\infty}^{\infty} f(t)e^{-i\omega t}dt, \end{aligned}$$

so that, for any field,

$$\begin{aligned} \int dtdt'\overline{\phi}(t)D(t-t')\phi(t') &= \frac{1}{2\pi}\int dtdt'\overline{\phi}(t)\int d\omega D(\omega)e^{-i\omega t}e^{i\omega t'}\phi(t') \\ &= \frac{1}{2\pi}\int d\omega\int dt\overline{\phi}(t)e^{-i\omega t}D(\omega)\int dt'\phi(t')e^{i\omega t}. \end{aligned}$$

Performing the Fourier transform of Eq. (3.31) gives:

$$\int dtdt' \sum_{\substack{\mathbf{p},\mathbf{k}\\ i\in\{c,x\}}} (h^i_{\mathbf{k}}\Gamma^i_{\mathbf{k},\mathbf{p}})^2 \Psi^\dagger(t)\sigma_1^K D_{\mathbf{p},i}(t-t')\sigma_1^K\Psi(t') = \frac{1}{2\pi}\int d\omega \sum_{\substack{\mathbf{p},\mathbf{k}\\ i\in\{c,x\}}} (h^i_{\mathbf{k}}\Gamma^i_{\mathbf{k},\mathbf{p}})^2 \Psi^\dagger(\omega)D_{i,\mathbf{p}}(\omega)\Psi(-\omega),$$

where the momentum arguments (both system and decay baths) have been dropped for brevity. It has already been assumed that the bath is large enough that it can be considered as containing free bosons. This means that the bath's Green's functions are [21, 69–71]:

$$\begin{aligned} D^{R/A}_{\mathbf{p},i}(\omega) &= \frac{1}{\omega - \omega^{\Gamma^i}_{\mathbf{p}} \pm i\delta}, \\ D^K_{\mathbf{p},i}(\omega) &= -2\pi i(2n_b(\omega^{\Gamma^i}_{\mathbf{p}}) + 1)\delta(\omega - \omega^{\Gamma^i}_{\mathbf{p}}). \end{aligned} \tag{3.32}$$

Following Ref. [21], a standard series of assumptions is made about the baths. First, it is assumed that the bath frequencies $\omega^{\Gamma^i}_{\mathbf{p}}$ form a dense spectrum and that the coupling constants $\Gamma^i_{\mathbf{p},\mathbf{k}}$ are smooth functions of the bath frequencies. Further, the coupling between the photons (excitons) and the photonic (excitonic) decay bath is assumed constant and that each system momentum $\mathbf{k}$

couples to its own set of decay bath modes. The only momentum dependence of the couplings is defined by the exciton or photon fraction of the polaritons. The summation over bath momenta is replaced by an integral including the bath's density of states $N^i(\omega^{\Gamma^i})$:

$$\sum_{\mathbf{p},\mathbf{k}}(h^i_{\mathbf{k}}\Gamma^i_{\mathbf{p},\mathbf{k}})^2 \to \sum_{\mathbf{k}}(h^i_{\mathbf{k}})^2 \int d\omega^{\Gamma^i}\Gamma^i(\omega^{\Gamma^i})^2 N^i(\omega^{\Gamma^i}).$$

The integral over the bath energies can be performed for each of the three Green's functions. For the Keldysh part:

$$\begin{aligned}
&\sum_{\mathbf{k}}\frac{(h^i_{\mathbf{k}})^2}{2\pi}\int d\omega\overline{\psi}_{\mathbf{k},q}(\omega)\int d\omega^{\Gamma^i}\Gamma^i(\omega^{\Gamma^i})^2N^i(\omega^{\Gamma^i})D^K_i(\omega)\psi_{\mathbf{k},q}(-\omega)\\
=&\sum_{\mathbf{k}}\frac{(h^i_{\mathbf{k}})^2}{2\pi}\int d\omega\overline{\psi}_{\mathbf{k},q}(\omega)\int d\omega^{\Gamma^i}\Gamma^i(\omega^{\Gamma^i})^2N^i(\omega^{\Gamma^i})(-2\pi iF_{\chi_i}(\omega^{\Gamma^i})\delta(\omega-\omega^{\Gamma^i}))\psi_{\mathbf{k},q}(-\omega)\\
=&\sum_{\mathbf{k}}\frac{(h^i_{\mathbf{k}})^2}{2\pi}\int d\omega\overline{\psi}_{\mathbf{k},q}(\omega)(-2\pi i)\Gamma^i(\omega)^2N^i(\omega)F_{\chi_i}(\omega)\psi_{\mathbf{k},q}(-\omega)\\
=&\sum_{\mathbf{k}}\frac{1}{2\pi}\int d\omega\overline{\psi}_{\mathbf{k},q}(\omega)d^K_{\mathbf{k},i}(\omega)\psi_{\mathbf{k},q}(\omega),
\end{aligned}\tag{3.33}$$

where $F_{\chi_i}(\omega)=2n^i_b(\omega)+1$ has been introduced as the bath's distribution function.

The retarded and advanced parts are complex conjugates and can be evaluated using [88]

$$\frac{1}{\omega-\omega'\pm i\varepsilon}=P\frac{1}{\omega-\omega'}\mp i\pi\delta(\omega-\omega')$$

where P is the principal value integral. The retarded part is therefore:

$$\begin{aligned}
&\sum_{\mathbf{k}}\frac{(h^i_{\mathbf{k}})^2}{2\pi}\int d\omega\overline{\psi}_{\mathbf{k},cl}(\omega)\int d\omega^{\Gamma^i}\Gamma^i(\omega^{\Gamma^i})^2N^i(\omega^{\Gamma^i})D^R(\omega)\psi_{\mathbf{k},q}(-\omega)\\
=&\sum_{\mathbf{k}}\frac{(h^i_{\mathbf{k}})^2}{2\pi}\int d\omega\overline{\psi}_{\mathbf{k},cl}(\omega)\int d\omega^{\Gamma^i}\Gamma^i(\omega^{\Gamma^i})^2N^i(\omega^{\Gamma^i})\frac{1}{\omega-\omega^{\Gamma^i}+i\delta}\psi_{\mathbf{k},q}(-\omega)\\
=&\sum_{\mathbf{k}}\frac{(h^i_{\mathbf{k}})^2}{2\pi}\int d\omega\overline{\psi}_{\mathbf{k},cl}(\omega)\int d\omega^{\Gamma^i}\Gamma^i(\omega^{\Gamma^i})^2N^i(\omega^{\Gamma^i})\left(\frac{1}{\omega-\omega^{\Gamma^i}}-i\pi\delta(\omega-\omega^{\Gamma^i})\right)\psi_{\mathbf{k},q}(-\omega)\\
=&\sum_{\mathbf{k}}\frac{(h^i_{\mathbf{k}})^2}{2\pi}\int d\omega\overline{\psi}_{\mathbf{k},cl}(\omega)\left(\int d\omega^{\Gamma^i}\Gamma^i(\omega^{\Gamma^i})^2N^i(\omega^{\Gamma^i})\frac{1}{\omega-\omega^{\Gamma^i}}-i\pi\Gamma^i(\omega)^2N(\omega)\right)\psi_{\mathbf{k},q}(-\omega)\\
=&\sum_{\mathbf{k}}\frac{1}{2\pi}\int d\omega\overline{\psi}_{\mathbf{k},cl}(\omega)d^R_{\mathbf{k},i}(\omega)\psi_{\mathbf{k},q}(\omega).
\end{aligned}\tag{3.34}$$

This defines $d^R_{\mathbf{k},i}(\omega)$ and $d^K_{\mathbf{k},i}(\omega)$ as the self-energies from the decay baths, the real parts of which provide a renormalisation of the energies while the imaginary parts are the linewidths [71]:

$$d^K_{\mathbf{k},i}(\omega)=-2\pi i(h^i_{\mathbf{k}})^2\Gamma^i(\omega)^2N^i(\omega)F_{\chi_i}(\omega)$$

$$d^{R,A}_{\mathbf{k},i}(\omega) = (h^i_{\mathbf{k}})^2 \left(\int d\omega^{\Gamma^i} \Gamma^i(\omega^{\Gamma^i})^2 N^i(\omega^{\Gamma^i}) \frac{1}{\omega - \omega^{\Gamma^i}} \mp i\pi\Gamma^i(\omega)^2 N^i(\omega) \right).$$

The retarded and advanced self-energies are complex with the form $R_{\mathbf{k},i}(\omega) \mp i(h^i_{\mathbf{k}})^2\kappa_i(\omega)$ where the real part is:

$$R_{\mathbf{k},i}(\omega) = (h^i_{\mathbf{k}})^2 \int d\omega^{\Gamma^i} \frac{\Gamma^i(\omega^{\Gamma^i})^2 N^i(\omega^{\Gamma^i})}{\omega - \omega^{\Gamma^i}},$$

and the imaginary part is:

$$\kappa_i(\omega) = \pi\Gamma^i(\omega)^2 N^i(\omega).$$

The Keldysh part is $d^K_{\mathbf{k},i} = -2i(h^i_{\mathbf{k}})^2\kappa_i(\omega)F_{\chi_i}(\omega)$.

Any choice of the decay baths' distributions can be made [21], but if a Markovian bath, in which the bath's density of states and coupling to the system are constant, is chosen, $\Gamma^i(\omega^{\Gamma^i})^2 N^i(\omega^{\Gamma^i}) = {\Gamma^i}^2 N^i$, which is a constant. The energy shift due to the presence of the bath, $R_i(\omega)$, is zero and the linewidth is a constant, $\kappa_i(\omega) = \kappa_i$. The bath's occupation function is still dependent on the energy (frequency), so the distribution function retains its dependence on ω. The self-energy contributions from the decay bath are now:

$$\begin{aligned} d^K_{\mathbf{k},i}(\omega) &= -2i(h^i_{\mathbf{k}})^2\kappa_i F_{\chi_i}(\omega), \\ d^{R,A}_{\mathbf{k},i}(\omega) &= \mp i(h^i_{\mathbf{k}})^2\kappa_i. \end{aligned}$$

Inverting the Fourier transform of the retarded and advanced parts (between classical and quantum components of the fields) is simple. The constant terms appear in the action as

$$\frac{(h^i_{\mathbf{k}})^2\kappa_i}{2\pi} \int d\omega e^{-i\omega(t-t')} = (h^i_{\mathbf{k}})^2\kappa_i\delta(t-t')$$

which follows from the definition of the Dirac δ function [89, 90]:

$$\delta(t-t') = \frac{1}{2\pi} \int d\omega e^{i\omega(t-t')} = \delta(t'-t).$$

The Fourier transformation of the Keldysh part leads to a contribution $-2i(h^i_{\mathbf{k}})^2\kappa_i F_{\chi_i}(t-t')$ as the quantum-quantum component [21]. The Markovian, or white noise, environment used here is not the only possible choice, it is however justified since the energy interval of interest is small compared with the system energies so the bath's density of states will be approximately constant in this interval. In real units, $\omega_x \sim 1.5$eV and $\min(\omega_{up}(\mathbf{k}) - \omega_{lp}(\mathbf{k})) \sim 20$meV.

The action now contains only the polariton fields:

$$\begin{aligned} S[\Psi] &= \int dt \Bigg\{ \sum_{\mathbf{k}} \Psi^\dagger_{\mathbf{k}} (i\partial_t - \omega_{lp}(\mathbf{k}+\mathbf{k}_p) + \omega_p)\sigma_1^K \Psi_{\mathbf{k}} - \sqrt{2} F_{lp}(\overline{\psi}_{\mathbf{0},q} + \psi_{\mathbf{0},q}) \\ &\quad - \frac{1}{4} \sum_{\mathbf{k},\mathbf{k}',\mathbf{q}} V_{\mathbf{k},\mathbf{k}',\mathbf{q}} \left[\Psi^\dagger_{\mathbf{k}} \sigma_1^K \Psi_{\mathbf{k}-\mathbf{q}} \Psi^\dagger_{\mathbf{k}'} \Psi_{\mathbf{k}'+\mathbf{q}} + \Psi^\dagger_{\mathbf{k}} \Psi_{\mathbf{k}-\mathbf{q}} \Psi^\dagger_{\mathbf{k}'} \sigma_1^K \Psi_{\mathbf{k}'+\mathbf{q}} \right] \Bigg\} \\ &\quad + \iint dt dt' \sum_{\mathbf{k}} \Psi^\dagger_{\mathbf{k}}(t) \begin{pmatrix} 0 & -i\kappa_{lp}(\mathbf{k})\delta(t-t') \\ i\kappa_{lp}(\mathbf{k})\delta(t-t') & 2i \sum\limits_{i\in\{c,x\}} (h^i_{\mathbf{k}})^2 \kappa_i F_{\chi_i}(t-t') \end{pmatrix} \Psi_{\mathbf{k}}(t'). \end{aligned} \tag{3.35}$$

In the last line, the σ_1^K that proceeds and follows $((i\partial_t - \omega_{\mathbf{p}}^{\Gamma^i})\sigma_1^K)^{-1}$ in Eq. (3.31) has been applied to the matrix of the self-energies. In principle, all fields have a time argument and both integrals are double integrals over t and t'. There is no ambiguity in the first integral where the double measure of integration would lead to a factor $\delta(t-t')$ on all elements, so only the single time argument is used.

In the action, the summation over $i \in \{c, x\}$ lead to a contribution from each decay bath with a similar form. This is used to define the momentum dependent lower polariton decay in Eq. (3.35):

$$\kappa_{lp}(\mathbf{k}) = C^2(\mathbf{k}+\mathbf{k}_p)\kappa_c + X^2(\mathbf{k}+\mathbf{k}_p)\kappa_x. \tag{3.36}$$

If the exciton and photon decays are equal, then $\kappa_{lp}(\mathbf{k})$ is a constant due to the normalisation condition of the Hopfield coefficients.

3.2.6 Saddle points and the mean field equations

Having constructed an action in terms of the system fields only, the mean field properties can be investigated through the saddle points taken relative to both the classical and quantum fields [21, 70, 71]. This involves finding the solutions to

$$\frac{\delta S}{\delta \overline{\psi}_{\mathbf{k},cl}(t)} = 0 \qquad \text{and} \qquad \frac{\delta S}{\delta \overline{\psi}_{\mathbf{k},q}(t)} = 0.$$

The action of the derivative is to pick out only those terms that contain one or more copies of the field $\overline{\psi}_{\mathbf{k},\{cl,q\}}$:

$$\begin{aligned} \frac{\delta S}{\delta \overline{\psi}_{\mathbf{k},cl}(t)} &= \int dt \Big[(i\partial_t - \omega_{lp}(\mathbf{k}+\mathbf{k}_p) + \omega_p - i\kappa_{lp}(\mathbf{k}))\psi_{\mathbf{k},q}(t) \\ &\quad - \sum_{\mathbf{k}',\mathbf{q}} \frac{V_{\mathbf{k},\mathbf{k}',\mathbf{q}}}{2} \Big(\bar{\psi}_{\mathbf{k}',q}(t) \Psi^T_{\mathbf{k}-\mathbf{q}}(t) \Psi_{\mathbf{k}'+\mathbf{q}}(t) + \bar{\psi}_{\mathbf{k}',cl}(t) \Psi^T_{\mathbf{k}-\mathbf{q}}(t) \hat{\sigma}_1^K \Psi_{\mathbf{k}'+\mathbf{q}}(t) \Big) \Big], \end{aligned} \tag{3.37}$$

and

$$\frac{\delta S}{\delta\bar{\psi}_{\mathbf{k},q}(t)} = \int dt\Big[(i\partial_t-\omega_{lp}(\mathbf{k})+\omega_p+i\kappa_{lp}(\mathbf{k}+\mathbf{k}_p))\psi_{\mathbf{k},cl}(t)-\sqrt{2}F_{lp}\delta_{\mathbf{k},\mathbf{0}} - \sum_{\mathbf{k}',\mathbf{q}}\frac{V_{\mathbf{k},\mathbf{k}',\mathbf{q}}}{2}\Big(\bar{\psi}_{\mathbf{k}',q}(t)\Psi^T_{\mathbf{k}-\mathbf{q}}(t)\hat{\sigma}_1^K\Psi_{\mathbf{k}'+\mathbf{q}}(t)+\bar{\psi}_{\mathbf{k}',cl}(t)\Psi^T_{\mathbf{k}-\mathbf{q}}(t)\Psi_{\mathbf{k}'+\mathbf{q}}(t)\Big)\Big] +2i\sum_{i\in\{c,x\}}(h^i_{\mathbf{k}})^2\kappa_i\int dtdt' F_{\chi_i}(t-t')\psi_{\mathbf{k},q}(t'). \tag{3.38}$$

There always exists a solution to the saddle point equations such that the quantum part is zero [69–71] at which point $\frac{\delta S}{\delta\bar{\psi}_{\mathbf{k},cl}(t)}=0$ is satisfied automatically. This corresponds to the purely classical solution and the classical component of the field at the saddle point, ψ^{sp}_{cl}, satisfies:

$$(i\partial_t-\omega_{lp}(\mathbf{k}+\mathbf{k}_p)+\omega_p+i\kappa_{lp}(\mathbf{k}))\psi^{sp}_{\mathbf{k},cl}(t)-\sqrt{2}F_{lp}\delta_{\mathbf{k},\mathbf{0}}-\sum_{\mathbf{k}',\mathbf{q}}\frac{V_{\mathbf{k},\mathbf{k}',\mathbf{q}}}{2}\bar{\psi}^{sp}_{\mathbf{k}',cl}(t)\psi^{sp}_{\mathbf{k}-\mathbf{q},cl}(t)\psi^{sp}_{\mathbf{k}'+\mathbf{q},cl}(t)=0. \tag{3.39}$$

Dividing through by the $\sqrt{2}$ factor in front of the external pump, leads to the cGPE from the mean field analysis [29, 30] with $\psi^{\rm mf}=\psi^{sp}_{cl}/\sqrt{2}$ [21]:

$$(i\partial_t-\omega_{lp}(\mathbf{k}+\mathbf{k}_p)+\omega_p+i\kappa_{lp}(\mathbf{k}))\psi^{\rm mf}_{\mathbf{k}}(t)-F_{lp}\delta_{\mathbf{k},\mathbf{0}}-\sum_{\mathbf{k}',\mathbf{q}}V_{\mathbf{k},\mathbf{k}',\mathbf{q}}\left(\bar{\psi}^{\rm mf}_{\mathbf{k}'}(t)\psi^{\rm mf}_{\mathbf{k}-\mathbf{q}}(t)\psi^{\rm mf}_{\mathbf{k}'+\mathbf{q}}(t)\right)=0. \tag{3.40}$$

A steady state solution to the cGPE is proposed (a choice made for ψ) and the mean field calculated. A physical solution requires that the steady state is stable to small fluctuations around the mean field [29, 41]. Only if this condition is satisfied can other quantities, such as the luminescence, absorption or spectral weight, be calculated [21, 91].

3.2.7 Fluctuations about the mean field

To analyse the stability of the mean field, small fluctuations $\delta\psi_{cl}$ and $\delta\psi_q$ are added to the fields in the action. The action of coherently pumped polaritons is given by Eq. (3.35) and can be written slightly more compactly as:

$$S[\Psi] = \int dt\Bigg\{\sum_{\mathbf{k}}\Big[\Psi^\dagger_{\mathbf{k}}\left(A(\mathbf{k})\sigma_1^K-\kappa_{lp}(\mathbf{k})\sigma_2^K\right)\Psi_{\mathbf{k}}+F_{lp}\delta_{\mathbf{0},\mathbf{k}}(\overline{\psi}_{\mathbf{k},q}+\psi_{\mathbf{k},q})\Big] -\frac{1}{4}\sum_{\mathbf{k},\mathbf{k}',\mathbf{q}}V_{\mathbf{k},\mathbf{k}',\mathbf{q}}\Big[\Psi^\dagger_{\mathbf{k}}\sigma_1^K\Psi_{\mathbf{k}-\mathbf{q}}\Psi^\dagger_{\mathbf{k}'}\Psi_{\mathbf{k}'+\mathbf{q}}+\Psi^\dagger_{\mathbf{k}}\Psi_{\mathbf{k}-\mathbf{q}}\Psi^\dagger_{\mathbf{k}'}\sigma_1^K\Psi_{\mathbf{k}'+\mathbf{q}}\Big]\Bigg\} +2i\iint dtdt'\sum_{\substack{\mathbf{k}\\ i\in\{c,x\}}}\overline{\psi}_{\mathbf{k},q}(t)(h^i_{\mathbf{k}})^2\kappa_i F_{\chi_i}(t-t')\psi_{\mathbf{k},q}(t'). \tag{3.41}$$

The fields are written as vectors in the Keldysh basis of classical and quantum fields, and the Pauli matrix

$$\sigma_2^K = \begin{pmatrix} 0 & i \\ -i & 0 \end{pmatrix},$$

and shorthand

$$A(\mathbf{k}) = [i\partial_t - \omega_{lp}(\mathbf{k}_p + \mathbf{k}) + \omega_p]$$

have been introduced. The steady state solution that satisfies the saddle point has the form:

$$\Psi_{\mathbf{k}} = \begin{pmatrix} \psi^{sp}_{\mathbf{k},cl} \\ 0 \end{pmatrix} = \begin{pmatrix} \sqrt{2}\psi^{\mathrm{mf}}_{\mathbf{k}} \\ 0 \end{pmatrix}$$

where the quantum part is zero. Small fluctuations in energy and momentum around the steady state are added. The momenta of the fluctuations appear in the momentum signature of the fields and the fluctuations around each state momentum are the same up to the requirement of momentum conservation of the fluctuations (the steady state solution already satisfies momentum conservation). If momentum conservation cannot be achieved with a finite value of the momentum fluctuation (as is the case for terms linear in the fluctuation fields) then the term in the action is not permitted. Fluctuations in both the classical (around the finite valued steady state solution) and quantum (zero valued steady state solution) fields occur and a Nambu vector for the steady state solution and fluctuations is constructed

$$\Delta\Psi_{\mathbf{k}+\rho} = \begin{pmatrix} \delta\psi_{\mathbf{k}+\rho,cl} \\ \delta\overline{\psi}_{\mathbf{k}-\rho,cl} \\ \delta\psi_{\mathbf{k}+\rho,q} \\ \delta\overline{\psi}_{\mathbf{k}-\rho,q} \end{pmatrix}$$

where ρ is the momentum argument of the fluctuations, and the summation covers all possible momenta around the steady state. Although the momenta of the fluctuations ρ could be included in the momenta $\mathbf{k}, \mathbf{k}', \mathbf{q}$, this would allow fluctuations from two modes to appear at the same place. Therefore the distinction between the momenta of the mean field modes $\mathbf{k}, \mathbf{k}', \mathbf{q}$ and the momenta of the fluctuations ρ which are then restricted such that the momentum ranges around the modes do not overlap. To include fluctuations in the action, the forms

$$\psi_{cl} = \psi^{sp} + \delta\psi_{cl}; \qquad \psi_q = \delta\psi_q$$

are substituted into the Eq. (3.41) which gives half the terms in the action with fluctuations. The other half is found by considering the change of variables,

$$\int_{-a}^{a} dx f(x) \;=\; -\int_{a}^{-a} dx f(-x) \;=\; \frac{1}{2}\left[\int_{-a}^{a} dx f(x) - \int_{a}^{-a} dx f(-x)\right] \tag{3.42}$$

and summation

$$\sum_{i=a}^{b} f_i = \frac{1}{2}\left[\sum_{i=-a}^{b} f_i + \sum_{i=-b}^{a} f_{-i}\right]. \tag{3.43}$$

In the first two terms of the action and in the last term, all the fields have the same momentum signature and including the fluctuations is straightforward. When the fluctuations are included, the first term in Eq. (3.41) becomes:

$$\int dt \sum_{\mathbf{k},\rho} \begin{array}{l} [\overline{\psi}^{sp}_{\mathbf{k},cl}\left(A(\mathbf{k}) - i\kappa(\mathbf{k})\right)\delta\psi_{\mathbf{k}+\rho,q} + \delta\overline{\psi}_{\mathbf{k}+\rho,cl}\left(A(\mathbf{k}+\rho) - i\kappa(\mathbf{k}+\rho)\right)\delta\psi_{\mathbf{k}+\rho,q} \\ +\delta\overline{\psi}_{\mathbf{k}+\rho,q}\left(A(\mathbf{k}) + i\kappa_{lp}(\mathbf{k})\right)\psi^{sp}_{\mathbf{k},cl} + \delta\overline{\psi}_{\mathbf{k}+\rho,q}\left(A(\mathbf{k}+\rho) + i\kappa_{lp}(\mathbf{k}+\rho)\right)\delta\psi_{\mathbf{k}+\rho,cl}] \end{array}$$

the first and third terms are linear in the fluctuations and so are not allowed. The second (pump) term in Eq. (3.41) contains only a single quantum component of the field and is also linear in fluctuations. The pump term is also not affected by the fluctuations due to the $\delta_{\mathbf{0},\mathbf{k}}$ factor which links to the physical restriction that the pump couples only to polaritons with momentum $\mathbf{k} = \mathbf{0}$. The last term of Eq. (3.41) is quadratic in the quantum components of the fields and also in fluctuations:

$$2i\iint dtdt' \sum_{\substack{\mathbf{k},\rho \\ i\in\{c,x\}}} \left(\delta\overline{\psi}_{\mathbf{k}+\rho,q}(t)(h^i_{\mathbf{k}+\rho})^2\kappa_i F_{\chi_i}(t-t')\delta\psi_{\mathbf{k}+\rho,q}(t')\right).$$

The interaction term contains four fields at different momenta and the condition of momentum conservation is imposed at the steady state level and on the fluctuations on top of the steady state. To understand fully how the fluctuation fields appear in the interaction term, the momentum of each field is considered to fluctuate independently: each of the four fields has its own set of fluctuations, the relations between the momenta of these fluctuations will be found and then momentum conservation used to eliminate terms as necessary and determine the new interaction strengths.

The momentum signatures of the fluctuations are:

$$\begin{aligned} \mathbf{k} &\rightarrow \mathbf{k} + \rho_1 \\ \mathbf{k} - \mathbf{q} &\rightarrow \mathbf{k} - \mathbf{q} + \rho_2 \\ \mathbf{k}' &\rightarrow \mathbf{k}' + \rho_3 \\ \mathbf{k}' + \mathbf{q} &\rightarrow \mathbf{k}' + \mathbf{q} + \rho_4 \end{aligned}$$

and the aim is to find the relations between ρ_1, ρ_2, ρ_3 and ρ_4 in each of the interaction terms. The fields are all expanded according to the standard form, with the fluctuations around each field contributing a summation over the different momenta ρ_i. The summation over the original momenta and the interaction coefficient are not of interest at this stage and will be restored in

due course. The first of the two interaction terms is expanded out in the basis of fields plus fluctuations:

$$\begin{aligned}\Psi^\dagger_{\mathbf{k}}\sigma_1^K\Psi_{\mathbf{k}-\mathbf{q}}\Psi^\dagger_{\mathbf{k}'}\Psi_{\mathbf{k}'+\mathbf{q}} = &\Big(\overline{\psi}_{\mathbf{k},cl}\sum_{\rho_2}\delta\psi_{\mathbf{k}-\mathbf{q}+\rho_2,q} + \sum_{\rho_1,\rho_2}\delta\overline{\psi}_{\mathbf{k}+\rho_1,cl}\delta\psi_{\mathbf{k}-\mathbf{q}+\rho_2,q} \\ &+ \sum_{\rho_1}\delta\overline{\psi}_{\mathbf{k}+\rho_1,cl}\psi_{\mathbf{k}-\mathbf{q},cl} + \sum_{\rho_1,\rho_2}\delta\overline{\psi}_{\mathbf{k}+\rho_1,cl}\delta\psi_{\mathbf{k}-\mathbf{q}+\rho_2,cl}\Big) \\ &\times\Big(\overline{\psi}_{\mathbf{k}',cl}\psi_{\mathbf{k}'+\mathbf{q},cl} + \overline{\psi}_{\mathbf{k}',cl}\sum_{\rho_4}\delta\psi_{\mathbf{k}'+\mathbf{q}+\rho_4,cl} + \sum_{\rho_3}\delta\overline{\psi}_{\mathbf{k}'+\rho_3,cl}\psi_{\mathbf{k}'+\mathbf{q},cl} \\ &+ \sum_{\rho_3,\rho_4}\delta\overline{\psi}_{\mathbf{k}'+\rho_3,cl}\delta\psi_{\mathbf{k}'+\mathbf{q}+\rho_4,cl} + \sum_{\rho_3,\rho_4}\delta\overline{\psi}_{\mathbf{k}'+\rho_3,q}\delta\psi_{\mathbf{k}'+\mathbf{q}+\rho_4,q}\Big) \qquad (3.44)\end{aligned}$$

Expanding the first half leads to 20 terms; the second half is simply the substitution $\delta\psi_\rho \to \delta\overline{\psi}_{-\rho}$ and $\delta\overline{\psi}_\rho \to \delta\psi_{-\rho}$. To break this down, the terms in the first bracket are considered in order, and the restrictions on the ρ_i that are necessary to satisfy momentum conservation of the polariton scattering noted.

From the first term:

$$\begin{aligned}\sum_{\rho_2}\overline{\psi}_{\mathbf{k},cl}\delta\psi_{\mathbf{k}-\mathbf{q}+\rho_2,q}\overline{\psi}_{\mathbf{k}',cl}\psi_{\mathbf{k}'+\mathbf{q},cl} &\qquad \text{Linear in fluctuations}\\ \sum_{\rho_2,\rho_4}\overline{\psi}_{\mathbf{k},cl}\delta\psi_{\mathbf{k}-\mathbf{q}+\rho_2,q}\overline{\psi}_{\mathbf{k}',cl}\delta\psi_{\mathbf{k}'+\mathbf{q}+\rho_4,cl} &\qquad \Rightarrow \rho_2 = -\rho_4\\ \sum_{\rho_2,\rho_3}\overline{\psi}_{\mathbf{k},cl}\delta\psi_{\mathbf{k}-\mathbf{q}+\rho_2,q}\delta\overline{\psi}_{\mathbf{k}'+\rho_3,cl}\psi_{\mathbf{k}'+\mathbf{q},cl} &\qquad \Rightarrow \rho_2 = \rho_3\\ \sum_{\rho_2,\rho_3,\rho_4}\overline{\psi}_{\mathbf{k},cl}\delta\psi_{\mathbf{k}-\mathbf{q}+\rho_2,q}\delta\overline{\psi}_{\mathbf{k}'+\rho_3,cl}\delta\psi_{\mathbf{k}'+\mathbf{q}+\rho_4,cl} &\qquad \Rightarrow \rho_3 = \rho_2+\rho_4\\ \sum_{\rho_2,\rho_3,\rho_4}\overline{\psi}_{\mathbf{k},cl}\delta\psi_{\mathbf{k}-\mathbf{q}+\rho_2,q}\delta\overline{\psi}_{\mathbf{k}'+\rho_3,q}\delta\psi_{\mathbf{k}'+\mathbf{q}+\rho_4,q} &\qquad \Rightarrow \rho_3 = \rho_2+\rho_4\end{aligned}$$

From the second term:

$$\begin{aligned}\sum_{\rho_1,\rho_2}\delta\overline{\psi}_{\mathbf{k}+\rho_1,cl}\delta\psi_{\mathbf{k}-\mathbf{q}+\rho_2,q}\overline{\psi}_{\mathbf{k}',cl}\psi_{\mathbf{k}'+\mathbf{q},cl} &\qquad \Rightarrow \rho_1 = \rho_2\\ \sum_{\rho_1,\rho_2,\rho_4}\delta\overline{\psi}_{\mathbf{k}+\rho_1,cl}\delta\psi_{\mathbf{k}-\mathbf{q}+\rho_2,q}\overline{\psi}_{\mathbf{k}',cl}\delta\psi_{\mathbf{k}'+\mathbf{q}+\rho_4,cl} &\qquad \Rightarrow \rho_1 = \rho_2+\rho_4\\ \sum_{\rho_1,\rho_2,\rho_3}\delta\overline{\psi}_{\mathbf{k}+\rho_1,cl}\delta\psi_{\mathbf{k}-\mathbf{q}+\rho_2,q}\delta\overline{\psi}_{\mathbf{k}'+\rho_3,cl}\psi_{\mathbf{k}'+\mathbf{q},cl} &\qquad \Rightarrow \rho_1+\rho_3 = \rho_2\\ \sum_{\rho_1,\rho_2,\rho_3,\rho_4}\delta\overline{\psi}_{\mathbf{k}+\rho_1,cl}\delta\psi_{\mathbf{k}-\mathbf{q}+\rho_2,q}\delta\overline{\psi}_{\mathbf{k}'+\rho_3,cl}\delta\psi_{\mathbf{k}'+\mathbf{q}+\rho_4,cl} &\qquad \Rightarrow \rho_1+\rho_3 = \rho_2+\rho_4\\ \sum_{\rho_1,\rho_2,\rho_3,\rho_4}\delta\overline{\psi}_{\mathbf{k}+\rho_1,cl}\delta\psi_{\mathbf{k}-\mathbf{q}+\rho_2,q}\delta\overline{\psi}_{\mathbf{k}'+\rho_3,q}\delta\psi_{\mathbf{k}'+\mathbf{q}+\rho_4,q} &\qquad \Rightarrow \rho_1+\rho_3 = \rho_2+\rho_4\end{aligned}$$

From the third term:

$$\sum_{\rho_1} \delta\overline{\psi}_{\mathbf{k}+\rho_1,q}\psi_{\mathbf{k}-\mathbf{q},cl}\overline{\psi}_{\mathbf{k}',cl}\psi_{\mathbf{k}'+\mathbf{q},cl} \qquad \text{Linear in fluctuations}$$

$$\sum_{\rho_1,\rho_4} \delta\overline{\psi}_{\mathbf{k}+\rho_1,q}\psi_{\mathbf{k}-\mathbf{q},cl}\overline{\psi}_{\mathbf{k}',cl}\delta\psi_{\mathbf{k}'+\mathbf{q}+\rho_4,cl} \qquad \Rightarrow \rho_1 = \rho_4$$

$$\sum_{\rho_1,\rho_3} \delta\overline{\psi}_{\mathbf{k}+\rho_1,q}\psi_{\mathbf{k}-\mathbf{q},cl}\delta\overline{\psi}_{\mathbf{k}'+\rho_3,cl}\psi_{\mathbf{k}'+\mathbf{q},cl} \qquad \Rightarrow \rho_1 = -\rho_3$$

$$\sum_{\rho_1,\rho_3,\rho_4} \delta\overline{\psi}_{\mathbf{k}+\rho_1,q}\psi_{\mathbf{k}-\mathbf{q},cl}\delta\overline{\psi}_{\mathbf{k}'+\rho_3,cl}\delta\psi_{\mathbf{k}'+\mathbf{q}+\rho_4,cl} \qquad \Rightarrow \rho_1 + \rho_3 = \rho_4$$

$$\sum_{\rho_1,,\rho_3,\rho_4} \delta\overline{\psi}_{\mathbf{k}+\rho_1,q}\psi_{\mathbf{k}-\mathbf{q},cl}\delta\overline{\psi}_{\mathbf{k}'+\rho_3,q}\delta\psi_{\mathbf{k}'+\mathbf{q}+\rho_4,q} \qquad \Rightarrow \rho_1 + \rho_3 = \rho_4$$

From the fourth term:

$$\sum_{\rho_1,\rho_2} \delta\overline{\psi}_{\mathbf{k}+\rho_1,q}\delta\psi_{\mathbf{k}-\mathbf{q}+\rho_2,cl}\overline{\psi}_{\mathbf{k}',cl}\psi_{\mathbf{k}'+\mathbf{q},cl} \qquad \Rightarrow \rho_1 = \rho_2$$

$$\sum_{\rho_1,\rho_2,\rho_4} \delta\overline{\psi}_{\mathbf{k}+\rho_1,q}\delta\psi_{\mathbf{k}-\mathbf{q}+\rho_2,cl}\overline{\psi}_{\mathbf{k}',cl}\delta\psi_{\mathbf{k}'+\mathbf{q}+\rho_4,cl} \qquad \Rightarrow \rho_1 = \rho_2 + \rho_4$$

$$\sum_{\rho_1,\rho_2,\rho_3} \delta\overline{\psi}_{\mathbf{k}+\rho_1,q}\delta\psi_{\mathbf{k}-\mathbf{q}+\rho_2,cl}\delta\overline{\psi}_{\mathbf{k}'+\rho_3,cl}\psi_{\mathbf{k}'+\mathbf{q},cl} \qquad \Rightarrow \rho_1 + \rho_3 = \rho_2$$

$$\sum_{\rho_1,\rho_2,\rho_3,\rho_4} \delta\overline{\psi}_{\mathbf{k}+\rho_1,q}\delta\psi_{\mathbf{k}-\mathbf{q}+\rho_2,cl}\delta\overline{\psi}_{\mathbf{k}'+\rho_3,cl}\delta\psi_{\mathbf{k}'+\mathbf{q}+\rho_4,cl} \qquad \Rightarrow \rho_1 + \rho_3 = \rho_2 + \rho_4$$

$$\sum_{\rho_1,\rho_2,\rho_3,\rho_4} \delta\overline{\psi}_{\mathbf{k}+\rho_1,q}\delta\psi_{\mathbf{k}-\mathbf{q}+\rho_2,cl}\delta\overline{\psi}_{\mathbf{k}'+\rho_3,q}\delta\psi_{\mathbf{k}'+\mathbf{q}+\rho_4,q} \qquad \Rightarrow \rho_1 + \rho_3 = \rho_2 + \rho_4$$

The Nambu vector form requires a single fluctuation field, which means that the $|\rho_i|$ have to be equal. Any terms that are cubic in the fluctuations are discarded since enforcing equal amplitudes of momenta would now break momentum conservation (the linear terms have already been discarded as discussed above and the mean field states already satisfy momentum conservation). Several possible combinations of momentum fluctuation arguments are now possible, as detailed in table 3.3

ρ_1	ρ_3	ρ_2	ρ_4
$\pm\rho$		$\pm\rho$	
$\pm\rho$			$\pm\rho$
	$\pm\rho$	$\pm\rho$	
	$\pm\rho$		$\pm\rho$
$\pm\rho$	$\mp\rho$		
		$\pm\rho$	$\mp\rho$
$\pm\rho$	$\pm\rho$	$\mp\rho$	$\mp\rho$
$\pm\rho$	$\mp\rho$	$\pm\rho$	$\mp\rho$

Table 3.3: Momentum signatures of fluctuations according to momentum conservation in a single momentum field on top of state that satisfies momentum conservation.

The implications of the momentum conservation are the same for the second part of the interaction term. For constructing the complete action of general fluctuations, it is useful to expand out as before:

$$\begin{aligned}\Psi^\dagger_{\mathbf{k}}\Psi_{\mathbf{k}-\mathbf{q}}\Psi^\dagger_{\mathbf{k}}\sigma_1^K\Psi_{\mathbf{k}-\mathbf{q}} = \Big(&\overline{\psi}_{\mathbf{k},cl}\psi_{\mathbf{k}-\mathbf{q},cl} + \overline{\psi}_{\mathbf{k},cl}\sum_{\rho_2}\delta\psi_{\mathbf{k}-\mathbf{q}+\rho_2,cl} \\ &+ \sum_{\rho_1}\delta\overline{\psi}_{\mathbf{k}+\rho_1,cl}\psi_{\mathbf{k}-\mathbf{q},cl} + \sum_{\rho_1,\rho_2}\delta\overline{\psi}_{\mathbf{k}+\rho_1,cl}\delta\psi_{\mathbf{k}-\mathbf{q}+\rho_2,cl} \\ &+ \sum_{\rho_1,\rho_2}\delta\overline{\psi}_{\mathbf{k}+\rho_1,q}\delta\psi_{\mathbf{k}-\mathbf{q}+\rho_2,q}\Big) \\ \times\Big(&\overline{\psi}_{\mathbf{k}',cl}\sum_{\rho_4}\delta\psi_{\mathbf{k}'+\mathbf{q}+\rho_4,q} + \sum_{\rho_3,\rho_4}\delta\overline{\psi}_{\mathbf{k}'+\rho_3,cl}\delta\psi_{\mathbf{k}'+\mathbf{q}+\rho_4,q} \\ &+ \sum_{\rho_3}\delta\overline{\psi}_{\mathbf{k}'+\rho_3,cl}\psi_{\mathbf{k}'+\mathbf{q},cl} + \sum_{\rho_3,\rho_4}\delta\overline{\psi}_{\mathbf{k}'+\rho_3,cl}\delta\psi_{\mathbf{k}'+\mathbf{q}+\rho_4,cl}\Big). \end{aligned} \tag{3.45}$$

Again, considering the terms resulting from the first bracket individually is convenient.

From the first term:

$$\sum_{\rho_4}\overline{\psi}_{\mathbf{k},cl}\psi_{\mathbf{k}-\mathbf{q},cl}\overline{\psi}_{\mathbf{k}',cl}\delta\psi_{\mathbf{k}'+\mathbf{q}+\rho_4,q} \qquad \text{Linear in fluctuations}$$

$$\sum_{\rho_3,\rho_4}\overline{\psi}_{\mathbf{k},cl}\psi_{\mathbf{k}-\mathbf{q},cl}\delta\overline{\psi}_{\mathbf{k}'+\rho_3,cl}\delta\psi_{\mathbf{k}'+\mathbf{q}+\rho_4,q} \qquad \Rightarrow \rho_3 = \rho_4$$

$$\sum_{\rho_3}\overline{\psi}_{\mathbf{k},cl}\psi_{\mathbf{k}-\mathbf{q},cl}\delta\overline{\psi}_{\mathbf{k}'+\rho_3,cl}\psi_{\mathbf{k}'+\mathbf{q},cl} \qquad \text{Linear in fluctuations}$$

$$\sum_{\rho_3,\rho_4}\overline{\psi}_{\mathbf{k},cl}\psi_{\mathbf{k}-\mathbf{q},cl}\delta\overline{\psi}_{\mathbf{k}'+\rho_3,cl}\delta\psi_{\mathbf{k}'+\mathbf{q}+\rho_4,cl} \qquad \Rightarrow \rho_3 = \rho_4$$

From the second term:

$$\sum_{\rho_2,\rho_4}\overline{\psi}_{\mathbf{k},cl}\delta\psi_{\mathbf{k}-\mathbf{q}+\rho_2,cl}\overline{\psi}_{\mathbf{k}',cl}\delta\psi_{\mathbf{k}'+\mathbf{q}+\rho_4,q} \qquad \Rightarrow \rho_2 = -\rho_4$$

$$\sum_{\rho_2,\rho_3,\rho_4}\overline{\psi}_{\mathbf{k},cl}\delta\psi_{\mathbf{k}-\mathbf{q}+\rho_2,cl}\delta\overline{\psi}_{\mathbf{k}'+\rho_3,cl}\delta\psi_{\mathbf{k}'+\mathbf{q}+\rho_4,q} \qquad \Rightarrow \rho_3 = \rho_2 + \rho_4$$

$$\sum_{\rho_2,\rho_3}\overline{\psi}_{\mathbf{k},cl}\delta\psi_{\mathbf{k}-\mathbf{q}+\rho_2,cl}\delta\overline{\psi}_{\mathbf{k}'+\rho_3,cl}\psi_{\mathbf{k}'+\mathbf{q},cl} \qquad \Rightarrow \rho_2 = \rho_3$$

$$\sum_{\rho_2,\rho_3,\rho_4}\overline{\psi}_{\mathbf{k},cl}\delta\psi_{\mathbf{k}-\mathbf{q}+\rho_2,cl}\delta\overline{\psi}_{\mathbf{k}'+\rho_3,cl}\delta\psi_{\mathbf{k}'+\mathbf{q}+\rho_4,cl} \qquad \Rightarrow \rho_3 = \rho_2 + \rho_4$$

From the third term:

$$\sum_{\rho_1,\rho_4}\delta\overline{\psi}_{\mathbf{k}+\rho_1,cl}\psi_{\mathbf{k}-\mathbf{q},cl}\overline{\psi}_{\mathbf{k}',cl}\delta\psi_{\mathbf{k}'+\mathbf{q}+\rho_4,q} \qquad \Rightarrow \rho_1 = \rho_4$$

$$\sum_{\rho_1,\rho_3,\rho_4} \delta\overline{\psi}_{\mathbf{k}+\rho_1,cl}\psi_{\mathbf{k}-\mathbf{q},cl}\delta\overline{\psi}_{\mathbf{k}'+\rho_3,cl}\delta\psi_{\mathbf{k}'+\mathbf{q}+\rho_4,q} \qquad \Rightarrow \rho_1+\rho_3=\rho_4$$

$$\sum_{\rho_1,\rho_3} \delta\overline{\psi}_{\mathbf{k}+\rho_1,cl}\psi_{\mathbf{k}-\mathbf{q},cl}\delta\overline{\psi}_{\mathbf{k}'+\rho_3,cl}\psi_{\mathbf{k}'+\mathbf{q},cl} \qquad \Rightarrow \rho_1=-\rho_3$$

$$\sum_{\rho_1,\rho_3,\rho_4} \delta\overline{\psi}_{\mathbf{k}+\rho_1,cl}\psi_{\mathbf{k}-\mathbf{q},cl}\delta\overline{\psi}_{\mathbf{k}'+\rho_3,cl}\delta\psi_{\mathbf{k}'+\mathbf{q}+\rho_4,cl} \qquad \Rightarrow \rho_1+\rho_3=\rho_4$$

From the fourth term:

$$\sum_{\rho_1,\rho_2,\rho_4} \delta\overline{\psi}_{\mathbf{k}+\rho_1,cl}\delta\psi_{\mathbf{k}-\mathbf{q}+\rho_2,cl}\overline{\psi}_{\mathbf{k}',cl}\delta\psi_{\mathbf{k}'+\mathbf{q}+\rho_4,q} \qquad \Rightarrow \rho_1=\rho_2+\rho_4$$

$$\sum_{\rho_1,\rho_2,\rho_3,\rho_4} \delta\overline{\psi}_{\mathbf{k}+\rho_1,cl}\delta\psi_{\mathbf{k}-\mathbf{q}+\rho_2,cl}\delta\overline{\psi}_{\mathbf{k}'+\rho_3,cl}\delta\psi_{\mathbf{k}'+\mathbf{q}+\rho_4,q} \qquad \Rightarrow \rho_1+\rho_3=\rho_2+\rho_4$$

$$\sum_{\rho_1,\rho_2,\rho_3} \delta\overline{\psi}_{\mathbf{k}+\rho_1,cl}\delta\psi_{\mathbf{k}-\mathbf{q}+\rho_2,cl}\delta\overline{\psi}_{\mathbf{k}'+\rho_3,cl}\psi_{\mathbf{k}'+\mathbf{q},cl} \qquad \Rightarrow \rho_1+\rho_3=\rho_4$$

$$\sum_{\rho_1,\rho_2,\rho_3,\rho_4} \delta\overline{\psi}_{\mathbf{k}+\rho_1,cl}\delta\psi_{\mathbf{k}-\mathbf{q}+\rho_2,cl}\delta\overline{\psi}_{\mathbf{k}'+\rho_3,cl}\delta\psi_{\mathbf{k}'+\mathbf{q}+\rho_4,cl} \qquad \Rightarrow \rho_1+\rho_3=\rho_2+\rho_4$$

From the fifth term:

$$\sum_{\rho_1,\rho_2,\rho_4} \delta\overline{\psi}_{\mathbf{k}+\rho_1,q}\delta\psi_{\mathbf{k}-\mathbf{q}+\rho_2,q}\overline{\psi}_{\mathbf{k}',cl}\delta\psi_{\mathbf{k}'+\mathbf{q}+\rho_4,q} \qquad \Rightarrow \rho_1=\rho_2+\rho_4$$

$$\sum_{\rho_1,\rho_2,\rho_3,\rho_4} \delta\overline{\psi}_{\mathbf{k}+\rho_1,q}\delta\psi_{\mathbf{k}-\mathbf{q}+\rho_2,q}\delta\overline{\psi}_{\mathbf{k}'+\rho_3,cl}\delta\psi_{\mathbf{k}'+\mathbf{q}+\rho_4,q} \qquad \Rightarrow \rho_1+\rho_3=\rho_2+\rho_4$$

$$\sum_{\rho_1,\rho_2,\rho_3} \delta\overline{\psi}_{\mathbf{k}+\rho_1,q}\delta\psi_{\mathbf{k}-\mathbf{q}+\rho_2,q}\delta\overline{\psi}_{\mathbf{k}'+\rho_3,cl}\psi_{\mathbf{k}'+\mathbf{q},cl} \qquad \Rightarrow \rho_1+\rho_3=\rho_2$$

$$\sum_{\rho_1,\rho_2,\rho_3,\rho_4} \delta\overline{\psi}_{\mathbf{k}+\rho_1,q}\delta\psi_{\mathbf{k}-\mathbf{q}+\rho_2,q}\delta\overline{\psi}_{\mathbf{k}'+\rho_3,cl}\delta\psi_{\mathbf{k}'+\mathbf{q}+\rho_4,cl} \qquad \Rightarrow \rho_1+\rho_3=\rho_2+\rho_4$$

For the calculation of the inverse Green's functions, only terms that are quadratic in the fluctuations are kept; the terms that are quartic in the fluctuations that satisfy momentum conservation are considered to be small compared to those that are quadratic in the fluctuations. The action that is quadratic in fluctuations includes a summation over the momenta of the fluctuations:

$$\begin{aligned}
&iS[\Delta\Psi] = \\
&\int dt\Big\{\sum_{\mathbf{k},\rho}[\delta\overline{\psi}_{\mathbf{k}+\rho,cl}\left(A(\mathbf{k}+\rho)-i\kappa(\mathbf{k}+\rho)\right)\delta\psi_{\mathbf{k}+\rho,q}+\delta\overline{\psi}_{\mathbf{k}+\rho,q}\left(A(\mathbf{k}+\rho)+i\kappa(\mathbf{k}+\rho)\right)\delta\psi_{\mathbf{k}+\rho,cl}] \\
&-\frac{1}{4}\sum_{\substack{\mathbf{k},\mathbf{k}',\mathbf{q}\\ \rho}}\Big[V_{\mathbf{k},\mathbf{k}',\mathbf{q}-\rho}(\overline{\psi}_{\mathbf{k},cl}\delta\psi_{\mathbf{k}-\mathbf{q}+\rho,q}\overline{\psi}_{\mathbf{k}',cl}\delta\psi_{\mathbf{k}'+\mathbf{q}-\rho,cl}+\overline{\psi}_{\mathbf{k},cl}\delta\psi_{\mathbf{k}-\mathbf{q}+\rho,cl}\overline{\psi}_{\mathbf{k}',cl}\delta\psi_{\mathbf{k}'+\mathbf{q}-\rho,q}) \\
&+V_{\mathbf{k},\mathbf{k}'+\rho,\mathbf{q}-\rho}(\overline{\psi}_{\mathbf{k},cl}\delta\psi_{\mathbf{k}-\mathbf{q}+\rho,cl}\delta\overline{\psi}_{\mathbf{k}'+\rho,cl}\psi_{\mathbf{k}'+\mathbf{q},cl}+\overline{\psi}_{\mathbf{k},cl}\delta\psi_{\mathbf{k}-\mathbf{q}+\rho,q}\delta\overline{\psi}_{\mathbf{k}'+\rho,cl}\psi_{\mathbf{k}'+\mathbf{q},cl}) \\
&+V_{\mathbf{k}+\rho,\mathbf{k}',\mathbf{q}}(\delta\overline{\psi}_{\mathbf{k}+\rho,cl}\delta\psi_{\mathbf{k}-\mathbf{q}+\rho,q}\overline{\psi}_{\mathbf{k}',cl}\psi_{\mathbf{k}'+\mathbf{q},cl}+\delta\overline{\psi}_{\mathbf{k}+\rho,q}\delta\psi_{\mathbf{k}-\mathbf{q}+\rho,cl}\overline{\psi}_{\mathbf{k}',cl}\psi_{\mathbf{k}'+\mathbf{q},cl})
\end{aligned}$$

$$+ V_{\mathbf{k}+\rho,\mathbf{k}',\mathbf{q}+\rho}(\delta\overline{\psi}_{\mathbf{k}+\rho,q}\psi_{\mathbf{k}-\mathbf{q},cl}\overline{\psi}_{\mathbf{k}',cl}\delta\psi_{\mathbf{k}'+\mathbf{q}+\rho,cl} + \delta\overline{\psi}_{\mathbf{k}+\rho,cl}\psi_{\mathbf{k}-\mathbf{q},cl}\overline{\psi}_{\mathbf{k}',cl}\delta\psi_{\mathbf{k}'+\mathbf{q}+\rho,q})$$
$$+ V_{\mathbf{k},\mathbf{k}'+\rho,\mathbf{q}}(\overline{\psi}_{\mathbf{k},cl}\psi_{\mathbf{k}-\mathbf{q},cl}\delta\overline{\psi}_{\mathbf{k}'+\rho,cl}\delta\psi_{\mathbf{k}'+\mathbf{q}+\rho,q} + \overline{\psi}_{\mathbf{k},cl}\psi_{\mathbf{k}-\mathbf{q},cl}\delta\overline{\psi}_{\mathbf{k}'+\rho,cl}\delta\psi_{\mathbf{k}'+\mathbf{q}+\rho,cl})$$
$$+ V_{\mathbf{k}+\rho,\mathbf{k}'-\rho,\mathbf{q}+\rho}(\delta\overline{\psi}_{\mathbf{k}+\rho,q}\psi_{\mathbf{k}-\mathbf{q},cl}\delta\overline{\psi}_{\mathbf{k}'-\rho,cl}\psi_{\mathbf{k}'+\mathbf{q},cl} + \delta\overline{\psi}_{\mathbf{k}+\rho,cl}\psi_{\mathbf{k}-\mathbf{q},cl}\delta\overline{\psi}_{\mathbf{k}'-\rho,cl}\psi_{\mathbf{k}'+\mathbf{q},cl})\Big]\Big\}$$
$$- 2i\iint dtdt' \sum_{\substack{\mathbf{k},\rho \\ i\in\{c,x\}}} \left(\delta\overline{\psi}_{\mathbf{k}+\rho,q}(t)(h^i_{\mathbf{k}+\rho})^2\kappa_i F_{\chi_i}(t-t')\delta\psi_{\mathbf{k}+\rho,q}(t')\right) \tag{3.46}$$

All quantities of interest will be calculated in energy-momentum space so the Fourier transform is performed. In Eq. (3.46), only half the necessary fields are present, the remaining fields are restored by using Eqs. (3.42) and (3.43), and the action including fluctuations has the form:

$$iS[\Delta\Psi] = \int d\omega \sum_\rho \Delta\Psi^\dagger_\rho(\omega) \begin{pmatrix} 0 & [D^{-1}]^A \\ [D^{-1}]^R & [D^{-1}]^K \end{pmatrix} \Delta\Psi_\rho(\omega) \tag{3.47}$$

where $[D^{-1}]^{\{R/A/K\}} = [D^{-1}]^{\{R/A/K\}}(\omega,\rho)$ and R, A, K indicate the retarded, advanced and Keldysh components of the inverse Green's function respectively. The summation over the fluctuation momenta ρ is included explicitly, while the system's steady state momenta are hidden. Without making an explicit choice of the system momenta $\mathbf{k}, \mathbf{k}'$ and $\mathbf{q}$, nothing more can be said about the general form of the inverse Green's functions. The fluctuations are written using a Nambu vector form [21]:

$$\Delta\Psi_\rho(\omega) = \begin{pmatrix} \delta\psi_{\rho,cl}(\omega) \\ \delta\bar{\psi}_{-\rho,cl}(-\omega) \\ \delta\psi_{\rho,q}(\omega) \\ \delta\bar{\psi}_{-\rho,q}(-\omega) \end{pmatrix}, \tag{3.48}$$

where each $\delta\psi$ has the structure $(\delta\psi_1, \delta\psi_2 \ldots)^T$ for system momenta $\mathbf{k}_m = 1, 2 \ldots$ and the fluctuations are around these momenta ($_{\pm\rho}(\pm\omega) \rightarrow_{\mathbf{k}_m\pm\rho} (\omega_m \pm \omega)$). Here, ω is the energy fluctuation away from the system momentum (energy conservation on ω could have been used instead of momentum conservation to justify discarding terms linear and cubic in the fluctuations).

3.2.8 Inversion of Keldysh rotation: physical quantities

To calculate physical observables such as the luminescence and absorption spectra of the polariton system, the Keldysh rotation is inverted to find the forwards ($<$) and backwards ($>$) Green's functions [21, 70, 71]:

$$\begin{aligned} D^{<,>} &= \frac{1}{2}(D^K \mp (D^R - D^A)); \\ D^< &= -i\langle\psi_f\psi_b^\dagger\rangle, \\ D^> &= -i\langle\psi_b\psi_f^\dagger\rangle. \end{aligned} \tag{3.49}$$

$D^<$ describe the average density of particles in a system with energy ω and momentum ρ, while $D^>$ is the density of states available to an additional particle [88]. The incoherent luminescence and absorption spectra *around* the mean field can be defined as [21]:

$$L(\omega,\rho) = \frac{i}{2\pi}D^<(\omega,\rho), \tag{3.50}$$

$$A(\omega,\rho) = \frac{i}{2\pi}D^>(\omega,\rho). \tag{3.51}$$

The finite occupations from the mean field are not included; these are spectra of the fluctuations only. One important feature is that $D^{R,A,K}$ all contain $\det([D^{-1}]^R)$ in the denominator; if this is zero while the numerator remains non-zero, then the luminescence or absorption diverges, indicating that the mean field solution is unstable and that there is a transition to another phase.

In experiments polaritons are observed through the photon losses from the microcavities. The photon luminescence is obtained by extracting the photon part through multiplication by the (momentum dependent) photon fraction $C^2(\rho+\mathbf{k}_p)$, defined in section 2.3:

$$L_{phot} = C^2(\rho+\mathbf{k}_p)L_{lp}. \tag{3.52}$$

The spectral weight is defined as the difference between the absorption and luminescence. In terms of the Green's functions [91],

$$SW(\omega,\rho) = A(\omega,\rho) - L(\omega,\rho) = \frac{i}{2\pi}(D^R - D^A), \tag{3.53}$$

or $1/(2\pi)$ times the spectral response [72] or spectral function [88].

3.3 Pump only case and OPO threshold

As in previous studies of polariton OPO, the first step is to investigate the case of a single pump mode with a well defined energy and momentum [28, 29]. The mean field occupations and complex amplitudes are calculated and fluctuations are then added to obtain the inverse Green's functions according to the scheme outlined in the previous section. At this point, it is useful to set the convention that the pump *strength* refers to F_{lp} while the pump *power* is $I_p = |F_{lp}|^2$.

3.3.1 Pump only mean field and fluctuations

The pump only mean field is found by choosing $\mathbf{k} = \mathbf{k}' = \mathbf{q} = \mathbf{0}$, where the polariton scattering remains within the pump mode. This can be done either in Eq. (3.40) or in the action and the saddle point then calculated, the latter approach is followed here. The action in the case of a

single mode at the pump is:

$$S[\Psi_{\mathbf{0}}] = \int dt\Bigg\{\Psi_{\mathbf{0}}^{\dagger}(i\partial_t-\omega_{lp}(\mathbf{k}_p)+\omega_p)\sigma_1^K\Psi_{\mathbf{0}}-\sqrt{2}F_{lp}(\overline{\psi}_{\mathbf{0},q}+\psi_{\mathbf{0},q})-\frac{1}{2}V_{\mathbf{0},\mathbf{0},\mathbf{0}}\Psi_{\mathbf{0}}^{\dagger}\sigma_1^K\Psi_{\mathbf{0}}\Psi_{\mathbf{0}}^{\dagger}\Psi_{\mathbf{0}}\Bigg\}$$
$$+\iint dtdt'\Psi_{\mathbf{0}}^{\dagger}(t)\begin{pmatrix}0 & -i\kappa_{lp}(\mathbf{0})\delta(t-t')\\ i\kappa_{lp}(\mathbf{0})\delta(t-t') & 2i\sum\limits_{i\in\{c,x\}}(h_{\mathbf{0}}^i)^2\kappa_i F_{\chi_i}(t-t')\end{pmatrix}\Psi_{\mathbf{0}}(t') \tag{3.54}$$

where the interaction term has a factor 1/2 instead of 1/4 since when all four fields have the same momentum, $\Psi_{\mathbf{k}}^{\dagger}\sigma_1^K\Psi_{\mathbf{k}}\Psi_{\mathbf{k}}^{\dagger}\Psi_{\mathbf{k}}=\Psi_{\mathbf{k}}^{\dagger}\Psi_{\mathbf{k}}\Psi_{\mathbf{k}}^{\dagger}\sigma_1^K\Psi_{\mathbf{k}}$. The cGPE for the complex amplitude of the pump mode $\psi_{\mathbf{0}}^{\mathrm{mf}}$ and the applied pump F_{lp} is [19, 28, 30]:

$$[i\partial_t-\omega_{lp}(\mathbf{k}_p)+\omega_p-V_{\mathbf{0},\mathbf{0},\mathbf{0}}|\psi_{\mathbf{0}}^{\mathrm{mf}}(t)|^2+i\kappa_{lp}(\mathbf{0})]\psi_{\mathbf{0}}^{\mathrm{mf}}(t)-F_{lp}=0. \tag{3.55}$$

This is rearranged for F_{lp}:

$$F_{lp}=[i\partial_t-\omega_{lp}(\mathbf{k}_p)+\omega_p-V_{\mathbf{0},\mathbf{0},\mathbf{0}}|\psi_{\mathbf{0}}^{\mathrm{mf}}(t)|^2+i\kappa_{lp}(\mathbf{0})]\psi_{\mathbf{0}}^{\mathrm{mf}}(t). \tag{3.56}$$

The simplest possible form of the mean field is a plane wave $\psi_{\mathbf{k}_p}^{\mathrm{mf}}(t)=\psi_{\mathbf{k}_p}^{\mathrm{mf}}e^{i\omega_p t}$ in the lab frame [28–30]. Due to the gauge transformation to the pump frame, a plane wave at the pump mode is simply $\psi_{\mathbf{0}}^{\mathrm{mf}}$. In the steady state, the partial derivative gives zero and

$$F_{lp}=-\left[\omega_{lp}(\mathbf{k}_p)-\omega_p+V_{\mathbf{0},\mathbf{0},\mathbf{0}}|\psi_{\mathbf{0}}^{\mathrm{mf}}|^2-i\kappa_{lp}(\mathbf{0})\right]\psi_{\mathbf{0}}^{\mathrm{mf}}. \tag{3.57}$$

To proceed further, the pump power $I_p=|F_{lp}|^2$ is calculated:

$$I_p=\left[(\omega_{lp}(\mathbf{k}_p)-\omega_p+V_{\mathbf{0},\mathbf{0},\mathbf{0}}n_p)^2+\kappa_{lp}^2(\mathbf{0})\right]n_p \tag{3.58}$$

where $n_p=|\psi_{\mathbf{0}}^{mf}|^2$ is the polariton occupation at the pump mode. Since all quantities are real, I_p can be plotted as a function of n_p; n_p is the input parameter for the theoretical analysis while in experiments and numerical simulations F_{lp} or I_p is controlled directly. For many calculations, the complex amplitude $\psi_{\mathbf{0}}^{\mathrm{mf}}$ is required. The pump is applied externally, so can have any form. In particular, choosing F_{lp} to be real (and positive) gives:

$$F_{lp}=(+)\sqrt{\left[(\omega_{lp}(\mathbf{k}_p)-\omega_p+V_{\mathbf{0},\mathbf{0},\mathbf{0}}n_p)^2+\kappa_{lp}^2(\mathbf{0})\right]n_p}, \tag{3.59}$$

and Eq. (3.57) can be solved for complex $\psi_{\mathbf{0}}^{\mathrm{mf}}$.

Including fluctuations (with momenta $\mathbf{k}$) is straightforward as there is only one mode and

$$\psi_{cl}\to\sqrt{2}\psi_{\mathbf{0}}^{\mathrm{mf}}+\sum_{\mathbf{k}}\delta\psi_{\mathbf{k},cl} \quad ; \quad \psi_q\to\sum_{\mathbf{k}}\delta\psi_{\mathbf{k},q}$$

are substituted into the mean field action (Eq. (3.54)). The action with the fluctuations included is similar to Eq. (3.46), but there are no complications due to the presence of many modes. Keeping only terms that are second order in the fluctuations:

$$
\begin{aligned}
iS[\Delta\Psi] = \int dt \Big\{ & \sum_{\mathbf{k}} [\delta\overline{\psi}_{\mathbf{k},cl} \left(A(\mathbf{k}) - i\kappa_{lp}(\mathbf{k})\right) \delta\psi_{\mathbf{k},q} + \delta\overline{\psi}_{\mathbf{k},q} \left(A(\mathbf{k}) + i\kappa_{lp}(\mathbf{k})\right) \delta\psi_{\mathbf{k},cl}] \\
& - \frac{1}{2} \sum_{\mathbf{k}} \Delta\Psi^{\dagger}_{\mathbf{k}} \begin{pmatrix} 0 & 0 & V_{++}|\psi_{\mathbf{0},cl}|^2 & 0 \\ 0 & 0 & V_{+-}\overline{\psi}^2_{\mathbf{0},cl} & V_{--}|\psi_{\mathbf{0},cl}|^2 \\ V_{++}|\psi_{\mathbf{0},cl}|^2 & V_{+-}\psi^2_{\mathbf{0},cl} & 0 & 0 \\ 0 & V_{--}|\psi_{\mathbf{0},cl}|^2 & 0 & 0 \end{pmatrix} \Delta\Psi_{\mathbf{k}} \Big] \Big\} \\
& + 2i \iint dt dt' \sum_{\substack{\mathbf{k} \\ i\in\{c,x\}}} \Big(\delta\overline{\psi}_{\mathbf{k},q}(t) (h^i_{\mathbf{k}})^2 \kappa_i F_{\chi_i}(t-t') \delta\psi_{\mathbf{k},q}(t') \Big).
\end{aligned} \tag{3.60}
$$

The interaction term uses the Nambu vector of all fluctuations defined in Eq. (3.48) and the interaction strengths include the momentum signatures of the fluctuations. In the off-diagonal terms, $V_{+-} = V_{\mathbf{0},\mathbf{0},\mathbf{k}} = V_{\mathbf{0},\mathbf{0},-\mathbf{k}} = V_{\mathbf{0},\mathbf{k},-\mathbf{k}} = g_{\mathrm{x}} X^2(\mathbf{k}_p) X(\mathbf{k}_p + \mathbf{k}) X(\mathbf{k}_p - \mathbf{k})$, and the diagonal terms contain fluctuations with the same signature: $V_{\pm\pm} = g_{\mathrm{x}} X^2(\mathbf{k}) X^2(\mathbf{k}_p \pm \mathbf{k})$.

Performing the Fourier transform into the energy basis, the partial derivative becomes ω. The additional terms are found using Eqs. (3.42) and (3.43) and the result is written in the form of Eq. (3.47) with the sub-matrices:

$$
[D^{-1}]^R = \frac{1}{2} \begin{pmatrix} \omega - \alpha^+ + i\kappa^+_{lp} & -\beta \\ -\overline{\beta} & -\omega - \alpha^- - i\kappa^-_{lp} \end{pmatrix}, \tag{3.61}
$$

$$
[D^{-1}]^A = \frac{1}{2} \begin{pmatrix} \omega - \alpha^+ - i\kappa^+_{lp} & -\beta \\ -\overline{\beta} & -\omega - \alpha^- + i\kappa^-_{lp} \end{pmatrix}, \tag{3.62}
$$

$$
[D^{-1}]^K = \frac{1}{2} \begin{pmatrix} 2i \sum\limits_{i\in\{c,x\}} (h^i_{\mathbf{k}})^2 \kappa_i F^+_{\chi_i} & 0 \\ 0 & 2i \sum\limits_{i\in\{c,x\}} (h^i_{-\mathbf{k}})^2 \kappa_i F^-_{\chi_i} \end{pmatrix}. \tag{3.63}
$$

In general, the properties are set by the mean field occupation and ϕ^{sp}_{cl} is replaced by $\sqrt{2}\psi^{\mathrm{mf}}$ and the factor $1/2$ is removed from the interaction terms. The $\pm$ superscripts indicate the sign of the energy and momentum arguments: a positive sign indicates momenta and energies above the pump mode while a negative sign is for values below the pump mode. Since the summation includes both positive and negative values of momenta, the signs really indicate the relation between the momentum arguments of the elements. For example, the diagonal elements of the inverse retarded Green's function have the symmetry

$$
[D^{-1}]^R_{2,2}(\omega, \mathbf{k}) = \left([D^{-1}]^R_{1,1}(-\omega, -\mathbf{k}) \right)^*.
$$

In Eqs. (3.61) and (3.62) the following shorthands have been introduced and will be used throughout:

$$\alpha^{\pm} = \omega_{lp}(\mathbf{k}_p \pm \mathbf{k}) - \omega_p + 2V_{\pm\pm}|\psi_{\mathbf{0}}^{\mathrm{mf}}|^2; \tag{3.64}$$

$$\beta = V_{+-}(\psi_{\mathbf{0}}^{\mathrm{mf}})^2. \tag{3.65}$$

The information contained in the inverse retarded Green's function is the same as that encoded in the linear response matrix [21]. In the linear response analysis, the equation for the eigenvalues ω is $L(\mathbf{k}) - \omega \mathbb{1}_2$ where [28, 30]

$$L(\delta k) = \begin{pmatrix} \omega_{lp}(-) - \omega_p - i\kappa_{lp}^- + 2V_{p--}|P|^2 & V_{p+-}P^2 \\ -V_{p+-}P^{*2} & -\omega_{lp}(+) + \omega_p - i\kappa_{lp}^+ - 2V_{p++}|P|^2 \end{pmatrix}. \tag{3.66}$$

Comparing Eqs. (3.61) and (3.66) leads to the conclusion that $L(\mathbf{k}) = -2\sigma_z[D^{-1}]^R(0, -\mathbf{k})$ where the $-\mathbf{k}$ signature is a result of different sign conventions in defining the fluctuations [28, 30].

Solving $\det([D^R]^{-1}) = 0$ for complex ω is equivalent to finding the complex eigenvalues in linear response analysis. The real parts of ω give the spectra of the excitations while the imaginary parts determine whether the mean field is stable to small amplitude fluctuations. If an imaginary part is positive, then the proposed state is unstable [92]. The determinant is

$$\begin{aligned} \det([D^R]^{-1}) &= \frac{1}{4}\Big((-\omega - \alpha^- - i\kappa_{lp}^-)(\omega - \alpha^+ + i\kappa_{lp}^+) - |\beta|^2\Big) \\ &= \frac{1}{4}\Big(-\omega^2 - \omega[\alpha^- - \alpha^+ + i(\kappa_{lp}^- + \kappa_{lp}^+)] - i(\kappa_{lp}^+\alpha^- - \kappa_{lp}^-\alpha^+) \\ &\qquad + \alpha^-\alpha^+ - |\beta|^2 + \kappa_{lp}^-\kappa_{lp}^+\Big). \end{aligned} \tag{3.67}$$

The complex eigenvalues $\omega \Rightarrow \omega^{\pm}$ are:

$$\begin{aligned} \omega^{\pm} = \frac{1}{2}\Big(&\alpha^+ - \alpha^- - i(\kappa_{lp}^+ + \kappa_{lp}^-) \\ &\pm \sqrt{(\alpha^+ + \alpha^-)^2 - 4|\beta|^2 - (\kappa_{lp}^- - \kappa_{lp}^+)^2 + 2i(\alpha^- + \alpha^+)(\kappa_{lp}^- - \kappa_{lp}^+)}\Big). \end{aligned} \tag{3.68}$$

The pump-only state is unstable if the imaginary part of ω^+ or ω^- is positive. The transition occurs when $\Im(\omega^{\pm}) = 0$ or

$$\frac{\kappa_{lp}^+ + \kappa_{lp}^-}{2} = \pm\Im\left(\sqrt{\left[\frac{\alpha^+ + \alpha^-}{2} - i\frac{\kappa_{lp}^+ - \kappa_{lp}^-}{2}\right]^2 - V_{p+-}^2|\psi_{mf}|^4}\right).$$

For the imaginary part of one of the eigenvalues to become positive, or vary at all from $-i(\kappa_{lp}^- + \kappa_{lp}^+)/2$, the discriminant must be negative. When this occurs, the real parts of the eigenvalues

become equal:

$$\Re(\omega^{\pm}) = \frac{\alpha^{+} - \alpha^{-}}{2}. \tag{3.69}$$

Meanwhile, when the discriminant of the square root is positive, the eigenvalues have the same (negative) imaginary part, but their real parts differ [28, 30].

The determinant of the inverse retarded Green's function is a complex function, so the condition $\det([D^{-1}]^R) = 0$ is equivalent to the real and imaginary parts of $\det([D^{-1}]^R)$ equal to zero simultaneously [21]. Splitting the determinant into its real and imaginary parts gives:

$$\Re[\det([D^{-1}]^R)] = \frac{1}{4}(-\omega^2 - \omega(\alpha^{-} - \alpha^{+}) + \alpha^{-}\alpha^{+} + \kappa_{lp}^{-}\kappa_{lp}^{+} - |\beta|^2), \tag{3.70}$$

$$\Im[\det([D^{-1}]^R)] = \frac{1}{4}\left(-\omega(\kappa_{lp}^{-} + \kappa_{lp}^{+}) + \alpha^{+}\kappa_{lp}^{-} - \alpha^{-}\kappa_{lp}^{+}\right), \tag{3.71}$$

which are solved for real ω. The real part, $\Re[\det([D^{-1}]^R)] = 0$, gives the poles $\omega \to \xi^{\pm}(\mathbf{k})$, and the imaginary part, $\Im[\det([D^{-1}]^R)] = 0$, gives an effective chemical potential $\omega \to \mu_{\text{eff}}(\mathbf{k})$:

$$\xi^{\pm}(\mathbf{k}) = \frac{\alpha^{+} - \alpha^{-}}{2} \pm \frac{1}{2}\sqrt{(\alpha^{-} + \alpha^{+})^2 + 4\kappa_{lp}^{-}\kappa_{lp}^{+} - 4|\beta|^2}, \tag{3.72}$$

$$\mu_{\text{eff}}(\mathbf{k}) = \frac{\alpha^{+}\kappa_{lp}^{-} - \alpha^{-}\kappa_{lp}^{+}}{\kappa_{lp}^{+} + \kappa_{lp}^{-}}. \tag{3.73}$$

The determinant is zero for a real ω when the effective chemical potential crosses the poles, $\xi^{\pm}(\mathbf{k}) = \mu_{\text{eff}}(\mathbf{k})$.

3.3.2 Inversion of pump only Green's functions

From the inverse Green's functions, the retarded, advanced and Keldysh Green's functions, D^R, D^A and D^K are calculated. In the pump only case, the matrix F_s, which describes the occupations of the system, can also be calculated. Taking the inverse of $[D^{-1}]^R$ gives:

$$D^R = \frac{1}{2\det([D^{-1}]^R)}\begin{pmatrix} -\omega - \alpha^{-} - i\kappa_{lp}^{-} & \beta \\ \overline{\beta} & \omega - \alpha^{+} + i\kappa_{lp}^{+} \end{pmatrix}. \tag{3.74}$$

The advanced Green's function is the Hermitian conjugate of the retarded Green's function [70, 71]. Since $\det([D^R]^{-1}) = \det([D^A]^{-1})^*$, D^R and D^A can be written with the same denominator:

$$D^R = \frac{\det([D^{-1}]^A)}{\det([D^{-1}]^A)}D^R = \frac{\det([D^{-1}]^R)^*}{2|\det([D^{-1}]^R)|^2}\begin{pmatrix} -\omega - \alpha^{-} - i\kappa_{lp}^{-} & \beta \\ \overline{\beta} & \omega - \alpha^{+} + i\kappa_{lp}^{+} \end{pmatrix}, \tag{3.75}$$

$$D^A = \frac{\det([D^{-1}]^R)}{\det([D^{-1}]^R)}D^A = \frac{\det([D^{-1}]^R)}{2|\det([D^{-1}]^R)|^2}\begin{pmatrix} -\omega - \alpha^{-} + i\kappa_{lp}^{-} & \beta \\ \overline{\beta} & \omega - \alpha^{+} - i\kappa_{lp}^{+} \end{pmatrix}. \tag{3.76}$$

The Keldysh Green's function is calculated using Eq. (3.11) as:

$$D^K = -\frac{i}{4|\det([D^{-1}]^R)|^2}\begin{pmatrix} \kappa_{lp}^+ F_\chi^+ |-\omega-\alpha^- - i\kappa_{lp}^-|^2 & \kappa_{lp}^+ F_\chi^+(-\omega-\alpha^- - i\kappa_{lp}^-)\beta \\ +\kappa_{lp}^- F_\chi^- |\beta|^2 & +\kappa_{lp}^- F_\chi^-(\omega-\alpha^+ - i\kappa_{lp}^+)\beta \\ \kappa_{lp}^+ F_\chi^+(-\omega-\alpha^- + i\kappa_{lp}^-)\overline{\beta} & \kappa_{lp}^- F_\chi^- |\omega-\alpha^+ + i\kappa_{lp}^+|^2 \\ +\kappa_{lp}^- F_\chi^-(\omega-\alpha^+ + i\kappa_{lp}^+)\overline{\beta} & +\kappa_{lp}^+ F_\chi^+ |\beta|^2 \end{pmatrix} \tag{3.77}$$

with $\alpha^\pm, \beta$ and $^\pm$ as before, and the summation over the two baths in the inverse Green's function has been summarised by defining

$$F_\chi^\pm = \sum_{i\in\{c,x\}} (h_{\pm\mathbf{k}}^i)^2 \kappa_i F_{\chi i}^\pm. \tag{3.78}$$

In principle the distribution matrix F_s can be calculated directly from the Keldysh Green's function, but it is simpler to use the second expression of Eq. (3.10) since the off-diagonal elements of $[D^{-1}]^K$ are zero, then

$$F_s = \frac{1}{f_{den}}\begin{pmatrix} f_a & f_b \\ f_c & f_d \end{pmatrix} \tag{3.79}$$

with the elements

$$f_{den} = 2\big(|\beta|^2 - \kappa_{lp}^+\kappa_{lp}^-\big)\big(\kappa_{lp}^- - \kappa_{lp}^+\big)^2 - 2\kappa_{lp}^+\kappa_{lp}^-\big(2\omega+\alpha^- - \alpha^+\big)^2, \tag{3.80}$$

$$\begin{aligned} f_a = {} & |\beta|^2\big(\kappa_{lp}^- - \kappa_{lp}^+\big)\big(F_\chi^-\kappa_{lp}^- + F_\chi^+\kappa_{lp}^+\big) \\ & - F_\chi^+\kappa_{lp}^-\kappa_{lp}^+\Big(\big(\kappa_{lp}^- - \kappa_{lp}^+\big)^2 + \big(2\omega+\alpha^- - \alpha^+\big)^2\Big), \end{aligned} \tag{3.81}$$

$$f_b = \beta\kappa_{lp}^+\kappa_{lp}^-\big(F_\chi^- + F_\chi^+\big)\Big(2\omega+\alpha^- - \alpha^+ + i(\kappa_{lp}^- - \kappa_{lp}^+)\Big), \tag{3.82}$$

$$f_c = -\overline{\beta}\kappa_{lp}^+\kappa_{lp}^-\big(F_\chi^- + F_\chi^+\big)\Big(2\omega+\alpha^- - \alpha^+ - i(\kappa_{lp}^- - \kappa_{lp}^+)\Big) = -f_b^*, \tag{3.83}$$

$$\begin{aligned} f_d = {} & -|\beta|^2\big(\kappa_{lp}^- - \kappa_{lp}^+\big)\big(F_\chi^-\kappa_{lp}^- + F_\chi^+\kappa_{lp}^+\big) \\ & + F_\chi^-\kappa_{lp}^-\kappa_{lp}^+\Big(\big(\kappa_{lp}^- - \kappa_{lp}^+\big)^2 + \big(2\omega+\alpha^- - \alpha^+\big)^2\Big). \end{aligned} \tag{3.84}$$

3.3.3 Inversion of Keldysh rotation: physical quantities

In order to obtain information about the polariton system, physical quantities are of interest. In particular the incoherent luminescence and absorption around a stable steady state solution and their difference, the spectral weight, can be calculated if the proposed mean field steady state is stable.

The luminescence $L(\omega, \mathbf{k})$ and absorption $A(\omega, \mathbf{k})$ are given by Eqs. (3.50) and (3.51). The

matrices of the physical Green's functions, $D^<$ and $D^>$, are:

$$D^< = \frac{-i}{2|\det([D^{-1}]^R)|^2}\begin{pmatrix} D_a^< & D_b^< \\ D_c^< & D_d^< \end{pmatrix}, \tag{3.85}$$

$$\begin{aligned}
D_a^< &= \frac{1}{2}\left(\kappa_{lp}^+ F_\chi^+[(\omega+\alpha^-)^2+(\kappa_{lp}^-)^2]+\kappa_{lp}^- F_\chi^-|\beta|^2\right) \\
&\quad -2\left[(-\omega-\alpha^-)\Im(\det([D^{-1}]^R))+\kappa_{lp}^-\Re(\det([D^{-1}]^R))\right], \\
D_b^< &= \frac{\beta}{2}[\kappa_{lp}^+ F_\chi^+(-\omega-\alpha^- - i\kappa_{lp}^-)+\kappa_{lp}^- F_\chi^-(\omega-\alpha^+ - i\kappa_{lp}^+)]-2\beta\Im(\det([D^{-1}]^R)), \\
D_c^< &= \frac{\overline{\beta}}{2}[\kappa_{lp}^+ F_\chi^+(-\omega-\alpha^- + i\kappa_{lp}^-)+\kappa_{lp}^- F_\chi^-(\omega-\alpha^+ + i\kappa_{lp}^+)]-2\overline{\beta}\Im(\det([D^{-1}]^R)), \\
D_d^< &= \frac{1}{2}\left(\kappa_{lp}^- F_\chi^-[(\omega-\alpha^+)^2+(\kappa_{lp}^+)^2]+\kappa_{lp}^+ F_\chi^+|\beta|^2\right) \\
&\quad -2\left[(\omega-\alpha^+)\Im(\det([D^{-1}]^R))-\kappa_{lp}^+\Re(\det([D^{-1}]^R))\right],
\end{aligned}$$

$$D^> = \frac{-i}{2|\det([D^{-1}]^R)|^2}\begin{pmatrix} D_a^> & D_b^> \\ D_c^> & D_d^> \end{pmatrix}, \tag{3.86}$$

$$\begin{aligned}
D_a^> &= \frac{1}{2}\left(\kappa_{lp}^+ F_\chi^+[(\omega+\alpha^-)^2+(\kappa_{lp}^-)^2]+\kappa_{lp}^- F_\chi^-|\beta|^2\right) \\
&\quad +2\left[(-\omega-\alpha^-)\Im(\det([D^{-1}]^R))+\kappa_{lp}^-\Re(\det([D^{-1}]^R))\right], \\
D_b^> &= \frac{\beta}{2}[\kappa_{lp}^+ F_\chi^+(-\omega-\alpha^- - i\kappa_{lp}^-)+\kappa_{lp}^- F_\chi^-(\omega-\alpha^+ - i\kappa_{lp}^+)]+2\beta\Im(\det([D^{-1}]^R)), \\
D_c^> &= \frac{\overline{\beta}}{2}[\kappa_{lp}^+ F_\chi^+(-\omega-\alpha^- + i\kappa_{lp}^-)+\kappa_{lp}^- F_\chi^-(\omega-\alpha^+ + i\kappa_{lp}^+)]+2\overline{\beta}\Im(\det([D^{-1}]^R)), \\
D_d^> &= \frac{1}{2}\left(\kappa_{lp}^- F_\chi^-[(\omega-\alpha^+)^2+(\kappa_{lp}^+)^2]+\kappa_{lp}^+ F_\chi^+|\beta|^2\right) \\
&\quad +2\left[(\omega-\alpha^+)\Im(\det([D^{-1}]^R))-\kappa_{lp}^+\Re(\det([D^{-1}]^R))\right].
\end{aligned}$$

For a physical observable the $\psi^\dagger\psi$ term is chosen which corresponds to the $(1,1)$ term in the matrices. The luminescence is then:

$$L = \frac{1}{4\pi|\det([D^{-1}]^R)|^2} D_a^< \tag{3.87}$$

and the absorption:

$$A = \frac{1}{4\pi|\det([D^{-1}]^R)|^2} D_a^>. \tag{3.88}$$

The spectral weight is defined as the difference between the luminescence and absorption in Eq.

(3.53). It is therefore proportional to

$$D^A - D^R = \frac{-i}{|\det([D^{-1}]^R)|^2} \begin{pmatrix} \Im(\det([D^{-1}]^R))(-\omega - \alpha^-) & \Im(\det([D^{-1}]^R))\beta \\ +\kappa_{lp}^- \Re(\det([D^{-1}]^R)) & \\ \Im(\det([D^{-1}]^R))\overline{\beta} & \Im(\det([D^{-1}]^R))(\omega - \alpha^+) \\ & -\kappa_{lp}^+ \Re(\det([D^{-1}]^R)) \end{pmatrix}. \quad (3.89)$$

$D^<, D^>$ and $D^R - D^A$ all have a denominator $|\det([D^{-1}]^R)|^2$. If $\det([D^{-1}]^R) = 0$ for a combination of $|\psi_{mf}|^2, \omega, \mathbf{k}$, then the denominator of all elements is zero and the quantities will diverge unless the numerator is also zero. In Eqs. (3.85) - (3.89), the matrix elements have been written in terms of the real and imaginary parts of $\det([D^{-1}]^R)$. When the determinant is zero the elements of $D^{<,>}$ all contain finite numerators from the Keldysh contribution so the luminescence and absorption diverge. Although all parts of $D^R - D^A$ can be written in terms of $\Im, \Re(\det([D^{-1}]^R))$, these appear linearly in the numerator but quadratically in the denominator. The denominator therefore goes to zero faster than the numerator and the spectral weight also diverges at the phase transition.

3.3.4 Eigenvalues of the distribution matrix

The distribution matrix, Eqs.(3.79)-(3.84), is of interest in its own right as it describes the difference between this driven-dissipative system and an equilibrium system where [69–71]

$$F_{EQ} = \coth\left(\frac{\omega}{2T}\right) \mathbb{1},$$

where $\mathbb{1}$ is the unit matrix. The eigenvalues of F_s can be calculated (taking general $F_\chi^+ \neq F_\chi^-$):

$$\lambda_{F_s} = \frac{1}{2f_{den}} \left(f_a + f_d \pm \sqrt{(f_a - f_d)^2 + 4f_b f_c} \right). \quad (3.90)$$

F_s and hence its eigenvalues diverge if $f_{den} = 0$. Considering the denominator:

$$f_{den} = \left(|\beta|^2 - \kappa_{lp}^- \kappa_{lp}^+\right)\left(\kappa_{lp}^- - \kappa_{lp}^+\right)^2 - \kappa_{lp}^+ \kappa_{lp}^- \left(2\omega + \alpha^- - \alpha^+\right)^2$$

and solving $f_{den} = 0$ for ω gives

$$\omega(\mathbf{k}) = \frac{\alpha^+ - \alpha^-}{2} \pm \frac{(\kappa_{lp}^- - \kappa_{lp}^+)}{2} \sqrt{\frac{|\beta|^2}{\kappa_{lp}^+ \kappa_{lp}^-} - 1} \quad (3.91)$$

which is independent of the bath distributions in F_χ. Although the term 'effective chemical potential' was used to describe Eq. (3.73), calculated from $\Im(\det([D^{-1}]^R)) = 0$, Eq. (3.91) is really the effective chemical potential since it controls the divergence of the distribution. When $f_{den} = 0$, the numerators of Eqs. (3.81) - (3.84) remain finite and the distribution matrix diverges at the phase transition. As will be seen later, these quantities coincide in the limit of constant

polariton decay and Eq. (3.73) is used in all plots.

3.3.5 Limits of constants

So far, the form of the decay bath's occupation has not been specified and the lower polariton decay is momentum dependent as defined in Eq. (3.36). Two assumptions can be made: 1) that the decay bath energies are large enough compared to the range of energies of interest for $F_{\chi_i}(\pm) \approx 1$ to be valid; 2) that the exciton and photon decays are equal which makes the polariton decay momentum independent. The first assumption is physical since the range of energies of interest is small compared to the energies of the decay baths [21, 72], the second simplification is not physical since the polariton decay is strongly momentum dependent [15]. This latter simplification is a useful reference since much of the work on the polariton OPO regime does not account for momentum dependent decay [28, 30, 41].

1) Simplification: $F_{\chi_i} = 1$ When both decay baths are assumed to be energetically far from the system, the diagonal terms of the Keldysh part of the inverse Green's function are still momentum dependent, but contain only the Hopfield coefficients and the exciton and photon decay rates. The terms with $F_\chi^\pm$ factors in Eqs. (3.63) and (3.77)- (3.88) reduce to $C^2(\mathbf{k}_p + \mathbf{k})\kappa_c + X^2(\mathbf{k}_p + \mathbf{k})\kappa_x = \kappa_{lp}^\pm$. The effect is to introduce additional factors of the polariton decay. For example, the Keldysh Green's function is unaffected in form, but now reads:

$$D^K = -\frac{i}{4|\det[D^{-1}]^R|^2}\begin{pmatrix} (\kappa_{lp}^+)^2|-\omega-\alpha^- - i\kappa_{lp}^-|^2 & (\kappa_{lp}^+)^2(-\omega-\alpha^- - i\kappa_{lp}^-)\beta \\ +(\kappa_{lp}^-)^2|\beta|^2 & (+\kappa_{lp}^-)^2(\omega-\alpha^+ - i\kappa_{lp}^+)\beta \\ (\kappa_{lp}^+)^2(-\omega-\alpha^- + i\kappa_{lp}^-)\overline{\beta} & (\kappa_{lp}^-)^2|\omega-\alpha^+ + i\kappa_{lp}^+|^2 \\ +(\kappa_{lp}^-)2(\omega-\alpha^+ + i\kappa_{lp}^+)\overline{\beta} & +(\kappa_{lp}^+)^2|\beta|^2 \end{pmatrix}.$$

2) Limit: $\kappa_{lp}(\mathbf{k}) = \kappa_{lp}$ When the exciton and photon decays are assumed equal, Eqs. (3.72) and (3.73) become

$$\xi^\pm(\mathbf{k}) = \frac{\alpha^+ - \alpha^-}{2} \pm \frac{1}{2}\sqrt{(\alpha^- + \alpha^+)^2 + 4(\kappa_{lp}^2 - |\beta|^2)}, \tag{3.92}$$

$$\mu_{\text{eff}}(\mathbf{k}) = \frac{\alpha^+ - \alpha^-}{2}, \tag{3.93}$$

and $f_{den} = 0$ at

$$\omega(\mathbf{k}) = \frac{\alpha^+ - \alpha^-}{2} \tag{3.94}$$

which is the same as Eq. (3.93); the divergences of the distribution matrix coincide with the effective chemical potential in the limit of constant decay. Eqs. (3.92) and (3.93) define where $\det([D^{-1}]^R) = 0$.

The complex eigenvalues from $\det([D^{-1}]^R) = 0$ are:

$$\omega^{\pm}(\mathbf{k}) = \frac{\alpha^+ - \alpha^-}{2} - i\kappa_{lp} \pm \sqrt{\left(\frac{\alpha^+ + \alpha^-}{2}\right)^2 - |\beta|^2}, \tag{3.95}$$

the real part of which is the same as Eqs. (3.93) and (3.94) when the square root is imaginary.

If the limit of constant polariton decay is applied after the distributions of the two decay baths are set to unity, the distribution matrix simplifies to

$$F_s = \begin{pmatrix} -1 & \frac{2\beta}{2\omega+\alpha^- -\alpha^+} \\ \frac{2\overline{\beta}}{2\omega+\alpha^- -\alpha^+} & 1 \end{pmatrix}. \tag{3.96}$$

3.3.6 Effective temperature

In equilibrium, the distribution matrix is $\coth(\omega/2T)$, and diverges as $2T/\omega$ in the limit of small ω [69–71]. Thus, from a small ω expansion, the temperature T of an equilibrium system can be inferred. In non-equilibrium systems, an effective temperature defined along similar lines can be convenient for describing the system. It may also provide constraints on the effective noise term in a Langevin description of a system, or as an analogy of a thermometer whereby two coupled systems (or parts of a system) with the same effective temperature are in equilibrium [93]. One area in which the effective temperature occurs frequently is the study of driven amorphous materials (e.g. shaken sand) [94, 95] in which the effective temperature is identified as being associated with the degrees of freedom that are affected over long time scales [96, 97].

By examining the distribution matrix in the Keldysh description of a system, an effective temperature, characterised by a $1/\omega$ divergence, may appear in systems that are far from equilibrium [72, 73, 98–100]. In the polariton system studied, the short time scales are associated with the decay baths that have been integrated out, so the description contains only the slow dynamics.

In the limit of constant polariton decay and decay baths that are energetically far from the system, the eigenvalues of the distribution matrix, Eq. (3.96), are:

$$\begin{aligned} \lambda_{F_s} &= \pm\sqrt{1 + \frac{4|\beta|^2}{(2\omega + \alpha^- - \alpha^+)^2}} \\ &\approx \frac{2|\beta|}{2\omega + \alpha^- - \alpha^+}. \end{aligned} \tag{3.97}$$

These diverge when $\omega = (\alpha^+ - \alpha^-)/2$ (the divergence is of the form $1/(\omega - \omega_z)$ [72]) leading to

$$T_{\text{eff}} = |\beta| = X^2(\mathbf{k}_p)X(\mathbf{k}_p + \mathbf{k})X(\mathbf{k}_p - \mathbf{k})|\psi_{\mathbf{0}}^{\text{mf}}|^2. \tag{3.98}$$

There is also a trivial divergence of λ_{F_s} at the pump; where the fluctuations in energy and momentum are zero. The effective temperature of the polaritons as a result of the fluctuations

around the mean field is set by the 'blue shift' of the polariton dispersion caused by the finite occupation of the pump mode $n_p = |\psi_{\mathbf{0}}^{\mathrm{mf}}|^2$. There are local minima at $\mathbf{k} = \mathbf{0}, 2\mathbf{k}_p$; the signal and idler states form near these local minima. If the momentum dependence of the polariton decay is retained (exciton decay less than photon decay), the numerator in the distribution matrix is not cancelled and there no longer is a simple algebraic definition of an effective temperature.

3.4 OPO regime: three modes

Having determined that a system of coherently pumped polaritons restricted to the pump mode is unstable towards the appearance of new modes, one near $\mathbf{k} = \mathbf{0}$ and the other near $2\mathbf{k}_p$, the next step is to make a new ansatz that includes additional modes [19, 29, 30, 41]. This is done for two additional modes, the signal and idler, within the Keldysh formalism and gives cGPEs describing the mean field occupation of these modes. In the following, the momentum dependence of the polariton decay is retained, although it is usually considered constant [1,29,41] or different decays applied to the individual modes [30].

3.4.1 Mean field and cGPEs

There are several points at which the restriction to three modes can be made, all of which give the same result. The momenta in the interaction term are also restricted so that only these three modes are allowed as the result of the scattering. It is possible to make the ansatz as early as the Hamiltonian by restricting to three momenta and therefore only the operators $\hat{a}_{\mathbf{k}_s}, \hat{a}_{\mathbf{k}_p}$ and $\hat{a}_{\mathbf{k}_i}$ appear in the Hamiltonian.

The more common approach is to make the substitution of three plane wave modes into the cGPE [29, 30, 41]. With the gauge transformation, this means substituting the new ansatz (in the gauge transformed system)

$$\psi^{\mathrm{mf}} = S\delta_{\mathbf{k},-\tilde{\mathbf{k}}}e^{i\tilde{\omega}t} + P\delta_{\mathbf{k},\mathbf{0}} + I\delta_{\mathbf{k},+\tilde{\mathbf{k}}}e^{-i\tilde{\omega}t} \tag{3.99}$$

into Eq. (3.40). The signal is at an energy $\tilde{\omega}$ and momentum $\tilde{\mathbf{k}}$ below the pump (which is at zero), while the idler is (by energy conservation) above the pump by the same amounts. The mean field steady state can be calculated by requiring that $\partial_t S = \partial_t P = \partial_t I = 0$. The pump F_{lp} is the same as below threshold.

Here, the restriction to the three modes is made at the level of the Keldysh action. The fields are therefore formally subdivided into spaces around each of the three modes: $\psi = \psi_s + \psi_p + \psi_i$. Each mode j has momentum $\mathbf{k}_j$, and in principle the three fields could each contain summations

over momenta. The Keldysh action reads:

$$
\begin{aligned}
S_{OPO} \;=\; & \int dt\Big(-\sqrt{2}F_{lp}(\bar{\psi}_{p,q}+\psi_{p,q}) + \sum_{j=s,p,i}\Big[\bar{\psi}_{j,cl}(i\partial_t-\omega_{lp}(\mathbf{k}_j)+\omega_p-i\kappa_{lp})\psi_{j,q} \\
& +\bar{\psi}_{j,q}(i\partial_t-\omega_{lp}(\mathbf{k}_j)+\omega_p+i\kappa_{lp})\psi_{j,cl})\Big] - \Big\{\sum_{j=s,p,i}\frac{V_{jjjj}}{2}(\bar{\psi}_{j,cl}\bar{\psi}_{j,q}(\psi_{j,cl}^2+\psi_{j,q}^2) + \\
& V_{sisi}\big[(\bar{\psi}_{s,cl}\bar{\psi}_{i,cl}+\bar{\psi}_{s,q}\bar{\psi}_{i,q})(\psi_{s,cl}\psi_{i,q}+\psi_{s,q}\psi_{i,cl})\big] \\
& +\frac{V_{ppsi}}{2}\big[2(\bar{\psi}_{s,cl}\bar{\psi}_{i,cl}+\bar{\psi}_{s,q}\bar{\psi}_{i,q})\psi_{p,cl}\psi_{p,q}+(\bar{\psi}_{s,cl}\bar{\psi}_{i,q}+\bar{\psi}_{s,q}\bar{\psi}_{i,cl})(\psi_{p,cl}^2+\psi_{p,q}^2)\big] \\
& +\sum_{j=s,i}V_{pjpj}\big[(\bar{\psi}_{p,cl}\bar{\psi}_{j,cl}+\bar{\psi}_{p,q}\bar{\psi}_{j,q})(\psi_{p,cl}\psi_{j,q}+\psi_{p,q}\psi_{j,cl})\big]+h.c.\Big\}\Big) \\
& +2i\iint dtdt'\sum_{j=s,p,i}\bar{\psi}_{j,q}(t)\sum_{i\in\{c,x\}}(h^i_{\mathbf{k}_j})^2\kappa_i F_{\chi_i}(t-t')\psi_{j,q}(t'). \qquad (3.100)
\end{aligned}
$$

The interaction coefficients are now written with indices that indicate exactly which modes are involved in each scattering process: $V_{i,j,k,l}=g_{\mathrm{x}}X(\mathbf{k}_i)X(\mathbf{k}_j)X(\mathbf{k}_k)X(\mathbf{k}_l)$ for $\mathbf{k}_{i,j,k,l}\in\mathbf{k}_s,\mathbf{k}_p,\mathbf{k}_i$.

The saddle points are taken with respect to the three modes and the quantum fields set to zero to find the cGPEs describing the three modes:

$$
\begin{aligned}
\frac{\delta S}{\delta\overline{\psi}_{s,q}}=0 \;\Rightarrow\; & \Big(i\partial_t-\omega_{lp}(\mathbf{k}_s)+\omega_p+i\kappa_{lp}(\mathbf{k}_s)-\frac{V_{ssss}}{2}\overline{\psi}^{sp}_{s,cl}\psi^{sp}_{s,cl}-V_{spsp}\overline{\psi}^{sp}_{p,cl}\psi^{sp}_{p,cl} \\
& -V_{sisi}\overline{\psi}^{sp}_{i,cl}\psi^{sp}_{i,cl}\Big)\psi^{sp}_{s,cl}-\frac{V_{ppsi}}{2}\overline{\psi}^{sp}_{i,cl}(\psi^{sp}_{p,cl})^2=0; \qquad (3.101) \\
\frac{\delta S}{\delta\overline{\psi}_{p,q}}=0 \;\Rightarrow\; & \Big(i\partial_t-\omega_{lp}(\mathbf{k}_p)+\omega_p+i\kappa_{lp}(\mathbf{k}_p)-V_{spsp}\overline{\psi}^{sp}_{s,cl}\psi^{sp}_{s,cl}-\frac{V_{pppp}}{2}\overline{\psi}^{sp}_{p,cl}\psi^{sp}_{p,cl} \\
& -V_{pipi}\overline{\psi}^{sp}_{i,cl}\psi^{sp}_{i,cl}\Big)\psi^{sp}_{p,cl}-V_{ppsi}\overline{\psi}^{sp}_{p,cl}\psi^{sp}_{s,cl}\psi^{sp}_{i,cl}-\sqrt{2}F_{lp}=0; \qquad (3.102) \\
\frac{\delta S}{\delta\overline{\psi}_{i,q}}=0 \;\Rightarrow\; & \Big(i\partial_t-\omega_{lp}(\mathbf{k}_i)+\omega_p+i\kappa_{lp}(\mathbf{k}_i)-V_{sisi}\overline{\psi}^{sp}_{s,cl}\psi^{sp}_{s,cl}-V_{pipi}\overline{\psi}^{sp}_{p,cl}\psi^{sp}_{p,cl} \\
& -\frac{V_{iiii}}{2}\overline{\psi}^{sp}_{i,cl}\psi^{sp}_{i,cl}\Big)\psi^{sp}_{i,cl}-\frac{V_{ppsi}}{2}\overline{\psi}^{sp}_{s,cl}(\psi^{sp}_{p,cl})^2=0. \qquad (3.103)
\end{aligned}
$$

Making the substitution of the mean field: $\psi^{\mathrm{mf}}_j=\sqrt{2}\psi^{sp}_{j,cl}$ and dividing through by $\sqrt{2}$ leads to:

$$
\begin{aligned}
0=\; & \Big(i\partial_t-\omega_{lp}(\mathbf{k}_s)+\omega_p+i\kappa_{lp}(\mathbf{k}_s)-V_{ssss}\overline{\psi}^{\mathrm{mf}}_{s,cl}\psi^{\mathrm{mf}}_{s,cl}-2V_{spsp}\overline{\psi}^{\mathrm{mf}}_{p,cl}\psi^{\mathrm{mf}}_{p,cl} \\
& -2V_{sisi}\overline{\psi}^{\mathrm{mf}}_{i,cl}\psi^{\mathrm{mf}}_{i,cl}\Big)\psi^{\mathrm{mf}}_{s,cl}-V_{ppsi}\overline{\psi}^{\mathrm{mf}}_{i,cl}(\psi^{\mathrm{mf}}_{p,cl})^2; \\
0=\; & \Big(i\partial_t-\omega_{lp}(\mathbf{k}_p)+\omega_p+i\kappa_{lp}(\mathbf{k}_p)-2V_{spsp}\overline{\psi}^{\mathrm{mf}}_{s,cl}\psi^{\mathrm{mf}}_{s,cl}-V_{pppp}\overline{\psi}^{\mathrm{mf}}_{p,cl}\psi^{\mathrm{mf}}_{p,cl} \\
& -2V_{pipi}\overline{\psi}^{\mathrm{mf}}_{i,cl}\psi^{\mathrm{mf}}_{i,cl}\Big)\psi^{\mathrm{mf}}_{p,cl}-2V_{ppsi}\overline{\psi}^{\mathrm{mf}}_{p,cl}\psi^{\mathrm{mf}}_{s,cl}\psi^{\mathrm{mf}}_{i,cl}-F_{lp};
\end{aligned}
$$

$$0 = \Big(i\partial_t - \omega_{lp}(\mathbf{k}_i) + \omega_p + i\kappa_{lp}(\mathbf{k}_i) - 2V_{sisi}\overline{\psi}^{\rm mf}_{s,cl}\psi^{\rm mf}_{s,cl} - 2V_{pipi}\overline{\psi}^{\rm mf}_{p,cl}\psi^{\rm mf}_{p,cl} - V_{iiii}\overline{\psi}^{\rm mf}_{i,cl}\psi^{\rm mf}_{i,cl}\Big)\psi^{\rm mf}_{i,cl} - V_{ppsi}\overline{\psi}^{\rm mf}_{s,cl}(\psi^{\rm mf}_{p,cl})^2.$$

Assuming that the steady states can be described as plane waves with complex amplitudes S, P, I, the signal and idler momenta are defined relative to the pump as $\mathbf{k}_s = \mathbf{k}_p - \tilde{\mathbf{k}}$ and $\mathbf{k}_i = \mathbf{k}_p + \tilde{\mathbf{k}}$. The energies are: $\omega_s = \omega_p - \tilde{\omega}$ and $\omega_i = \omega_p + \tilde{\omega}$, and the mean fields are as in Eq. (3.99):

$$\psi^{\rm mf}_s = S\delta_{\mathbf{k},-\tilde{\mathbf{k}}}e^{i\tilde{\omega}t}, \tag{3.104}$$

$$\psi^{\rm mf}_p = P, \tag{3.105}$$

$$\psi^{\rm mf}_i = I\delta_{\mathbf{k},\tilde{\mathbf{k}}}e^{-i\tilde{\omega}t}. \tag{3.106}$$

This gives the three coupled cGPEs of the OPO regime [30]

$$\begin{aligned}
0 = &\Big(i\partial_t - \omega_{lp}(\mathbf{k}_p - \tilde{\mathbf{k}}) + \omega_p + i\kappa_{lp}(\mathbf{k}_p - \tilde{\mathbf{k}}) - V_{ssss}|S|^2 - 2V_{spsp}|P|^2 - 2V_{sisi}|I|^2\Big)Se^{i\tilde{\omega}t} \\
&- V_{ppsi}I^*P^2e^{i\tilde{\omega}t}; \\
0 = &\Big(i\partial_t - \omega_{lp}(\mathbf{k}_p) + \omega_p + i\kappa_{lp}(\mathbf{k}_p) - 2V_{spsp}|S|^2 - V_{pppp}|P|^2 - 2V_{pipi}|I|^2\Big)P \\
&- 2V_{ppsi}P^*SI - F_{lp}; \\
0 = &\Big(i\partial_t - \omega_{lp}(\mathbf{k}_p + \tilde{\mathbf{k}}) + \omega_p + i\kappa_{lp}(\mathbf{k}_p + \tilde{\mathbf{k}}) - 2V_{sisi}|S|^2 - 2V_{pipi}|P|^2 - V_{iiii}|I|^2\Big)Ie^{-i\tilde{\omega}t} \\
&- V_{ppsi}S^*P^2.
\end{aligned}$$

In the steady state, the amplitudes of the modes are constant so all $i\partial_t(M)$ are zero, and the exponentials give factors $i(\pm i\tilde{\omega}) = \mp\tilde{\omega}$ in the equations for the signal and idler states. The exponential itself cancels after the time derivative is taken.

It is convenient to simplify the notation:

$$\kappa(\mathbf{k}_{s,p,i}) \to \kappa_{s,p,i}, \qquad \omega_{lp}(\mathbf{k}_{s,p,i}) \to \varepsilon_{s,p,i}, \qquad X(\mathbf{k}_{s,p,i}) \to X_{s,p,i}, \qquad n_{s,p,i} = |S|^2_,|P|^2_,|I|^2$$

and write the interactions using the Hopfield coefficients for the time being. The three coupled equations that describe the mean field occupation of the OPO state are [29]:

$$[\varepsilon_s - \tilde{\omega} - \omega_p - i\kappa_s + g_{\rm x}X_s^2(X_s^2n_s + 2X_p^2n_p + 2X_i^2n_i)]S + g_{\rm x}X_sX_p^2X_iP^2I^* = 0, \tag{3.107}$$

$$[\varepsilon_p - \omega_p - i\kappa_p + g_{\rm x}X_p^2(2X_s^2n_s + X_p^2n_p + 2X_i^2n_i)]P + 2g_{\rm x}X_sX_p^2X_iSP^*I + F_{lp} = 0, \tag{3.108}$$

$$[\varepsilon_i + \tilde{\omega} - \omega_p - i\kappa_i + g_{\rm x}X_i^2(2X_s^2n_s + 2X_p^2n_p + X_i^2n_i)]I + g_{\rm x}X_sX_p^2X_iS^*P^2 = 0. \tag{3.109}$$

These contain the external pump F_{lp} which can be chosen to be real since the phase is set externally, and four complex quantities: S, P, I and $\tilde{\omega}$.

The complex mode amplitudes have the form $M = |M|e^{i\theta_m}$; the phase of the pump mode is locked to the external pump and is determined from Eq. (3.108), but there is freedom in the

choice of the signal and idler phases. The relation between them is well defined [87], but their values are spontaneously chosen at each realisation of an experiment [41, 87]. In the calculation of the mean field, the phase of one of these modes can be chosen freely. The signal is chosen to be real and the idler phase is then determined by the steady state equations (Eqs. (3.107) - (3.109)). This phase freedom means that a shift of the signal phase e.g. $\theta_s \to \theta_s + \Delta\theta$, would be accompanied by a simultaneous change in the idler phase in the opposite direction, $\theta_i \to \theta_i - \Delta\theta$, while the equations of motion remain unchanged [41], therefore one of S and I can be chosen to be real.

The energy $\tilde{\omega}$ is real for a physical solution. The remaining complex quantities are therefore P and I. The signal momentum is also an unknown, but to solve the mean field equations, it has to be set (arbitrarily); here $\mathbf{k}_s = \mathbf{0}$ is used. The choice of the signal momentum is investigated in chapter 4.

In the first instance, the mean field occupations of the three modes are of interest. This requires some fairly substantial rearrangement which is detailed below. For simplicity, the following shorthand is introduced into the mean field equations:

$$\begin{aligned}
\xi_s &= \varepsilon_s - \omega_p + g_{\mathrm{x}} X_s^2 (X_s^2 n_s + 2X_p^2 n_p + 2X_i^2 n_i), \\
\xi_p &= \varepsilon_p - \omega_p + g_{\mathrm{x}} X_p^2 (2X_s^2 n_s + X_p^2 n_p + 2X_i^2 n_i), \\
\xi_i &= \varepsilon_i - \omega_p + g_{\mathrm{x}} X_i^2 (2X_s^2 n_s + 2X_p^2 n_p + X_i^2 n_i), \\
\eta &= g_{\mathrm{x}} X_s X_p^2 X_i.
\end{aligned}$$

First, Eq. (3.107) is rearranged for P^2:

$$P^2 = -\frac{(\xi_s - \tilde{\omega} - i\kappa_s)S}{\eta I^*}. \tag{3.110}$$

This is then substituted into Eq. (3.109) the result multiplied by I^*:

$$(\xi_i + \tilde{\omega} - i\kappa_i)n_i - (\xi_s - \tilde{\omega} - i\kappa_s)n_s = 0.$$

The real and imaginary parts must be zero independently and are therefore considered separately. From the imaginary part,

$$-\kappa_i n_i + \kappa_s n_s = 0,$$

so

$$n_i = \frac{\kappa_s}{\kappa_i} n_s = \Gamma_{si} n_s, \tag{3.111}$$

$$X_i^2 n_i = \frac{\kappa_s X_i^2}{\kappa_i X_s^2} X_s^2 n_s = \gamma_{si} X_s^2 n_s, \tag{3.112}$$

where the abbreviations Γ_{si} and γ_{si} have been introduced as ratios of the decay rates at the

different momenta, the second of which is scaled by the exciton fraction of the polaritons. This is an expression of the Manley-Rowe condition and states that the occupation of the idler mode is proportional to the signal mode [29, 31, 58]. If the polariton decay is constant ($\kappa_x = \kappa_c$) then the signal and idler occupations are the same.

Meanwhile, the real part:

$$(\xi_i + \tilde{\omega})n_i - (\xi_s - \tilde{\omega})n_s = 0,$$

is rearranged for $\tilde{\omega}$:

$$\tilde{\omega} = \frac{\xi_s n_s - \xi_i n_i}{n_i + n_s} = \frac{\xi_s - \xi_i \Gamma_{si}}{1 + \Gamma_{si}}. \tag{3.113}$$

This is a function of n_s and n_p. Restoring the definitions of ξ_s and ξ_i and writing n_i in terms of n_s leads to

$$\tilde{\omega} = R + Tn_s, \tag{3.114}$$

where

$$\begin{aligned} R &= \frac{\epsilon_s - \Gamma_{si}\epsilon_i - \omega_p + \Gamma_{si}\omega_p + 2g_{\mathrm{x}}X_p^2(X_s^2 - X_i^2)n_p}{1 + \Gamma_{si}}, \\ T &= \frac{g_{\mathrm{x}}X_s^2[X_s^2(1 + \gamma_{si}) - X_i^2(2 + \gamma_{si})]}{1 + \Gamma_{si}}. \end{aligned}$$

The next step is to find the relation between n_p and n_s. Eq. (3.110) is used to calculate

$$|P|^4 = n_p^2 = \frac{(\xi_s - \tilde{\omega})^2 + \kappa_p^2}{\Gamma_{si}\eta^2}. \tag{3.115}$$

ξ_s is written in a similar spirit to $\tilde{\omega}$

$$\xi_s = W + Qn_s, \tag{3.116}$$

and Q and W are defined as:

$$\begin{aligned} W &= \varepsilon_s - \omega_p + 2g_{\mathrm{x}}X_s^2X_p^2n_p, \\ Q &= g_{\mathrm{x}}X_s^2(X_s^2 + 2\gamma_{si}). \end{aligned}$$

$\tilde{\omega}$ from Eq. (3.114), and ξ_s from Eq. (3.116) are now substituted into Eq. (3.115):

$$n_p^2 = \frac{[(W + Qn_s) - (R + Tn_s)]^2 + \kappa_p^2}{\Gamma_{si}\eta^2}, \tag{3.117}$$

which is rearranged to form a quadratic equation for n_s:

$$an_s^2 + bn_s + c = 0$$

with

$$
\begin{aligned}
a &= (Q+T)^2 \\
&= \left[2g_{\mathrm{x}}X_s^4(1+2\gamma_{si}) - g_{\mathrm{x}}X_s^2X_i^2(2+\gamma_{si})\right]^2, \\
b &= 2W(Q+R+T)+2RT \\
&= 2\Big(\varepsilon_s - \omega_p + 2g_{\mathrm{x}}X_s^2X_p^2n_p\Big)\left(\frac{\epsilon_s - \Gamma_{si}\epsilon_i - \omega_p + \Gamma_{si}\omega_p + 2g_{\mathrm{x}}X_p^2(X_s^2-X_i^2)n_p}{1+\Gamma_{si}}\right. \\
&\quad \left. + g_{\mathrm{x}}X_s^2(X_s^2+2\gamma_{si}) + \frac{g_{\mathrm{x}}X_s^2[X_s^2(1+\gamma_{si}) - X_i^2(2+\gamma_{si})]}{1+\Gamma_{si}}\right) \\
&\quad + 2\left(\frac{\epsilon_s - \Gamma_{si}\epsilon_i - \omega_p + \Gamma_{si}\omega_p + 2g_{\mathrm{x}}X_p^2(X_s^2-X_i^2)n_p}{1+\Gamma_{si}}\right)\left(\frac{g_{\mathrm{x}}X_s^2(X_s^2(1+\gamma_{si}) - X_i^2(2+\gamma_{si}))}{1+\Gamma_{si}}\right), \\
c &= (W+R)^2 + \kappa_s^2 - \eta^2\Gamma_{si}n_p^2 \\
&= \left(\varepsilon_s - \omega_p + 2g_{\mathrm{x}}X_s^2X_p^2n_p + \frac{\epsilon_s - \Gamma_{si}\epsilon_i - \omega_p + \Gamma_{si}\omega_p + 2g_{\mathrm{x}}X_p^2(X_s^2-X_i^2)n_p}{1+\Gamma_{si}}\right)^2 \\
&\quad + \kappa_s^2 - \eta^2\Gamma_{si}n_p^2.
\end{aligned}
$$

In the quadratic equation for n_s, a depends only on the choice of the signal and pump momenta; while c and b are quadratic in the pump mode occupation. The signal occupation is then simply the result of solving the standard quadratic equation and has the solutions

$$n_s = \frac{-b \pm \sqrt{b^2 - 4ac}}{2a}.$$

For there to be OPO, n_s must be real and positive; for a given n_p, both possible n_s values are calculated; if neither is real and positive, the mean field signal occupation is zero and the pump strength F_{lp} is as calculated in the pump only case (note that with $n_s = n_i = 0$, Eq. (3.108) is exactly the pump only result of Eq. (3.57)). The occupations of the three modes $n_{s,p,i}$ can now be calculated if one is known; the rearrangement followed here assumes that n_p is the input quantity from which n_s, n_i and F_{lp} are calculated.

To relate the values here to the pump strength F_{lp}, Eq. (3.108) is rearranged:

$$F_{lp} = -(\xi_p - i\kappa_p)P - 2\eta SP^*I$$

In calculating $|F_{lp}|^2$, the SP^*I term is not straightforward, but from Eq. (3.107), can write:

$$S = \frac{-\eta P^2 I^*}{\xi_s - \tilde{\omega} - i\kappa_s} \tag{3.118}$$

so

$$F_{lp} = \left(-(\xi_p - i\kappa_p) + \frac{2\eta^2 n_i n_p(\xi_s - \tilde{\omega} + i\kappa_s)}{\xi_s - \tilde{\omega})^2 + \kappa_s^2}\right)P.$$

Taking the modulus squared gives the pump power:

$$I_p = |F_{lp}|^2 = n_p \left[\left(\xi_p - \frac{2\eta^2 n_i n_p (\xi_s - \tilde{\omega})}{(\xi_s - \tilde{\omega})^2 + \kappa_s^2} \right)^2 + \left(\kappa_p + \frac{2\kappa_s \eta^2 n_i n_p}{(\xi_s - \tilde{\omega})^2 + \kappa_s^2} \right)^2 \right]. \tag{3.119}$$

In all cases, the optical limiter regime of the pump mode is considered and in the absence of OPO, $|P|^2$ is monotonic in $|F_{lp}|^2$. The relations between $X_p^2 n_p$ and $X_s^2 n_s$ hold whatever the detuning of the laser from the lower polariton curve (i.e. optical limiter or bistable regime) but the mean field behaviours in the bistable regime would be much more complex and are not considered further.

In order to calculate more than the mode occupations, it is necessary to use the complex modes P, S, I. Since the values of $n_{s,p,i}$ are known, Eqs. (3.107)-(3.109) become:

$$(\Xi_s - \tilde{\omega})S + \eta P^2 I^* = 0, \tag{3.120}$$

$$\Xi_p P + 2\eta S P^* I + F_{lp} = 0, \tag{3.121}$$

$$(\Xi_i + \tilde{\omega})I + \eta S^* P^2 = 0, \tag{3.122}$$

with

$$\Xi_m = \varepsilon_m - \omega_p + 2g_{\mathrm{x}} X_m^2 (X_s^2 n_s + X_p^2 n_p + X_i^2 n_i) - g_{\mathrm{x}} X_m^4 n_m - i\kappa_m. \tag{3.123}$$

S from Eq. (3.118) is substituted into Eq. (3.121),

$$F_{lp} = \left(\frac{2\eta^2 n_p n_i}{\Xi_s - \tilde{\omega}} - \Xi_p \right) P,$$

and

$$P = \frac{F_{lp}}{\frac{2\eta^2 n_p n_i}{\Xi_s - \tilde{\omega}} - \Xi_p}$$

with $F_{lp} = \sqrt{|F_{lp}|^2} \in \mathbb{R}$. Since S can be chosen to be real, rearranging Eq. (3.122) for I gives the last of the mean field values of the system:

$$I = \frac{-\eta S^* P^2}{\Xi_i + \tilde{\omega}}. \tag{3.124}$$

3.4.2 Fluctuations and inverse Green's functions

To include fluctuations around the mean field of the OPO, the standard procedure is followed. Fluctuations exist around each of the three modes, but are restricted to share a single energy and momentum space. Therefore, the momenta of the fluctuations are restricted as described in section 3.2.7, while there are three copies of the fluctuations due to the three modes. The part of the action that is second order in the fluctuation fields is therefore between the vectors $\Delta\Psi_{\mathbf{k}}^\dagger$

and $\Delta\Psi_{\mathbf{k}}$ with:

$$\Delta\Psi_{\mathbf{k}} = \begin{pmatrix} \delta\Psi_{\mathbf{k},cl} \\ \delta\Psi_{\mathbf{k},q} \end{pmatrix}; \qquad \delta\Psi_{\mathbf{k},\{cl,q\}} = \begin{pmatrix} \delta\psi_{\mathbf{k},\{cl,q\},s} \\ \delta\overline{\psi}_{-\mathbf{k},\{cl,q\},s} \\ \delta\psi_{\mathbf{k},\{cl,q\},p} \\ \delta\overline{\psi}_{-\mathbf{k},\{cl,q\},p} \\ \delta\psi_{\mathbf{k},\{cl,q\},i} \\ \delta\overline{\psi}_{-\mathbf{k},\{cl,q\},i} \end{pmatrix}; \tag{3.125}$$

and the mode signature s, p, i defines the mode around which the fluctuations exist.

The inverse Green's functions can be written compactly [1,41,101], but here the elements are written out explicitly (since it is not especially easy to see the result of the summations). Since the inverse advanced Green's function is simply the Hermitian conjugate of the inverse retarded Green's function, $[D^{-1}]^R$ and $[D^{-1}]^K$ give all relevant terms. The symmetries under complex conjugation are noted, but not the symmetries that result from $\mathbf{k} \leftrightarrow -\mathbf{k}$ (and $\omega \leftrightarrow -\omega$).

The matrix elements of the inverse retarded Green's function are:

$$\begin{aligned}
[D^{-1}]^R_{(1,1)} &= \omega + \omega_p - \tilde{\omega} - \omega_{lp}(\mathbf{k}_s + \mathbf{k}) + i\kappa_{lp}(\mathbf{k}_s + \mathbf{k}) - 2g_{\mathrm{x}}X^2(\mathbf{k}_s + \mathbf{k})(X_s^2 n_s + X_p^2 n_p + X_i^2 n_i), \\
[D^{-1}]^R_{(1,2)} &= -2g_{\mathrm{x}}X(\mathbf{k}_s + \mathbf{k})X(\mathbf{k}_p + \mathbf{k})(X_p X_s SP^* + X_p X_i PI^*), \\
[D^{-1}]^R_{(1,3)} &= -2g_{\mathrm{x}}X(\mathbf{k}_s + \mathbf{k})X(\mathbf{k}_i + \mathbf{k})X_s X_i SI^*, \\
[D^{-1}]^R_{(1,4)} &= -g_{\mathrm{x}}X(\mathbf{k}_s + \mathbf{k})X(\mathbf{k}_s - \mathbf{k})X_s^2 S^2, \\
[D^{-1}]^R_{(1,5)} &= -2g_{\mathrm{x}}X(\mathbf{k}_s + \mathbf{k})X(\mathbf{k}_p - \mathbf{k})X_s X_p SP \\
[D^{-1}]^R_{(1,6)} &= -g_{\mathrm{x}}X(\mathbf{k}_s + \mathbf{k})X(\mathbf{k}_i - \mathbf{k})(X_p^2 P^2 + 2X_s X_i SI), \\
[D^{-1}]^R_{(2,1)} &= ([D^{-1}]^R_{(1,2)})^* = -2g_{\mathrm{x}}X(\mathbf{k}_s + \mathbf{k})X(\mathbf{k}_p + \mathbf{k})(X_s X_p S^* P + X_p X_i P^* I), \\
[D^{-1}]^R_{(2,2)} &= \omega + \omega_p - \omega_{lp}(\mathbf{k}_p + \mathbf{k}) + i\kappa_{lp}(\mathbf{k}_p + \mathbf{k}) - 2g_{\mathrm{x}}X^2(\mathbf{k}_+\mathbf{k})(X_s^2 n_s + X_p^2 n_p + X_i^2 n_i), \\
[D^{-1}]^R_{(2,3)} &= ([D^{-1}]^R_{(1,2)}) = -2g_{\mathrm{x}}X(\mathbf{k}_p + \mathbf{k})X(\mathbf{k}_i + \mathbf{k})(X_s X_p SP^* + X_p X_i PI^*), \\
[D^{-1}]^R_{(2,4)} &= -2g_{\mathrm{x}}X(\mathbf{k}_s - \mathbf{k})X(\mathbf{k}_p + \mathbf{k})X_s X_p SP, \\
[D^{-1}]^R_{(2,5)} &= -g_{\mathrm{x}}X(\mathbf{k}_p + \mathbf{k})X(\mathbf{k}_p - \mathbf{k})(X_p^2 P^2 + 2X_s X_i SI), \\
[D^{-1}]^R_{(2,6)} &= -2g_{\mathrm{x}}X(\mathbf{k}_p + \mathbf{k})X(\mathbf{k}_i - \mathbf{k})X_p X_i PI, \\
[D^{-1}]^R_{(3,1)} &= ([D^{-1}]^R_{(1,3)})^* = -2g_{\mathrm{x}}X(\mathbf{k}_s + \mathbf{k})X(\mathbf{k}_i + \mathbf{k})X_s X_i S^* I, \\
[D^{-1}]^R_{(3,2)} &= ([D^{-1}]^R_{(1,2)})^* = -2g_{\mathrm{x}}X(\mathbf{k}_p + \mathbf{k})X(\mathbf{k}_i + \mathbf{k})(X_s X_p S^* P + X_p X_i P^* I), \\
[D^{-1}]^R_{(3,3)} &= \omega + \omega_p + \tilde{\omega} - \omega_{lp}(\mathbf{k}_i + \mathbf{k}) + i\kappa_{lp}(\mathbf{k}_i + \mathbf{k}) - 2g_{\mathrm{x}}X^2(\mathbf{k}_i + \mathbf{k})(X_s^2 n_s + X_p^2 n_p + X_i^2 n_i), \\
[D^{-1}]^R_{(3,4)} &= -g_{\mathrm{x}}X(\mathbf{k}_s - \mathbf{k})X(\mathbf{k}_i + \mathbf{k})(X_p^2 P^2 + 2X_s X_i SI), \\
[D^{-1}]^R_{(3,5)} &= -2g_{\mathrm{x}}X(\mathbf{k}_p - \mathbf{k})X(\mathbf{k}_i + \mathbf{k})X_p X_i PI, \\
[D^{-1}]^R_{(3,6)} &= -g_{\mathrm{x}}X(\mathbf{k}_i + \mathbf{k})X(\mathbf{k}_i - \mathbf{k})X_i^2 I^2, \\
[D^{-1}]^R_{(4,1)} &= ([D^{-1}]^R_{(1,4)})^* = -g_{\mathrm{x}}X(\mathbf{k}_s + \mathbf{k})X(\mathbf{k}_s - \mathbf{k})X_s^2 (S^*)^2, \\
[D^{-1}]^R_{(4,2)} &= ([D^{-1}]^R_{(2,4)})^* = -2g_{\mathrm{x}}X(\mathbf{k}_s - \mathbf{k})X(\mathbf{k}_p + \mathbf{k})X_s X_p S^* P^*,
\end{aligned}$$

$$
\begin{aligned}
[D^{-1}]^R_{(4,3)} &= ([D^{-1}]^R_{(3,4)})^* = -g_{\mathrm{x}}X(\mathbf{k}_s-\mathbf{k})X(\mathbf{k}_i+\mathbf{k})(X_p^2(P^*)^2+2X_sX_iS^*I^*),\\
[D^{-1}]^R_{(4,4)} &= \omega+\omega_p-\tilde{\omega}-\omega_{lp}(\mathbf{k}_s-\mathbf{k})-i\kappa_{lp}(\mathbf{k}_s-\mathbf{k})-2g_{\mathrm{x}}X^2(\mathbf{k}_s-\mathbf{k})(X_s^2n_s+X_p^2n_p+X_i^2n_i),\\
[D^{-1}]^R_{(4,5)} &= -2g_{\mathrm{x}}X(\mathbf{k}_s-\mathbf{k})X(\mathbf{k}_p-\mathbf{k})(X_sX_pS^*P+X_pX_iP^*I),\\
[D^{-1}]^R_{(4,6)} &= -2g_{\mathrm{x}}X(\mathbf{k}_s-\mathbf{k})X(\mathbf{k}_i-\mathbf{k})X_sX_iS^*I,\\
[D^{-1}]^R_{(5,1)} &= ([D^{-1}]^R_{(1,5)})^* = -2g_{\mathrm{x}}X(\mathbf{k}_s+\mathbf{k})X(\mathbf{k}_p-\mathbf{k})X_sX_pS^*P^*,\\
[D^{-1}]^R_{(5,2)} &= ([D^{-1}]^R_{(2,5)})^* = -g_{\mathrm{x}}X(\mathbf{k}_p+\mathbf{k})X(\mathbf{k}_p-\mathbf{k})(X_p^2(P^*)^2+2X_sX_iS^*I^*),\\
[D^{-1}]^R_{(5,3)} &= ([D^{-1}]^R_{(3,5)})^* = -2g_{\mathrm{x}}X(\mathbf{k}_p-\mathbf{k})X(\mathbf{k}_i+\mathbf{k})X_pX_iP^*I^*,\\
[D^{-1}]^R_{(5,4)} &= ([D^{-1}]^R_{(4,5)})^* = -2g_{\mathrm{x}}X(\mathbf{k}_s-\mathbf{k})X(\mathbf{k}_p-\mathbf{k})(X_sX_pSP^*+X_pX_iPI^*),\\
[D^{-1}]^R_{(5,5)} &= \omega+\omega_p-\omega_{lp}(\mathbf{k}_p-\mathbf{k})-i\kappa_{lp}(\mathbf{k}_p-\mathbf{k})-2g_{\mathrm{x}}X^2(\mathbf{k}_p-\mathbf{k})(X_s^2n_s+X_p^2n_p+X_i^2n_i),\\
[D^{-1}]^R_{(5,6)} &= ([D^{-1}]^R_{(4,5)}) = -2g_{\mathrm{x}}X(\mathbf{k}_p-\mathbf{k})X(\mathbf{k}_i-\mathbf{k})(X_sX_pS^*P+X_pX_iP^*I),\\
[D^{-1}]^R_{(6,1)} &= ([D^{-1}]^R_{(1,6)})^* = -g_{\mathrm{x}}X(\mathbf{k}_s+\mathbf{k})X(\mathbf{k}_i-\mathbf{k})(X_p^2(P^*)^2+2X_sX_iS^*I^*),\\
[D^{-1}]^R_{(6,2)} &= ([D^{-1}]^R_{(2,6)})^* = -2g_{\mathrm{x}}X(\mathbf{k}_p+\mathbf{k})X(\mathbf{k}_i-\mathbf{k})X_pX_iP^*I^*,\\
[D^{-1}]^R_{(6,3)} &= ([D^{-1}]^R_{(3,6)})^* = -g_{\mathrm{x}}X(\mathbf{k}_i+\mathbf{k})X(\mathbf{k}_i-\mathbf{k})X_i^2(I^*)^2,\\
[D^{-1}]^R_{(6,4)} &= ([D^{-1}]^R_{(4,6)})^* = -2g_{\mathrm{x}}X(\mathbf{k}_s-\mathbf{k})X(\mathbf{k}_i-\mathbf{k})X_sX_iSI^*,\\
[D^{-1}]^R_{(6,5)} &= ([D^{-1}]^R_{(4,5)})^* = -2g_{\mathrm{x}}X(\mathbf{k}_p-\mathbf{k})X(\mathbf{k}_i-\mathbf{k})(X_sX_pSP^*+X_pX_iPI^*),\\
[D^{-1}]^R_{(6,6)} &= \omega+\omega_p+\tilde{\omega}-\omega_{lp}(\mathbf{k}_i-\mathbf{k})-i\kappa_{lp}(\mathbf{k}_i-\mathbf{k})-2g_{\mathrm{x}}X^2(\mathbf{k}_i-\mathbf{k})(X_s^2n_s+X_p^2n_p+X_i^2n_i).
\end{aligned}
$$

As in the pump only case, the inverse retarded Green's function is related to the matrix from the linear response analysis. The rotation is slightly different: $L=-\sigma_{z,6}[D^{-1}]^R(0,\mathbf{k})$ due to differences in the fluctuation signatures used in obtaining the linear response matrix [41]. Where $\sigma_{z,6}$ is

$$
\sigma_{z,6}=\begin{pmatrix}
1 & 0 & 0 & 0 & 0 & 0\\
0 & 1 & 0 & 0 & 0 & 0\\
0 & 0 & 1 & 0 & 0 & 0\\
0 & 0 & 0 & -1 & 0 & 0\\
0 & 0 & 0 & 0 & -1 & 0\\
0 & 0 & 0 & 0 & 0 & -1
\end{pmatrix}.
$$

The use of σ_z comes from writing $[D^{-1}]^R$ and L in terms of four sub-matrices [1, 41]. Since calculating the determinant of $[D^{-1}]^R$ in the OPO leads to an equation for ω^6, the rotation to the linear response matrix is performed to analyse the stability of the OPO state since the eigenvalues can still be calculated.

The inverse Keldysh Green's function, $[D^{-1}]^K(\omega,\mathbf{k})$, is similar to the pump only case (Eq. (3.61)), with diagonal elements:

$$
[D^{-1}]^K_{(1,1)}=i\sum_{i\in\{c,x\}}(h^i_{\mathbf{k}_s+\mathbf{k}})^2\kappa_iF_{\chi_i}(\omega_p-\tilde{\omega}+\omega),
$$

$$
\begin{aligned}
[D^{-1}]^K_{(2,2)} &= i \sum_{i\in\{c,x\}} (h^i_{\mathbf{k}_p+\mathbf{k}})^2 \kappa_i F_{\chi_i}(\omega_p+\omega),\\
[D^{-1}]^K_{(3,3)} &= i \sum_{i\in\{c,x\}} (h^i_{\mathbf{k}_i+\mathbf{k}})^2 \kappa_i F_{\chi_i}(\omega_p+\tilde{\omega}+\omega),\\
[D^{-1}]^K_{(4,4)} &= i \sum_{i\in\{c,x\}} (h^i_{\mathbf{k}_s-\mathbf{k}})^2 \kappa_i F_{\chi_i}(\omega_p-\tilde{\omega}-\omega),\\
[D^{-1}]^K_{(5,5)} &= i \sum_{i\in\{c,x\}} (h^i_{\mathbf{k}_s-\mathbf{k}})^2 \kappa_i F_{\chi_i}(\omega_p-\omega),\\
[D^{-1}]^K_{(6,6)} &= i \sum_{i\in\{c,x\}} (h^i_{\mathbf{k}_s-\mathbf{k}})^2 \kappa_i F_{\chi_i}(\omega_p+\tilde{\omega}-\omega).
\end{aligned}
$$

In all calculations, the simplification $F_{\chi_i}(\omega) = 1$ is considered, so the inverse Keldysh Green's function is much more compact:

$$
[D^{-1}]^K = i \begin{pmatrix}
\kappa_{lp}(\mathbf{k}_s+\mathbf{k}) & 0 & 0 & 0 & 0 & 0\\
0 & \kappa_{lp}(\mathbf{k}_p+\mathbf{k}) & 0 & 0 & 0 & 0\\
0 & 0 & \kappa_{lp}(\mathbf{k}_i+\mathbf{k}) & 0 & 0 & 0\\
0 & 0 & 0 & \kappa_{lp}(\mathbf{k}_s-\mathbf{k}) & 0 & 0\\
0 & 0 & 0 & 0 & \kappa_{lp}(\mathbf{k}_p-\mathbf{k}) & 0\\
0 & 0 & 0 & 0 & 0 & \kappa_{lp}(\mathbf{k}_i-\mathbf{k})
\end{pmatrix}. \tag{3.126}
$$

Inverting the Keldysh rotation is always done numerically in the OPO regime.

3.5 Results in the pump only case (numerical)

In this section, the pump only state and OPO threshold is analysed according to the calculations outlined in section 3.3 for three ratios of the exciton to photon decay: $\kappa_c = \kappa_x, 10\kappa_x$ and $100\kappa_x$, in which the photon decay is held constant and the exciton decay reduced. The first ratio gives constant polariton decay and the results have been published in Ref. [1]. When the exciton decay is much less than the photon decay, the polariton decay $\kappa_{lp}(\mathbf{k})$ is strongly momentum dependent, as shown in Fig. 3.2, where the photon decay is kept constant ($\kappa_c = 0.05$) and the exciton decay is reduced. Restoring the momentum dependence of the polariton decay is useful for closer comparison with experiments where polaritons with low momenta are much more visible than those with higher momenta [15]. The effects of changing the pump properties or choosing a different value for the signal momentum could also be explored, but this is not done in the present Keldysh analysis.

In all calculations, a system of non-dimensional units, where the exciton-photon interconversion rate $\Omega_R/2$ is rescaled to unity, as detailed in appendix A, is used. The pump is applied resonantly to the lower polariton dispersion at $\mathbf{k}_p = (k_p, 0) = (1.5, 0)$ and the minimum of the photon dispersion coincides with the exciton energy. In all cases, the pump mode occupation

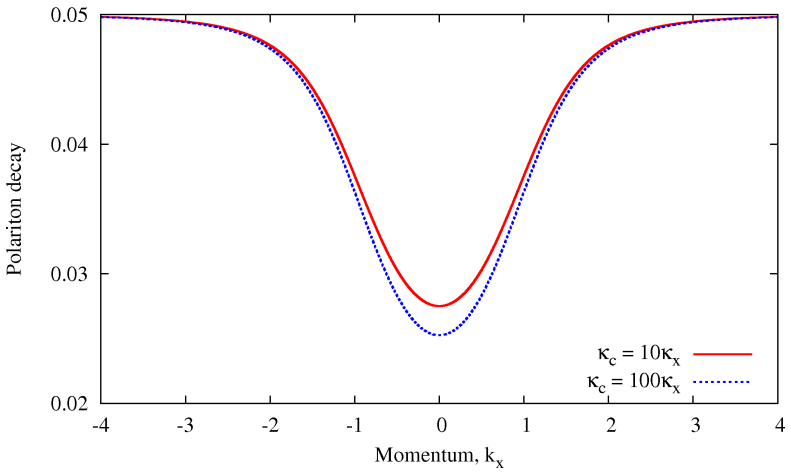

Figure 3.2: Momentum dependence of the polariton decay for two ratios of exciton and photon decays. The photon decay is kept constant at $\kappa_c = 0.05$ while the exciton decay is reduced. The polariton losses are greater at higher momenta than at $\mathbf{k} = \mathbf{0}$.

is monotonic in pump strength since the parameters are chosen such that the system is in the optical limiter regime.

3.5.1 $\kappa_c = \kappa_x$

First, the simple case of constant polariton decay is investigated [1]. Fig. 3.3 shows that there are two regions around $k_x = 0$ and $k_x = 2|\mathbf{k}_p|$ (in the lab frame) where the pump mode becomes unstable to small fluctuations. These appear as the pump mode occupation increases above some lower threshold value and then becomes stable again at higher mode occupations, which defines an 'upper threshold'. Since the system is in the optical limiter regime of the pump mode, increasing pumping can be used to mean increasing n_p.

In Fig. 3.4, $\xi^{\pm}(\mathbf{k})$, $\mu_{\text{eff}}(\mathbf{k})$, $\Re(\omega^{\pm}(\mathbf{k}))$ and $\Im(\omega^{\pm}(\mathbf{k}))$ from Eqs. (3.92), (3.93) and (3.95), are plotted for a range of stable pump mode occupations. When pumping is increased, the instability threshold is approached from below and the imaginary parts of the complex eigenvalues $\Im(\omega^{\pm}(\mathbf{k}))$ start to split while the real parts combine in four places. This leads to the double tails seen at low n_p in Fig. 3.3. When the four maxima in the imaginary parts of the complex eigenvalues first appear, two are located near the pump momentum, one at a much higher and one at a much lower momentum. As the transition is approached, the peaks in the imaginary parts grow and those that were below the pump momentum move towards each other and $k_x = 0$, while those that were above the pump momentum move towards $k_x = 2|\mathbf{k}_p|$.

For a strong pump (high n_p), the pump mode becomes stable to small fluctuations again. Just above this upper threshold, there are only two places where $\Im(\omega^{+}(\mathbf{k})) \neq \Im(\omega^{-}(\mathbf{k}))$: one near $k_x = 0$ and one near $k_x = 2|\mathbf{k}_p|$. As the pump strength is further increased these peaks eventually disappear while the real parts of the eigenvalues ($\Re(\omega^{\pm}(\mathbf{k}))$) separate and become

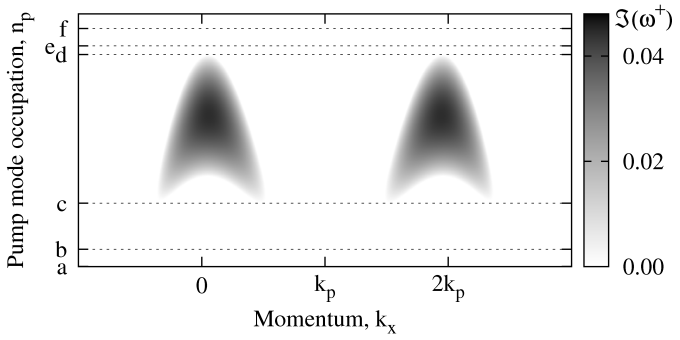

Figure 3.3: Regions of unstable single-mode pump-only state, $\Im(\omega^{\pm}) > 0$, symmetric around the pump momentum $\mathbf{k}_p$. The letters and dotted lines correspond to the pump mode occupations used in Fig. 3.4 (a is $n_p = 1 \times 10^{-4}$ and cannot be resolved from the horizontal axis). Since the pump mode is in the optical limiter regime, the pump strength F_p is monotonic in n_p so either could be used to label the y-axis.

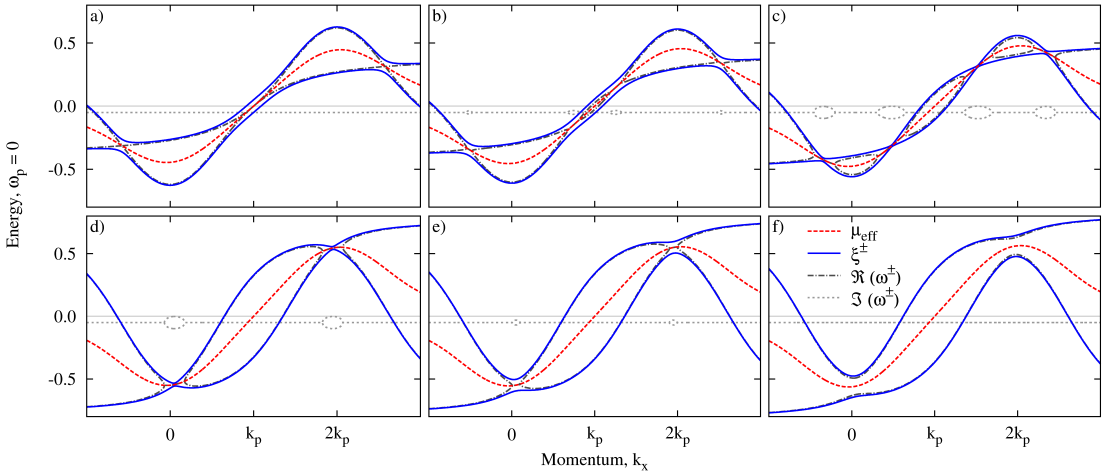

Figure 3.4: Solutions to $\det([D^{-1}]^R) = 0$ for the stable pump mode occupations indicated in Fig. 3.3. Red dotted: μ_{eff} from $\Im(\det([D^{-1}]^R(\mu_{\text{eff}}, \mathbf{k}))) = 0$ where $\mu_{\text{eff}} \in \mathbb{R}$; solid blue: $\xi^{\pm}$ from $\Re(\det([D^{-1}]^R(\xi^{\pm}, \mathbf{k}))) = 0$ where $\xi^{\pm} \in \mathbb{R}$; dark grey dashed: $\Re(\omega^{\pm})$ and grey dashed: $\Im(\omega^{\pm})$ from $\det([D^{-1}]^R(\omega^{\pm}, \mathbf{k})) = 0$ where $\omega^{\pm} \in \mathbb{C}$. Top row: approaching lower threshold from below: a) $n_p = 1 \times 10^{-4}$; b) $n_p = 0.02$; c) $n_p = 0.073$. Bottom row: increasing n_p above 'upper threshold': d) $n_p = 0.245$; e) $n_p = 0.255$; f) $n_p = 0.275$.

increasingly close to the poles ($\xi^{\pm}(\mathbf{k})$).

In general, the poles, $\xi^{\pm}(\mathbf{k})$ (solid blue lines in Fig. 3.4) pinch together at the momenta where $\Im(\omega^{\pm}(\mathbf{k}))$ is closest to 0. The values of $\xi^{\pm}(\mathbf{k})$ are very close to the spectra, $\Re(\omega^{\pm}(\mathbf{k}))$, apart from where $\Im(\omega^{\pm}(\mathbf{k}))$ split (or differ from $\Im(\omega^{\pm}(\mathbf{k})) = -\kappa_{lp}$). At these points, the effective chemical potential is equal to the real parts of the eigenvalues. The phase transition occurs where the real and imaginary parts of the determinant of the inverse retarded Green's function become

zero simultaneously, which indicates diverging luminescence in the normal state and is where $\mu_{\text{eff}}(\mathbf{k}) = \xi^{\pm}(\mathbf{k})$.

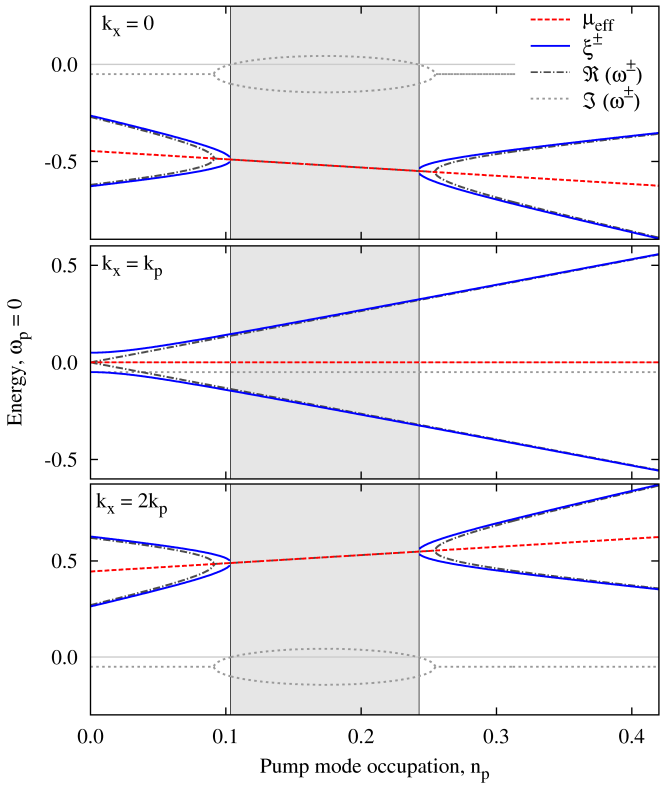

Figure 3.5: As Fig. 3.4 but at selected momenta. The unstable region is indicated in grey. Top: $k_x = 0$ i.e. at the expected signal, the chemical potential μ_{eff} decreases with increasing n_p to cross $\xi^{\pm}$ when $\Im(\omega^{+}) = 0$; middle: $k_x = |\mathbf{k}_p|$, μ_{eff} never crosses $\xi^{\pm}$ and $\Im(\omega^{\pm}) < 0$ for any n_p i.e. there is no instability directly at the pump; bottom: $k_x = |2\mathbf{k}_p|$ i.e. at the expected idler, the chemical potential μ_{eff} increases with increasing n_p to cross $\xi^{\pm}$ when $\Im(\omega^{+}) = 0$.

To show clearly what happens across the instability threshold, the behaviour of $\Re(\omega^{\pm}(\mathbf{k}))$, $\Im(\omega^{\pm}(\mathbf{k}))$, $\xi^{\pm}(\mathbf{k})$ and $\mu_{\text{eff}}(\mathbf{k})$ are examined over a range of pump mode occupations three momenta in the lab frame: $k_x = k_p$, 0 and $|2\mathbf{k}_p|$. As can be seen in Fig. 3.5, at the pump, $\Im(\omega^{\pm}) < 0$ and $\mu_{\text{eff}} \neq \xi^{\pm}$ at any n_p which indicates that there is no instability *at* the pump mode as expected for the choice of parameters that ensures that the system is in the optical limiter regime. Meanwhile, for $k_x = 0$ the effective chemical potential μ_{eff} decreases as the density is increased and crosses $\xi^{\pm}$ in two places indicating the lower and upper thresholds. Around $k_x = 2|\mathbf{k}_p|$, the effective chemical potential is increasing with increasing density.

In Fig. 3.5, the mode crossing is seen to occur exactly at the transition from a stable to an unstable region, where $\Im(\omega^{\pm}) = 0$. This behaviour of pinching and crossing is expected from Eqs. (3.92) and (3.93), and is analogous to other bosonic condensations, where the phase transition is

associated with the chemical potential crossing one of the energy modes [3, 21]. The increasing chemical potential, and therefore the closest analogy to equilibrium BEC, is around the expected idler, not the signal.

The effective temperature that can be defined in this case is plotted in Fig. 3.6. The shape of $T_{\text{eff}}(\mathbf{k})$ is set by the X^4 contribution in $V_{p_{+-}}$ and has minima at momenta $k_x = 0$ and $k_x = |2\mathbf{k}_p|$ in the lab frame. In the OPO transition, the 'condensation' happens into signal and idler modes with momenta close to the lowest effective temperature.

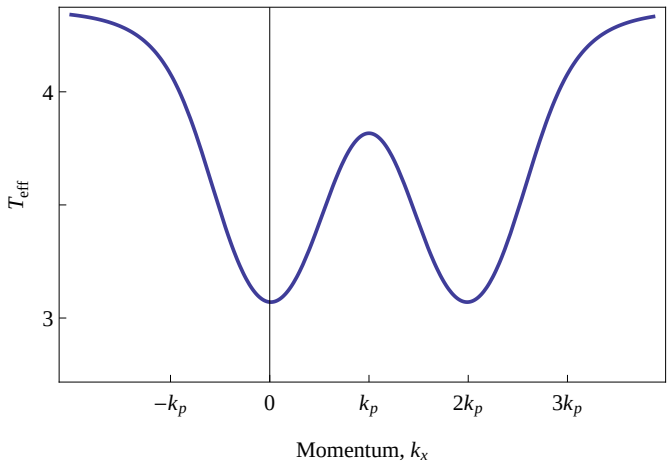

Figure 3.6: The effective temperature, $T_{\text{eff}}(\mathbf{k})$ as defined by Eq. (3.98), with a local maximum at the applied pump and global minima at $k_x = 0, |2\mathbf{k}_p|$. The pump mode occupation provides a purely multiplicative factor.

When the single mode ansatz is stable, the incoherent luminescence, absorption and spectral weight around the pump mode can be calculated. The pump mode occupations of Figs. 3.4 c and 3.4 d, close to the border of the unstable region, are considered. Further away from the thresholds, the $\det([D^{-1}]^R)$ is larger so the luminescence will be weaker; the two samples chosen are representative of the general behaviour of the poles.

Below the lower threshold, Fig. 3.7 a, four peaks appear in around the pump mode, above the 'upper threshold', Fig. 3.7 b, there are only two peaks centred near $k_x = 0$ and $k_x = |2\mathbf{k}_p|$. These peaks in the incoherent luminescence correspond to where the imaginary parts of the eigenvalues split and the smallest value of $\det([D^{-1}]^R)$.

One effect of assuming a constant polariton decay is that the peaks in the polariton luminescence appear symmetric about the pump mode, reflecting the pairwise scattering process. In experiments, only the photonic component of polaritons can be measured and the signal, which has a higher photon fraction, appears stronger than the idler [27, 82]. Thus, in the lower panels of Fig. 3.7, the luminescence is rescaled according to the photon fraction (Eq. (3.52)) and the photon luminescence is stronger at low momenta, as expected.

The absorption (top row of Fig. 3.8) follows the same general pattern as the luminescence,

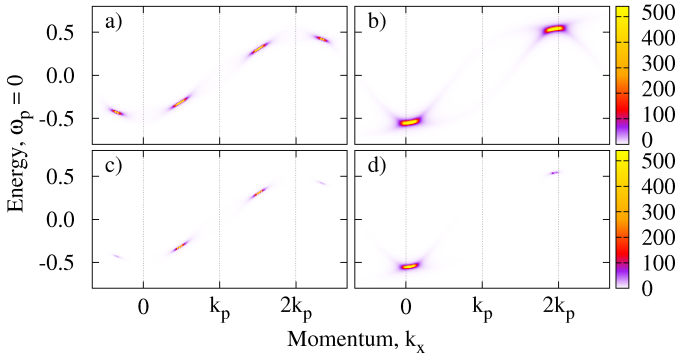

Figure 3.7: Incoherent polariton (top) and photon (bottom) luminescence near the instability thresholds. Left: below lower threshold $n_p = 0.073$; right: above upper threshold $n_p = 0.245$.

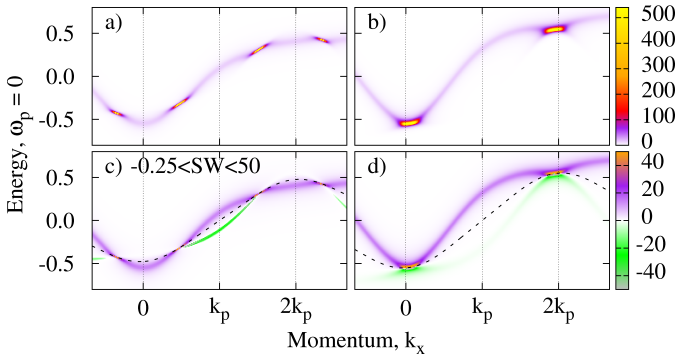

Figure 3.8: Polariton absorption (upper) and spectral weight (lower) near the instability thresholds. Left: below lower threshold $n_p = 0.073$; right: above upper threshold $n_p = 0.245$. The scales for positive spectral weight are the same, at weak pumping, there is only weak negative spectral weight and the range is curtailed for visibility. The dashed line in the lower panels is the effective chemical potential $\mu_{\text{eff}}(\mathbf{k})$ of Fig. 3.4.

but is generally stronger on the upper branch of the spectrum. As seen in Figs. 3.8 c and 3.8 d, there are regions of negative spectral weight where the luminescence is greater than the absorption. At weak pumping, the spectral weight is only very weakly negative (the negative part of the spectral weight range in Fig. 3.8 c has been greatly reduced to show this), this occurs for energies below the chemical potential and away from the peaks in the luminescence. Above the upper threshold, the regions of negative spectral weight occur above the effective chemical potential for momenta less than k_p and below the chemical potential for momenta above k_p.

In Fig. 3.9, the incoherent luminescence has been plotted for all momenta $\mathbf{k} = (k_x, 0)$ and energies below the pump energy (around the signal only). For weak pumping, the two peaks are broad and the one at the lower energy is weaker than the one at higher energy. Comparing this to Fig. 3.7 a, this shows that the peak at higher momentum dominates, which is consistent with the weaker luminescence on the side of the ring away from the pump in Fig. 3.10. Above the

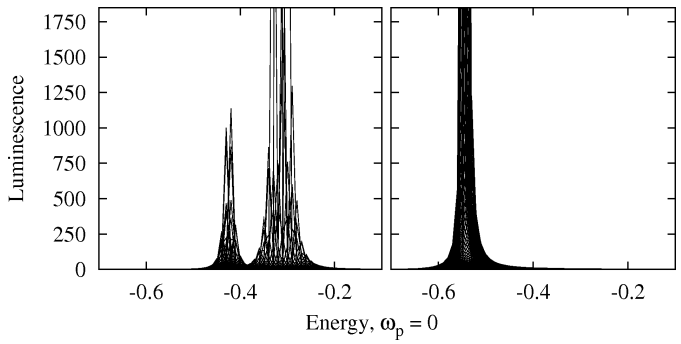

Figure 3.9: Incoherent luminescence at energies below ω_p for a large rang of momenta. Left: $n_p = 0.073$, below the lower threshold, the peak at higher energy dominates; right: $n_p = 0.245$ above the upper threshold, the single peak is at a lower energy and is much narrower than the two peaks present for a weaker pump.

upper threshold, the peak in the luminescence is narrower in energy.

Lastly, the luminescence is integrated over energy and plotted in two-dimensional momentum space where $\mathbf{k} = (k_x, k_y)$. The four peaks in the (ω, k_x) plots (Fig. 3.7 and 3.8) are a signature of a ring structure in the luminescence near the lower threshold; with a higher occupation on the side closest to the pump. Just above the upper threshold, the instability develops at a unique momentum $\mathbf{k}_s = (k_s, 0)$ and only two distinct peaks associated with developing signal and idler states are observed. The OPO transition can therefore be described using a distinct *pair* of new modes if the pump is decreased through the upper threshold of the instability.

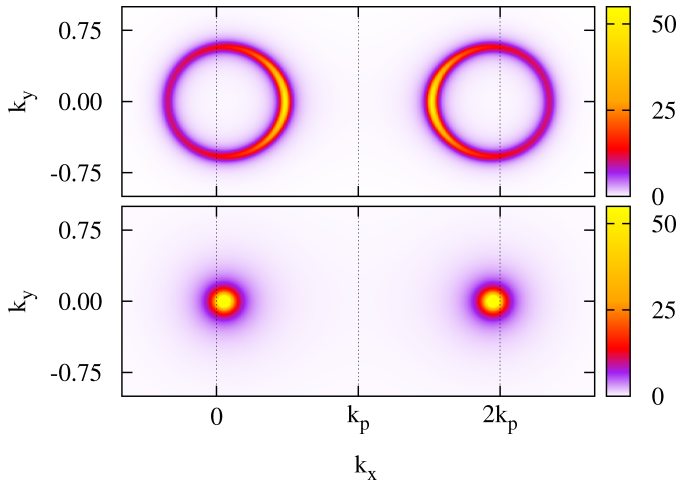

Figure 3.10: Incoherent polariton luminescence in 2-D momentum space after integrating over energy. Top: below lower threshold, $n_p = 0.073$; bottom: above upper threshold, $n_p = 0.245$.

3.5.2 $\kappa_c = 10\kappa_x$

When the photon decay rate is ten times the exciton decay rate, the pump mode becomes unstable at a weaker pump strength than when the polariton decay is constant and the return to stability is slow as shown by the large blue region in the left hand side of Fig. 3.11. There is also a double peak in the imaginary parts even when the pump mode is stable. The imaginary parts of the eigenvalues are determined by Eq. (3.68) which always has a contribution:

$$-\frac{\kappa^+ + \kappa^-}{2}$$

which has a double dip (peak) structure as shown in the right hand side of Fig. 3.11.

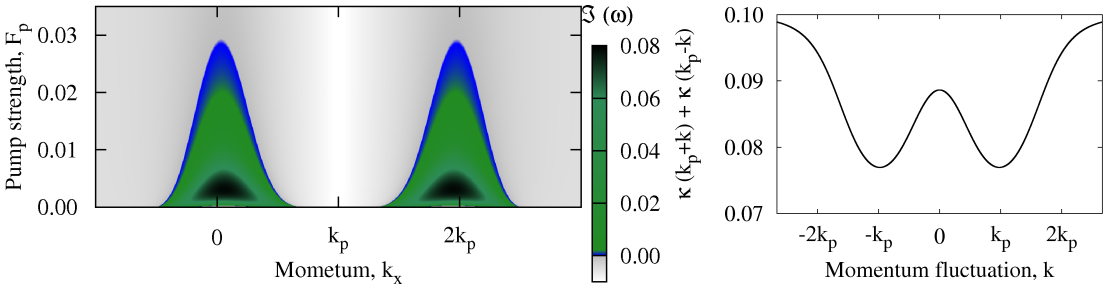

Figure 3.11: Left: imaginary part of the eigenvalue that becomes positive (blue, green, black region) for $\kappa_c = 10\kappa_x$. The return to stability is at a higher pump strength than for equal decays. Right: background variation in imaginary part of eigenvalues for $\kappa_c = 10\kappa_x$, the two dips are at real momenta 0 and $2k_p$, here they are plotted in terms of the momentum fluctuations around the pump mode.

According to Eq. (3.68) the two possible eigenvalues always have different imaginary parts, but, unlike when the polariton decay is constant, the real parts do not stick together at all points where the imaginary parts split [28]. Further, the real parts of the complex eigenvalues are the same as the poles $\xi^{\pm}$, as seen in Fig. 3.12. The effective chemical potential, given by Eq. (3.73), does not lie exactly half way between the poles. At low pump strengths it is closer to the upper branch of the spectrum at low momenta and closer to the lower branch at high momenta, while at high pump strengths, it approaches the upper branch near $k = 2k_p$ and the lower branch near $k = 0$.

Physical quantities are again calculated for a stable pump mode below the lower and above the upper thresholds. The luminescence is slightly weaker around the expected signal than around the idler, reflecting that polaritons are collect in the higher momentum states from which their decay is slower. At low pump strengths, Fig. 3.12 a and b, the poles are pinched significantly and the incoherent polariton (Fig. 3.13 a) and photon (Fig. 3.13 c) luminescence plots display corresponding peaks (for the pump strength of Fig. 3.12 b). Near the upper threshold, the poles are barely pinched, reflecting the slow return to stability in Fig. 3.11. Around $k_x = 0$, the lower of the two branches has a higher occupation (and hence luminescence) while around $k_x = 2k_p$,

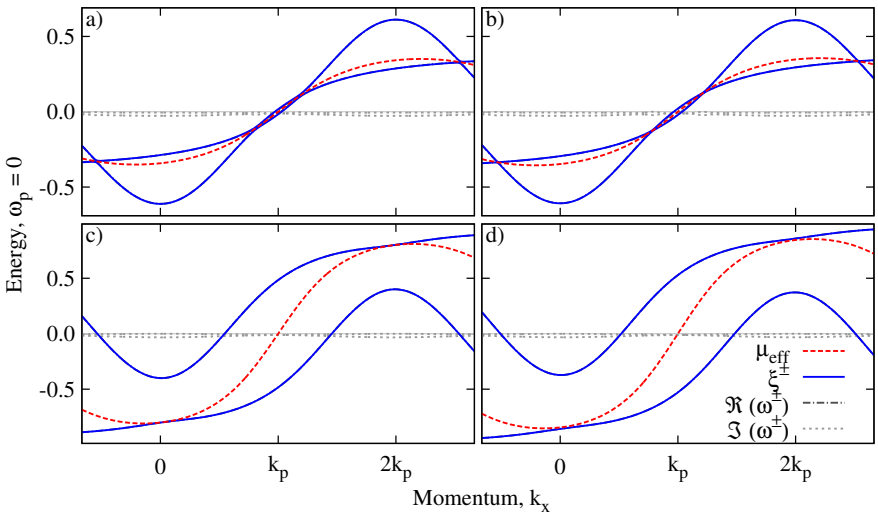

Figure 3.12: Poles and eigenvalues for $\kappa_c = 10\kappa_x$ a) $n_p = 0.010$, b) $n_p = 0.014$ below the instability threshold; c) $n_p = 0.366$, d) $n_p = 0.400$ on return to stable pump. $\mu_{\rm eff}$ is given by Eq. (3.73).

the upper branch dominates. The peaks in the luminescence are narrow in energy, but appear broad in momentum. The lower photon fraction of the polaritons at high momenta again means that the visible (photon) luminescence is greatest at low momenta despite the larger polariton occupation at higher momenta.

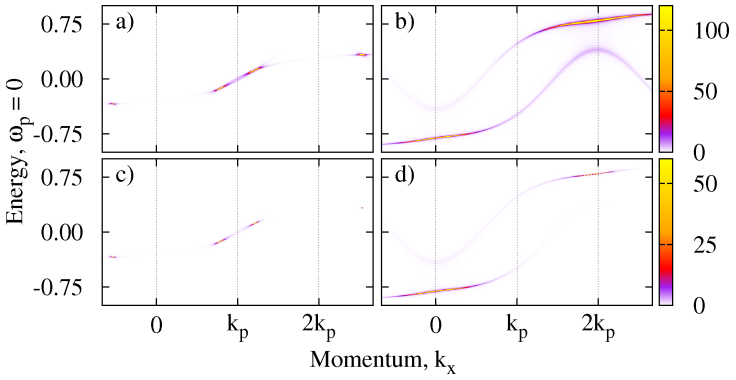

Figure 3.13: Polariton (top) and photon (bottom) luminescence in energy-momentum space for $\kappa_c = 10\kappa_x$. a, c) $n_p = 0.014$ below the lower instability threshold, b,d) $n_p = 0.366$ above the upper threshold.

The absorption and spectral weight plotted in Fig. 3.14 are similar to the luminescence and to the case of constant decay. The main difference is that the spectral weight is negative over much larger regions; at low pump strengths, positive spectral weight occurs both above and below $\mu_{\rm eff}$. Above the upper threshold, most of the region where the spectral weight is negative

is found at energies below the effective chemical potential.

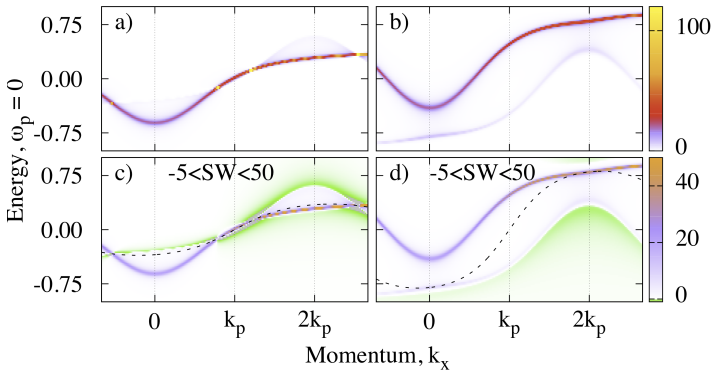

Figure 3.14: Polariton absorption (top) and spectral weight (bottom) in energy-momentum space for $\kappa_c = 10\kappa_x$. a, c) $n_p = 0.014$ below the lower instability threshold, b,d) $n_p = 0.366$ above the upper threshold.

Integrating the luminescence over energy, and plotting in 2-D momentum space, makes the features seen in Fig. 3.13 clearer. In Fig. 3.15 a, the fairly even rings seen in the case of constant polariton decay, Fig. 3.10, are distorted on the sides closest to the pump, and the luminescence is stronger at higher momenta. The ring with $k_x > k_p$ is strongest due to the lower polariton decay in this region. Above the upper threshold, Fig. 3.15, the only significant difference to the case of constant polariton decay is that the peak around $k_x = 0$ is weaker than that near $k_x = 2k_p$.

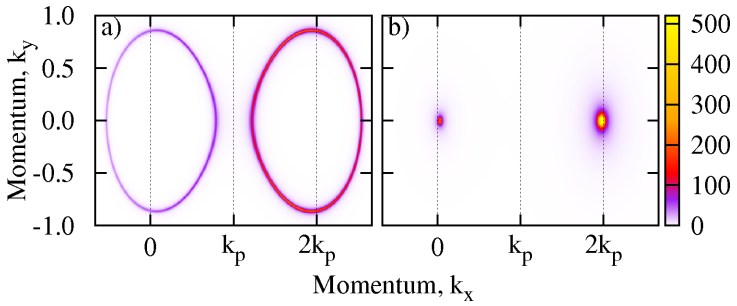

Figure 3.15: Polariton luminescence integrated over energy and plotted in 2-D momentum space for $\kappa_c = 10\kappa_x$. a) $n_p = 0.014$ below the lower instability threshold $0 < L < 50$, b) $n_p = 0.366$ above the upper threshold $0 < L < 520$.

3.5.3 $\kappa_c = 100\kappa_x$

Taking the photon decay to 100 times the exciton decay, leads to a pump mode that is unstable for all but the lowest pump mode occupations (the stable example is for $n_p = 0.0049$). For pump strengths that are relevant to the lower polariton model, the unstable region covers a much larger

range of momenta. The region where the instabilities are large is, however, small and at low pump strengths. The weakly unstable tail persists to all pump strengths considered, as seen in the left hand side of Fig. 3.16.

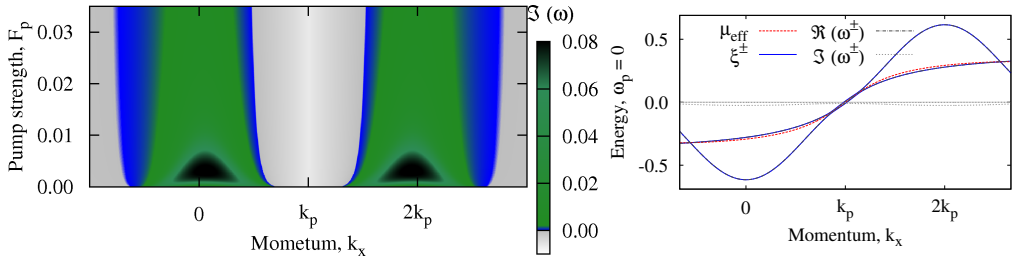

Figure 3.16: Left: imaginary part of the eigenvalue that becomes positive (blue, green, black region) for $\kappa_c = 100\kappa_x$ for the moderate pump strengths (and pump mode densities) considered, there is no upper threshold of the unstable region. Right: poles and eigenvalues for $\kappa_c = 100\kappa_x$ near instability threshold, $n_p = 0.0049$. The eigenvalues are plotted over the poles to show that the real parts of the eigenvalues lie on top of the poles $\xi^{\pm}$, μ_{eff} is given by Eq. (3.73).

In the right hand side of Fig. 3.16, the poles and the eigenvalues are plotted for the stable example at very low pump strength. The imaginary parts of the eigenvalues are seen to vary and the effective chemical potential is very close to crossing the poles so the system is very close to threshold. The polariton luminescence, absorption and spectral weight and the photon luminescence are calculated for this stable pump strength. Apart from further weakening around $k_x = 0$, the behaviours are exactly as below threshold when $\kappa_c = 10\kappa_x$, and the plots in Fig. 3.17 is very similar to the left hand sides of Figs. 3.13 and 3.14.

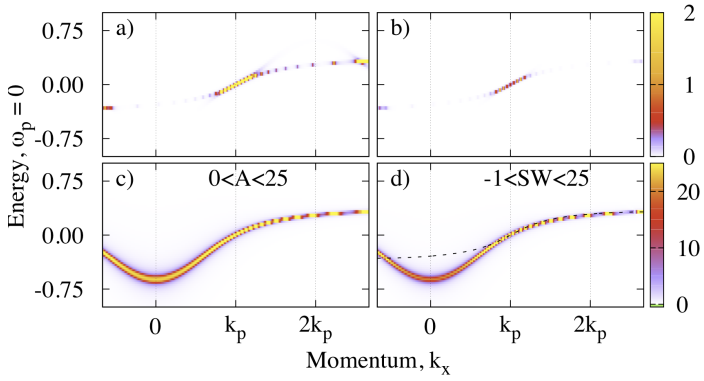

Figure 3.17: $\kappa_c = 100\kappa_x$ and $n_p = 0.0049$ below instability threshold. a) polariton luminescence, b) photon luminescence, c) polariton absorption, d) polariton spectral weight.

When the luminescence is integrated over energy, the features noted in Fig. 3.15 are even more pronounced. In Fig. 3.18, the distortion of the rings is tending towards a clear figure of eight shape, consistent with a study of polaritons under pulsed resonant excitation [82]. These

calculations are of the incoherent polariton luminescence around the pump mode, while the experiments also included the pump mode. There is no reason for energy and momentum (particularly momentum) conservation to give results that depend on whether the excitation is continuous or pulsed, so long as the polariton lifetimes are long enough for the scattering to occur.

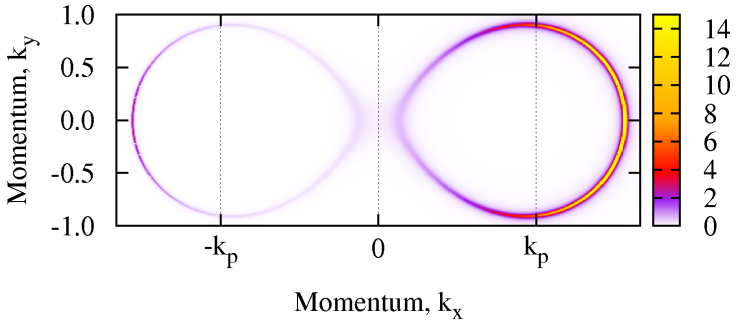

Figure 3.18: Polariton luminescence integrated over energy and plotted in 2-D momentum space for $\kappa_c = 100\kappa_x$.

The lack of an upper threshold is examined by looking at the behaviours at set momenta across a range of pump strengths. In Fig. **??**, the two sets of solutions to $\det([D^{-1}]^R) = 0$ are plotted at $k_x = 0, k_p$ and $2k_p$ which correspond to the expected signal, the pump and the expected idler respectively. As in Fig. 3.5, these momenta are broadly representative of the entire region around the pump mode. As mentioned in section 3.3, $\det([D^{-1}]^R) = 0$, which controls the transition, can be satisfied by $\mu_{\text{eff}} = \xi^{\pm}$; alternatively the transition can be said to occur when the imaginary part of a complex eigenvalue is positive. The condition for the pump mode to be stable ($\Im(\omega) < 0 \ \forall \ \mathbf{k}$) only gives the lower threshold; since the effective chemical potential only crosses the poles once, there is no upper threshold.

When the proposed steady state is unstable, the real parts of the complex eigenvalues (Eq. (3.68)) are not equal to the effective chemical potential, μ_{eff} (Eq. (3.73)). At $k_x = 0, 2k_p$, there is a small region where $\mu_{\text{eff}} = \Re(\omega^{\pm})$, but otherwise the two complex eigenvalues have different real parts. At the lower threshold, the real parts of the eigenvalues first differ significantly from the poles at the point where $\det([D^{-1}]^R) = 0$. As in the case of constant polariton decay, the chemical potential is increasing through the threshold around $k_x = 2k_p$ and decreasing around $k_x = 0$.

The case where $\kappa_c = 10\kappa_x$ differs only by a return to stability for the pump mode. As noted in section 3.5.2, the imaginary parts of the eigenvalues decrease slowly towards the upper threshold. It was noted that in Figs. 3.13 and 3.14, the quantities calculated above the upper threshold were broadened in energy-momentum space, and that in Fig. 3.12 there was little pinching of the poles towards the effective chemical potential around the return to stability. These features all reflect that the return to a stable pump mode is slowed when the exciton decay is reduced compared with the photon decay.

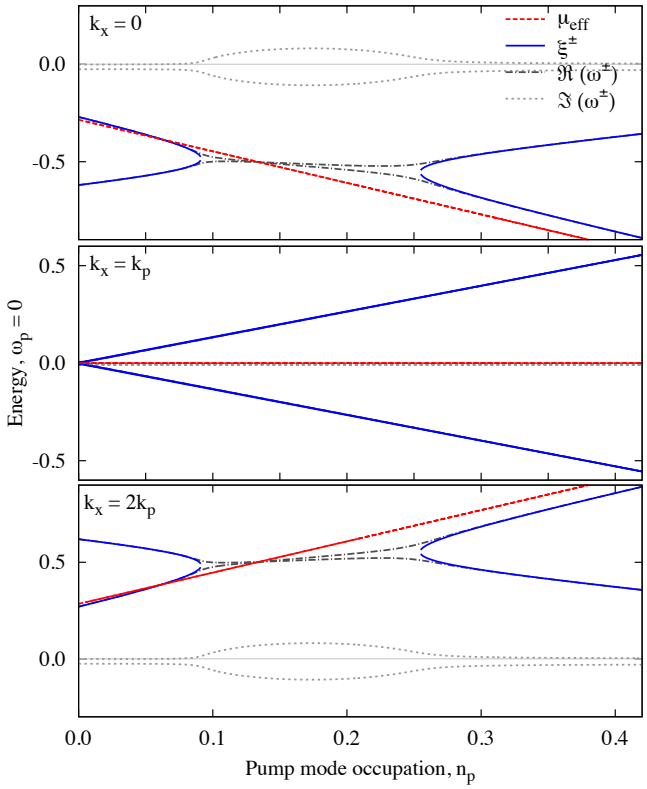

Figure 3.19: The poles and instabilities over a range of pump mode occupations (pump strengths) at three momenta. Top: $k_x = 0$; centre: $k_x = k_p$; bottom: $k_x = 2k_p$. There is no upper threshold at $k_x = 0\ 2k_p$.

3.6 Above OPO threshold, constant polariton decay

The three mode description of the OPO regime is analysed for the case of constant polariton decay. The steady state requires that the signal and idler momenta are specified [30]; the simplest choice of $\mathbf{k}_s = \mathbf{0}$ is used so $\mathbf{k}_i = 2\mathbf{k}_p$, although in experiments $\mathbf{k}_s$ is usually small but finite [33, 102].

The mean field occupations of the pump, $\mathbf{k}_p = (1.5, 0)$ and signal, $\mathbf{k}_s = \mathbf{0}$ are plotted in Fig. 3.20. The pump mode occupation in the absence of the signal and idler states is also included. In the OPO regime, the occupation of the pump mode is depleted due to scattering into the signal and idler modes which have equal occupation due to the constant polariton decay, as shown in Eq. (3.111).

Taking the determinant of the inverse retarded Green's function, and solving $\det([D^{-1}]^R(\omega, \mathbf{k})) = 0$ for $\omega^j \in \mathbb{C}$ gives the modes of the system ω^j. With the three mean field modes there are now six poles. A sample pump power near the upper threshold of the OPO region ($I_p = 9.016 I_{th}$ in Fig. 3.20) is considered, and the real and imaginary parts of the complex eigenvalues are

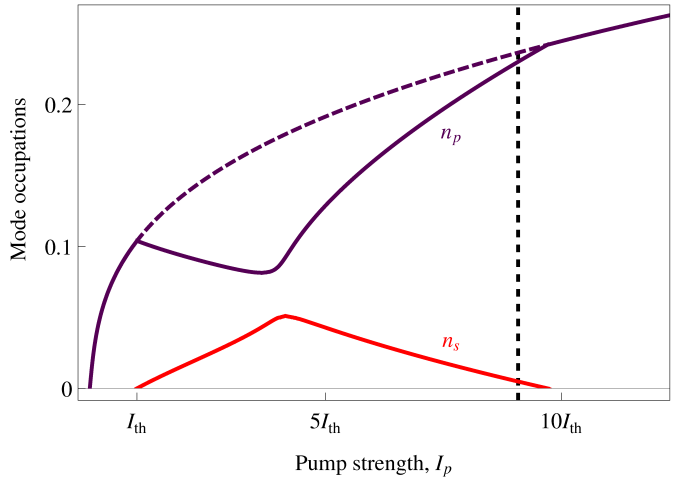

Figure 3.20: Signal, n_s (red), and pump, n_p (purple, the dashed part is the pump only ansatz within the OPO region) mode occupations within the OPO regime for $\mathbf{k}_p = (1.5, 0)$ and $\mathbf{k}_s = (0, 0)$. The dashed vertical line is the pump power considered for Figs. 3.21-3.23. The idler occupation n_i is the same as the signal occupation for constant polariton decay [29, 31, 58].

plotted in Fig. 3.21. (In reference to the contents of the following chapter, up to the difference in value of the polariton decay, this sample would lie in the blue region near the upper threshold of Fig. 4.23) These show that the steady state is stable ($\Im(\omega) < 0$), and that a Goldstone mode, characterised by $\Im(\omega) \to 0$ *and* $\Re(\omega) \to 0$ for $\mathbf{k} \to \mathbf{0}$, is present [41]. (The example here is along $k_y = 0$ so $k_x \to 0$ is of interest for the limiting behaviour.) The Goldstone mode is associated with the spontaneous symmetry breaking of the phase freedom of the signal and idler phases in the OPO regime. To remain within the three mode ansatz, it is assumed that the fluctuations in each mode are close in momenta and energy to that mode and the momentum range for plotting the results is therefore restricted to $|k_x - |\mathbf{q}|_m| \leq (|\mathbf{k}|_p - |\mathbf{k}|_s)/2$.

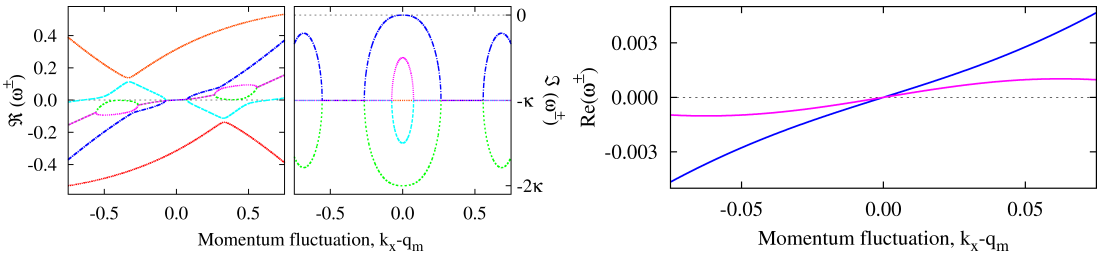

Figure 3.21: Real $\Re(\omega^j)$ (left) and imaginary parts $\Im(\omega^j)$ (centre) of the eigenvalues for the OPO state at pump power: $I_p = 9.016 I_{th}$. The dark blue curve corresponds to the Goldstone mode. Since all the imaginary parts of the poles are negative, the OPO ansatz is stable. In the right hand panel, the real parts of the spectra in a very small region around $\delta k = 0$ showing that, although $\mathbf{k}_s = (0, 0)$, there is still a finite slope of the Goldstone mode.

In the right hand side of Fig. 3.21, the very central region of the spectra is plotted. Although

in Fig. 3.21 the real parts of the spectra appear flat in the limit $\omega \to 0, \mathbf{k} \to 0$, in Fig. 3.21, it is clear that although $\mathbf{k}_s = (0, 0)$, the spectra are still sloped. In particular this slope is linear in the momentum fluctuation and is due to the finite flow induced by the pump. The imaginary part of the Goldstone mode is proportional to $-|\mathbf{k}|^2$ [41].

For the stable three mode description of the OPO regime, the incoherent luminescence is calculated. In Fig. 3.22, the contributions from around the signal, pump and idler modes are considered separately and the spectra ($\Re(\omega)$ from linear response) overlaid. There are clear variations in the occupations of the different branches according to the mode considered. For example, the outermost branches with increasing energy as the momentum of fluctuations increase are only noticeably occupied around the pump mode, while the parts of these branches characterised by decreasing energy with increasing momentum contribute to the luminescence around the signal mode for negative momentum of fluctuations and around the idler for positive momentum. The divergence caused by the Goldstone mode at $\omega_{s,i}, k_x = 0$ leads to significant peaks close to the signal and idler states. There is only a weak peak in the incoherent luminescence around the pump mode ($\omega_p, k_x = 0$), which is due to the secondary splitting in the imaginary parts of the eigenvalues (central (blue/green) lines in the right hand side of Fig. 3.21): in this case since the imaginary part pertinent to the pump mode is not zero, the luminescence does not diverge.

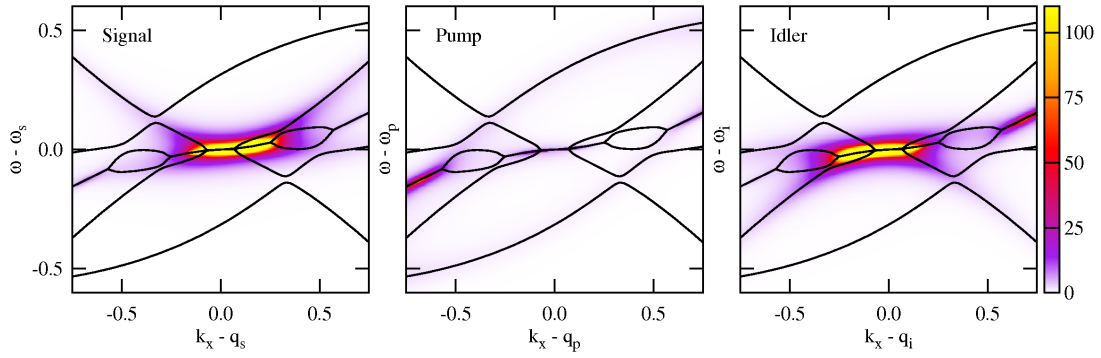

Figure 3.22: Incoherent polariton luminescence about the three OPO states with the spectra ($\Re(\omega)$) overlaid. The Goldstone mode leads to dominant luminescence around the signal and idler states, while the incoherent luminescence around the pump is much weaker.

In Fig. 3.23 the momenta and energies of Fig. 3.22 are shifted to the relevant mode ($k_x = 0 \to |\mathbf{q}|_m$ and $\omega_m = 0 \to \omega_p = 0$) to create a full picture of the incoherent luminescence around the OPO. The photon parts are included for completeness and to highlight the difference in visibility around the three modes due to the rate at which photons escape [82]. In particular, the weak peak at the pump mode becomes insignificant, and the incoherent luminescence is concentrated around the signal with a very small region around the idler mode, which are both due to the Goldstone mode. As for the luminescence calculated around the pump only mean field, the mean field occupations of the modes do not feature in the luminescence plots here. The signatures of

the Goldstone mode lie very close to the signal and idler modes and so are likely to be obscured by the luminescence from these modes in experiments.

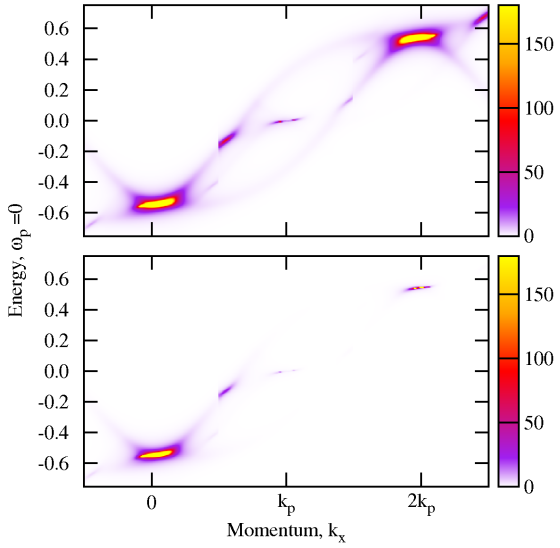

Figure 3.23: The incoherent luminescence around the three OPO states combined. Top: polariton, Bottom: photon.

3.7 OPO mean field with $\kappa_c = 100\kappa_x$

In Fig. 3.24, the pump and signal modes of the OPO regime are plotted for $\mathbf{k}_p(1.5, 0), \mathbf{k}_s = (0, 0)$ and $\kappa_c = 100\kappa_x$. The idler mode occupation is related to the signal occupation plotted by Eq. (3.111); for the values considered here, this gives $n_i = 0.51 n_s$; only n_s is plotted in Fig. 3.24.

Two features become noticeable: firstly there is OPO to extremely large pump powers, which is consistent with the lack of an upper threshold of the unstable region in the pump only case of Figs. 3.16 and **??**. This confirms that the OPO thresholds are determined by the imaginary part of the complex eigenvalues becoming zero and not by the condition $\det([D^{-1}]^R) = 0$. Secondly, as highlighted in the inset, there is bistability within the signal mode at low pumping: just above the OPO threshold, there are two possible signal mode occupations for a single pump power, the one chosen depends on whether the pump power is being increased or decreased.

Bistable behaviour of the signal mode has been observed experimentally [103], and in the three mode description of the OPO regime employed here, but under different conditions. In particular, the interplay of bistability and the OPO regime was studied for constant polariton decay in Ref. [30] where it was demonstrated that changing the detuning of the pump to the bistable regime did not forbid a finite signal occupation which could also be bistable. The bistability of the signal mode and the relation to the onset of the pump bistabilty were discussed

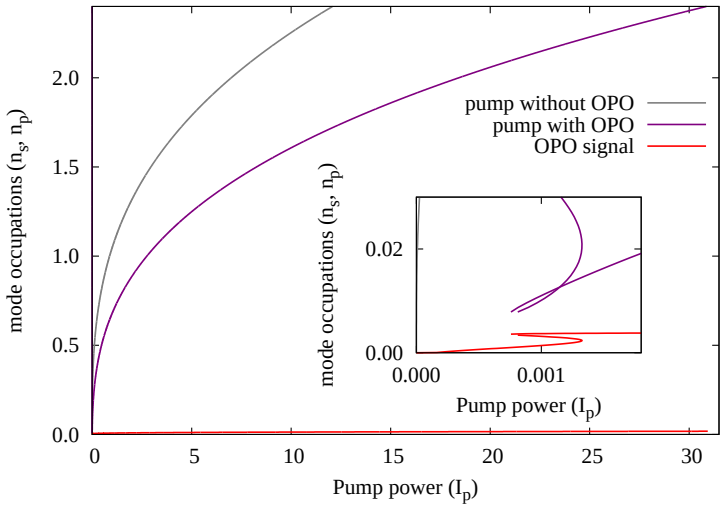

Figure 3.24: Mean field occupations of the OPO signal and pump modes for $\kappa_c = 100\kappa_x$ and $\mathbf{k}_p = (1.5, 0), \Delta^p = 0, \mathbf{k}_s = (0, 0), \kappa_c = 0.05$. There is a small but finite signal occupation to very high pump powers and the pump mode occupation is depleted relative to the pump only mean field. Close to the switch on of the OPO, there is bistability in the signal mode (and pump mode).

in terms of the pump detuning away from the lower polariton dispersion and of the energy mismatch of the OPO modes from the triple resonance condition $\omega_{lp}(\mathbf{k}_s) + \omega_{lp}(\mathbf{k}_i) = 2\omega_{lp}(\mathbf{k}_p)$. A bistable pump mode was also considered in Ref. [29], and again was accompanied by bistability in the signal mode occupation.

3.8 Keldysh conclusions

In this chapter, a Keldysh Green's function approach has been developed in detail for a system of exciton-polaritons that are introduced at a single pump energy and momentum. The Keldysh action of the system was derived first without restricting the number of modes allowed and the bath fields integrated out. To investigate the transition to the polariton OPO regime, the polaritons were restricted to remain within the pump mode. Small fluctuations around the pump mode were added to obtain the inverse Green's functions. The transition was defined as the point where the determinant of the inverse retarded Green's function is zero, and similarities between the phase transition in this far from equilibrium system and an equilibrium Bose-Einstein condensation transition were observed. In particular, the real poles of the system cross an effective chemical potential at the transition.

The physical properties of incoherent luminescence, absorption and spectral weight around the pump mode were calculated for pump strengths near the instability thresholds, but where the

pump mode was stable. The effects of changing the polariton decay from constant to strongly momentum dependent did not significantly affect the spectra, but did affect the occupations: when the polariton decay is constant, the luminescence is symmetric about the pump mode; as the exciton decay is weakened, the luminescence at high momenta becomes weaker. All examples studied have regions of negative spectral weight where the luminescence is stronger than the absorption. When the polariton decay is constant, these regions occur below the chemical potential for constant polariton decay and above the upper threshold; in all other cases, the regions of negative spectral weight appear both above and below the effective chemical potential which no longer lies exactly between the poles.

The effects of the momentum dependent polariton decay are seen very clearly when the incoherent luminescence is integrated over energy and plotted in 2-D momentum space. This is particularly dramatic below the lower threshold of the unstable region where the maximum of the polariton luminescence moves to the sides of the rings away from the pump while the sides closest to the pump become distorted, tending towards a figure of eight shape, rather than the almost circular rings with strongest luminescence on the sides closest to the pump seen in the case of constant polariton decay.

Finally, the simplest description of the OPO regime as a system of three modes was used to examine the above threshold case for constant polariton decay. In the example studied, the signal momentum was chosen to be zero, although this choice does not correspond to the maximum of the luminescence near either threshold. The OPO regime was found to be stable near the upper threshold and the incoherent luminescence plotted around the OPO states. The usefulness of the Keldysh approach which gives the occupations of the modes here becomes clear as the differences in the occupations around the three modes are significant. In particular, different branches of the spectra are occupied by the fluctuations around each mode; when the three modes are plotted together, the resulting incoherent luminescence spectrum is dominated by the signal and idler modes. This occurs due to the Goldstone mode which has $\Re(\omega(\mathbf{k})), \Im(\omega(\mathbf{k})) = 0$ at $\mathbf{k} = \mathbf{0}$, and it is clear that the Goldstone mode is associated with the signal and idler modes only. Meanwhile, if the polariton decay is taken to be strongly momentum dependent, there is no upper threshold of the OPO regime over a large range of pump powers, and at lower pump powers, there is also bistable behaviour within the OPO modes even though, at the single mode mean field level, the pump mode is in the optical limiter regime.

4 | The signal momentum

As seen in the previous chapter, the choice of the signal momentum in the OPO mean field equations has to be made by hand. Further, at any given pump strength within the optical limiter regime, the pump mode can be unstable for a range of momenta around $k_x = 0, 2|\mathbf{k}_p|$, or even at multiple locations. In this chapter, linear response analysis instead of the Keldysh formalism is used to see whether it is possible to use the simple linear response analysis to obtain a good estimate for the value of $\mathbf{k}_s$, and investigate the effects the chosen $\mathbf{k}_s$ may have on the OPO regime. Some experiments have considered the effects of the pump properties [27, 33], but the problem of choosing $\mathbf{k}_s$ and the effects of the pump properties have not been studied theoretically. The predictions obtained from linear response are checked via simulations of the mean field of the polaritons; all simulations, except those in Fig. 4.22 which were run by Dr. A. Zamora, were run by G. D. Dagvadorj and this work was done in discussion with Dr. A. Zamora.

4.1 Exciton-photon basis

The linear response analysis and the numerical integration both start from the complex Gross-Pitaevskii equations (cGPEs) describing polaritons either as coupled excitons and photons (the exciton-photon model) or as a system of the lower polaritons only. In general, the exciton-photon model is the more exact description of the polariton system [28], while the lower polariton model can be used to study a three mode description of the OPO regime.

Although the cGPEs can be found from the saddle points of the Keldysh action, they can also be obtained directly from the Hamiltonian. The cGPEs and linear response matrices are derived in section 4.1 for the exciton-photon model and in section 4.2 for the lower polariton model. As in the Keldysh analysis, in the lower polariton the pump only case and the three mode OPO are considered, while in the exciton-photon model the analysis is restricted to the pump only case only.

The cGPEs are derived in the exciton-photon basis in detail, and the decay baths are integrated out without resorting to the Keldysh formalism. The starting point is the exciton-photon Hamiltonian, Eqs. (2.2)- (2.5), a pair of coupled cGPEs can be derived for the photons ($\hat{a}_{\mathbf{k}}$) and excitons ($\hat{b}_{\mathbf{k}}$) which will include removing the decay baths ($\hat{A}_{\mathbf{p}}, \hat{B}_{\mathbf{p}}$ respectively).

4.1.1 Treatment of the decay baths

The derivation followed here is standard for a system coupled to a heat bath composed of an infinite set of harmonic oscillators [104] and is equivalent to the quasi-mode approximation used in Refs. [23, 31]. The starting point is the Heisenberg equation of motion for an operator $\hat{O}$:

$$i\partial_t \hat{O} = [\hat{O}, \hat{H}]$$

(here $\hat{O}$ is one of $\hat{a}_{\mathbf{k}}, \hat{b}_{\mathbf{k}}, \hat{A}_{\mathbf{p}}, \hat{B}_{\mathbf{p}}$). There are four types of operator in the exciton-photon Hamiltonian (Eqs. (2.2) - (2.5)) so there are four Heisenberg equations of motion:

$$i\partial_t \hat{a}_{\mathbf{k}} = \omega_c(\mathbf{k})\hat{a}_{\mathbf{k}} + \frac{\Omega_R}{2}\hat{b}_{\mathbf{k}} + F_{p,c}\delta_{\mathbf{k},\mathbf{k}_p} + \sum_{\mathbf{p}} \Gamma^a_{\mathbf{p},\mathbf{k}} \hat{A}_{\mathbf{p}}, \tag{4.1}$$

$$i\partial_t \hat{A}_{\mathbf{p}} = \omega_{\mathbf{p}}^{\Gamma^a} \hat{A}_{\mathbf{p}} + \Gamma^a_{\mathbf{p},\mathbf{k}} a_{\mathbf{k}}, \tag{4.2}$$

$$i\partial_t \hat{b}_{\mathbf{k}} = \omega_x(\mathbf{k})\hat{b}_{\mathbf{k}} + \frac{\Omega_R}{2}\hat{a}_{\mathbf{k}} + \sum_{\mathbf{p}} \Gamma^b_{\mathbf{p},\mathbf{k}} \hat{B}_{\mathbf{p}} + g_{\mathrm{x}} \sum_{\mathbf{k}',\mathbf{q}} \hat{b}^\dagger_{\mathbf{k}'} \hat{b}_{\mathbf{k}-\mathbf{q}} \hat{b}_{\mathbf{k}'}, \tag{4.3}$$

$$i\partial_t \hat{B}_{\mathbf{p}} = \omega_{\mathbf{p}}^{\Gamma^b} \hat{B}_{\mathbf{p}} + \Gamma^b_{\mathbf{p},\mathbf{k}} \hat{b}_{\mathbf{k}}. \tag{4.4}$$

The calculation for removing the photon decay bath is done in detail, the excitons follow the same method and require the same assumptions so the result is quoted. The photon decay bath, Eq. (4.2), allows for the solution:

$$\hat{A}_{\mathbf{p},\mathbf{k}}(t) = \hat{A}_{\mathbf{p},\mathbf{k}}(0)e^{-i\omega_{\mathbf{p}}^{\Gamma^a} t} - i\Gamma^a_{\mathbf{p},\mathbf{k}} \int_0^t \hat{a}_{\mathbf{k}}(\tau) e^{-i\omega_{\mathbf{p}}^{\Gamma^a}(t-\tau)} d\tau,$$

and Eq. (4.1) becomes:

$$i\partial_t \hat{a}_{\mathbf{k}} = \omega_c(\mathbf{k})\hat{a}_{\mathbf{k}} + \frac{\Omega_R}{2}\hat{b}_{\mathbf{k}} + F_{p,c}\delta_{\mathbf{k},\mathbf{k}_p} + \sum_{\mathbf{p}} \Gamma^a_{\mathbf{p},\mathbf{k}} \hat{A}_{\mathbf{p}}(0) e^{-i\omega_{\mathbf{p}}^{\Gamma^a} t} - i \sum_{\mathbf{p}} (\Gamma^a_{\mathbf{p},\mathbf{k}})^2 \int_0^t \hat{a}_{\mathbf{k}}(\tau) e^{-i\omega_{\mathbf{p}}^{\Gamma^a}(t-\tau)} d\tau. \tag{4.5}$$

The first three terms in Eq. (4.5) describe a system of two interacting bosonic species with coherent pumping. The fourth term is a random fluctuating force:

$$F^a_{\mathbf{k}}(t) = \sum_{\mathbf{p}} \Gamma^a_{\mathbf{p},\mathbf{k}} \hat{A}_{\mathbf{p}}(0) e^{-i\omega_{\mathbf{p}}^{\Gamma^a} t}, \tag{4.6}$$

and the final term, which describes the influence of the losses on the photons, is handled by making a series of assumptions about the nature of the decay bath.

First, a weak interaction between the system and the bath is assumed so $\hat{a}(t) = e^{-i\omega_c(\mathbf{k})}\tilde{a}(t)$ where the time variation of $\tilde{a}(t)$ is slow compared with the exponential factor. Since heat baths have effectively infinitely many degrees of freedom, all couplings between the system and the bath are comparable in size and $\Gamma^a_{\mathbf{p},\mathbf{k}} \approx \Gamma^a$ which is a constant. The $\sum_{\mathbf{p}}$ is replaced by an

integral over ω^{Γ^a} with a density of states $D(\omega^{\Gamma^a})$ so

$$-i\sum_{\mathbf{p}}(\Gamma^a_{\mathbf{p},\mathbf{k}})^2\int_0^t \tilde{a}_{\mathbf{k}}(\tau)e^{i\omega_c(\mathbf{k})(t-\tau)-i\omega_{\mathbf{p}}^{\Gamma^a}(t-\tau)}d\tau$$
$$= -i(\Gamma^a)^2\int_0^\infty D(\omega^{\Gamma^a})\int_0^t \tilde{a}_{\mathbf{k}}(\tau)e^{i\omega_c(\mathbf{k})(t-\tau)-i\omega^{\Gamma^a}(t-\tau)}d\tau d\omega^{\Gamma^a}.$$

It is now assumed that the decay bath spectrum is both dense and smooth as a function of ω^{Γ^a}, then $D(\omega^{\Gamma^a})\approx D(0)$ and

$$\int_0^\infty D(\omega^{\Gamma^a})\int_0^t \tilde{a}_{\mathbf{k}}(\tau)e^{i\omega_c(\mathbf{k})(t-\tau)-i\omega^{\Gamma^a}(t-\tau)}d\tau d\omega^{\Gamma^a}$$
$$= D(0)\int_0^t \hat{a}_{\mathbf{k}}(\tau)\left(\int_0^\infty e^{-\omega_c(\mathbf{k})(t-\tau)-i\omega^{\Gamma^a}(t-\tau)}d\omega^{\Gamma^a}\right)d\tau.$$

A change of variables from $\omega^{\Gamma^a}\rightarrow\omega'$ can be made with $\omega^{\Gamma^a}-\omega_c(\mathbf{k})=\omega'$. Since the system energy $\omega_c(\mathbf{k})$ is large (due to physically large exciton energy) the lower limit of the integral which now lies at $\omega'=-\omega_c(\mathbf{k})$ can be taken to $-\infty$ [104]. The resulting integral lis proportional to the Dirac delta-function $\delta(t-\tau)$ [89, 90],

$$\int_{-\infty}^\infty e^{-i\omega^{\Gamma^a}(t-\tau)}d\omega^{\Gamma^a}=2\pi\delta(t-\tau).$$

Since the delta-function has the property [104],

$$\int_0^t\delta(t-\tau)d\tau=\frac{1}{2},$$

the last term in Eq. (4.5) is now simply:

$$-i\pi(\Gamma^a)^2D(0)\int_0^t\hat{a}_{\mathbf{k}}(\tau)\delta(t-\tau)d\tau=-i\pi(\Gamma^a)^2D(0)\hat{a}_{\mathbf{k}}(t)=-i\kappa_c\hat{a}_{\mathbf{k}}$$

where $\kappa_c=\pi(\Gamma^a)^2D(0)$ quantifies the decay of the photons. The Heisenberg equation of motion for the photons, Eq. (4.1), now reads:

$$i\partial_t\hat{a}_{\mathbf{k}}=\omega_c(\mathbf{k})\hat{a}_{\mathbf{k}}+\frac{\Omega_R}{2}\hat{b}_{\mathbf{k}}+F_{p,c}\delta_{\mathbf{k},\mathbf{k}_p}+F^a_{\mathbf{k}}(t)-i\kappa_c\hat{a}_{\mathbf{k}}. \tag{4.7}$$

An identical treatment of the excitons simplifies Eq. (4.3) to:

$$i\partial_t\hat{b}_{\mathbf{k}}=\omega_x(\mathbf{k})\hat{b}_{\mathbf{k}}+\frac{\Omega_R}{2}\hat{a}_{\mathbf{k}}+F^b_{\mathbf{k}}(t)-i\kappa_x\hat{b}_{\mathbf{k}}+\sum_{\mathbf{k}',\mathbf{q}}g_{\mathrm{x}}\hat{b}^\dagger_{\mathbf{k}'}\hat{b}_{\mathbf{k}-\mathbf{q}}\hat{b}_{\mathbf{k}'+\mathbf{q}}. \tag{4.8}$$

The fluctuating forces do not affect the steady state and are set to zero throughout.

4.1.2 Complex Gross-Pitaevskii equations

In general, the field operator of a system can be written in terms of the creation and annihilation operators as [3]:

$$\hat{\phi} = \sum_i \varphi_i \hat{a}_i \tag{4.9}$$

where the summation is over all the states i of the system (the momenta). The Heisenberg equations of motion for these fields are:

$$i\partial_t \hat{\phi}_c = (\omega_c(\mathbf{k}) - i\kappa_c)\hat{\phi}_c + F_{p,c}\delta_{\mathbf{k},\mathbf{k}_p} + \frac{\Omega_R}{2}\hat{\phi}_x, \tag{4.10}$$

$$i\partial_t \hat{\phi}_x = (\omega_x(\mathbf{k}) + g_{\mathrm{x}}\hat{\phi}_x^\dagger\hat{\phi}_x - i\kappa_x)\hat{\phi}_x + \frac{\Omega_R}{2}\hat{\phi}_c. \tag{4.11}$$

In the Bogoliubov approximation, the operator $\hat{\phi}$ is replaced by a (complex) classical field or order parameter, ϕ [3]. This leads to a pair of coupled cGPEs describing the exciton-photon system [28, 59, 102]:

$$i\partial_t \phi_c = (\omega_c(\mathbf{k}) - i\kappa_c)\phi_c + F_{p,c}\delta_{\mathbf{k},\mathbf{k}_p} + \frac{\Omega_R}{2}\phi_x; \tag{4.12}$$

$$i\partial_t \phi_x = (\omega_x - i\kappa_x + g_x|\phi_x|^2)\phi_x + \frac{\Omega_R}{2}\phi_c. \tag{4.13}$$

4.1.3 Pump only mean field

The below threshold case of a single pump mode is examined first. The simplest choice is for the fields $\phi_{\{c,x\}}$ to have the plane wave form $P_{\{c,x\}}e^{-i\omega_p t}$ with complex amplitudes $P_{\{c,x\}}$. The pump energy, ω_p, is set by the properties of the laser pumping $F_{p,c} = fe^{-i\omega_p t}$. As in the Keldysh case, the amplitude f is chosen to be real. Making the substitution of the mean field gives [28, 64], for the photons:

$$\begin{aligned}
i\partial_t(P_c e^{-i\omega_p t}) &= (\omega_c(\mathbf{k}_p) - i\kappa_c)P_c e^{-i\omega_p t} + fe^{-i\omega_p t} + \frac{\Omega_R}{2}P_x e^{-i\omega_p t}, \qquad (4.14)\\
(i\partial_t P_c + \omega_p P_c)e^{-i\omega_p t} &= (\omega_c(\mathbf{k}_p) - i\kappa_c)P_c e^{-i\omega_p t} + fe^{-i\omega_p t} + \frac{\Omega_R}{2}P_x e^{-i\omega_p t},\\
i\partial_t P_c + \omega_p P_c &= (\omega_c(\mathbf{k}_p) - i\kappa_c)P_c + f + \frac{\Omega_R}{2}P_x \quad ,\\
i\partial_t P_c &= (\omega_c(\mathbf{k}_p) - \omega_p - i\kappa_c)P_c + f + \frac{\Omega_R}{2}P_x, \qquad (4.15)
\end{aligned}$$

and excitons:

$$\begin{aligned}
i\partial_t(P_x e^{-i\omega_p t}) &= (\omega_x(\mathbf{k}_p) + g_{\mathrm{x}}|P_x|^2 - i\kappa_x)P_x e^{-i\omega_p t} + \frac{\Omega_R}{2}P_c e^{-i\omega_p t}, \qquad (4.16)\\
(i\partial_t P_x + \omega_p)e^{-i\omega_p t} &= (\omega_x(\mathbf{k}_p) + g_{\mathrm{x}}|P_x|^2 - i\kappa_x)P_x e^{-i\omega_p t} + \frac{\Omega_R}{2}P_c e^{-i\omega_p t},
\end{aligned}$$

$$i\partial_t P_x + \omega_p = (\omega_x(\mathbf{k}_p) + g_{\mathrm{x}}|P_x|^2 - i\kappa_x)P_x + \frac{\Omega_R}{2}P_c,$$
$$i\partial_t P_x = (\omega_x(\mathbf{k}_p) - \omega_p + g_{\mathrm{x}}|P_x|^2 - i\kappa_x)P_x + \frac{\Omega_R}{2}P_c. \tag{4.17}$$

In the steady state, $i\partial_t P_{\{c,x\}} = 0$ [28]. Eq. (4.17) is rearranged for the photon field:

$$P_c = \frac{2}{\Omega_R}(\omega_p - \omega_x(\mathbf{k}_p) - g_{\mathrm{x}}|P_x|^2 + i\kappa_x)P_x \tag{4.18}$$

which is substituted into Eq. (4.15) to give:

$$0 = \frac{2}{\Omega_R}(\omega_c(\mathbf{k}_p) - \omega_p - i\kappa_c)(\omega_p - \omega_x(\mathbf{k}_p) - g_{\mathrm{x}}|P_x|^2 + i\kappa_x)P_x + f + \frac{\Omega_R}{2}P_x.$$

A little bit of rearrangement gives an equation for the external pump in terms of P_x:

$$\begin{aligned} f &= \Big[\frac{2}{\Omega_R}\left((\omega_x(\mathbf{k}_p) - \omega_p + g_{\mathrm{x}}|P_x|^2)(\omega_c(\mathbf{k}_p) - \omega_p) - \kappa_c\kappa_x\right) - \frac{\Omega_R}{2} \\ &\quad -i\frac{2}{\Omega_R}\left(\kappa_x(\omega_c(\mathbf{k}_p) - \omega_p) + \kappa_c(\omega_x(\mathbf{k}_p) - \omega_p + g_{\mathrm{x}}|P_x|^2)\right)\Big]P_x. \end{aligned} \tag{4.19}$$

The absolute value squared gives a real equation for the pump power $|F_{p,c}|^2$ in terms of the exciton occupation $|P_x|^2$:

$$\begin{aligned} |f|^2 &= \Big[\left(\frac{2}{\Omega_R}\left((\omega_x(\mathbf{k}_p) - \omega_p + g_{\mathrm{x}}|P_x|^2)(\omega_c(\mathbf{k}_p) - \omega_p) - \kappa_c\kappa_x\right) - \frac{\Omega_R}{2}\right)^2 \\ &\quad +\frac{4}{\Omega_R^2}\left(\kappa_x(\omega_c(\mathbf{k}_p) - \omega_p) + \kappa_c(\omega_x(\mathbf{k}_p) - \omega_p + g_{\mathrm{x}}|P_x|^2)\right)^2\Big]|P_x|^2. \end{aligned} \tag{4.20}$$

It is thus possible to plot $|f|^2, |P_{\{c,x\}}|^2$. Eqs. (4.19) and (4.18) can be used to find the complex amplitudes P_x, P_c if f, the (positive) square root of Eq. (4.20), is known.

Before examining the stability of the pump mode, the properties and behaviours of the mean field can be considered. There are two distinct behaviour of the pump mode: in the optical limiter regime, the exciton and photon populations increase monotonically with the pump power; if $\omega_p - \omega_{lp}(\mathbf{k}_p) \geq \sqrt{3}\kappa$, bistable behaviour can occur in which there are two possible exciton occupations for a given pump power and is characterised by a typical S-shaped curve [28,29]. As in the Keldysh analysis, the optical limiter regime is considered for all analyses.

4.1.4 Fluctuations around the pump steady state

Having found the mean field occupation, a linear response analysis (linear Bogoliubov-like theory [19, 28]) expanding in fluctuations around the pump mode is performed. To include small fluctuations around the mean field, the substitution $\phi \to \phi_0 + \Delta\phi$ is made into the cGPEs and only terms that are linear in the fluctuations $\Delta\phi$ are kept. This is then formed into a matrix

equation [28]:

$$i\partial_t \delta\vec{\phi} = L \cdot \delta\vec{\phi}$$

where $\delta\vec{\phi}$ is a vector formed of all the relevant $\Delta\phi$'s and their complex conjugates. In the exciton-photon basis,

$$\delta\vec{\phi} = \begin{pmatrix} \Delta\phi_x \\ \Delta\phi_c \\ \Delta\phi_x^* \\ \Delta\phi_c^* \end{pmatrix}. \tag{4.21}$$

The fluctuations can have any form, but it is useful to choose a plane wave. To include fluctuations, the substitution

$$\phi_{\{c,x\}} = P_{\{c,x\}} e^{-i\omega_p t}\delta_{\mathbf{k},\mathbf{k}_p} + \Delta\phi_{\{c,x\}} e^{-i(\omega_p+\delta\omega)t}\delta_{\mathbf{k},\mathbf{k}_p+\delta\mathbf{k}} \tag{4.22}$$

is made into the cGPEs (Eqs. (4.12) and (4.13)). The external laser pump f is not affected by fluctuations.

The photons are considered first:

$$\begin{aligned} i\partial_t(\phi_c) &= \omega_p P_c e^{-i\omega_p t} + (i\partial_t\Delta\phi_c + (\omega_p+\delta\omega)\Delta\phi_c)e^{-i(\omega_p+\delta\omega)t} \\ &= (\omega_c(\mathbf{k}_p) - i\kappa_c)P_c e^{-i\omega_p t} + f e^{-i\omega_p t} + \frac{\Omega_R}{2}P_x e^{-i\omega_p t} \\ &\quad +(\omega_c(\mathbf{k}_p+\delta\mathbf{k}) - i\kappa_c)\Delta\phi_c e^{-i(\omega_p+\delta\omega)t} + \frac{\Omega_R}{2}\Delta\phi_x e^{-i(\omega_p+\delta\omega)t}. \end{aligned} \tag{4.23}$$

Only terms linear in the fluctuations are kept, and the exponential factor common to all terms cancels to leave an equation for $\Delta\phi_c$:

$$(i\partial_t + \delta\omega)\Delta\phi_c = (\omega_c(\mathbf{k}_p+\delta\mathbf{k}) - \omega_p - i\kappa_c)\Delta\phi_c + \frac{\Omega_R}{2}\Delta\phi_x. \tag{4.24}$$

The excitons are slightly more complicated due to the interaction term (the exponents on P_x and $\Delta\phi_x$ have been dropped for brevity):

$$\begin{aligned} g_{\mathrm{x}}|\phi_x|^2\phi_x &= g_{\mathrm{x}}(|P_x|^2 + P_x\Delta\phi_x^* + P_x^*\Delta\phi_x + |\Delta\phi_x|^2)(P_x+\Delta\phi_x) \\ &= g_{\mathrm{x}}\big(|P_x|^2P_x + P_x^2\Delta\phi_x^* + |P_x|^2\Delta\phi_x + P_x|\Delta\phi_x|^2 + |P_x|^2\Delta\phi_x \\ &\quad +P_x|\Delta\phi_x|^2 + P_x^*\Delta\phi_x^2 + |\Delta\phi_x|^2\Delta\phi_x\big). \end{aligned}$$

The mean field and terms that are quadratic in the fluctuations are discarded to leave:

$$g_{\mathrm{x}}|\phi_x|^2\phi_x \quad\rightarrow\quad g_{\mathrm{x}}(P_x^2\Delta\phi_x^* + 2|P_x|^2\Delta\phi_x).$$

The rest of the exciton part is almost identical for the photon part, so, after dividing through by the exponential factor $e^{-i(\omega_p+\delta\omega)t}$, the equation of motion for fluctuations around the exciton

mean field is:

$$(i\partial_t + \delta\omega)\Delta\phi_x = (\omega_x(\mathbf{k}_p + \delta\mathbf{k}) - \omega_p + g_{\mathrm{x}}2|P_x|^2\Delta\phi_x - i\kappa_x)\Delta\phi_x + \frac{\Omega_R}{2}\Delta\phi_c + g_{\mathrm{x}}P_x^2\Delta\phi_x^*.$$

The remainder of the terms, $i\partial_t\Delta\phi^*_{\{c,x\}}$, are obtained immediately through [89]

$$i\partial_t O^\dagger = -(i\partial_t O)^\dagger$$

and the convention that the energy and momentum signatures of the conjugate fields are opposite. The linear response matrix in the exciton-photon model is the part without the $\delta\omega$ contribution since the spectra calculate $\delta\omega$ [28, 64] has the form:

$$L_{x-c} = \begin{pmatrix} A(\delta\mathbf{k}) & B \\ -B^* & -A(-\delta\mathbf{k}) \end{pmatrix} \tag{4.25}$$

with

$$A(\delta\mathbf{k}) = \begin{pmatrix} \omega_x(\mathbf{k}_p + \delta\mathbf{k}) + 2g_{\mathrm{x}}|P_x|^2 - \omega_p - i\kappa_x & \frac{\Omega_R}{2} \\ \frac{\Omega_R}{2} & \omega_c(\mathbf{k}_p + \delta\mathbf{k}) + \omega_p - i\kappa_c \end{pmatrix} \tag{4.26}$$

and

$$B = \begin{pmatrix} g_{\mathrm{x}}{P_x}^2 & 0 \\ 0 & 0 \end{pmatrix}. \tag{4.27}$$

The spectra are found by calculating the (complex) eigenvalues of Eq. (4.25). The real parts give the dispersions (the upper and lower polaritons and their 'images') while the imaginary parts determine whether the pump state is stable or not [28, 64]. If the imaginary part of one of the eigenvalues is positive for some combination of pump strength f and momentum fluctuation $\delta\mathbf{k}$, then the pump mode is unstable towards a new state at $\delta\mathbf{k}$. By defining $\mathbf{k} = \mathbf{k}_p - \delta\mathbf{k}$ the problem can be written in terms of the actual momenta $\mathbf{k}$ and $\mathbf{k}_p + \delta\mathbf{k} \to 2\mathbf{k}_p - \mathbf{k}$. The exciton-photon model is only valid at exciton densities that are low enough to allow excitons to be treated as weakly interacting bosons [15, 28], so behaviours at large values of f that lead to high exciton occupations (or densities) may not be realistic.

4.2 Lower Polariton basis

Although the results can be written down directly after the detailed derivation presented for the exciton-photon basis, the derivation is included here in brief to highlight the differences that appear with the Hopfield coefficients.

4.2.1 Treatment of the decay baths

The exciton and photon decay baths in the lower polariton Hamiltonian (Eq. (2.13)) are treated following the scheme outlined above for the exciton-photon model. As above, the two decay baths follow the same procedure, so the photon bath only is calculated in detail. First:

$$\begin{aligned} i\partial_t \hat{p}_{\mathbf{k}} &= \omega_{lp}(\mathbf{k})\hat{p}^\dagger_{\mathbf{k}} + g_{\mathrm{x}} \sum_{\mathbf{k}',\mathbf{q}} V_{\mathbf{k},\mathbf{k}',\mathbf{q}} \hat{p}^\dagger_{\mathbf{k}'} \hat{p}_{\mathbf{k}-\mathbf{q}} \hat{p}_{\mathbf{k}'+\mathbf{q}} \\ &\quad + \sum_{\mathbf{p}} \left(\Gamma^a_{\mathbf{p},\mathbf{k}} C(\mathbf{k}) \hat{A}_{\mathbf{p}} + \Gamma^b_{\mathbf{p},\mathbf{k}} X(\mathbf{k}) \hat{B}_{\mathbf{p}} \right) + F_{lp}\delta_{\mathbf{k},\mathbf{k}_p}, \qquad (4.28) \\ i\partial_t \hat{A}_{\mathbf{p}} &= \Gamma^a_{\mathbf{p},\mathbf{k}} C(\mathbf{k}) \hat{p}_{\mathbf{k}} + \omega_{\mathbf{p}}^{\Gamma^a} \hat{A}_{\mathbf{p}}. \qquad (4.29) \end{aligned}$$

Eq. (4.29) is exactly Eq. (4.2) with the substitution $a_{\mathbf{k}} \to C(\mathbf{k})p_{\mathbf{k}}$ so the solution is

$$\hat{A}_{\mathbf{p}} = \hat{A}_{\mathbf{p}}(0) e^{-i\omega_{\mathbf{p}}^{\Gamma^a} t} - iC(\mathbf{k})\Gamma^a_{\mathbf{p},\mathbf{k}} \int_0^t \hat{p}_{\mathbf{k}}(\tau) e^{-i\omega_{\mathbf{p}}^{\Gamma^a}(t-\tau)} d\tau$$

which means that

$$\sum_{\mathbf{p}} \Gamma^a_{\mathbf{p},\mathbf{k}} C(\mathbf{k}) \hat{A}_{\mathbf{p}} \to F^a_{lp,\mathbf{k}}(t) - i\pi\Gamma^a D(0) C^2(\mathbf{k}) \hat{p}_{\mathbf{k}} = F^a_{lp,\mathbf{k}}(t) - iC^2(\mathbf{k})\kappa_c \hat{p}_{\mathbf{k}}$$

where $F^a_{lp,\mathbf{k}}(t) = C(\mathbf{k})F^a_{\mathbf{k}}(t)$. Doing the same for the exciton decay bath $\hat{B}_{\mathbf{k}}$, leads to:

$$\begin{aligned} i\partial_t \hat{p}_{\mathbf{k}} &= \omega_{lp}(\mathbf{k})\hat{p}^\dagger_{\mathbf{k}} + g_{\mathrm{x}} \sum_{\mathbf{k}',\mathbf{q}} V_{\mathbf{k},\mathbf{k}',\mathbf{q}} \hat{p}^\dagger_{\mathbf{k}'} \hat{p}_{\mathbf{k}-\mathbf{q}} \hat{p}_{\mathbf{k}'+\mathbf{q}} \\ &\quad - i\left(C^2(\mathbf{k})\kappa_c + X^2(\mathbf{k})\kappa_x \right) + F^a_{lp,\mathbf{k}}(t) + F^b_{lp,\mathbf{k}}(t) + F_{lp}\delta_{\mathbf{k},\mathbf{k}_p}. \qquad (4.30) \end{aligned}$$

The pump $F_{lp} = f_{lp}e^{i\omega_p t}$ is proportional to the photon pump ($f_{lp} \propto f$) [30]. The polariton decay can be written in terms of the exciton and photon decays and the Hopfield coefficients with:

$$\kappa_{lp}(\mathbf{k}) = X^2(\mathbf{k})\kappa_x + C^2(\mathbf{k})\kappa_c. \qquad (4.31)$$

The cGPE is obtained by taking the final form of the Heisenberg equation of motion for a field that includes all states (by Eq. (4.9)) and considering only the mean field in which the field operator is replaced by a complex number and the fluctuating forces are zero. This leads to the lower polariton cGPE [19, 30, 41]:

$$i\partial_t \phi_{lp} = (\omega_{lp}(\mathbf{k}) - i\kappa_{lp} + V_{lp}|\phi_{lp}|^2)\phi_{lp} + F_{lp}\delta_{\mathbf{k},\mathbf{k}_p}. \qquad (4.32)$$

The interaction strength V_{lp} and the lower polariton dispersion ω_{lp} are defined in momentum space. Since the field ψ_{lp} can contain any number of momenta, the momentum arguments on V_{lp} depend on the momenta included in the approximation; once the momenta are known, then

$V_{lp} \to V_{\mathbf{k},\mathbf{k}',\mathbf{q}}$ according to the expansion of $|\phi_{lp}|^2\phi_{lp}$.

4.2.2 Pump only mean field and linear response

The mean field of the lower polaritons when there is a single mode is:

$$\phi_{lp} = P_{lp}e^{-i\omega t}\delta_{\mathbf{k},\mathbf{k}_p}. \tag{4.33}$$

Substituting into Eq. (4.32) leads to the mean field steady state equation for the polariton occupation $n_p = |P|^2$ at the pump mode [29, 30]:

$$f_{lp} = [\omega_{lp}(\mathbf{k}_p) - \omega_p + V_{lp}n_p - i\kappa_{lp}]P \tag{4.34}$$

$$|f_{lp}|^2 = [(\omega_{lp}(\mathbf{k}_p) - \omega_p + n_p)^2 + \kappa_{lp}^2]n_p. \tag{4.35}$$

Since the pump strength is real, f_{lp} depends on $n_p = |P|^2$ only.

The fluctuations around the mean field have the same form as in the exciton-photon model and the terms in the lower polariton model are calculated exactly as the terms in the equation for the exciton fluctuations (since both contain interactions). The additional difference is the momentum dependence of the polariton interaction. The linear response matrix, formed by keeping only terms linear in fluctuations is [19, 30, 31, 59]:

$$L_{lp} = \begin{pmatrix} \alpha^+ - i\kappa_{lp} & P_{lp}^2 \\ -P_{lp}^{*\,2} & -\alpha^- - i\kappa_{lp} \end{pmatrix} \tag{4.36}$$

where

$$\alpha^{\pm} = \omega_{lp}(\mathbf{k}_p \pm \delta\mathbf{k}) - \omega_p + 2|P_{lp}|^2 \tag{4.37}$$

as in the Keldysh analysis. The eigenvalues of L_{lp}, can be calculated exactly [30]:

$$\omega^{\pm} = \frac{\alpha^+ - \alpha^-}{2} - i\kappa_{lp} \pm \frac{1}{2}\sqrt{(\alpha^+ + \alpha^-)^2 - 4n_p^2}. \tag{4.38}$$

4.2.3 OPO mean field and linear response

In the lower polariton model, the OPO regime with three modes can also be investigated. A new ansatz consisting of three plane waves is made and substituted into the lower polariton cGPE [29, 30, 41]. The new polariton field has the form:

$$\phi_{lp} = \phi_s + \phi_p + \phi_i,$$

with each mode a plane wave:

$$\phi_m = Me^{-i\omega_m t}e^{i\mathbf{k}_m\cdot\mathbf{x}},$$

the effect of the second exponential is equivalent to $\delta_{\mathbf{k},\mathbf{k}_m}$ [30, 41].

The requirements of energy and momentum conservation within the OPO modes restrict the terms and the OPO regime is described by three coupled cGPEs, one for each of the signal, pump and idler modes [29, 30, 41]. The new ansatz is substituted into the polariton cGPE, Eq. (4.32), and the steady-state with $\partial_t P = \partial_t S = \partial_t I = 0$ taken. This gives three complex equations that can be solved to give the signal energy ϵ_s, the mode occupations n_s, n_p, n_i and the complex mode amplitudes S, P, I [29]. Some of the interaction terms introduce modes outside of the three mode ansatz; these are discarded. The steady-state equations of the OPO modes are [29, 30]

$$\begin{aligned} \Xi_s S + V_{sppi} P^2 I^* &= 0, & (4.39)\\ \Xi_p P + 2V_{sppi} S P^* I + f_{lp} &= 0, & (4.40)\\ \Xi_i I + V_{sppi} S^* P^2 &= 0, & (4.41) \end{aligned}$$

where, as in section 3.4, the shorthand

$$\begin{aligned} \Xi_m &= \omega_{lp}(\mathbf{k}_m) + 2(V_{mmss} n_s + V_{mmpp} n_p + V_{mmii} n_i) \\ &\quad -\epsilon_m - \omega_p - V_{mmmm} n_m - i\kappa_m \end{aligned} \tag{4.42}$$

is used. The mean field occupations and mode amplitudes are calculated as described in section 3.4.1.

The stability of the OPO regime at a given pump strength and $\mathbf{k}_s$ is determined from a linear response analysis of the three mode description. The linear response of the OPO regime is [41]

$$L_{OPO} = \begin{pmatrix} -M(\delta\mathbf{k}) & -Q(\delta\mathbf{k}) \\ Q^*(-\delta\mathbf{k}) & M^*(-\delta\mathbf{k}) \end{pmatrix} \tag{4.43}$$

with the submatrices

$$M_{m,n}(\delta\mathbf{k}) = \delta_{m,n}\left(\omega_m - \omega_{lp}(\mathbf{k}_m + \delta\mathbf{k}) + i\kappa_{lp}(\mathbf{k}_m + \delta\mathbf{k})\right) - 2\sum_{r,t=1}^{3} \delta_{m+r,n+t} V_{m^\pm,n^\pm,r,t} \psi_r^* \psi_t, \tag{4.44}$$

$$Q_{m,n}(\delta\mathbf{k}) = -\sum_{r,t=1}^{3} \delta_{m+n,r+t} V_{m\pm,n^\mp,r,t} \psi_r \psi_t. \tag{4.45}$$

The OPO regime is unstable if the imaginary part of one of the six eigenvalues is positive. If the OPO is stable, the maximum imaginary part is the Goldstone mode with $\omega_G \to 0$ at $\delta\mathbf{k} \to 0$ [41]; if the OPO is unstable, then eigenvalues with positive imaginary part at a finite momentum fluctuation exist. As a result of the restriction to linear fluctuations around each mode, the momentum fluctuation is restricted to forbid overlap between the modes.

4.3 Numerical integration of the cGPEs

The cGPEs (Eqs. (4.12), (4.13) and (4.32)) are integrated numerically in real space using an adaptive step size Runga-Kutta algorithm on a 256×256 lattice for a Gaussian pump to give the mean field polariton, exciton and photon densities $|\psi_{lp,x,c}|^2$. The non-dimensional time is related to the real time according to the Rabi frequency: $T_{real} = T_{non-dim}(2/\hbar\Omega_R)$. In all the numerical results reported here, the integration runs to $T_{tot} = 2.4 \times 10^5$ which corresponds to a real time of 72ns. The signal is identified as the largest distinct peak in the polariton or photon density with $\mathbf{k}_s < \mathbf{k}_p$ [26, 27, 33, 61].

In the numerical integration, the momentum dependent polariton interaction cannot be included since the real space form of the Hopfield coefficients is not used. Therefore a *simplified* version of the lower polariton model is used in which the polariton-polariton interaction strength is set to unity (the fields are rescaled by rescaling the exciton-exciton interaction constant).

Choice of parameters All calculations are performed in a non-dimensional system of units in which the exciton-photon interconversion rate $\Omega_R/2$, is unity as described in appendix A. In the simplified lower polariton model $V_{lp} = 1$, and in the exciton-photon model $g_{\mathrm{x}} = 0.00121$. The controllable parameters are the pump energy and momentum for which the choices $\omega_p = \omega_{lp}(\mathbf{k}_p) = -0.38$ and $\mathbf{k}_p = (1.4, 0)$ are usually made. In all sections except section 4.4.7, the momenta are restricted to the $k_y = 0$ plane so the vector form of all momentum arguments is dropped. Except in Fig. 4.24 where the exciton losses are reduced, the polariton, photon and exciton losses are all equal (and independent of momentum and energy) with $\kappa_{lp} = \kappa_c = \kappa_x = 0.045$.

4.4 Determining the signal momentum

The two models derived above are used to investigate whether the signal momentum can be estimated from a simple linear response analysis of the pump mode or from a three mode ansatz describing the OPO regime. In sections 4.4.1 - 4.4.3, the momentum of the most unstable eigenvalue (largest $\Im(\omega)$) is found and compared to the location of the signal found through numerical integration of the cGPEs. The signal, in the polariton or photon distributions, is identified as having the maximum polariton or photon occupation at a momentum below the pump momentum (and distinct from the pump). The effects of changing the pump parameters are considered in section 4.4.4.

The OPO regime in lower polariton model is considered in section 4.4.6 and the k_s value(s) for which the three mode description of the OPO regime is stable at a given pump strength are found. By appropriate rotation, a coordinate system where the pump is applied in the k_x plane can always be defined and, as long as there is only one signal, the coordinate system can be rotated such that the pump, signal and idler all lie along $k_y = 0$. When k_y is included in the

analysis in section 4.4.7, the fluctuations are considered in the 2-D momentum plane. Lastly, the momentum dependent interactions are included in the lower polariton model in section 4.4.8.

4.4.1 k_s in the simplified lower polariton model

In this section, the simplest model of the polariton system with constant polariton-polariton interaction is used. First, k_s is obtained directly from the numerical integration of the cGPE (Eq. (4.32)). Then the maximum of the imaginary parts of the eigenvalues (of Eq. (4.36)) is used to predict k_s. Finally, the signal momenta from the two methods are compared.

Numerical integration of the polariton cGPE

The lower polariton cGPE, Eq. (4.32), is integrated numerically for range of pump strengths covering the entire OPO region. In Fig. 4.1, the polariton density at the end of the simulation is plotted for two pump strengths. In both cases, there is OPO with a significant polariton occupation away from the applied pump and the signal is identified as the largest (distinct) peak with $k_s < k_p$.

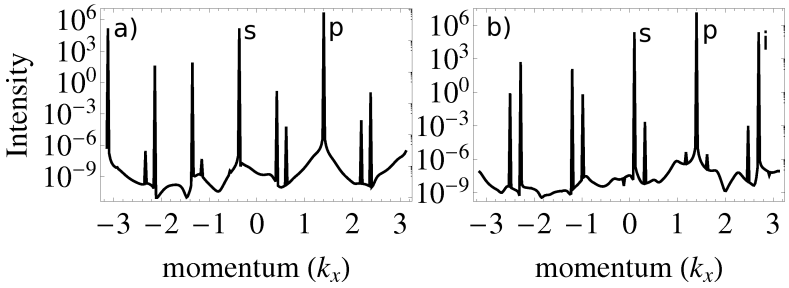

Figure 4.1: The polariton density distribution at the end of the integration period. The distinct modes (signal, s, pump, p and idler, i) are identified. a) weak pump, $F_{lp} = 0.015$; b) strong pump $F_{lp} = 0.051$ with satellite states.

For weak pumping, Fig. 4.1 a, the signal appears with negative momentum, and other peaks in the logarithmic plot are weak. When the applied pump is stronger, Fig. 4.1 b, the signal mode has $k_s \sim 0$, and distinct satellite states with momenta $k \sim -k_p, \sim -2k_p$ [19, 29, 31, 60–62] are visible. In the OPO regime, the macroscopic occupation of the distinct signal and idler modes is due to stimulated scattering into these modes [22, 26, 27, 33, 58]. The satellite modes are the result of multiple scattering events involving the three modes of the OPO regime [29, 31, 60, 61]; the OPO regime itself - the signal and idler modes - is the result of scattering involving pairs of pump polaritons only [18, 19, 26, 27, 30, 31, 41, 59]. The properties of these significantly weaker satellite states are not considered further. The background polariton density is $|\psi_{lp}|^2 \sim 10^{-8}$ throughout.

The signal occupation is plotted in Fig. 4.2 in both linear and logarithmic scales. There is no macroscopic occupation away from the pump, and therefore no OPO, for very weak pumping. As

the pumping is increased, the signal occupation increases sharply at $F_{lp} = F_{\rm on}$: there is a range of pump strengths where the signal occupation is large, and above $F_{lp} = F_{\rm off}$ there is again no largely occupied state away from the pump. When there is no OPO, any peak in the polariton density away from the pump which yields a definite k_s is weak and the result of spontaneous parametric scattering [82], rather than the stimulated scattering that leads to the macroscopic occupation of the OPO modes. The OPO regime is identified as having $|\psi_s|^2 > 10^4$ in the non-dimensional system of units used, and exists for a range of pump powers $F_{\rm on} \leq F_{lp} \leq F_{\rm off}$.

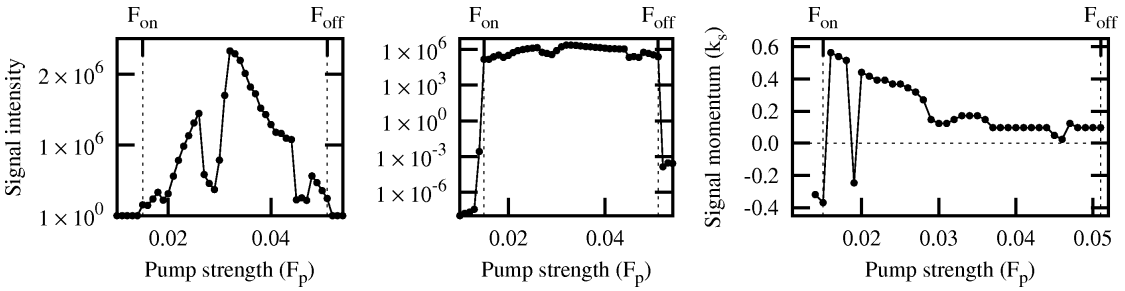

Figure 4.2: Value (left, linear scale, centre, logarithmic scale) and location (right) of the maximum signal at the end of the integration period. The OPO exists where there is a large signal occupation; the signal momentum is initially large and decreases to become small and positive over a range of pump strengths. ($F_p \Rightarrow F_{lp}$)

The signal momentum is extracted from the polariton density and plotted the right hand panel of Fig. 4.2. In the OPO region, k_s is initially negative, which corresponds to the polariton distribution at weak pumping in Fig. 4.1 a. On increasing the pumping, k_s becomes positive for a large range of pump strengths, with some variation. When k_s is first positive, its value is quite large, but it decreases to $k_s \sim 0.1$ for much of the OPO region. The polariton density distribution plotted in Fig. 4.1 b is at the last pump strength considered before the OPO switches off.

Linear response analysis

Even without the linear response analysis, the mean field gives some information about the expected behaviour. $|f_{lp}|^2$ is cubic in n_p which can lead to bistable behaviour under certain pumping parameters. The critical quantity is the detuning of the pump away from the lower polariton curve: if $\omega_p - \omega_{lp}(k_p) \equiv \Delta^p > \sqrt{3}\kappa_{lp}$, the pump mode is bistable [28–30, 86, 105]. Since $\omega_p = \omega_{lp}(k_p)$ is used here, the system is in the 'optical limiter' regime with a monotonic relation between the pump strength and the polariton occupation at the pump mode, as shown in the upper part of Fig. 4.3.

If the discriminant of Eq. (4.38) is positive, then the two eigenvalues have a common imaginary part, $\Im(\omega^{\pm}) = -\kappa_{lp}$, and the pump mode is stable. When the discriminant is negative, the imaginary parts of the eigenvalues are not equal, and it is possible to find the location of the maximum, $\Im(\omega^{+})$ which may become positive. The imaginary part of ω^{+} is plotted in the right hand panel of Fig. 4.3 for a range of pump strengths covering the full OPO regime and over a

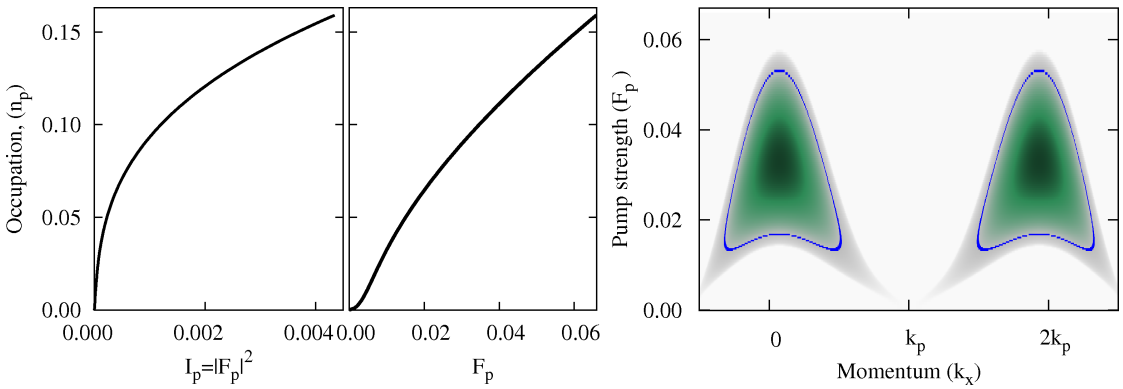

Figure 4.3: Mean field, steady state pump mode polariton occupation (left, with the pump power, centre, with the pump strength) and the imaginary parts of eigenvalues $\Im(\omega) > -\kappa_{lp}$ (right). The blue line (region, $-0.0011 < \Im(\omega^+) < 0.0011$) shows the border of the unstable region with $\Im(\omega^+) > 0$. ($F_p \Rightarrow F_{lp}$)

broad range of momenta above and below the pump mode. The imaginary parts first split in two places, while at higher pump strengths there is a single maximum. There are no satellite states seen in the linear response since the fluctuations are restricted to pairs of polaritons with energy and momentum conservation.

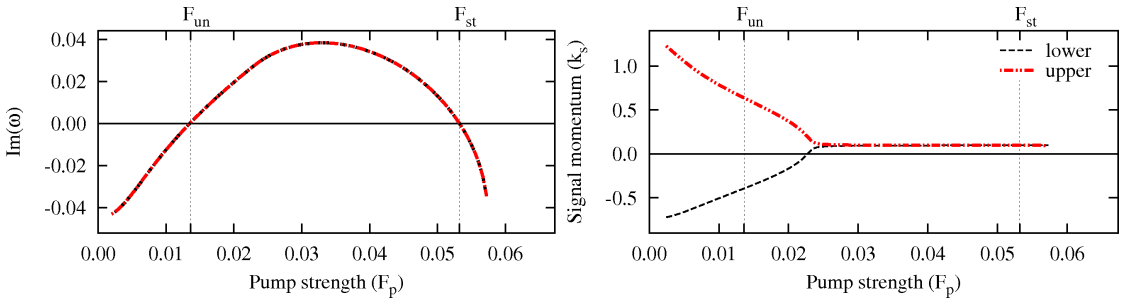

Figure 4.4: Left: maxima of imaginary parts; right: the signal momentum from linear response. The two possible values of k_s approach each other smoothly. ($F_p \Rightarrow F_{lp}$)

At very weak pumping, the peaks in the imaginary parts of the eigenvalues predict two k_s values, one positive, one negative, both of which are far from zero. As the pump becomes unstable at $F_{\rm un}$, k_s is already smaller than at the weakest pump strengths. As the pump strength is increased, the maximum value of $\Im(\omega)$ reaches a maximum and then decreases to again become negative at $F_{\rm st}$. There is an intermediate pump strength at which the two possible k_s values become indistinguishable; the two possible values of k_s approach this point evenly. Once there is a single k_s value, this value is constant until the discriminant of Eq. 4.38 becomes positive. By the argument that the signal appears with the maximum of the imaginary part, which would indicate there are initially two possible k_s values or two signal modes.

In Fig. 4.5, the k_s from linear response is plotted over the signal part of the imaginary parts to highlight where the peaks in the imaginary parts lie in relation to the borders of the unstable region. The pump mode first becomes unstable at a momentum slightly closer to zero than the maximum value for which there is a positive imaginary part. A single value of k_s occurs for comparatively weak pumping, for a k_s in the centre of the unstable region, but before the imaginary part reaches its maximum value. The idler momentum is not considered here but can be calculated easily using the momentum conservation imposed by the OPO scattering.

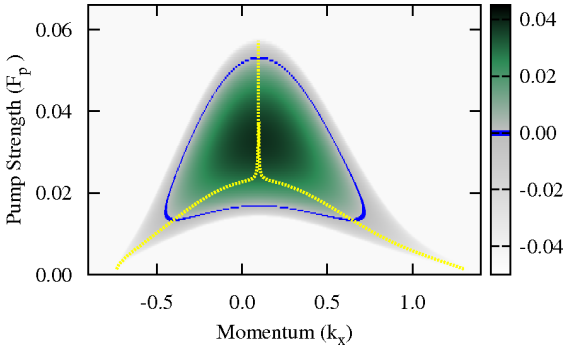

Figure 4.5: Detail of Fig. 4.3 (the imaginary part of the eigenvalues that becomes positive) around $k_x = 0$ with the locations of the maxima (yellow dotted lines) overlaid, showing where the k_s values lie against the background instabilities. ($F_p \Rightarrow F_{lp}$)

Discussion

There is qualitatively similar behaviour of k_s from the two approaches for a range of pump powers: as pumping is increased, there is a threshold pump strength; the value for k_s is initially moderate, tends towards a small positive value and then remains more or less constant until the second threshold after which no k_s can be identified. For the simple linear response approach to be a useful tool as part of the cGPE analysis of the OPO regime, there should also be quantitative agreement in k_s

In Fig. 4.6, the signal momenta and transitions from both methods are plotted together (Figs. 4.2 b and 4.4 b combined). There are two key aspects to consider: the thresholds of the OPO and unstable regions and the actual k_s value. The single mode becomes unstable to small fluctuations for pump strengths close to the switch on of the OPO. The OPO switches off for a slightly weaker pump than the return stability of the single mode: $F_{\text{off}} < F_{st}$. The single mode ansatz is unstable to small fluctuations for the definite OPO region.

The most significant variation in the signal position from the two approaches occurs for intermediate pump strengths where the k_s from the linear response analysis decreases much more rapidly than the k_s found from the numerical integration. For the higher pump strengths, the signal momentum from both approaches is $k_s \approx 0.1$, with variations in the numerical result of ± 0.1. The actual wave-vector is given by: $q_s = k_s\sqrt{\Omega_R m_c}$. For an example Rabi splitting

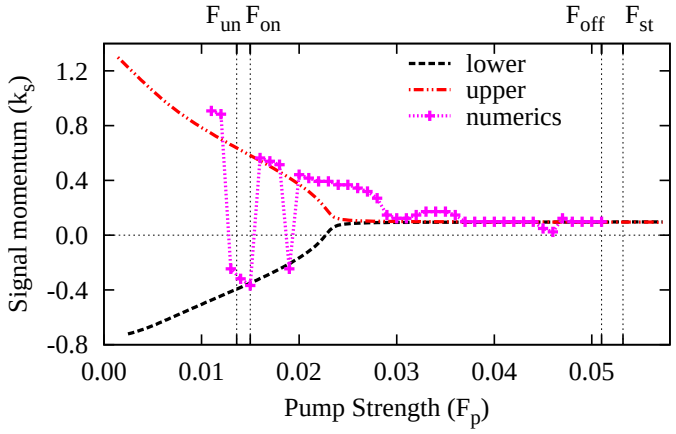

Figure 4.6: Comparison of (transitions and) k_s from the two methods. The two approaches give similar values for k_s over a range of pump strengths. Magenta (dotted and crosses), as Fig. 4.2; red (dash-dotted), black (dashed) as Fig. 4.4. ($F_p \Rightarrow F_{lp}$)

$\Omega_R = 5$meV and a cavity photon mass $m_c = 2.5 \times 10^{-4} m_e$ [18], this gives $q_s = 0.11\mu\text{m}^{-1}$.

4.4.2 k_s in the exciton-photon model

To confirm the behaviour observed in the simplified lower polariton model of the previous section, this section performs the same analysis in the exciton-photon model.

Numerical integration of coupled cGPEs

Once again a range of pump strengths is considered which covers the entire OPO regime. In finding the signal from the numerical data, the maximum in the photon occupation is considered. Examples of photon densities for weak and strong pumping are shown in Fig. 4.7.

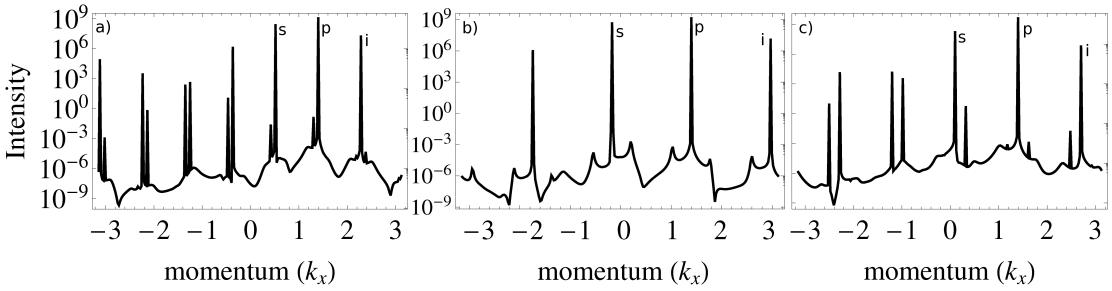

Figure 4.7: The photon density at the end of the integration period and the distinct modes (signal, s, pump, p and idler, i) identified. a): weak pump, $F_{p,c} = 1.8$; b) $F_{p,c} = 2.3$ for which k_s is negative; c) strong pump, $F_{p,c} = 5.0$ with satellite states near $-k_p$ and $-2k_p$.

Many features observed in the lower polariton model (Fig. 4.1), including the distinct satellite

states at strong pumping, are also present here. At low pump strengths (Fig. 4.7 a) there is a double peak around $k = 0$ with the peak nearest the pump dominant. The distribution of the peaks is similar to that seen in the polariton case under weak pumping, but there the dominant peak gave a negative k_s and the other peaks were much weaker. The photon density is lower at momenta above the pump, leading to an idler that is weaker than the signal. This reflects the fact that polaritons couple less strongly to the photons at higher momenta [31, 59, 82, 106]. In the centre panel of Fig. 4.7, an example of the photon distribution that gives a negative k_s at an intermediate f is plotted.

A well defined signal exists for a range of pumping strengths between $F_{\rm on}$ and $F_{\rm off}$. The photon density at the signal and the resulting k_s are plotted in Fig. 4.8.

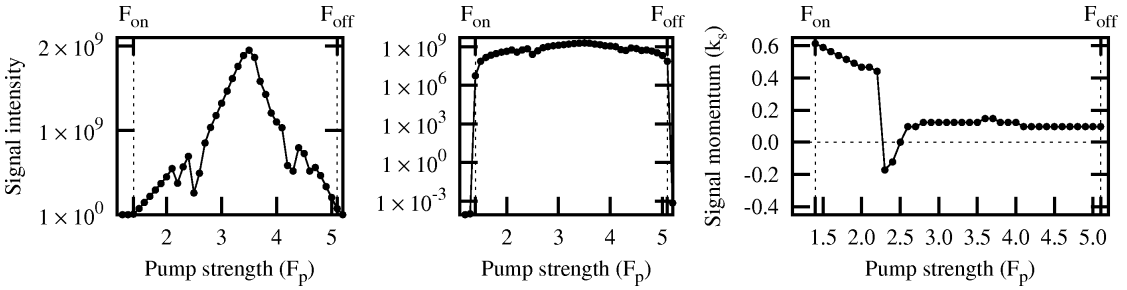

Figure 4.8: Left and centre: signal intensity showing clear region of macroscopic occupation ($|\psi|^2 > 10^6$) which is the OPO region. Right: location of the signal, $k_s < k_p$, at the end of the integration period.

The location of the signal when the OPO switches on gives again a moderate, positive value of k_s. Instead of decreasing reasonably smoothly from its initial value towards its constant value, k_s switches suddenly to a negative value. As pumping is increased further, k_s increases smoothly towards a small positive value which it maintains until the OPO switches off at $F_{\rm off}$.

Linear response analysis

The mean field is calculated by substituting the single mode Eq. (4.33), into the coupled cGPEs, Eqs. (4.12) and (4.13) and taking the steady state, $i\partial_t\psi = 0$. The exciton, $n_x = |\psi_x|^2$ and photon $n_c = |\psi_x|^2$ occupations in the mean field, are calculated and plotted in the left and cental panels of Fig. 4.9. Since the pumping is such that the system is in the 'optical limiter' regime, both n_x and n_c are monotonic in the pump strength. The imaginary parts of the eigenvalues, plotted in the right hand panel of Fig. 4.9, behave exactly as in the lower polariton model, showing two regions of variation at lower pump strengths which combine to a single region for a stronger pump.

When the maximum values of the imaginary parts of the eigenvalues ($\Im(\omega^{\pm})$ of Eq. (4.25)) are considered, a small difference between the value of $\Im(\omega)$ is the two tails is seen and continues to pump strengths where the pump mode is unstable. This is plotted in Fig. 4.10 a, where

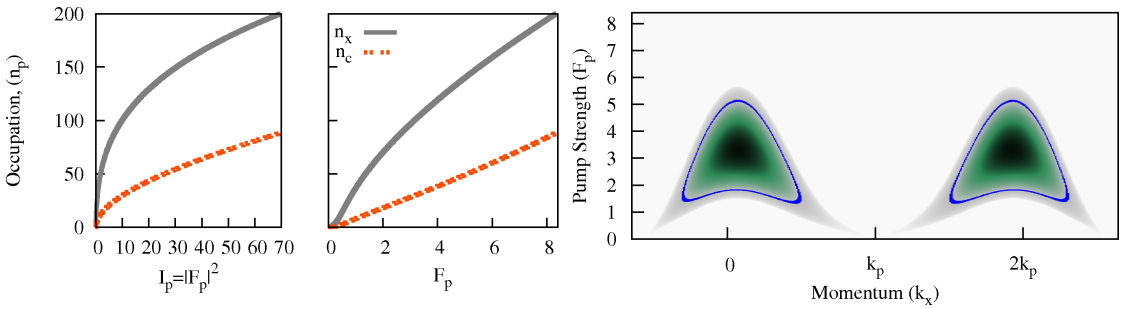

Figure 4.9: Left: Pump mode exciton n_x, centre: photon n_c occupations in the mean field steady state, right: imaginary parts of the eigenvalues with $\Im(\omega) > -\kappa$.

$\Im(\omega^{\pm})$ is larger for the potential k_s that lies closer to the pump. The pump strength at which the instability first appears is $F_{un(XC)}$; increasing the pump strength further leads to a single peak in the imaginary parts. Although both potential k_s values are included in Fig. 4.10 b, the upper (positive) value is the more unstable point.

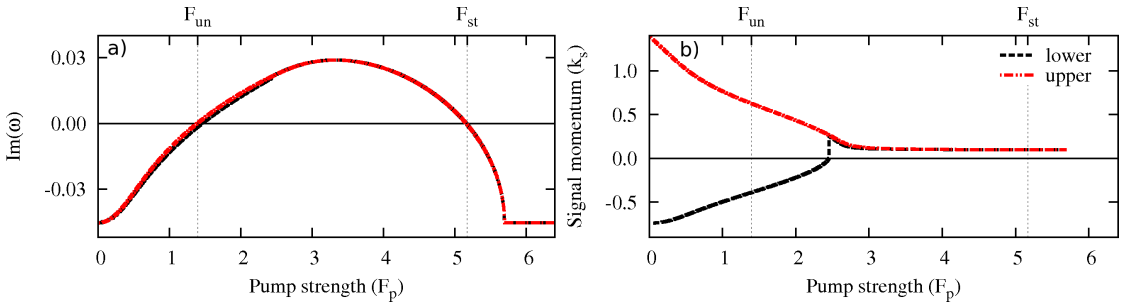

Figure 4.10: a) maxima of the imaginary parts and b) resulting k_s. The peak closer to the pump (red, dash-dotted, giving the upper value of k_s) becomes unstable at a slightly lower pump strength than the lower (negative, black, dashed) momentum peak.

Another difference to the polariton model exists in how the two potential k_s values become one. Instead of a smooth join between the two branches, there is a sharp jump to a single value of k_s. Once there is a single possible k_s, it decreases slightly to a constant value which is maintained until after the pump mode has become stable again at F_{st}.

In Fig. 4.11 a, the (positive) imaginary part of the eigenvalue is plotted for a range of pump strengths near the transition to a single possible k_s. There is initially a double peak; the one at lower momentum being the weaker. As the pump strength is increased, both peaks grow, but the two peaks do not move together particularly fast. Instead, the dip between the two peaks is filled in and there is a single broad peak that slopes between what were the two distinct peaks. This gives the sudden switch to a single signal location which is not the two peaks occurring at a single place, but the lower momentum peak becoming one edge of a plateau, while the higher momentum peak is the highest point.

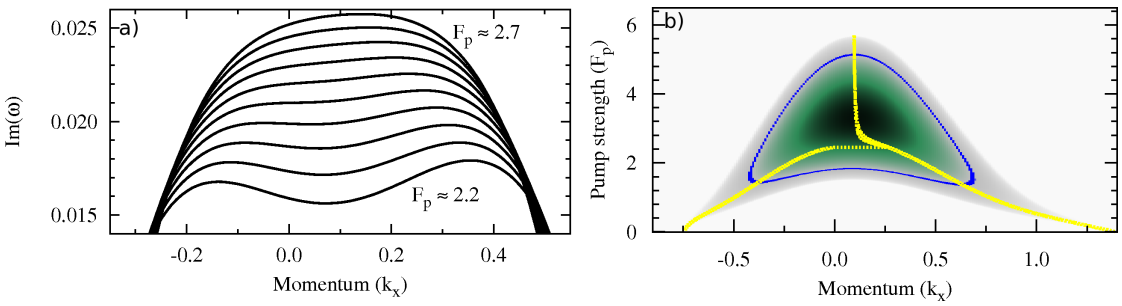

Figure 4.11: a) imaginary part near $k = 0$ for a range of pump strengths near the sharp jump in k_s that occurs when the two peaks combine. b) detail of Fig. 4.9 (the imaginary part of the eigenvalues that becomes positive) with the locations of the maxima (yellow dotted lines) overlaid, showing where the k_s values lie against the background instabilities.

The signal momentum from linear response is plotted over the signal part of the imaginary parts of the eigenvalues in Fig. 4.11 b. The details of how the two peaks become one are not clearly visible in the density plot.

Discussion

Considering the differences between the OPO region and the signal momentum from the two approaches is again necessary. The OPO region with a macroscopic occupation of a signal mode appears for the pump strength at which the pump mode becomes unstable, and the signal switches off for a pump strength near that for which the pump mode becomes again stable to small fluctuations. In both cases, the difference in pump strength is less that the single step in pump strength used for the numerical samples.

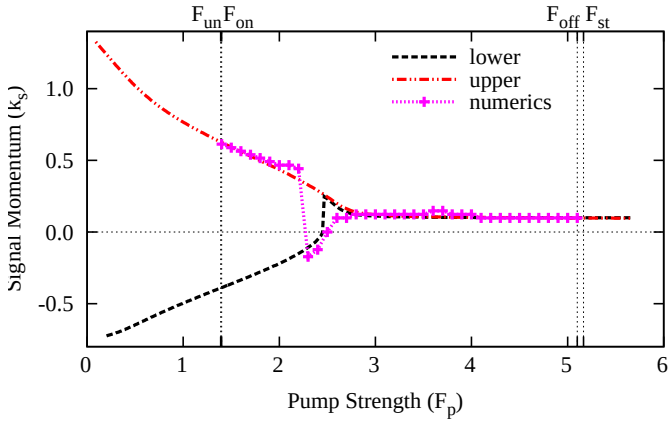

Figure 4.12: Comparison of the OPO transitions and signal momentum in the exciton-photon model. Magenta (dotted): from Fig. 4.8; red (dash-dotted), black (dashed): as in Fig. 4.10.

As shown in Fig. 4.12, the two approaches give a similar value of k_s over much of the region

considered. At higher pump strengths, there is a single momentum from the two approaches over a significant range of pump strengths. There is more variation for a weaker pump, but the negative k_s seen in the numerics, is close to the lower branch from the linear response, which has the smaller imaginary part.

The numerical integration gives a k_s that, once it becomes negative, increases gradually to reach a small positive value that is maintained for much of the remainder of the OPO region. If the two peaks remained distinct throughout until the coalescence (as in the simplified lower polariton model, Fig. 4.4), rather than exhibiting the sharp disappearance of the lower momentum peak, then it is expected that the signal momentum from the numerics would follow this curve closely. For the range of pump strengths where k_s is (approximately) constant, it has a value $k_s \approx 0.1$, which is the same as in the simplified lower polariton model.

4.4.3 Comparison of models

The previous two sections have shown that the simple linear response analysis gives a reasonable estimate of the signal momentum within the polariton OPO for at least a range of pump strengths for the parameters considered. That the signal momentum is constant over a large range of pumping strengths suggests that using the linear response analysis to determine a single k_s for a given set of pump (system) parameters will improve the accuracy of the description of the OPO regime to some extent. The two models used give, for the same pump parameters, $k_s \approx 0.1$ for much of the OPO region.

The only major discrepancies between the results of the linear response analysis and the numerical integration, are at moderate pump strengths in the simplified lower polariton model. The behaviours of the imaginary parts of the eigenvalues are very similar in both models; with the differences appearing in the numerical results.

It is important to remember that when the single mode ansatz is unstable the question remains as to what the new state is and whether it is stable. The double peak nature of the eigenvalues at weak pumping suggest that at this point the new ansatz should contain two signal and idler modes, while at higher pump strengths there are only two additional modes. In section 4.4.6, the OPO is assumed to consist of three distinct modes: the mean field can be calculated and the stability of the proposed steady state again evaluated using linear response.

Having determined that there is at least qualitative agreement between the k_s values obtained by identifying the most unstable eigenvalue of the linear response analysis of the steady state and the actual k_s value from numerical integration of the cGPE(s), the linear response approach can be used to further investigate the choice of k_s. The exciton-photon model should be used unless the nature of the three mode description of the OPO regime is of interest for which the lower polariton model has to be used.

4.4.4 Changing the pump properties.

Experimental work has investigated the variation of the signal properties with changing pump energy and momentum [33]. Using the exciton-photon model (for which there is extremely good agreement between the linear response prediction of k_s and the exact value) and choosing pump parameters that remain within the optical limiter regime ($\omega_p - \omega_{lp}(\mathbf{k}_p) = \Delta^p < \sqrt{3}\kappa_{x,c}$), the effects of changing k_p and Δ^p are investigated. Three values of Δ^p: $-0.05, 0, +0.05$, and pump momenta over a large range: $0.5 \leq k_p \leq 3.5$ are considered; in most of the results only the pump momenta that lead to an unstable single mode are present. The mean field occupations are calculated for $n_p < 250$.

Although the three values of Δ^p used keep the system within the optical limiter regime, the pump mode is still affected by these variations, as shown in Fig. 4.13 where the mean field exciton occupation is plotted against pump strength (f) and k_p. For all values of the detuning of the pump away from the lower polariton dispersion, the occupation increases fastest with pump strength at lower k_p. At positive detuning, the system is still in the optical limiter regime, but is starting to show the s-shape that characterises the bistable regime [28, 29]. In Fig. 4.13 d, the three values of the pump detuning are plotted for a single k_p showing that for a given pump momentum, increasing the detuning leads to higher n_p for a given f, apart from at very weak pumping where the positive detuning of the pump leads to slower increase in the pump mode occupation.

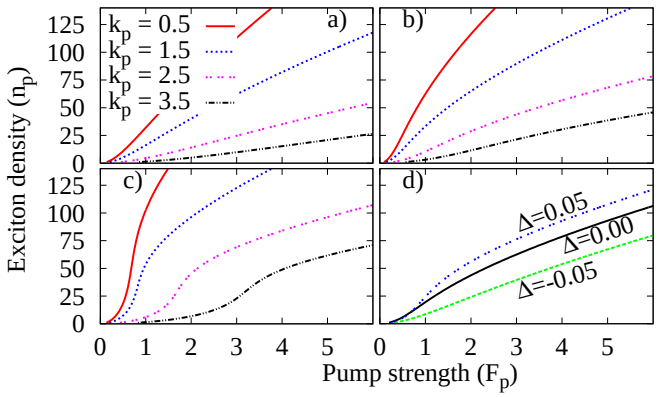

Figure 4.13: Exciton occupation in the pump mode with pump strength $F_{p,c}$ for different three values of the detuning of the pump from the lower polariton dispersion and several k_p values. a) $\Delta^p = -0.05$; b) $\Delta^p = 0$; c) $\Delta^p = 0.05$ for a range of k_p; d) $k_p = 1.5$, all three values of Δ^p.

In Fig. 4.14, the locations of the peaks in the imaginary parts of the eigenvalues are plotted for a range of pump momenta with $\Delta^p = 0$ over a large range of exciton occupations, including where the pump mode is stable, but there is at least one maximum of the imaginary parts of the eigenvalues. This shows that the k_s behaviour observed for a single k_p is general, and also that way in which a single k_s appears depends on the pump momentum with a smooth join for

sufficiently low pump momenta while at higher momenta there is a sharp join. For very low k_p, the pump mode is always stable to small fluctuations and the system never enters the OPO regime. As k_p is increased the OPO instabilities remain, but the single k_s and the disappearance of any possible k_s occur at much higher exciton occupations (and pump strengths).

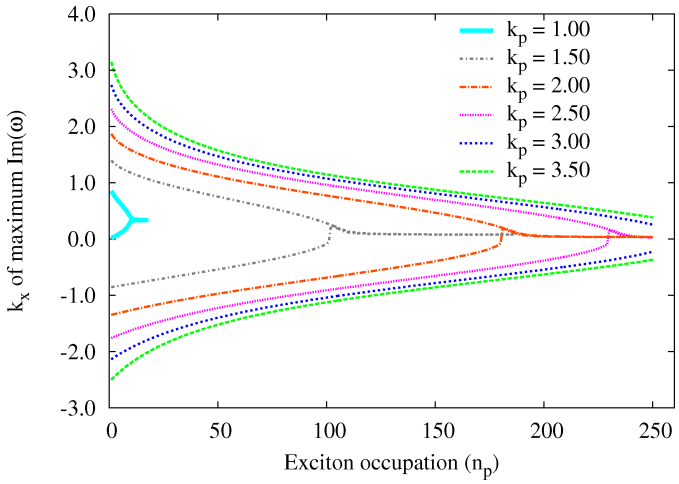

Figure 4.14: Signal momentum for a range of k_p for $\Delta^p = 0$. As k_p is increased, the pump strengths at which there is a single k_s and at which there is no longer any identifiable k_s increase. This considers the exciton occupation which is linked to the pump strengths according to Fig. 4.13 b.

From Fig. 4.14 three particular points of interest for any pump properties can be identified: where the pump mode first becomes unstable, 'switch on' or lower threshold; the lowest f (or f_{lp}) for which there is a single peak in the instability 'coalescence'; where the pump mode becomes stable again, 'switch off' (the upper threshold which may not exist for moderate n_p values).

To investigate any effects that changing the pump properties may have on the signal momentum, k_s is calculated for a range of pump momenta and energies. The mean field pump mode occupations plotted in Fig. 4.13 are representative. The signal momenta at switch off and coalescence are plotted in Fig. 4.15 a and b for a range of pump momenta and different values of the detuning, in which it is seen that, in agreement with experiments [105, 107], changing the pump energy at a given k_p does not affect k_s. However, there is some variation of k_s with k_p both at switch off and coalescence which is somewhat at variance with experimental results where no variation of the signal angle (or momentum) with pump angle is reported [33, 107].

Considering now the case of the pump applied resonantly to the lower polariton dispersion, $\Delta^p = 0$, a small variation in k_s between coalescence and switch off is observed, with the final value of k_s being slightly lower than the initial single value. In Fig. 4.15 c, it is also seen that there is an upper limit on k_p above which there is no return to stability for the pump strengths considered.

The pump strengths at the two stability thresholds and at the point where a single k_s appears

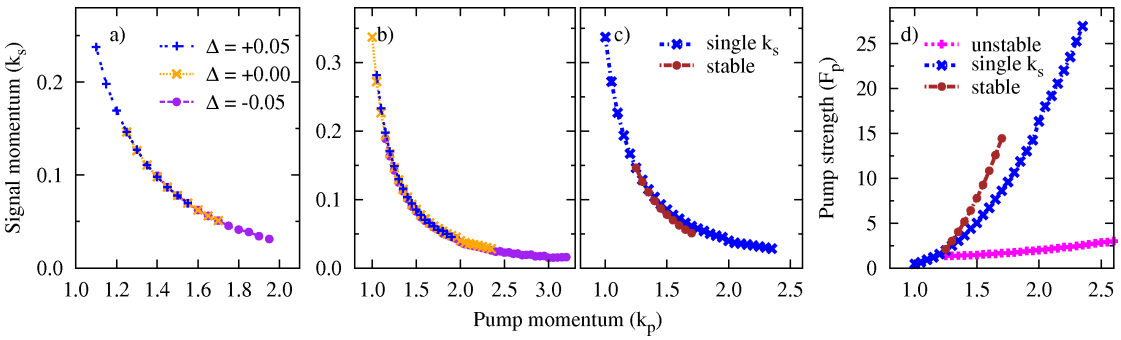

Figure 4.15: k_s at a) switch off and b) single value with changing k_p for different values of the pump detuning Δ^p. Where the three values of Δ^p give a k_s value for the same k_p, the values are indistinguishable. c) $\Delta^p = 0$, k_s values at two points: single k_s and return to stability for a range of k_p. d) $\Delta^p = 0$, pump strengths the two stability thresholds and the coalescence point; there can be a single k_s value even when the pump mode remains stable.

are plotted with k_p in Fig. 4.15 d in which it is seen that the region for which two k_s values are possible increases rapidly with k_p as the difference between the pump strengths of the lower threshold and coalescence point grows. The pump strength at which the pump mode becomes unstable increases slowly with k_p; returning to Fig. 4.13, it can be seen that this actually corresponds to a decrease in the exciton occupation at which instability occurs. Although a single signal momentum and hence a clear OPO could exist at large momenta, this is clearly limited by the pump strengths that can be used. There is no upper threshold within the range of exciton occupations considered for pump momenta greater than about 1.8.

In other studies of the OPO regime and the signal properties, the signal energy has been considered [30, 33]. Since the linear response approach is being used, the signal energy is defined as the real part of the eigenvalue at the k_s identified via the maximum of the imaginary part $(\Re(\omega, k_s))$. (The location of the peak in the imaginary part gives k_s, so the real part, which is the associated spectrum gives the energy.) The signal at coalescence is plotted in Fig. 4.16 for a positive detuning of the pump away from the lower polariton curve and for a range of pump momenta. The single k_s point is chosen since it covers a larger range of pump momenta. In all cases, the behaviours at large k_p are limited by the consideration of the effects within the microcavity at high exciton density. In particular, the underlying assumption of the exciton-photon model is that the excitons can be treated as effective bosons is only valid at low and moderate exciton occupations [31].

From Figs. 4.15 and 4.16, it can be seen that as the pump momentum is increased and the signal momentum decreases, the signal energy increases. This is broadly consistent with experiments studying the effect of changing the pump properties on the resulting signal where the signal energy increased, but the momentum was not observed to vary with k_p [33]. However, the variation in the energy is much greater than the variation in the momentum. There are two distinct points: for the pump mode to become unstable, k_p must be sufficiently large;

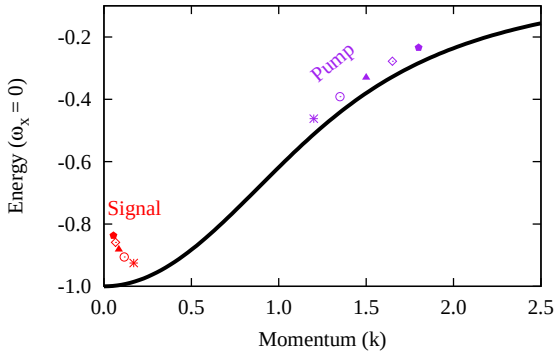

Figure 4.16: Pump energy and real part of eigenvalue at various k_p for $\Delta^p = +0.05$ when there is a single k_s (clean OPO). The solid line is the lower polariton dispersion.

increasing the pump momentum (and hence energy if the pump's relation to the unperturbed lower polariton dispersion remains unchanged) leads to a signal momentum that is closer to zero and with increasing energy.

4.4.5 Note on experimental observation

The precision of the experimental results is finite and linked to the size of the pump spot. Also, the theoretical analysis considers a single k_p and picks out the single k_s value to the precision of the calculation. In experiments, the excitation is provided by a finite sized spot and thus has a limited resolution and the exciting laser will not be exactly monochromatic. An experimental momentum resolution of $0.2\mu\text{m}^{-1}$ which using a Rabi splitting of 6.5meV [107] and a photon mass $2.5 \times 10^{-4} m_0$, gives a resolution of 0.16 in the non-dimensional system of units, which is about the same as the total variance of k_s at switch off seen in Fig. 4.15. The much larger variance observed in Fig. 4.15 includes pump momenta for which the pump only ansatz is stable at all pump strengths.

Comparing the value of k_s predicted by the simple linear response analysis with experimental data can be done. Although experiments often describe the signal as having an emission angle that is normal to the sample $\theta = 0°$, the actual peak in the signal emission is at a finite angle, typically about 1° [33, 107]. With a Rabi frequency of 6meV, $\omega_{lp}(0) \approx 1.4587$ [33] and using $m_c = 2.5 \times 10^{-4} m_0$ gives $k_s \approx 0.105$ in the non-dimensional units. Where transforming from experimental angles to momenta in μm^{-1} uses [23, 26, 59]:

$$k = \frac{\omega_{lp}(k)}{\hbar c \sin(\theta)}. \tag{4.46}$$

Another experiment gives the signal centred at 2° or $k_s \approx 0.25\mu\text{m}^{-1}$ [61]. The Rabi splitting of 6meV gives a non-dimensional value of ≈ 0.204.

The outstanding question may relate to the definition of the OPO signal as occurring near

$k = 0$ so any large momentum signals are considered as precursors to the transition to the OPO regime in experiments, although some experimental results do show double peaks in the energy spectrum at a given angle at low and moderate pump strengths that have not been discussed [61,107]. Secondly, although the pump mode is unstable at these large potential signal momenta and the signal occupation at these momenta is large in the numerical simulations, the peak in the signal occupation as seen in e.g. Fig 4.8, does not occur until well after the signal momentum has reached its near-constant value. Lastly, the finite energy distribution of the pump spot does not affect the signal properties, but the finite momentum distribution does so any experimental pump includes a (small) range of k_p and hence a range of k_s. Taking a pump spot size of $\sim 100\mu$m [26,27] to give a k_p variation of $0.01\mu\text{m}^{-1}$ the variation of k_p in the non-dimensional system of units is 0.012 for $\Omega_R = 6.5$ and $m_c = 2.5 \times 10^{-4} m_0$.

Although the linear response analysis presented here implies that there is no upper limit on k_p for OPO to occur, this is not the case in experiments where no OPO is observed for excitation at large angles (k_p) [27]. One physical limitation is that the OPO threshold density must be below the exciton saturation density [27], as seen in Fig. 4.14, increasing k_p increases the exciton density at the pump mode for which there is a single k_s. If the OPO is defined as having a single signal (single k_s value) then at large k_p this may not occur before the exciton saturation density is reached (as discussed in section 2.1, the model used does not include the effects of exciton saturation).

4.4.6 Effect on the OPO regime

To investigate the effect on the OPO regime, a full range of $\mathbf{k}_s = (k_s, 0)$ values are considered for $\mathbf{k}_p = (1.4, 0)$ and $\Delta^p = 0$. The mean field occupations of the simplified lower polariton model are calculated using Eqs. (4.39)-(4.42) and the eigenvalues of the linear response matrix calculated for $|k_x| < |k_p - k_s|/2$. For each k_s and pump strength f_{lp}, two questions are asked: whether the OPO regime exists (non-zero n_s) and whether it is stable (all imaginary parts of eigenvalues ≤ 0 to the level of numerical accuracy at $k_y = 0$). In Fig. 4.17 a, the signal mode occupation is plotted and in Fig. 4.17 b, a phase diagram showing the three possible behaviours: no OPO, unstable OPO and stable OPO, is constructed. The signal momenta determined in section 4.4.1 is overlaid.

At low pump strengths, the three mode description of the OPO regime is stable for a range of k_s on the side towards the pump. As the pumping is increased, this region narrows slightly and moves towards $k_s = 0$. Further increase of the pumping leads to a region where the OPO regime is unstable for all k_s for which it exists. At the highest pump strengths, there is again a region where the OPO regime is stable, this time for most of the k_s values for there is a finite signal mode occupation, which is near $k_s = 0$ and centred on a small positive k_s. Only at the highest pump strengths does the k_s from the single mode linear response analysis lie consistently within the region of stable three mode description of the OPO regime.

The stable regions at lower pump strength are for k_s values that agree with the exact numerics,

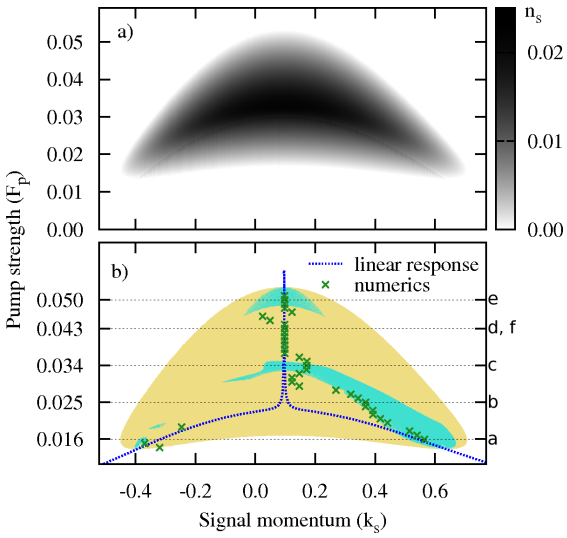

Figure 4.17: a) signal mode occupation with $F_p \Rightarrow f_{lp}$ and k_s; b) regions of stable (blue-green, dark) and unstable OPO (golden, light) with k_s from section 4.4.1 (dark blue dotted lines: linear response; green crosses: numerical data); the horizontal gridlines are the pump strengths of the polariton distributions examined in Fig. 4.18.

but not with the single mode linear response; the numerical prediction lies at the lower k_s edge of the stable region. The five polariton density profiles in Fig. 4.18 correspond to the five pump strengths in Fig. 4.17. Finding k_s as the largest peak in the polariton density below the pump gives k_s values that give stable OPO for the pump strength considered. For $f_{lp} = 0.43$, the three mode description of the OPO regime is unstable at all k_s values; the corresponding polariton density in Fig. 4.18 d is 'noisy' with large occupations at many momenta compared with the other samples where the pump, signal and idler modes are clear in the logarithmic plot. In Fig. 4.18, the polariton density profile at $f_{lp} = 0.043$ is plotted in linear scale. Although the signal is clear, there are additional modes that have large occupation that are not consistent with a scheme involving satellite states equally spaced at lower and higher momenta.

4.4.7 k_s with non-zero k_y

So far, with the pump applied at $k_y = 0$, it has been assumed that the signal will therefore appear at $k_y = 0$ too, and the analysis has been restricted to the plane with $k_y = 0$. In chapter 3, the incoherent luminescence was calculated in 2-D momentum space and had a ring shaped structure for weak pumping. This suggests that at low pump strengths, there are not just two possible values of the signal momentum, but an infinite number. Studies considering fluctuations within the OPO regime consider $\mathbf{k}_s = (k_s, 0)$, which is always possible by a suitable choice of the k_y axis, and that the fluctuations are restricted to exist in the $k_y = 0$ plane too [41].

Here, the possibility for the signal to appear with finite k_y is investigated within the simplified

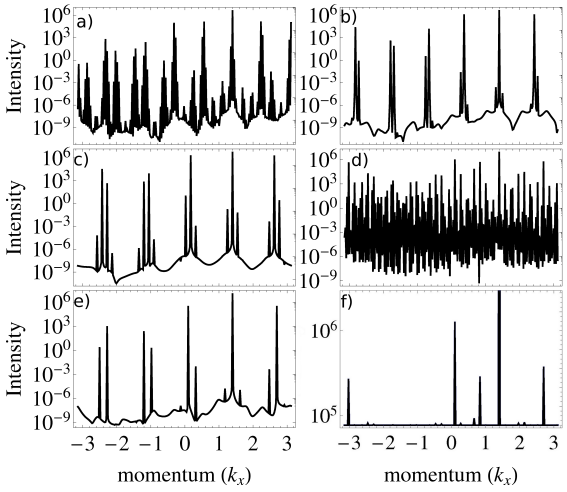

Figure 4.18: Polariton density profiles at various pumpings across OPO regime. a)-e) Log scale profiles: a) $f_{lp} = 0.016$, b) $f_{lp} = 0.025$, c) $f_{lp} = 0.034$, d) $f_{lp} = 0.043$, e) $f_{lp} = 0.050$, f) $f_{lp} = 0.043$, linear scale.

lower polariton model. First linear response analysis is performed for a pump applied with $\mathbf{k}_p = (k_p, 0)$, but without restricting the fluctuations to lie in the plane of the pump. The analysis is then extended to the OPO regime where the signal is chosen with $\mathbf{k}_s = (k_s, 0)$ and the appearance of instabilities with non-zero k_y considered. Finally, numerical results of the exciton-photon model with additional noise are presented for comparison.

Two examples of the imaginary parts of the eigenvalues around the pump mode (for momenta around the expected signal at $\mathbf{k} = \mathbf{0}$) within the simplified lower polariton model used in sections 4.4.1 and 4.4.6 are plotted in Fig. 4.19: the two behaviours observed in the incoherent luminescence are reproduced and the double peak structure extends into a ring. The instabilities around a mean field steady state are consistent with pulsed pumped experiments [82]; but with the distinct difference that there is a gap between the pump and the instability and hence occupation. Although the pump strengths considered here give and unstable pump mode, the behaviours are general.

If fluctuations in the k_y direction ($-(k_p - k_s)/2 < \delta k_y < (k_p - k_s)/2$) are included in the OPO linear response analysis, the range of stable OPO is reduced, as seen by comparing Figs. 4.17 b and 4.20. The small stable region with negative k_s is now unstable and the broad band of stable OPO characterised by decreasing k_s values with increasing f_{lp} is much narrower. This indicates regions where the OPO is stable at $k_y = 0$, in the plane of the pump and signal, but unstable towards small fluctuations at finite k_y.

In Fig. 4.21, the largest imaginary part of the eigenvalues is plotted for the signal momenta $\mathbf{k}_s = (k_s, 0)$ and several pump strengths, as identified in Fig. 4.20, showing the different types of unstable behaviour seen across the phase diagram. It is interesting to examine both where the OPO is unstable to fluctuations in δk_x as well as where the instability occurs at finite k_y.

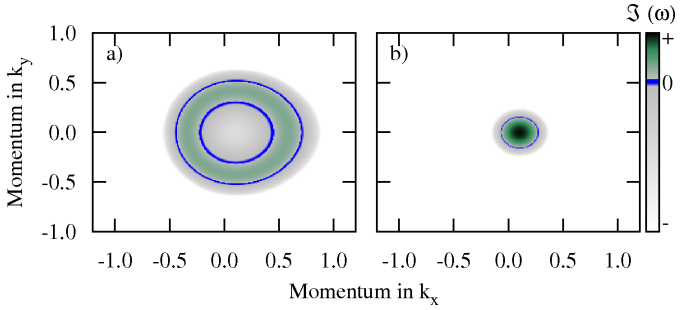

Figure 4.19: Unstable eigenvalues (positive imaginary part) for weak and strong pumping, f_{lp} within unstable region, showing the two distinct behaviours: a ring shape at low pump strengths giving an ill-defined signal; at higher pump strengths, there is a single region of instability and a well defined k_s.

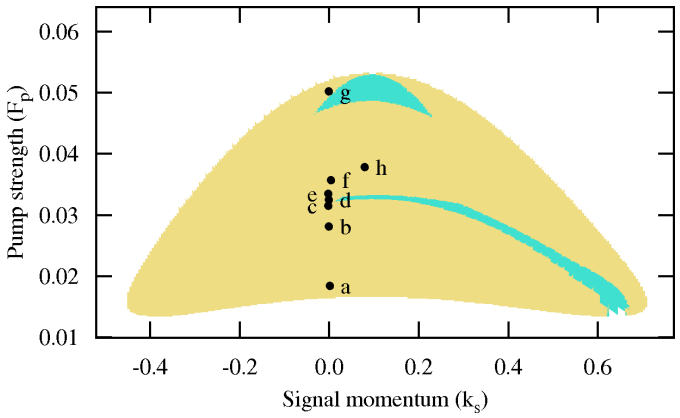

Figure 4.20: Regions of stable and unstable OPO when fluctuations in k_y are included. The stable regions are reduced compared with Fig. 4.17b. The letters refer to the samples shown in Fig. 4.21.

The samples for $k_s = 0$ are considered first. Very close to threshold, Fig. 4.21 a, the OPO is unstable symmetrically around $k_y = 0$ and around $\delta k_x = 0$; this symmetry around the axes is present in all samples considered. The most unstable regions are lobes at moderate δk_x, but there are also unstable regions far from $k_y = 0$, and a weakly unstable ring in the centre. As the pump strength is increased, the instabilities at large k_y vanish while the central ring joins to the lobes to form a distorted oval around the modes, as show in Fig. 4.21 b. The most unstable points are still at $k_y = 0$ and finite δk_x. On increasing the pump strength further, the lobes at $k_y = 0$ become progressively weaker while the instabilities at finite k_y decrease more slowly. Eventually, there are small unstable regions around $k_x = 0$ but with finite k_y as shown in Fig. 4.21 c; this reduces the unstable region compared to the $k_y = 0$ case. There is then a small range of pump strengths, near the maximum signal occupation where a signal mode with $k_s = 0$ is stable.

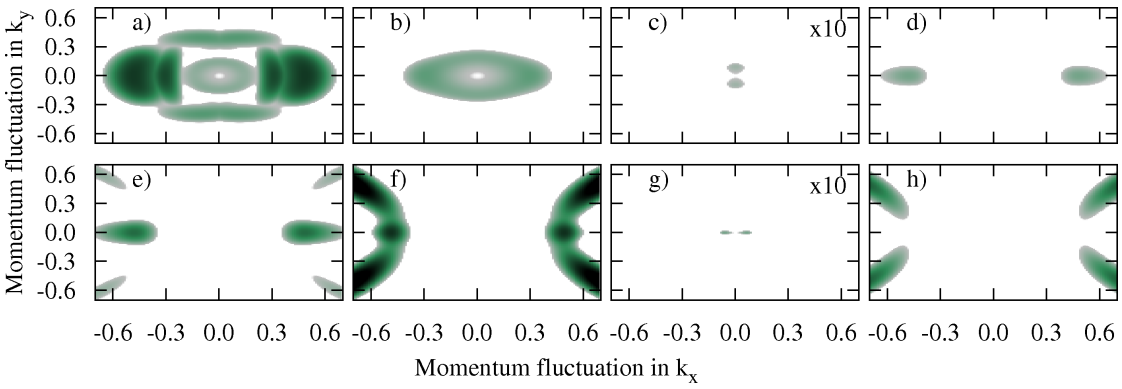

Figure 4.21: Unstable eigenvalues (positive imaginary part) around the OPO for fluctuations in k_x and k_y. a) - g), $\mathbf{k}_s = (0, 0)$ a) $f_{lp} = 0.0184, n_p = 0.054$; b) $f_{lp} = 0.0281, n_p = 0.046$; c) $f_{lp} = 0.0316, n_p = 0.048$, $\times 10$ for visibility; d) $f_{lp} = 0.0325, n_p = 0.052$; e) $f_{lp} = 0.0332, n_p = 0.056$; f) $f_{lp} = 0.0357, n_p = 0.070$; g) $f_{lp} = 0.0502, n_p = 0.128$, $\times 10$ for visibility; h) $\mathbf{k}_s = (0.08, 0)$, $f_{lp} = 0.0378, n_p = 0.075$.

The OPO is next unstable in two regions centred on $k_y = 0$ as shown in Fig. 4.21 d. As the pumping becomes stronger, unstable regions far from $k_y = 0$ appear, Fig. 4.21 e, that grow to eventually form semicircular unstable regions, Fig. 4.21 f. It is noted that the positive imaginary part is largest for large k_y, and the peak at $k_y = 0$ becomes less pronounced as the pumping is increased. Eventually, the OPO becomes stable near the upper threshold. For $k_s = 0$, there is another region of unstable OPO immediately before the upper threshold is reached. This region is common to the stability with and without the inclusion of fluctuations at finite k_y and Fig. 4.21 g where the small unstable regions are centred on $k_y = 0$ is consistent with this.

To understand how the broad stable region near the maximum signal occupation becomes so narrow, a sample with finite k_s is examined. In Fig. 4.21 h, it is seen that at finite signal momentum, the large k_y behaviour observed in Fig. 4.21 f is general, but the two peaks at $k_y = 0$ that appear earlier (Fig. 4.21 e) are not present for finite k_s.

The discussion of the nature of the instabilities can be related back to the polariton profiles discussed in the preceding section. Considering that the mean field profiles plotted in Fig. 4.18 are in the $k_y = 0$ plane, the instabilities along this axis in the plots of Fig. 4.21 can be discussed. Roughly speaking, Fig. 4.18 a corresponds to Fig. 4.19 a; Fig. 4.18 b to Fig. 4.21 a and b; Fig. 4.18 c to Fig. 4.21 h; Fig. 4.18 d and f to Fig. 4.21 f (the samples shown remain similar to higher pump strengths); Fig. 4.18 e to Fig. 4.21 g and Fig. 4.19 b. From this, it becomes clear that the instabilities around the OPO regime do not give much indication of the polariton profile if the choice of k_s is not correct.

However, one crucial feature must be highlighted: except for Fig. 4.21 e, f and h, the OPO is stable, but for a different value of k_s to that used in the calculation of the instabilities around the OPO. This highlights that if the OPO regime is investigated with a k_s that is far from the stable k_s, the instabilities are strong (compare Fig. 4.21 a, b with Fig. 4.21 d, g).

To better understand the linear response behaviour in 2-D momentum, and highlight any features that may be visible in experiments, the photon density at pump strengths in similar regions of the OPO phase diagram can be analysed. Noise is added to the cGPEs describing the exciton-photon model, Eqs. (4.12) and (4.13) (when the mean field occupations are calculated numerically, all occupation is at $k_y = 0$). The numerical simulation now uses truncated Wigner methods, and the cGPEs have the form [64, 108]:

$$i\partial_t\psi_c = (\omega_c(k) - i\kappa_c)\psi_c + \frac{\Omega_R}{2}\psi_x + f + i\sqrt{\kappa_c}\eta_c \tag{4.47}$$

$$i\partial_t\psi_x = (\omega_x(k) + g_x(|\psi_x|^2 - V_{rc}) - i\kappa_x)\psi_x + \frac{\Omega_R}{2}\psi_c + i\sqrt{\kappa_x}\eta_x \tag{4.48}$$

where $\eta_{c,x} = dW_{x,c}/dt$ is Wiener differential noise with [64, 108]:

$$\langle dW^*_{x,c}(\mathbf{r}, t)dW_{x,c}(\mathbf{r}', t')\rangle = \delta(\mathbf{r} - \mathbf{r}')\delta(t - t');$$
$$\langle dW_{x,c}(\mathbf{r}, t)dW_{x,c}(\mathbf{r}', t')\rangle = 0.$$

The additional term $g_x V_{rc}\psi_x$ accounts for the artificially induced density at zero pumping [64, 108].

The photon density at four pump strengths is plotted in Fig. 4.22. Near the lower threshold, the ring shape of the signal is very similar to the ring seen in the linear response analysis of the pump only case, Fig. 4.19 a. When the pump strength is increased, the ring shrinks, compare Fig. 4.22 b with Fig. 4.22 a. There are two possible explanations for this: it could correspond the coalescence of the two possible k_s values seen in the pump only linear response analysis, or it could reflect a ring shape in instabilities of the OPO states as plotted in Fig. 4.21 b. The ring shape is also present in the satellite states. The first explanation is more likely since the pump strength in Fig. 4.22 b is $f = 2.2$ which is just below the coalescence of the linear response peaks (see Fig. 4.10). The disappearance of a ring shaped structure as pump strength is increased leads identifying the OPO transition as occurring at the 'coalescence' point - or single peak - rather than when the pump mode becomes unstable - ring shaped signal [109].

As the upper threshold is approached, Fig. 4.22 c, the photon density becomes distributed in broad bands and the signal is not easily identified. As discussed in section 4.4.6, noisy behaviour in the mean field polariton distribution corresponds to an OPO that is unstable according to linear response analysis. Interestingly, when noise is added into the exciton-photon model, satellite bands evenly spaced in k_y appear. Just before the OPO switches off, Fig. 4.22 d, the OPO modes are along $k_y = 0$ with finite widths in k_y. This is consistent with the region of OPO that is stable to fluctuations in k_x and k_y that occurs just before the OPO switch off.

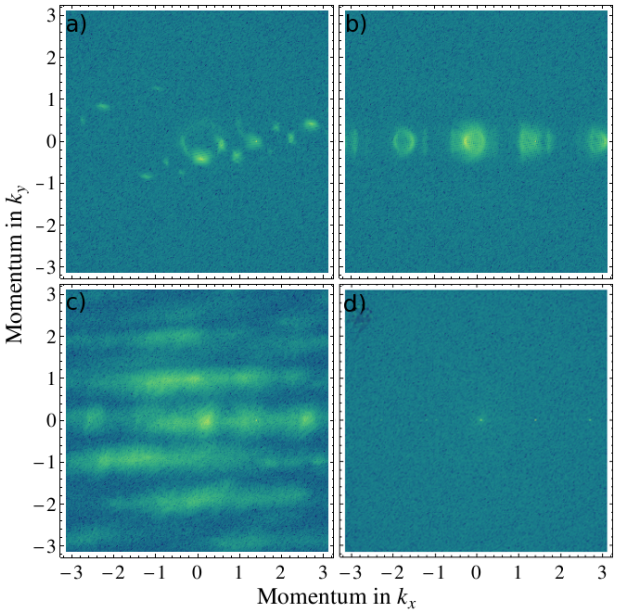

Figure 4.22: Plots of $\log(|\Psi_c|^2)$ in $k_x - k_y$ space at pump strengths across the OPO region. a) $f = 1.6$ near the lower threshold, the signal appears on a ring with low density at $\mathbf{k} = \mathbf{0}$ ($|\psi|^2 < 10^9$), b) $f = 2.2$ part way into the OPO region, the signal is a large spot, but with a ring structure discernible ($|\psi|^2 < 10^9$), c) $f = 3.6$ the signal is difficult to identify since there is a band of moderate photon density and additional bands equally spaced in k_y are also present ($|\psi|^2 < 500$), d) $f = 5.0$ near the upper threshold, the peaks in the photon occupation are very sharp with $k_y \approx 0$ ($|\psi|^2 < 10^9$).

4.4.8 k_s with momentum dependent polariton interactions

So far, the discussion has considered the exciton-photon model which gives a very good description of the polariton system or a simplified lower polariton model in which the polariton-polariton interaction strength is momentum independent. Using the linear response analysis of the pump only ansatz in the exciton-photon model to predict k_s gives good agreement with numerical simulations. In the simplified lower polariton model, the best way to predict k_s at low pump strengths is to find where the three mode ansatz of the OPO regime is stable while at higher pump strengths the linear response analysis of the pump mode is sufficient. Here, the linear response analysis of the pump only and three mode descriptions is performed in the full lower polariton model in which the momentum dependence of the polariton interactions is restored; the pump is applied at $\mathbf{k}_p = (1.5, 0)$ with $\Delta^p = 0$, and fluctuations are restricted to the $k_y = 0$ plane.

In Fig. 4.23, the peaks in the imaginary parts of the eigenvalues of the pump only linear response are plotted over the regions of stable and unstable OPO. The discrepancy seen in Fig. 4.17 b is still present, but is less pronounced and the stable band at moderate pumping exists for a large range of both positive and negative k_s. The sharp jump in the k_s value predicted by

the pump only linear response, seen in the exciton-photon model but not in the simplified lower polariton model, is again present, and the two subsequent k_s values are marked. The stable band at low pump strengths has a complicated structure, which is not discussed further.

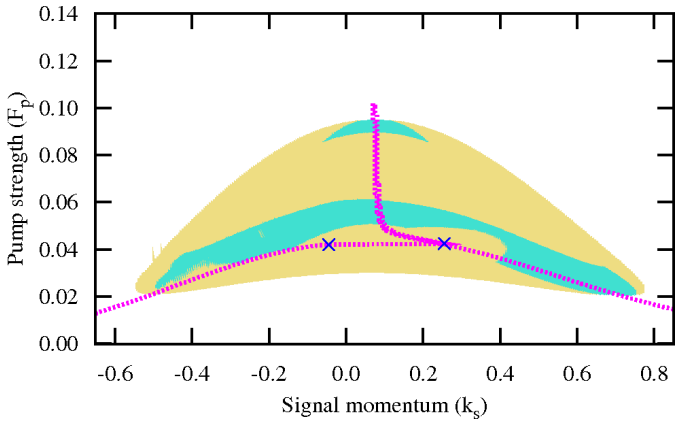

Figure 4.23: In the full lower polariton model, there is better agreement between k_s predicted by pump only linear response and the region where the OPO is stable to fluctuations with $k_y = 0$. Pink dashed lines: k_s from pump linear response; golden regions: unstable OPO; blue regions: stable OPO; dark blue crosses: subsequent k_s values at coalescence, the jump is as seen in the exciton-photon model. ($\mathbf{k}_p = (1.5, 0)$; $F_p \Rightarrow f_{lp}$)

To determine whether it is worth applying a predicted k_s in the OPO regime when the polariton decay is momentum dependent ($\kappa_x < \kappa_c$), the OPO regime with $\kappa_c = 10\kappa_x$ is considered. Fig. 4.24 shows that the OPO regime exists but that the three mode description is never stable for $-0.5|\mathbf{k}_p| < k_s < 0.6|\mathbf{k}_p|$ ($\mathbf{k}_p = (1.5, 0)$).

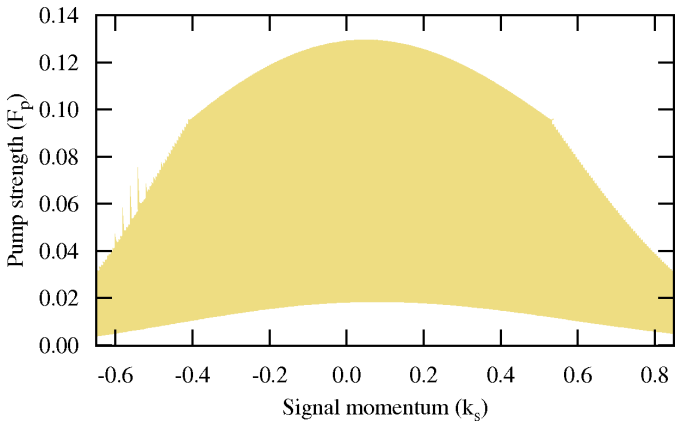

Figure 4.24: Full Lower Polariton model: OPO is always unstable for $\kappa_c = 10\kappa_x$. ($\mathbf{k}_p = (1.5, 0)$; $F_p \Rightarrow f_{lp}$ and fluctuations are restricted to $k_y = 0$.)

4.5 Signal momentum conclusions

In this chapter, the cGPEs of the exciton-photon and lower polariton descriptions of the coherently pumped polariton system were derived from the Heisenberg equations of motion. The exciton-photon and a simplified version of the lower polariton model with $V_{lp} = 1$ were used to investigate the potential of using linear response analysis to predict the signal momentum of the OPO regime. The k_s predicted in the exciton-photon model matches very closely to the exact solution, while in the simplified lower polariton model, the k_s from the simulations coincided with where the three mode ansatz is stable to fluctuations with zero momentum in the k_y direction at low pump strengths and with the most unstable point found through the linear response of the pump only case at higher pumping.

When the OPO regime is stable, the polariton distribution is not very noisy around the distinct peaks marking the signal, pump and idler states, perhaps with additional satellite states which do not necessarily lead to the three mode description of the OPO regime becoming unstable. It is interesting to note that stable OPO is possible for a continuous range of pump strengths until near where the signal reaches its maximum occupation. There is then an unstable region that occurs as the signal occupation decreases from its maximum value and a further stable region for very weak signal (low n_s) just before the signal switches off. It is not just the signal momentum that determines whether the OPO is stable or not, but the pump strength is a major factor, more so than the signal occupation since the band of stable OPO at low pump strengths covers most of the signal occupations in the OPO regime.

Including the 2-D momentum in the analysis leads to two main features. Firstly, at low pump strengths the instability occurs on a ring and therefore there is no single k_s, while at higher pump strengths there is a single region of instability centred at $k_y = 0$. Secondly, the pump strengths and k_s values for which the OPO is stable are reduced. Momentum dependent polariton decay where $\kappa_c = 10\kappa_x$, expands the k_s range over which there is a finite signal occupation at the mean field level, but. in the example considered, there were no k_s, F_p combinations for which the three mode description of the OPO regime was stable.

When the momentum dependence of the polariton interactions and decay are included, the OPO regime becomes unstable for all pump strengths. It was noted in section 3.7, that the signal mode can become bistable while the pump is in the optical limiter regime, and the interplay between instability to small amplitude fluctuations and bistability could be interesting.

5 | Conclusions

This thesis has explored the transition of a system of coherently pumped polaritons into the OPO regime, and the properties of the OPO signal and idler states. Here, the main results are summarised and some areas for further investigation mentioned. First, the detailed Hamiltonians for the polariton system were written down and the Hopfield coefficients derived in chapter 2.

In chapter 3, Keldysh Green's functions techniques were employed to find the spectra resulting from a linear response analysis and gain access to the occupations of the spectra. It was found that the phase transition to the polariton OPO regime can be described in analogy with equilibrium Bose-Einstein condensation as an effective chemical potential can be identified which crosses the normal modes (poles) at the transitions (lower and upper thresholds). Interestingly, when the exciton decay is taken to be much less than the photon decay this still defines an upper threshold although the pump only state remains unstable at all pump strengths above the lower threshold. In the OPO regime, which is modelled using three modes (one for each of signal, pump and idler), the occupations of the spectra depend on the mode considered. Of particular relevance is the observation that the Goldstone mode, due to the spontaneous breaking of the $U(1)$ phase symmetry of the OPO signal and idler [41], which is tied to the signal and idler modes as the pump mode does not have a large incoherent occupation at the zero of the fluctuation. Combining the three states creates an incoherent luminescence spectrum around the OPO states that is very similar that seen around the pump mode just above the return to stability.

Chapter 4 considered whether an informed choice can be made for the signal momentum in models of the OPO regime. In the mean field steady state description of the OPO regime which includes the signal and idler modes as well as the pump mode, it is necessary to choose the signal (and hence idler) momentum by hand. A detailed comparison showed that the value of k_s predicted by the linear response analysis of the pump only (below OPO threshold) case agrees well with the actual value from the numerical integration. In particular, there is very good quantitative agreement in the exciton-photon model, while the simplified lower polariton model only has qualitative agreement between the two methods. There is, however, qualitative agreement between both models near the upper threshold, and the k_s values near the switch off of the OPO (high pump strengths) agree between both methods and models. In the simplified lower polariton model, the k_s values for which the three mode description of the OPO is stable

give quantitative agreement with the numerical integration at low pump strengths, while in the broad stable region near the switch off of the signal and idler, it is the below threshold value of k_s that agrees with the numerical simulation. Changing the pump properties, both momentum and detuning away from the lower polariton dispersion, affects the thresholds of the instabilities and the pump strengths for which there is a single k_s value, but the variation of the k_s value itself is small.

Fluctuations having non-zero k_y were considered in the Keldysh formalism, where the incoherent polariton luminescence, integrated over energy, showed a clear ring-shaped structure below the lower threshold. For constant polariton decay, the rings are almost circular and the luminescence is strongest on the side closest to the pump. When the exciton decay was made much weaker than the photon decay and the polariton decay was therefore strongly momentum dependent, the peak in the luminescence moved to the side away from the pump and the rings became deformed towards a clear 8 shape centred on the pump. At high pump strengths (above the upper threshold) the signal and idler had a single peak centred on $k_y = 0$.

Including fluctuations in the k_y direction in the linear response analysis of the pump only case of the simplified lower polariton model showed the same features: the pump mode becomes unstable at low pump strengths at all points on a ring that contracts to a single peak at higher pump strengths. In the OPO regime the k_s, F_p combinations for which the OPO is stable are reduced by instabilities that occur only at finite k_y. Significant photon populations in k_y were only observed in the numerical integration when additional noise terms were included: the ring shape of the signal at low pump strengths (and its contraction to a single point) was observed, and at higher pump strengths bands of moderated photon occupation, equally spaced in k_y, appeared.

Lastly, the momentum dependent polariton interactions were restored and the stable OPO regime (for fluctuations with momentum in the k_x direction only) found to be larger than in the simplified lower polariton model. When the exciton decay was reduced, the OPO regime becomes unstable at all pump strengths and k_s values considered.

Starting from the work presented in this thesis, there are various areas in which further investigation could be done; some of these are mentioned below.

Continuing with the Keldysh analysis, a rotation into the amplitude-phase basis of the fluctuations would enable the calculation of the first order correlation functions in both space and time [21, 77]. These have already been calculated numerically [68], so the calculation, starting from the matrices for $D^<(\omega, \mathbf{k})$ in the pump only and OPO regimes would determine where the second order approximation is accurate.

In the pump only case, the Keldysh analysis could be performed in the exciton-photon basis. As seen in the discussion of k_s, this would not give much new information, but could be a useful confirmation of the below threshold behaviours, especially when the exciton decay is less than the photon decay, as the incoherent luminescence of the photons is directly accessible. This could be particularly useful for understanding ring of incoherent luminescence below the lower threshold

and the shift of the maximum occupation from the pump side of the rings to the side away from the pump when the decays are made uneven. The build up of excitons at high momenta should also be observable in this description.

The work on determining the signal momentum has several areas that could be developed with some interest for experiments. Given the effects of $\kappa_x < \kappa_c$ on the incoherent luminescence around the pump mode, it could be interesting to investigate how these more realistic decays would affect $\mathbf{k}_s$. Bistability of the pump and signal modes has been recognised [25, 28–30, 110–112], but this study has focused on a pump in the optical limiter regime. The nature of the signal mode and whether there is bistability between possible $\mathbf{k}_s$ values either on the ring or in the $k_y = 0$ plane could be interesting. It might also be interesting to investigate what parameters lead to a bistable signal mode and clarify whether the bistability condition of the pump mode changes when the exciton decay is less than the photon decay.

The real part of the Goldstone mode of the OPO regime is linear, and the imaginary part quadratic in $\delta\mathbf{k}$ at low momenta [41], but the parameter dependence has not been investigated in detail. Given that the Goldstone mode may often be obscured in experiments due to the emission from the signal, finding parameters for which its range may extend beyond the signal beam might lead to its observation. If $\Re(\omega_G) = a\,\delta\mathbf{k}$ and $\Im(\omega_G) = b\,\delta\mathbf{k}^2$, finding a and b in terms of controllable parameters (e.g. $\omega_c(\mathbf{0}) - \omega_x, \mathbf{k}_p$) would be interesting. The first check might be to confirm that the Goldstone mode is not destroyed by restoring the momentum dependence of the polariton decay.

Lastly, it may be possible to describe the OPO regime more precisely by including satellite states as observed in all numerical simulations. The many state solution to the cGPEs could be formulated using a Floquet spectrum [113, 114] with the states equally spaced in energy and momentum.

A | Non-dimensional units

All results were calculated in a non-dimensional system of units where energies are rescaled according to the Rabi frequency Ω_R. The rescaling applies in both the exciton-photon and lower polariton models, and is done at the level of the coupled exciton and photon cGPEs.

The cGPEs for excitons and photons restricted to a single momentum $\mathbf{k}$, where $a_{\mathbf{k}} \Rightarrow \phi_c; b_{\mathbf{k}} \Rightarrow \phi_x$, is:

$$i\partial_t \begin{pmatrix} a_{\mathbf{k}} \\ b_{\mathbf{k}} \end{pmatrix} = \begin{pmatrix} \omega_c(\mathbf{k}) - i\kappa_c & \frac{\Omega_R}{2} \\ \frac{\Omega_R}{2} & \omega_x(\mathbf{k}) + g_{\mathrm{x}}|b_{\mathbf{k}}|^2 - i\kappa_x \end{pmatrix} \begin{pmatrix} a_{\mathbf{k}} \\ b_{\mathbf{k}} \end{pmatrix} + \begin{pmatrix} F_{p,c} \\ 0 \end{pmatrix}.$$

Because the exciton mass is several (many) orders of magnitude greater than the photon mass m_c, the exciton dispersion is assumed flat $\omega_x(\mathbf{k}) = \omega_x$ while the dispersion of the (cavity) photons is [15] ($\hbar = 1$ throughout):

$$\omega_c(\mathbf{k}) = \omega_c(\mathbf{0}) + \frac{|\mathbf{k}|^2}{2m_c}.$$

The minimum of the photon energy can be described in terms of the detuning Δ^0 away from the exciton energy which can be controlled experimentally: $\omega_c(\mathbf{0}) = \omega_x + \Delta^0$ [15, 22, 24, 60].

The exciton energy can be found directly in the literature, but it is convenient to shift the energy scale of the entire system such that the zero of energy is ω_x. The strength of the exciton-exciton contact interaction can be calculated theoretically [115] $g_{\mathrm{x}} = 6e^2 a_x/\epsilon \approx 3\mu\mathrm{eV}(\mu\mathrm{m})^2$ (e is electric charge, a_x is exciton Bohr radius, ϵ is dielectric constant) and has also been inferred from experiments $2\mu\mathrm{eV}(\mu\mathrm{m})^2 < g_{\mathrm{x}} < 10\mu\mathrm{eV}(\mu\mathrm{m})^2$ [36, 116] and depends on the microcavity structure studied [116].

Typical experimental values of $\Omega_R = \min(\omega_{up}(\mathbf{k}) - \omega_{lp}(\mathbf{k}))$ are $5\mathrm{meV} < \Omega_R < 10\mathrm{meV}$ [15, 22, 27, 86, 111, 117] although some samples may have much larger values [19]. The detuning of the minimum of the photon dispersion away from the exciton energy has a significant effect on the excitonic and photonic fractions of the polaritons, more importantly, if $|\Delta^0| = |\omega_c(\mathbf{0}) - \omega_x|$ is large ($\gg \Omega_R/2$) the polaritons become indistinguishable from exctions (lower polaritons) and photons (upper polaritons) [15]. In all results, $\Delta^0 = 0$ has been used.

There are a couple of other tuneable parameters that do not appear in the above cGPEs: the detuning Δ^p of the monochromatic pump laser from resonance with the lower polariton dispersion, and the pump momentum $\mathbf{k}_p$. If Δ^p is too positive there are two main effects: the

pump only state may become bistable with two pump mode occupations allowed for a single pump strength [28, 29]; the mixing between the upper and lower polaritons becomes significant and the simpler lower polariton model would become invalid [28, 41]. The implication of the latter concern is that $\Delta^p < \Omega_R/2$ for the lower-polariton model to be valid [28, 41]. The value of $\mathbf{k}_p$ for OPO in experiments is typically in the range $1 < |\mathbf{k}_p| < 2\mu\text{m}^{-1}$ [33, 61, 82].

In table A.1, some experimental values of the system parameters are listed. The range and complexity of the parameters motivates using a non-dimensional system of units where a few parameters can be varied in calculations and the results applied to different experimental systems by appropriate rescaling.

Parameter	value	units
ω_x	1400 - 1600	meV
Δ^0	-2 - 6	meV
Ω_R	2.5 - 10	meV
g_x	0.002 - 0.01	$\text{meV}(\mu\text{m})^2$
τ_x	100 - 2500	ps
τ_c	1 - 100	ps
m_c	$2\times10^{-5}m_0$ - $3\times10^{-5}m_0$	$\text{meV}^{-1}\mu\text{m}^{-2}$
Δ^p	-2.5 - 2.5 ($\Omega_R = 5$)	meV
$\lvert\mathbf{k}_p\rvert$	1 - 2	μm^{-1}

Table A.1: Summary of some values of exciton-photon system parameters [15] (m_0 is the free electron mass and m_c is the cavity photon mass). The exciton lifetimes, $\tau_x = 150$ps for a CdTe based quantum well [118] and $\tau_x = 2500$ps for a GaAs based quantum well [119].

To create a non-dimensional system of units for the polariton system, $\Omega_R/2 = 1$ is chosen as the energy scale (the entire cGPE is multiplied by $2/\Omega_R$):

$$\frac{2}{\Omega_R}i\partial_t\begin{pmatrix}a_\mathbf{k}\\ b_\mathbf{k}\end{pmatrix} = \begin{pmatrix}\frac{2}{\Omega_R}(\omega_x+\Delta^0+\frac{|\mathbf{k}|^2}{2m_c}-i\kappa_c) & 1\\ 1 & \frac{2}{\Omega_R}(\omega_x+g_\text{x}|b_\mathbf{k}|^2-i\kappa_x)\end{pmatrix}\begin{pmatrix}a_\mathbf{k}\\ b_\mathbf{k}\end{pmatrix}+\begin{pmatrix}\frac{2}{\Omega_R}F_{p,c}\\ 0\end{pmatrix}.$$

As mentioned previously, ω_x ($2\omega_x/\Omega_R$)is a real shift in the energy scale of the problem so the zero of energy can be set as $\omega_x = 0$. Let: $\Delta' = 2\Delta^0/\Omega_R, \kappa'_{\{x,c\}} = 2\kappa_{\{x,c\}}/\Omega_R, t' = t\Omega_R/2$ then

$$\begin{aligned} i\partial_{t'}\begin{pmatrix}a_\mathbf{k}\\ b_\mathbf{k}\end{pmatrix} &= \begin{pmatrix}\Delta'+\frac{2}{\Omega_R}\frac{|\mathbf{k}|^2}{2m_c}-i\kappa'_c & 1\\ 1 & \frac{2}{\Omega_R}g_\text{x}|b_\mathbf{k}|^2-i\kappa'_x\end{pmatrix}\begin{pmatrix}a_\mathbf{k}\\ b_\mathbf{k}\end{pmatrix}+\begin{pmatrix}\frac{2}{\Omega_R}F_{p,c}\\ 0\end{pmatrix}\\ &= \begin{pmatrix}\Delta'+|\mathbf{q}|^2-i\kappa'_c & 1\\ 1 & g'_\text{x}|b_\mathbf{k}|^2-i\kappa'_x\end{pmatrix}\begin{pmatrix}a_\mathbf{k}\\ b_\mathbf{k}\end{pmatrix}+\begin{pmatrix}F\\ 0\end{pmatrix}, \end{aligned} \tag{A.1}$$

where $\mathbf{q} = \mathbf{k}/\sqrt{m_c\Omega_R}$, $F = 2F_{p,c}/\Omega_R$ and $g'_\text{x} = 2g_\text{x}/\Omega_R$. In the exciton-photon model analysis, this is the end of the rescaling procedure. By rescaling $a_\mathbf{k}, b_\mathbf{k} \to a'_\mathbf{k}, b'_\mathbf{k} = \sqrt{2g_\text{x}/\Omega_R}(a_\mathbf{k}, b_\mathbf{k})$, the

exciton-exciton interaction can be normalised too, with the effect of rescaling the fields, and

$$i\partial_{t'}\begin{pmatrix} a'_{\mathbf{k}} \\ b'_{\mathbf{k}} \end{pmatrix} = \begin{pmatrix} \Delta' + |\mathbf{q}|^2 - i\kappa'_c & 1 \\ 1 & |b'_{\mathbf{k}}|^2 - i\kappa'_x \end{pmatrix}\begin{pmatrix} a'_{\mathbf{k}} \\ b'_{\mathbf{k}} \end{pmatrix} + \begin{pmatrix} F' \\ 0 \end{pmatrix} \tag{A.2}$$

with $F' = \frac{2}{\Omega_R}\sqrt{\frac{2g_x}{\Omega_R}}F_{p,c}$. All results for the lower polariton model are presented in the non-dimensional system of units of Eq. (A.2), while results in the exciton-photon model are in the units of Eq. (A.1). This has reduced the number of parameters in the cGPEs from 7 to 3 (4 in the exciton-photon model where the fields are not rescaled according to g_x), as summarised in table A.2. The two pump quantities Δ^p and $\mathbf{k}_p$ scale according to their type: Δ^p is an energy so $\delta' = 2\Delta^p/\Omega_R$ while $\mathbf{k}_p$ is a momentum and $\mathbf{k}'_p = \mathbf{q}_p = \mathbf{k}_p/\sqrt{\Omega_R m_c}$.

Parameter	minimum value	maximum value
Δ'	-0.8	0.8
κ'_x	0.00016	0.004
κ'_c	0.004	0.08
δ'	-1	1
$\mathbf{k}'_p = \mathbf{q}_p$	0.9	1.8

Table A.2: Summary of scaled values of exciton-photon system parameters for the choice: $\Omega_R = 5, m_c = 0.25$ ($2.5 \times 10^{-5} m_0$), relevant to the non-dimensional model described above.

The normal (dimensional) expressions for the polariton dispersions and the Hopfield Coefficients are given by Eqs. (2.15), (2.21) and (2.22). In the rescaled units they read:

$$\begin{aligned} \omega_{up,lp}(\mathbf{q}) &= \frac{\Delta' + |\mathbf{q}|^2}{2} \pm \frac{1}{2}\sqrt{(\Delta' + |\mathbf{q}|^2)^2 + 4}, \\ X_{lp}(\mathbf{q}) &= \frac{\omega_{lp}(\mathbf{q}) - \Delta' - |\mathbf{q}|^2}{\sqrt{(\omega_{lp}(\mathbf{q}) - \Delta' - |\mathbf{q}|^2)^2 + 1}}, \\ C_{lp}(\mathbf{q}) &= \frac{1}{\sqrt{(\omega_{lp}(\mathbf{q}) - \Delta' - |\mathbf{q}|^2)^2 + 1}}. \end{aligned}$$

In the lower polariton model, the non-dimensionalised cGPE is:

$$i\partial_{t'}\phi = [\omega_{lp}(\mathbf{q}) - i\kappa'_{lp}(\mathbf{q}) + X^4_{lp}|\phi|^2]\phi + F'_{p,lp} \tag{A.3}$$

in which the fields ϕ, and the pump $F'_{p,lp}$ are rescaled such that $g_{\mathrm{x}} \to 1$ in the interaction term. In all results, the values used are non-dimensional although the notation is typically that of the dimensional case.

Bibliography

[1] K. Dunnett and M. H. Szymańska. Keldysh field theory for nonequilibrium condensation in a parametrically pumped polariton system. *Phys. Rev. B*, 93:195306, May 2016.

[2] L. D. Landau and E. M. Lifshitz. *Statistical Physics, part 1.* Elsevier, 3rd edition, 1980.

[3] L. Pitaevskii and S. Stringari. *Bose-Einstein Condensation.* Number 116 in International Series of Monographs on Physics. Oxford University Press, 2003.

[4] E. M. Lifshitz and L. P. Pitaeveskii. *Statistical Physics, part 2.* Pergamon Press, 1980.

[5] N. Proukakis, S. Gardiner, M. Davis, and M. Szymańska, editors. *Quantum Gases: Finite Temperature and Non-Equilibrium Dynamics.* Imperial College Press, 2013.

[6] M. H. Anderson, J. R. Ensher, M. R. Matthews, C. E. Wieman, and E. A. Cornell. Observation of bose-einstein condensation in a dilute atomic vapor. *Science*, 269(5221):198–201, Jul 1995.

[7] K. B. Davis, M. O. Mewes, M. R. Andrews, N. J. van Druten, D. S. Durfee, D. M. Kurn, and W. Ketterle. Bose-einstein condensation in a gas of sodium atoms. *Phys. Rev. Lett.*, 75:3969–3973, Nov 1995.

[8] C. C. Bradley, C. A. Sackett, and R. G. Hulet. Bose-Einstein condensation of lithium: Observation of limited condensate number. *Phys. Rev. Lett.*, 78:985–989, Feb 1997.

[9] D. G. Fried, T. C. Killian, L. Willmann, D. Landhuis, S. C. Moss, D. Kleppner, and T. J. Greytak. Bose-Einstein condensation of atomic hydrogen. *Phys. Rev. Lett.*, 81:3811–3814, Nov 1998.

[10] J. J. Hopfield. Theory of the contribution of excitons to the complex dielectric constant of crystals. *Phys. Rev.*, 112:1555–1567, Dec 1958.

[11] D. D. Sell, S. E. Stokowski, R. Dingle, and J. V. DiLorenzo. Polariton reflectance and photoluminescence in high-purity GaAs. *Phys. Rev. B*, 7:4568–4586, May 1973.

[12] C. H. Henry and J. J. Hopfield. Raman scattering by polaritons. *Phys. Rev. Lett.*, 15:964–966, Dec 1965.

[13] R. G. Ulbrich and C. Weisbuch. Resonant brillouin scattering of excitonic polaritons in gallium arsenide. *Phys. Rev. Lett.*, 38:865–868, Apr 1977.

[14] C. Weisbuch, M. Nishioka, A. Ishikawa, and Y. Arakawa. Observation of the coupled exciton-photon mode splitting in a semiconductor quantum microcavity. *Phys. Rev. Lett.*, 69:3314–3317, Dec 1992.

[15] H. Deng, H. Haug, and Y. Yamamoto. Exciton-polariton Bose-Einstein condensation. *Rev. Mod. Phys.*, 82:1489–1537, May 2010.

[16] B. Nelsen, G. Liu, M. Steger, D. W. Snoke, R. Balili, K. West, and L. Pfeiffer. Dissipationless flow and sharp threshold of a polariton condensate with long lifetime. *Phys. Rev. X*, 3(4):041015, Nov 2013.

[17] M. Steger, G. Liu, B. Nelsen, C. Gautham, D W. Snoke, R. Balili, L. Pfeiffer, and K. West. Long-range ballistic motion and coherent flow of long-lifetime polaritons. *Phys. Rev. B*, 88(23):235314, Dec 2013.

[18] J. Keeling and N. G. Berloff. Exciton-polariton condensation. *Contemporary Physics*, 52:131–151, Feb 2011.

[19] I. Carusotto and C. Ciuti. Quantum fluids of light. *Rev. Mod. Phys.*, 85:299–366, Feb 2013.

[20] J. Kasprzak, M. Richard, S. Kundermann, A. Baas, P. Jeambrun, J. M. J. Keeling, F. M. Marchetti, M. H. Szymańska, R. André, J. L. Staehli, V. Savona, P. B. Littlewood, Deveaud B., and Le Si Dang. Bose-Einstein condensation of exciton polaritons. *Nature*, 443:409–414, Sep 2006.

[21] M. H. Szymańska, J. Keeling, and P. B. Littlewood. Mean-field theory and fluctuation spectrum of a pumped decaying Bose-Fermi system across the quantum condensation transition. *Phys. Rev. B*, 75:195331, May 2007.

[22] P. G. Savvidis, J. J. Baumberg, R. M. Stevenson, M. S. Skolnick, D. M. Whittaker, and J. S. Roberts. Angle-resonant stimulated polariton amplifier. *Phys. Rev. Lett.*, 84:1547–1550, Feb 2000.

[23] C. Ciuti, P. Schwendimann, B. Deveaud, and A. Quattropani. Theory of the angle-resonant polariton amplifier. *Phys. Rev. B*, 62:R4825–R4828, Aug 2000.

[24] R. Houdré, C. Weisbuch, R. P. Stanley, U. Oesterle, and M. Ilegems. Nonlinear emission of semiconductor microcavities in the strong coupling regime. *Phys. Rev. Lett.*, 85:2793–2796, Sep 2000.

[25] N. A. Gippius, S. G. Tikhodeev, V. D. Kulakovsii, D. N. Krizhanovskii, and A. I. Tartakovskii. Nonlinear dynamics of polariton scattering in semiconductor microcavity: bistablity vs. stimulated scattering. *Europhys. Lett.*, 67(6):997, Sep 2004.

[26] R. M. Stevenson, V. N. Astratov, M. S. Skolnick, D. M. Whittaker, M. Emam-Ismail, A. I. Tartakovskii, P. G. Savvidis, J. J. Baumberg, and J. S. Roberts. Continuous wave observation of massive polariton redistribution by stimulated scattering in semiconductor microcavities. *Phys. Rev. Lett.*, 85:3680–3683, Oct 2000.

[27] J. J. Baumberg, P. G. Savvidis, R. M. Stevenson, A. I. Tartakovskii, M. S. Skolnick, D. M. Whittaker, and J. S. Roberts. Parametric oscillation in a vertical microcavity: A polariton condensate or micro-optical parametric oscillation. *Phys. Rev. B*, 62:R16247–R16250, Dec 2000.

[28] C. Ciuti and I. Carusotto. Quantum fluid effects and parametric instabilities in microcavities. *Phys. Status Solidi B*, 242(11):2224–2245, Sep 2005.

[29] D. M. Whittaker. Effects of polariton-energy renormalization in the microcavity optical parametric oscillator. *Phys. Rev. B*, 71:115301, Mar 2005.

[30] M. Wouters and I. Carusotto. Parametric oscillation threshold of semiconductor microcavities in the strong coupling regime. *Phys. Rev. B*, 75:075332, Feb 2007.

[31] C. Ciuti, P. Schwendimann, and A. Quattropani. Theory of polariton parametric interactions in semiconductor microcavities. *Semicond. Sci. Technol.*, 18:S279–S293, Oct 2003.

[32] A. Baas, J.-Ph. Karr, M. Romanelli, A. Bramati, and E. Giacobino. Quantum degeneracy of microcavity polaritons. *Phys. Rev. Lett.*, 96:176401, May 2006.

[33] R. Butté, M. S. Skolnick, D. M. Whittaker, D. Bajoni, and J. S. Roberts. Dependence of stimulated scattering in semiconductor microcavities on pump power, angle, and energy. *Phys. Rev. B*, 68:115325, Sep 2003.

[34] Y. Guo, C. K. Kao, E. H. Li, and K. S. Chiang. *Nonlinear photonics.* Springer series in photonics. Springer, 2002.

[35] R. W. Boyd. *Nonlinear optics.* Academic Press, 3rd edition, 2008.

[36] A. Amo, J. Lefrère, S. Pigeon, C. Adrados, C. Ciuti, I. Carusotto, R. Houdré, E. Giacobino, and A. Bramati. Superfluidity of polaritons in semiconductor microcavities. *Nature Physics*, 5(11):805–810, Nov 2009.

[37] A. V. Kavokin, J. J. Baumberg, G. Malpuech, and F. P. Laussy. *Microcavities.* Oxford University Press, 2007.

[38] N. Masumoto, N. Y. Kim, T. Byrnes, K. Kusudo, A. Löffler, S. Höfling, A. Forchel, and Y. Yamamoto. Exciton-polariton condensates with flat bands in a two-dimensional kagome lattice. *New Journal of Physics*, 14(6):065002, June 2012.

[39] G. Dasbach, C. Diederichs, J. Tignon, C. Ciuti, Ph. Roussignol, C. Delalande, M. Bayer, and A. Forchel. Polarization inversion via parametric scattering in quasi-one-dimensional microcavities. *Phys. Rev. B*, 71:161308, Apr 2005.

[40] T. Lecomte, V. Ardizzone, M. Abbarchi, C. Diederichs, A. Miard, A. Lemaitre, I. Sagnes, P. Senellart, J. Bloch, C. Delalande, J. Tignon, and P. Roussignol. Optical parametric oscillation in one-dimensional microcavities. *Phys. Rev. B*, 87:155302, Apr 2013.

[41] M. Wouters and I. Carusotto. Goldstone mode of optical parametric oscillators in planar semiconductor microcavities in the strong-coupling regime. *Phys. Rev. A*, 76:043807, Oct 2007.

[42] R. Balili, V. Hartwell, D. W. Snoke, L. Pfeiffer, and K. West. Bose-Einstein condensation of microcavity polaritons in a trap. *Science*, 316(5827):1007–1010, May 2007.

[43] N. W. Sinclair, J. K. Wuenschell, Z. Vörös, B. Nelsen, D. W. Snoke, M. H. Szymanska, A. Chin, J. Keeling, L. N. Pfeiffer, and K. W. West. Strain-induced darkening of trapped excitons in coupled quantum wells at low temperature. *Phys. Rev. B*, 83:245304, Jun 2011.

[44] R. Balili, B. Nelsen, D. W. Snoke, L. Pfeiffer, and K. West. Role of the stress trap in the polariton quasiequilibrium condensation in gaas microcavities. *Phys. Rev. B*, 79:075319, Feb 2009.

[45] R. Balili, B. Nelsen, D. W. Snoke, R. H. Reid, L. Pfeiffer, and K. West. Huge splitting of polariton states in microcavities under stress. *Phys. Rev. B*, 81:125311, Mar 2010.

[46] A. Askitopoulos, H. Ohadi, P. Savvidis, H. Zaharias, A. Kavokin, and P. Lagoudakis. Condensation of polaritons through optical confinement: increased coherence and reduced threshold. In *CLEO: 2013*, page CM2M.5. Optical Society of America, June 2013.

[47] G. H. Lodden and R. J. Holmes. Electrical excitation of microcavity polaritons by radiative pumping from a weakly coupled organic semiconductor. *Phys. Rev. B*, 82:125317, Sep 2010.

[48] G. Lerario, A. Cannavale, D. Ballarini, L. Dominici, M. De Giorgi, M. Liscidini, D. Gerace, D. Sanvitto, and G. Gigli. Room temperature bloch surface wave polaritons. *Opt. Lett.*, 39(7):2068–2071, Apr 2014.

[49] M. Mazzeo, A. Genco, Gambino S., Ballarini D., F. Mangione, O. Di Stefano, S. Patanè, S. Savasta, D. Sanvitto, and G. Gigli. Ultrastrong light-matter coupling in electrically doped microcavity organic light emitting diodes. *Applied Physics Letters*, 104(23):3303, June 2014.

[50] S. Gambino, M. Mazzeo, A. Genco, O. Di Stefano, S. Savasta, S. Patanè, D. Ballarini, F. Mangione, G. Lerario, D. Sanvitto, and G. Gigli. Exploring light-matter interaction phenomena under ultrastrong coupling regime. *ACS Photonics*, 1(10):1042–1048, Oct 2014.

[51] T. Schwartz, J. A. Hutchison, C. Genet, and T. W. Ebbesen. Reversible switching of ultrastrong light-molecule coupling. *Phys. Rev. Lett.*, 106:196405, May 2011.

[52] S. Kéna-Cohen, S. A. Maier, and D. D. C. Bradley. Ultrastrongly coupled exciton-polaritons in metal-clad organic semiconductor microcavities. *Advanced Optical Materials*, 1(11):827–833, Nov 2013.

[53] D. Ballarini, M. De Giorgi, S. Gambino, G. Lerario, M. Mazzeo, A. Genco, G. Accorsi, C. Giansante, S. Colella, S. D'Agostino, P. Cazzato, D. Sanvitto, and G. Gigli. Polariton-induced enhanced emission from an organic dye under the strong coupling regime. *Advanced Optical Materials*, 2(11):1076–1081, Nov 2014.

[54] D. G. Lidzey, D. D. C. Bradley, M. S. Skolnick, T. Virgili, S. Walker, and D. M. Whittaker. Strong exciton-photon coupling in an organic semiconductor microcavity. *Nature*, 395:53–55, Sep 1998.

[55] I. G. Savenko, O. V. Kibis, and I. A. Shelykh. Asymmetric quantum dot in a microcavity as a nonlinear optical element. *Phys. Rev. A*, 85:053818, May 2012.

[56] S. De Liberato, C. Ciuti, and C. C. Phillips. Terahertz lasing from intersubband polariton-polariton scattering in asymmetric quantum wells. *Phys. Rev. B*, 87:241304, Jun 2013.

[57] C. Ciuti, G. Bastard, and I. Carusotto. Quantum vacuum properties of the intersubband cavity polariton field. *Phys. Rev. B*, 72:115303, Sep 2005.

[58] D. M. Whittaker. Classical treatment of parametric processes in a strong-coupling planar microcavity. *Phys. Rev. B*, 63:193305, Apr 2001.

[59] C. Ciuti, P. Schwendimann, and A. Quattropani. Parametric luminescence of microcavity polaritons. *Phys. Rev. B*, 63:041303, Jan 2001.

[60] P. G. Savvidis, C. Ciuti, J. J. Baumberg, D. M. Whittaker, M. S. Skolnick, and J. S. Roberts. Off-branch polaritons and multiple scattering in semiconductor microcavities. *Phys. Rev. B*, 64:075311, Jul 2001.

[61] A. I. Tartakovskii, D. N. Krizhanovskii, D. A. Kurysh, V. D. Kulakovskii, M. S. Skolnick, and J. S. Roberts. Polariton parametric scattering processes in semiconductor microcavities observed in continuous wave experiments. *Phys. Rev. B*, 65:081308, Feb 2002.

[62] F. M. Marchetti and M. H. Szymańska. Vortices in polariton OPO superfluids. In V. Timofeev and D. Sanvitto, editors, *Exciton Polaritons in Microcavities*, volume 172 of *Springer Series in Solid-State Sciences*, pages 173–213. Springer Berlin Heidelberg, 2012.

[63] D. Sanvitto, D. N. Krizhanovskii, D. M. Whittaker, S. Ceccarelli, M. S. Skolnick, and J. S. Roberts. Spatial structure and stability of the macroscopically occupied polariton state in the microcavity optical parametric oscillator. *Phys. Rev. B*, 73:241308, Jun 2006.

[64] I. Carusotto and C. Ciuti. Spontaneous microcavity-polariton coherence across the parametric threshold: Quantum monte carlo studies. *Phys. Rev. B*, 72:125335, Sep 2005.

[65] H. Haug, T. D. Doan, H. Thien Cao, and D. B. Tran Thoai. Temporal first- and second-order correlations in a polariton condensate. *Phys. Rev. B*, 85:205310, May 2012.

[66] D. N. Krizhanovskii, D. Sanvitto, A. P. D. Love, M. S. Skolnick, D. M. Whittaker, and J. S. Roberts. Dominant effect of polariton-polariton interactions on the coherence of the microcavity optical parametric oscillator. *Phys. Rev. Lett.*, 97:097402, Aug 2006.

[67] A. Kavokin, G. Malpuech, and F.P. Laussy. Polariton laser and polariton superfluidity in microcavities. *Physics Letters A*, 306(4):187 – 199, Jan 2003.

[68] G. Dagvadorj, J. M. Fellows, S. Matyjaśkiewicz, F. M. Marchetti, I. Carusotto, and M. H. Szymańska. Nonequilibrium phase transition in a two-dimensional driven open quantum system. *Phys. Rev. X*, 5:041028, Nov 2015.

[69] A. Altland and B. Simons. *Condensed Matter Field Theory.* Cambridge University Press, 2nd edition, 2010.

[70] A. Kamenev. Many-body theory of non-equilibrium systems. In H. Bouchiat, Y. Gefen, G. Montambaux, and J. Dalibard, editors, *Les Houches, Session LXXXI, 2004 Nanophysics: Coherence and Transport.* Elsevier, 2005.

[71] A. Kamenev. *Field theory of non-equilibrium systems.* Cambridge University Press, 2011.

[72] E. G. Dalla Torre, S. Diehl, M. D. Lukin, S. Sachdev, and P. Strack. Keldysh approach for nonequilibrium phase transitions in quantum optics: Beyond the Dicke model in optical cavities. *Phys. Rev. A*, 87:023831, Feb 2013.

[73] M. Buchhold, P. Strack, S. Sachdev, and S. Diehl. Dicke-model quantum spin and photon glass in optical cavities: Nonequilibrium theory and experimental signatures. *Phys. Rev. A*, 87:063622, June 2013.

[74] A.-W. de Leeuw, H. T. C. Stoof, and R. A. Duine. Schwinger-Keldysh theory for Bose-Einstein condensation of photons in a dye-filled optical microcavity. *Phys. Rev. A*, 88:033829, Sep 2013.

[75] S. Gopalakrishnan, B. L. Lev, and P. M. Goldbart. Atom-light crystallization of Bose-Einstein condensates in multimode cavities: Nonequilibrium classical and quantum phase transitions, emergent lattices, supersolidity, and frustration. *Phys. Rev. A*, 82:043612, Oct 2010.

[76] J. Marino and S. Diehl. Driven markovian quantum criticality. *Phys. Rev. Lett.*, 116:070407, Feb 2016.

[77] M. H. Szymańska, J. Keeling, and P. B. Littlewood. Non-equilibrium quantum condensation in an incoherently pumped dissipative system. *Phys. Rev. Lett.*, 96:230602, June 2006.

[78] J. Keeling, M. H. Szymańska, and P. B. Littlewood. Keldysh Green's function approach to coherence in a non-equilibrium steady state: connecting Bose-Einstein condensation and lasing. In G. Slavcheva and P. Roussignol, editors, *Optical Generation and Control of Quantum Coherence in Semiconductor Nanostructures*, Nanoscience and Technology, pages 293–329. Springer, Berlin Heidelberg, 2010.

[79] M. Yamaguchi, K. Kamide, R. Nii, T. Ogawa, and Y. Yamamoto. Second thresholds in BEC-BCS-laser crossover of exciton-polariton systems. *Phys. Rev. Lett.*, 111:026404, July 2013.

[80] M. Yamaguchi, K. Kamide, T. Ogawa, and Y. Yamamoto. BEC-BCS-laser crossover in coulomb-correlated electron-hole-photon systems. *New Journal of Physics*, 14(6):065001, June 2012.

[81] S. A. Moskalenko and D. W. Snoke. *Bose-Einstein Condensation of excitons and biexcitons.* Cambridge University Press, 2000.

[82] W. Langbein. Spontaneous parametric scattering of microcavity polaritons in momentum space. *Phys. Rev. B*, 70:205301, Nov 2004.

[83] G. Rochat, C. Ciuti, V. Savona, C. Piermarocchi, A. Quattropani, and P. Schwendimann. Excitonic bloch equations for a two-dimensional system of interacting excitons. *Phys. Rev. B*, 61:13856–13862, May 2000.

[84] A. Mehdizadeh, A. S. Vala, S. Shojaei, and M. Kalafi. The role of exciton-photon coupling in the temporal behaviour of a quantum dot-photonic crystal microcavity. *Phys. Status Solidi C*, 9(12):2517–2520, Dec 2012.

[85] L. D. Landau and E. M. Lifshitz. *Quantum Mechanics.* Pergamon Press, 1965.

[86] A. Baas, J. Ph. Karr, H. Eleuch, and E. Giacobino. Optical bistability in semiconductor microcavities. *Phys. Rev. A*, 69:023809, Feb 2004.

[87] A. Kavokin and G. Malpuech. Chapter 5 Resonant excitation case and parametric amplification. In *Cavity Polaritons*, volume 32 of *Thin Films and Nanostructures*, pages 147 – 181. Academic Press, 2003.

[88] L. P. Kadanoff and G. Baym. *Quantum Statistical Mechanics.* Addison-Wesley, 1989.

[89] K. F. Riley, M. P. Hobson, and S. J. Bence. *Mathematical Methods for Physics and Engineering*. Cambridge University Press, 3rd edition, 2009.

[90] D. W. Jordan and P. Smith. *Mathematical Techniques*. Oxford University Press, 4th edition, 2008.

[91] F. M. Marchetti, J. Keeling, M. H. Szymańska, and P. B. Littlewood. Absorption, photoluminescence, and resonant Rayleigh scattering probes of condensed microcavity polaritons. *Phys. Rev. B*, 76:115326, Sep 2007.

[92] H. Kleinert. *Path Integrals in Quantum Mechanics, Statistics and Polymer Physics*. World Scientific, 1990.

[93] M. S. Bourzutschky and M. C. Cross. Coupled map models for chaos in extended systems. *Chaos*, 2:173–181, Apr 1992.

[94] E. Bouchbinder and J. S. Langer. Nonequilibrium thermodynamics of driven amorphous materials. ii. effective-temperature theory. *Phys. Rev. E*, 80:031132, Sep 2009.

[95] C. Song, P. Wang, and H. A. Makse. Experimental measurement of an effective temperature for jammed granular materials. *Proceedings of the National Academy of Sciences of the United States of America*, 102(7):2299–2304, Feb 2005.

[96] L. F. Cugliandolo, J. Kurchan, and L. Peliti. Energy flow, partial equilibration, and effective temperatures in systems with slow dynamics. *Phys. Rev. E*, 55:3898–3914, Apr 1997.

[97] P. Sollich, S. Fielding, and P. Mayer. Fluctuation-dissipation relations and effective temperatures in simple non-mean field systems. *Journal of Physics: Condensed Matter*, 14(7):1683, Feb 2002.

[98] A. Caso, L. Arrachea, and G. S. Lozano. Defining the effective temperature of a quantum driven system from current-current correlation functions. *The European Physical Journal B*, 85:266, Aug 2012.

[99] L. M. Sieberer, S. D. Huber, E. Altman, and S. Diehl. Non-equilibrium functional renormalization for driven-dissipative Bose-Einstein condensation. *Phys. Rev. B*, 89:134310, Apr 2014.

[100] P. C. Hohenberg and B. I. Shraiman. Chaotic behaviour of an extended system. *Physica D*, 37:109–115, July 1989.

[101] M. Wouters and I. Carusotto. Absence of long-range coherence in the parametric emission of photonic wires. *Phys. Rev. B*, 74:245316, Dec 2006.

[102] A. C. Berceanu, L. Dominici, I. Carusotto, D. Ballarini, E. Cancellieri, G. Gigli, M. H. Szymańska, D. Sanvitto, and F. M. Marchetti. Multicomponent polariton superfluidity in the optical parametric oscillator regime. *Phys. Rev. B*, 92:035307, Jul 2015.

[103] A. Baas, J.-Ph. Karr, M. Romanelli, A. Bramati, and E. Giacobino. Optical bistability in semiconductor microcavities in the nondegenerate parametric oscillation regime: analogy with the optical parametric oscillator. *Phys. Rev. B*, 70:161307, Oct 2004.

[104] H. Haken. *Light, Volume 1, Waves, Photons, Atoms.* North-Holland, 1981.

[105] S. S. Gavrilov. Blowup dynamics of coherently driven polariton condensates. *Phys. Rev. B*, 90:205303, Nov 2014.

[106] D. Sarchi, M. Wouters, and V. Savona. Polariton parametric photoluminescence in spatially inhomogeneous systems. *Phys. Rev. B*, 79:165315, Apr 2009.

[107] V. D. Kulakovskii, A. I. Tartakovskii, D. N. Krizhanovskii, N. A. Gippius, M. S. Skolnick, and J. S. Roberts. Nonlinear effects in a dense two-dimensional exciton-polariton system in semiconductor microcavities. *Nanotechnology*, 12(4):475, Dec 2001.

[108] E. Altman, L. M. Sieberer, L. Chen, S. Diehl, and J. Toner. Two-dimensional superfluidity of exciton polaritons requires strong anisotropy. *Phys. Rev. X*, 5(1):011017, Feb 2015.

[109] D. N. Krizhanovskii, S. S. Gavrilov, A. P. D. Love, D. Sanvitto, N. A. Gippius, S. G. Tikhodeev, V. D. Kulakovskii, D. M. Whittaker, M. S. Skolnick, and J. S. Roberts. Self-organization of multiple polariton-polariton scattering in semiconductor microcavities. *Phys. Rev. B.*, 77:115336, Mar 2008.

[110] S. S. Gavrilov, A. S. Brichkin, Ya. V. Grishina, C. Schneider, S. Höfling, and V. D. Kulakovskii. Blowup dynamics of coherently driven polariton condensates: Experiment. *Phys. Rev. B*, 92:205312, Nov 2015.

[111] I. Carusotto and C. Ciuti. Probing microcavity polariton superfluidity through resonant Rayleigh scattering. *Phys. Rev. Lett.*, 93:166401, Oct 2004.

[112] D.V. Skryabin, O.A. Egorov, A.V. Gorbach, and F. Lederer. One-dimensional polariton solitons and soliton waveguiding in microcavities. *Superlattices and Microstructures*, 47(1):5 – 9, 2010. Proceedings of the 9th International Conference on Physics of Light-Matter Coupling in Nanostructures, {PLMCN} 2009 (Lecce - Italy).

[113] P. Hartman. *Ordinary Differential Equations.* Wiley & Sons, 1964.

[114] D. W. Jordan and P. Smith. *Nonlinear Ordinary Differential Equations.* Oxford University Press, 4th edition, 2007.

[115] C. Ciuti, V. Savona, C. Piermarocchi, A. Quattropani, and P. Schwendimann. Threshold behavior in the collision broadening of microcavity polaritons. *Phys. Rev. B*, 58:R10123–R10126, Oct 1998.

[116] L. Ferrier, E. Wertz, R. Johne, D. D. Solnyshkov, P. Senellart, I. Sagnes, A. Lemaître, G. Malpuech, and J. Bloch. Interactions in confined polariton condensates. *Phys. Rev. Lett.*, 106:126401, Mar 2011.

[117] J. O. Hamp, A. K. Balin, F. M. Marchetti, D. Sanvitto, and M. H. Szymańska. Spontaneous rotating vortex rings in a parametrically driven polariton fluid. *EPL (Europhysics Letters)*, 110(5):57006, June 2015.

[118] A. Polhmann, R. Hellmann, E. O. Göbel, D. R. Yakovlev, W. Ossau, A. Waag, R. N. Bicknell-Tassius, and G. Landwehr. Exction lifetimes in CdTe/CdMnTe single quantum wells. *Applied Physics Letters*, 61(24):2929, Dec 1992.

[119] J. Feldmann, G. Peter, E. O. Göbel, P. Dawson, K. Moore, C. Foxon, and R. J. Elliott. Linewidth dependence of radiative exciton lifetimes in quantum wells. *Phys. Rev. Lett.*, 59:2337–2340, Nov 1987.